

TOWARD TWO-DIMENSIONALLY ORDERED
SUBSTITUTED POLYACETYLENES: ORDERED MONOMER AND
PREFORMED POLYMER APPROACH

By

RIGOBERTO C. ADVINCULA

A DISSERTATION PRESENTED TO THE GRADUATE SCHOOL OF THE
UNIVERSITY OF FLORIDA IN PARTIAL FULFILLMENT
OF THE REQUIREMENTS FOR THE DEGREE OF
DOCTOR OF PHILOSOPHY

UNIVERSITY OF FLORIDA

1994

*This dissertation is dedicated to my parents,
Atty. Benedicto F. Advincula and Evelina C. Advincula
for their love, support, encouragement, and desire
to see their children live fruitful lives.*

ACKNOWLEDGMENTS

So many special people deserve to be acknowledged. My experience with graduate school would not be the same without them. First and foremost, let me begin with my advisor, Dr. Randy S. Duran. The guidance, opportunities, encouragement, and experience he bestowed on me are greatly appreciated.

My thanks also go to the other professors on the "polymer floor," G. Butler, K. Wagener, and J. Reynolds. Their experience in the science of polymers as well as encouragement are appreciated. In the organic division, I wish to thank Dr. J. Zoltewicz for his advice and friendship. In the chemistry department, I am indebted to Dr. J. Helling. To the other members of my graduate committee, Professors M. Vala and C. Batich, I wish to thank them for their availability. My thanks to Dr. D. Shah of the department of chemical engineering for making the learning of surface science interesting.

My stay in France would not be as fruitful and exciting without the guidance and encouragement of Dr. J. Le Moigne. The friendship of the professors, students, and staff of IPCMS-GMO group are greatly appreciated. Special thanks to L. Oswald, for her friendship and assistance, and to H. Hilberer, for the availability of his dissertation work.

I wish to acknowledge technical support from Oriel Corporation through Mr. C. Calling, KSV Instruments, and the analytical support group of the Institut Charles Sadron, Strasbourg through Mr. M. Keyser.

Special thanks go to the secretarial staff who always had a ready smile most specially to Mrs. Lorraine Williams, who was always available and willing to help and "never busy."

I want to thank all my past and present peers at the "polymer floor," J. Roberts, R. Bodalia, A. Thibodeaux, T. Herod, P. Bernal, W. Sigmund, J. Adams, W. Rettig, M. Naumann, H. Fadel, H. Zhou, S. Kim, D. Tao, B. Sankaran, F. Zuluaga, P. Balandra, D. Smith, C. Marmo, J. Portmess, K. Novak, and to the rest of the past and present groups of Dr. Wagener and Dr. Reynolds. I want to thank J. Roberts especially for his friendship and the academic experience we shared as colleagues.

I wish to thank my family in the Philippines for their encouragement and support for all these years. The most special acknowledgment is to my wife Carolyn, who is equally deserving of a Ph.D. for her love, encouragement, support, and prayers for me.

TABLE OF CONTENTS

	Page
ACKNOWLEDGMENTS	iii
ABSTRACT	ix
CHAPTERS	
1 INTRODUCTION.....	1
The Outlook of Nonlinear Optical Materials	1
The Phenomena of Nonlinear Optics.....	3
Organic Materials for Nonlinear Optics.....	6
Polymers for Third Order Nonlinear Optical Materials	10
Substituted Polyacetylenes	17
Cyclopolymerization of Unconjugated Diynes.....	22
The Langmuir-Blodgett Technique.....	27
The Monolayer Phenomena.....	28
Langmuir-Blodgett Apparatus	29
LB Vertical Deposition Technique	32
Polymers at the Air-Water Interface	34
Theory of Polymer Behavior at the Interface.....	39
Comparison with small molecules.....	41
Polymer relaxation and equilibrium at the interface.....	42
Polymers and water.....	44
Interactions of polymers at the interface	45
Langmuir-Blodgett Films and Materials for Nonlinear optics	45
Summary and Overview of the Dissertation	46
2 EXPERIMENTAL.....	50
Materials.....	50
Monomers and Polymers	50
Monoacetylenic Liquid Crystalline Monomers.....	50
Polyethynylbenzoate Polymers.....	51
Monomer synthesis	52
Typical polymerization	55
Synthesis of Poly(diethylpropargylmalonate).....	57
Monomer preparation	57
Typical polymerization	58
General Instrumentation.....	61
Langmuir-Blodgett Technique.....	63
Langmuir Monolayer Film Studies	63
Langmuir-Blodgett film deposition.....	64
Surface Analytical Techniques at the Air-water Interface	66

Surface potentiometer	66
UV-vis spectroscopy at the interface	68
Brewster angle microscopy and reflectivity.....	71
3 APPROACH I	
POLYMERIZATION OF ORDERED MONOMERS.....	74
Introduction	74
Liquid Crystalline Monomers at the Interface	74
Objectives.....	76
Bulk Characteristics of the Monomers	77
Langmuir Monolayer Film Studies	79
Surface Pressure-Area Isotherms	79
Stability of the Monolayer.....	81
Brewster Angle Microscopy	83
Analysis of Results.....	88
LB Film Deposition and Characterization	89
Deposition.....	89
UV Spectra of LB Films.....	90
X-ray of LB Films	91
Polymerization of LB Films.....	92
Polymerization.....	92
Monolayer polymerization	
attempt at the air-water interface.....	92
Polymerization of LB Films.....	93
Analysis of Results.....	95
Summary	99
4 APPROACH II A	
POLY(ETHYNYLBENZOATE ESTER) POLYMERS.....	100
Introduction	
Design of Polymers	100
Synthesis of Monomers and Polymers	102
Analysis of Characterization Data	109
Monolayer Studies	113
Surface Pressure-Area Isotherm	113
Surface Potential	116
Isobaric Creep Stability	118
Temperature Dependence.....	119
UV-Vis Measurements	120
Poly(ethynylbenzoate alkyl esters)	
Alkyl Chain Length	125
Isotherm measurements.....	127
Hysteresis.....	129
Temperature Dependence.....	131
Surface Potential Measurements	133
Brewster Angle Microscopy	140
Deposition of LB films	145
Summary	152

5 APPROACH II(B)	
POLY(DIETHYLDIPROPARGYLMALONATE).....	155
Introduction	155
Synthesis of the Polymer.....	158
Thermogravimetric Analysis	166
Langmuir-Blodgett Film Investigations	168
Langmuir Film Studies	
Monolayer structure and orientation	168
Surface-pressure area isotherm.....	168
Surface potential isotherms.....	174
UV-vis measurements at the air-water interface	180
Brewster angle microscopy (BAM)	183
Relative reflectivity	189
Analysis of Results.....	191
The Chemical Structure of the Repeat Unit.....	193
The ester side group	194
Methylene hydrogens	197
Hysteresis	
Compression -expansion cycles.....	199
Surface pressure-area isotherm hysteresis behavior.....	200
Surface potential-area isotherm hysteresis behavior.....	203
Brewster angle microscopy (BAM) and reflectivity-hysteresis	206
In situ UV-vis spectroscopy	212
Deposition to Substrates.....	224
Multilayer Deposition of Pure Polymers	224
Polarized ATR-FTIR.....	225
Alternating Multilayers	227
Summary.....	231
6 CONCLUSION	
COMPARISON OF APPROACHES AND	
PROCESSABILITY OF SUBSTITUTED POLYACETYLENES.....	234
Polymerization of LB films	
reactive functional group and initiators.....	234
Poly(ethynylbenzoate)configuration and	
lateral alkyl side chain length.....	235
Poly(diethyldipropargylmalonate)	
Molecular weight and alternate layers.....	236
APPENDICES	
A NONLINEAR OPTICS	
THE THEORETICAL VIEWPOINT	238
B THE CONJUGATED	
POLYMER BACKBONE	245

C SURFACE POTENTIAL AND DIPOLE MOMENT.....	252
REFERENCES	254
BIOGRAPHICAL SKETCH	267

Abstract of Dissertation Presented to the Graduate School of the University of Florida in Partial Fulfillment of the Requirements for the Degree of Doctor of Philosophy

TOWARD TWO-DIMENSIONALLY ORDERED
SUBSTITUTED POLYACETYLENES: ORDERED MONOMER AND
PREFORMED POLYMER APPROACH

by
Rigoberto C. Advincula

April 1994

Chairman: Professor Randolph S. Duran
Major Department: Chemistry

The Langmuir Blodgett approach was used to enhance ordering of substituted polyacetylenes. The ordered monomer and preformed polymer approaches were taken. The monolayer properties of both monomers and polymers were analyzed by surface pressure-mean molecular area isotherms, their hysteresis, and stability behavior. In addition, surface potential, Brewster Angle Microscopy, and UV-vis spectroscopy were used to investigate the film behavior. Langmuir-Blodgett films were built-up using the vertical deposition technique.

Three liquid crystalline monoacetylene monomers were investigated. Greater monolayer stability was observed at lower subphase temperatures and the use of an interactant. Z and Y type multilayers were formed by deposition on a hydrophobic substrate. X-ray and UV-vis confirmed the multilayer integrity of these films. No polymerization was observed at the air-water interface but polymerization was observed with γ -irradiation with some degradation of the mesogenic substituent.

The use of preformed polymers, was investigated initially with a series of poly(ethynylbenzoate) polymers. The stiffness and length of the lateral substituent has an effect on the backbone microstructure. The polymers were synthesized using the metathesis catalyst, WCl₆. The results were discussed in terms of the configuration and conformation adopted by the polymer in the bulk and monolayer films. It was found that a better configuration amenable for planarity is achieved with a head-to-head trans-transoidal configuration. The length of the alkyl chain is important in facilitating monolayer behavior.

Poly(diethylpropargylmalonate), a polymer with improved configuration, was synthesized via cyclopolymerization. The behavior of the polymer at the air-water interface was studied. Comparison was made of high and low molecular weight derivatives. The contribution of the ester group and the backbone on the monolayer behavior was analyzed. Interesting conformation dynamics of the polymer backbone was observed by UV-vis spectroscopy. The low molecular weight derivative had an overall better monolayer behavior than the high molecular weight polymer. Successful deposition of both polymers was made using the vertical deposition technique. LB films up to 30 layers on glass and silicon substrates gave an average transfer ratio of 1.0 ± 0.05 . Interesting superlattice structures were also made by alternating with stearic acid layers.

CHAPTER 1

INTRODUCTION

Two decisive aspects in the field of science are tradition and innovation. Tradition is the basis for it is the cumulation of wisdom in the body of knowledge. To know what a subject is all about and to control it creates self-confidence, thus paving the way for innovations. Innovation is the adventure, since with the challenge comes the risk of calling into question (or even losing) one's own scientific identity, gained through tradition.

- Excerpt from a review article by Helmut Ringsdorf¹

The Outlook of Nonlinear Optical Materials

The development of mode-locked lasers capable of generating pulses of sub-nanosecond duration allowed the direct observation of nonlinear optical phenomena in materials. This was first reported by Franken et al. in 1961, by generating the second harmonic frequency of the incident light through a quartz crystal.² During that decade, most of the fundamental observations and discoveries were made. This paved the way for the invention of tunable wavelength dye lasers during the 1970s which utilized nonlinear effects such as harmonic generation, sum and difference frequency mixing, and stimulated Raman scattering.⁶ Most of these processes utilized inorganic semiconductors, and dielectric crystals as their nonlinear media. The early 1980s saw the advent of telecommunications using optical fibers, which has been the most important stimulus for the explosion of effort in nonlinear optics during the last decade.³ It is now common to find information carried on a laser beam in the processes of communication, information storage, information retrieval, printing,

and sensing. There is increasing effort to achieve even greater data processing capabilities, by using ultrafast electronic interactions and by harnessing the properties of laser light for highly parallel manipulation and interconnection of signals. This is the age of photonics.

It is but natural that most of the early experimental and theoretical investigations were concerned with inorganic materials since they constituted a major part of materials in solid state physics at that time. Because of the growth in new applications, it became apparent that new types of materials were needed. Attention was turned to organic materials, which gained a wide reputation during the 1980s as the next generation of "synthetic metals."⁴ It is no surprise that a very important property in these materials namely, a delocalized π -electron orbital system, would result in large nonlinear optical responses. In many cases, the observed effects are much larger than their inorganic counterparts.⁵ In recent years, a parallel can be drawn with the initial multidisciplinary effort that has been responsible for the growth of inorganics in integrated electronics technology. Although the field of nonlinear optics has traditionally been the stronghold of the physicists and electrical engineers, materials scientists and chemists are now playing an important role in its future development.

Thin films of organic or polymeric materials with large second and third order nonlinearities in combination with the semi-conductor based electronic circuitry offer the possibility of new phenomena and novel devices for laser modulation and deflection.⁶ Information control in optical circuitry, light valves, optical bistability and optical switches are but a few of the possibilities with organic systems. Other novel processes occurring through third-order nonlinearity such as degenerate four-wave mixing, phase conjugation, and third harmonic generation will rely greatly on the new organic systems that are being

developed. Of particular importance for conjugated organic systems is the fact that the origin of the nonlinear effect is the polarization of the π -electron cloud as opposed to displacements or rearrangement of nuclear coordinates in inorganic materials. As electrons are less massive than nuclei, these displacements, hence nonlinearity, can be intrinsically faster in organics than inorganics. In other words, the NLO property is limited only by the synthetic chemistry involved in extending this electron delocalization in conjugated systems. In addition, the properties of organic or polymeric materials may be varied to optimize associated properties, e.g. mechanical, thermal stability, and laser damage threshold, but preserve the electronic interactions responsible for the nonlinear optical effect.

The Phenomena of Nonlinear Optics

What are nonlinear optics then? *Nonlinear optics* are concerned with the nonlinear or anharmonic interaction of electromagnetic fields, generally in the optical frequency range with a medium, resulting in the alteration of phase, frequency, or other propagation characteristics of the incident light. In other words, incident light properties are altered after passing through a material in a nonlinear manner. This optical frequency range is usually of the order of 10^{13} - 10^{17} Hz which is above vibrational and rotational modes and below electronic resonances.

At relatively low light intensities that normally occur in nature, the optical properties of materials are quite independent of the intensity of illumination. If light waves are able to penetrate and pass through a medium, this occurs without any interaction between the waves. However, if the illumination is made sufficiently intense, the optical properties begin to depend on the intensity and

other characteristics of light. A typical activation energy (internal field), E_a of 3×10^{10} V/m is common, which is the energy that binds most electrons and ions. The light waves may then interact with each other as well as with the medium. The intensities necessary to observe these effects can only be obtained by using the output from a coherent light source such as a laser (light with incident intensity in the range of 10^{14} W/cm²). This is usually achieved by focusing powerful picosecond-duration pulses which are obtainable from mode-locked lasers. Another effect of light on matter is that it can sometimes induce changes in the chemical composition. This is in the area of *photochemistry*, which is differentiated from NLO phenomena in that the medium is chemically altered instead of just the incident light.

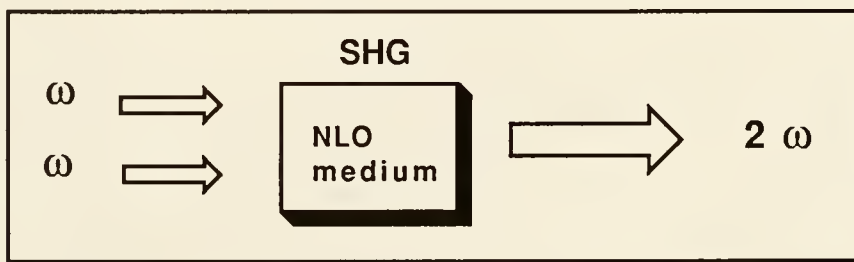


Figure 1-1. Schematic Illustration of the second harmonic generation (SHG), in which the incident light frequency (ω) is doubled (wavelength halved) upon passing through the nonlinear optically active medium.

The equation for describing the nonlinear phenomena can find some analogy in the classical force equation for springs. In a spring, displacement, x , is proportional to an external force, F . With increasing force, F , the spring stretches rapidly with a nonlinear relationship between x and F , such that at higher F , the nonlinear terms become important (in physics, the linear dependence of one physical quantity on another is almost always an approximation, which is valid only on a limited range of values). This can be described with a power series:

$$x = aF + bF^2 + cF^3 + \dots \quad (1.1)$$

Nonlinear optical phenomena can be similarly described by replacing x with polarization p and F with electric field E . When E is small, p is proportional to E (linear). With increasing E , the nonlinear contribution, E^2 and E^3 , terms become dominant:

$$p = \alpha E + \beta E^2 + \gamma E^3 + \dots \quad (1.2)$$

This equation shows the dependence of polarization at higher electric fields with constants representing the susceptibilities (magnitude of polarizability analogous to spring constant). A linear term α and second and third order nonlinear susceptibilities, β and γ , describe the microscopic susceptibility. This equation applies at the molecular level. At the macroscopic level the equation is given by

$$P = \epsilon_0 \chi^{(1)} E + \epsilon_0 \chi^{(2)} E^2 + \epsilon_0 \chi^{(3)} E^3 + \dots \quad (1.3)$$

where the macroscopic nonlinear susceptibilities are given by the second and third order nonlinear susceptibilities, $\chi^{(2)}$ and $\chi^{(3)}$, respectively, and ϵ_0 is permittivity of a vacuum. When the intermolecular interaction is weak, $\chi^{(2)}$ is approximately the sum of the β s of molecules in a unit volume. Similarly, $\chi^{(3)}$ is the sum of γ s. Simple additive relationships between the microscopic and macroscopic coefficients is often not the case, for example in an isotropic or centrosymmetric media, $\chi^{(2)} = 0$. Dispersion, degrees of freedom, spatial distributions, relationship of driving force frequencies, and variable magnetic and electric fields all affect the overall predictability between the microscopic and macroscopic terms. Detailed mathematical treatments of these effects can be found elsewhere; they are described somewhat further in Appendix A.

On the basis of the above discussion, a direct comparison between the polarizabilities of electron clouds in organic and nuclear displacements in inorganic materials can be made. In dielectric materials such as LiNbO₃, electronic polarization is not large because electrons are localized near atoms (analogous to stretching a strong spring). In semiconductors, electron clouds are widely spread, their displacement can be regarded like stretching a weak spring. Organic materials, especially long-chain conjugated molecules, have electrons delocalized one-dimensionally, i.e. they are regarded as natural quantum wires. The one dimensional characteristics lead to efficient electronic polarization induced by an electric field along the direction of the chain. Therefore compared to dielectric materials, large electronic polarizations are attainable.

Organic Materials for Nonlinear Optics

In the simplest form, π -electron cloud delocalization in organic materials is a consequence of the $\pi-\pi^*$ transition between the highest occupied molecular orbital (HOMO) and the lowest unoccupied molecular orbital (LUMO). The extension of this delocalization promotes a lowering of the energy of mixing between wavefunctions. In materials for nonlinear optics, other parameters are involved. Much theoretical research is based on determining these optimum parameters for hyperpolarizability. Among the most important are⁷

- (i) the susceptibility, $\chi^{(n)}$ (magnitude, phase, and sign),
- (ii) the recovery time, τ ,
- (iii) the real index of refraction, n ,
- (iv) the absorption coefficient, α ,
- (v) the relevant frequency domain, $\Delta\omega$.

A qualitative guideline based on the analysis of the wavefunction shape shows that simply extending the wave function overlap does not increase the inherent nonlinear susceptibility.⁸ For second order susceptibility, where noncentrosymmetry is important, β is found to be proportional to the product of the oscillator strength, f , and the dipole moment difference ($\Delta\mu$) between ground and excited state, $P_e - P_g$,

$$\beta \approx f(P_e - P_g) \quad (1.4)$$

For third order nonlinearity (γ) one must also promote wavefunction overlap by increasing the oscillator strength, f , and the wave function differences between the ground and excited states given by the wave function distribution, $L_e - L_g$

$$\gamma \approx f(L_e - L_g) \quad (1.5)$$

For both second and third order nonlinearity, note that f and $P_e - P_g$ or f and $L_e - L_g$ are not independent, thus tradeoffs are involved. Therefore a balance of the wavefunction overlap and wave function separation (or difference) must be considered simultaneously in optimizing nonlinear effects. A detailed treatment of the analysis is given in Appendix A.

Materials with second order nonlinear optical properties have received considerable effort among organic chemists. This is in part due to the large body of knowledge in the field of organic synthesis, where the synthesis of asymmetric systems is well known. To date, the largest $\chi^{(2)}$ values have been measured from organic molecular crystals.

The design of crystal structures with predictable symmetry is a main concern among theoreticians, and to this respect ordered films for $\chi^{(2)}$ consisting of amphiphiles or polymers have gained much attention. Theoretical structure-property relationships are important not only in translating microscopic

properties to macroscopic observations but also as a basis for the future design of these materials. Although numerous theoretical investigations have been made in formulating the fundamental guidelines for second order nonlinear optical materials, the following points are specific for third order nonlinear $\chi^{(3)}$ optical materials:

1. There is a power law dependence of γ on the number of carbon atoms in a conjugated chain, where γ is the molecular hyperpolarizability coefficient. The length, L, is defined as the distance along the x-direction between two carbon end sites:⁹

$$\gamma \approx L^{4.6 \pm 0.2} \quad (1.6)$$

Recent experimental verification suggest that large values of γ and correspondingly of $\chi^{(3)}$ require only chains of intermediate length of order 100-200 Å, e.g. oligomers, to low molecular weight range.^{190, 9} That is in long chains, conformational freedom can result in defects and twists which disrupt the conjugation. Therefore, the infinite length conjugated polymer chain may not be required for third order nonlinear optics. Reducing the width of the absorption band also enhances the $\chi^{(3)}$.⁸ Free electron and Huckel phenomenological models predict $\chi^{(3)}$ dependence for the polarizability on the conjugation length.

2. One dimensional systems possess the highest odd order nonlinearity per valence electron in one direction.⁷ This implies no actual advantage in two or three dimensional systems. Qualitatively, this is seen in comparison with Ge and GaAs semiconductors. Though the intrinsic value of γ is independent of symmetry, the lowering of symmetry in a conjugated chain by the incorporation of a donor and acceptor group at specific intervals has resulted in a one dimensional quantum well structure.^{8,9}

3. Specific functionalities in a conjugated system are evaluated as follows:¹⁰ Benzene, due to its aromatic character disrupts the conjugation and has an adverse effect on the polarizability tensor. The quinoidal form is more amenable to polarization but is not as easy to form. Triple bonds, notwithstanding the fact that they are π -electron richer than the double bonds, are geometrically more concentrated and form a less efficient delocalized structure.¹¹ The polyene system, on a length basis, is still the best system for electron delocalization. Recent hyperpolarizabilities have also been observed for sigma conjugated systems.¹²

4. Intermolecular forces of attraction such as H-bonding, ionic interactions, etc. can have the capacity to stabilize the twists in long conjugated chains and thus control the conformational defects.¹⁰ Thus they have value for structural organization at the molecular level. However, they do not have any beneficial effect on polarizability.

5. It is important to have some inherent form anisotropy in the molecules.¹³ In oriented *trans* polyacetylene, the tensor component parallel to the chain is higher than that perpendicular. This demonstrates that the nonlinear optical properties are entirely associated with the nonlinear polarizability of the π -electrons in the conjugated backbone.¹³

It is important that such theoretical guidelines, be validated with experimental work. Theoretical prediction and experimentation go hand in hand in testing their validity. The approach has been the building-up of large databases of actual systems and measuring intrinsic susceptibilities based on common parameters of measurement.¹⁴

Other than chemical modifications by synthesis, the control in molecular organization is deemed to be the most important aspect of nonlinear optical properties. Unlike electrical conductivity, molecular organization is critical,

more so in second-order nonlinear effects. It is necessary to create thin film structures especially for constructing quantum well structures. Well defined thickness, refractive index, and anisotropy are important for measurements in the waveguide geometry.¹⁵ Real device criteria include: uniform birefringence, minimized scattering losses, transparency, stability in ambient and operating environments, dimensional stability, and thickness control

Polymers for Third Order Nonlinear Optical Materials

The history of organic materials for NLO goes back about two decades. Urea was one of the early organic systems to demonstrate the potential of achieving large optical nonlinearities in organic crystals. Although many new interesting organic materials for second order effects have been investigated, the primary emphasis of this section will be with conjugated organic polymer systems for third order nonlinear optical properties with the exception of the poly(silanes).

Polymers have come a long way in being recognized as an important class of materials for electronic and optical applications. The development of polymers as structural materials has shown that they offer the flexibility of modifying molecular structure, conformation, order, and morphology. Therefore, they can be tailored to suit a specific application. In conjugated polymers for electrical conducting properties, this has not been much of a consideration. Conductivity is a bulk property which is heavily influenced by intrachain as well as interchain charge transport. In contrast, the current status of understanding of third order optical nonlinearity in conjugated polymers indicates the NLO behavior to be primarily a microscopic property. This poses specific challenges for developing conjugated polymers with these properties. Likewise, the lack of

processibility of these conjugated polymeric structures by conventional techniques is a consideration. Many conjugated polymers are insoluble in common organic solvents. Understanding of the microstructure and the role of solvent interaction have played an important role in building on the parent structure to improve solubility. Despite these seemingly difficult hurdles, conjugated polymers remain the best superior candidates to replace the inorganic GaAs system, both in sensitivity as well as speed of response.

Several examples of conjugated polymers with third order nonlinear optical properties are described briefly below:

Polydiacetylenes have an alternating double and triple bond backbone, making them relatively rigid compared to polyacetylenes. The most popular in the class of substituted polydiacetylenes has been the poly(dibutyl 4,19-dioxo-5,18-dioxa-3,20-diaza-10,12-docosadiynedioate) or poly(-n-BCMU), where n = 3,4 representing the number of methylene carbons between the urethane and the backbone.¹⁶ The presence of the urethane substituent facilitates coil-to-rigid rod stabilization of planar sequences. Multilayer LB films have been fabricated for waveguide applications.¹⁷ Polymers are formed in bulk or in situ at the air-water interface prior to deposition. Epitaxial polymerization of other diacetylene derivatives gives highly oriented crystals.¹⁸ Others (different R groups) that have been studied include PTS {poly[bis(*p*-toluenesulfonate)-2,4-hexadiyne-1,6-diol]}, pTDCU {poly[bis-(phenyl-urethane)-5,7-dodecadiyne-1,2-diol]},¹⁹ pDVDA1 {poly-[bis1,8-(*p*-methylphenyl)-octa-1,7-diene-3,5-diyne]},²⁰ 168pDA {poly{1-hexadecyl-6-(cadmiumoctanoate)-2,4-hexadiyne]},²¹ and pDCH {poly[bis1,6-(9carbazoyl)2,4-hexadiyne]}²²

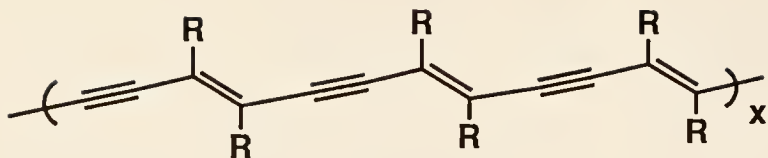


Figure 1-2. Polydiacetylene backbone with R, representing different substituents that can influence the backbone conformation. For instance in PTS, R = *p*-toluenesulfonate.

Polyaniline (PANI)²³ and polythiophenes (PT)²⁴ belong to a class of processible polymers made by oxidative chemical or electrochemical methods. They are well known for their electrical conducting properties. Different oxidation states of the emeraldine base forms of polyaniline have an effect on the NLO response. Doping results in the formation of more quinoidal structures. For polythiophenes, processibility has been improved with alkyl derivatization into poly(3-alkylthiophenes). Degenerate four wave mixing (DFWM) measurements showed sub-picosecond response time and spectral behavior, that could be explained by an inhomogeneously broadened absorption line.²⁵

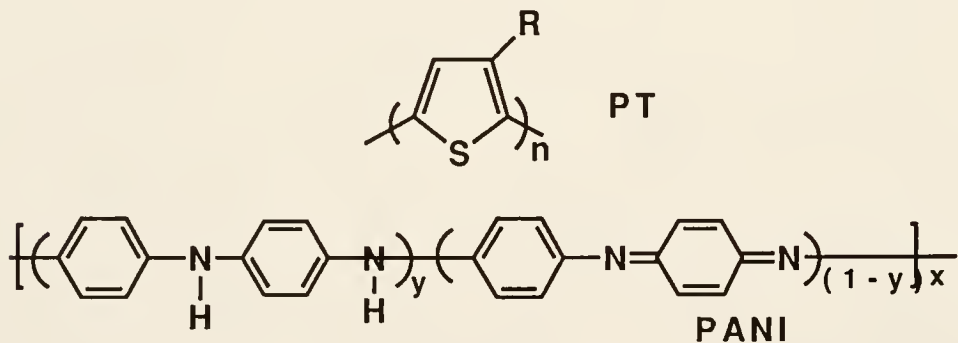


Figure 1-3. Polyaniline (PANI) and polythiophene (PT) polymers. R represents different alkyl chain lengths. Polyaniline is in the emeraldine base form.

Poly(*p*-phenylenevinylene), PPV, is well known from the precursor technique that has made it processible before the actual conjugated species is

produced.²⁶ High nonresonant values have been obtained from films of good optical and mechanical quality as prepared by film casting. This results from the interesting combination of phenyl and polyenic moieties e.g. poly(*p*-naphthalenevinylene) PNV.²⁷ Polyazomethines (PAM),²⁸ are isoelectronic and heteroatom containing analogues of poly(*p*-phenylenevinylene).

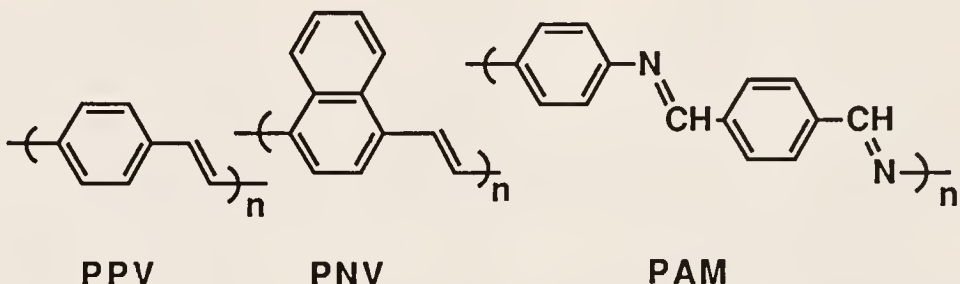


Figure 1-4. Chemical structures of Poly(phenylene) PPV, poly(naphthylene vinylene) PNV, poly(azomethine) PAM.

Poly(*p*-phenylene-benzobisthiazole) PBT,²⁹ polyquinolines,³⁰ and polyphenylene are rigid rod polymers processible in the melt form or by molecular composites with another polymer.

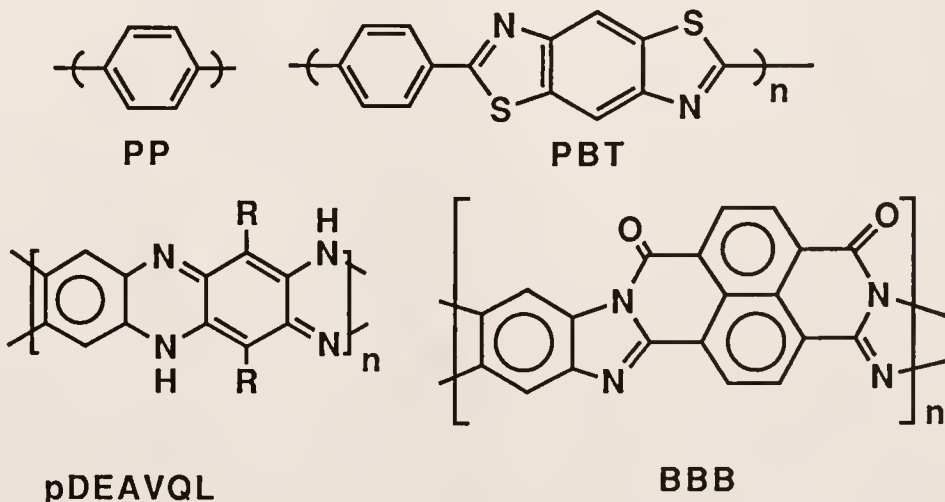


Figure 1-5. Chemical structures of Poly(phenylene) PP, Poly(benzothiazole) PBT, {poly[di(ethylaminovinyl) quinoxaline]} pDEAVQL, poly(benzimidazophenanthroline) BBB.

Polyacenes are the theoretical ladder type of polymers and many have been synthesized.³¹ Interesting routes to heteroaromatic ladder polymer structures make full use of the flexibility of organic synthesis. Examples of these heteroaromatic structures are pDPVQL {poly[di(piperidinovinyl)quinoxaline]}, pDEAVQL {poly[di(ethylamino-vinyl)quinoxaline]},³² and BBL or BBB poly(benzoimidazo-phenanthroline).³³

Poly(silane)s belong to a unique class of sigma conjugated polymers.³⁴ These are the only polymers among the group which do not contain the π -conjugated carbon backbone. The particular feature of polysilanes is the delocalization of sigma orbitals along the Si atom backbone. Examples are: pMPSi poly(methyl-phenylsilane),³⁵ pDHSi poly(di-n-hexylsilane),³⁶ and pDBPSi poly(di-*p*-butoxyphenylsilane).¹²

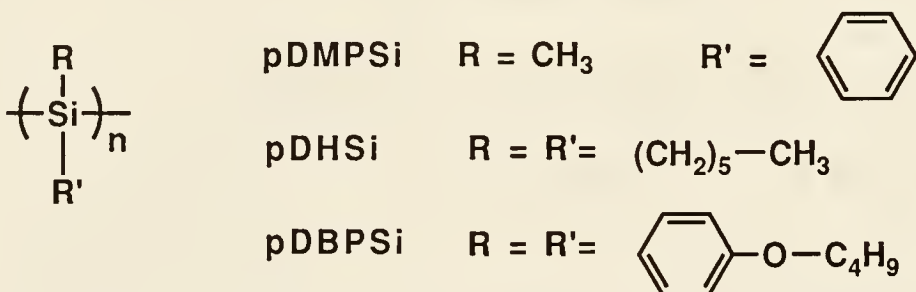


Figure 1-6. Chemical structures of pMPSi, poly(methyl-phenylsilane), pol(dihexylsilane) pDHSi, and poly(di-*p*-butoxyphenylsilane) pDBPSi.

Some $\chi^{(3)}$ properties for the above polymers and their measurement techniques are summarized in the Table 1-1.³⁷ From the table, it is seen that the highest third-order nonlinear optical values measured to date are with the polyacetylenes $(\text{CH})_x$.^{38,39}

Table 1-1. Conjugated polymers and their respective $\chi^{(3)}$ values as measured by THG or DFWM. In general non-resonant measurements are considered to be more important.

Polymer	Orientation	$\chi^{(3)}$ (esu) non-resonant	Technique and $\lambda(\mu\text{m})$	Ref.
Poly(diacetylenes)				
PTS		8.5×10^{-10}	THG 1.89	19
pTDCU		7×10^{-11}	THG 1.89	19
16-8pDA	LB	8×10^{-11}	THG 1.907	21
pVDA1	LC	10^{-11}	THG	20
pDCH		5×10^{-11}	THG 1.907	22
pDCH	epitax	2×10^{-10}	THG 1.907	22
Aromatic Polymers				
PPV		4×10^{-10}	DFWM 0.602	26
PNV		5×10^{-12}	DFWM	27
Hetero Aromatic Polymers				
PT	resonant	4.0×10^{-10}	DFWM 0.602	40
PANI	resonant	3.7×10^{-11}	THG 1.83	23
PAM		1.0×10^{-11}	THG 0.604	28
PBT		5.4×10^{-12}	DFWM 0.604	29
		1.4×10^{-11}	THG 1.907	29
Ladder Polymers				
pDEAVQL		3×10^{-10}	DFWM 0.532	32
pDPVQL		2.8×10^{-10}	DFWM 0.532	32
BBL		1.5×10^{-12}	DFWM 1.064	33
BBB		5.5×10^{-12}	DFWM 1.064	33
Polysilanes				
pDMPSi		1.5×10^{-12}	THG 1.064	35
		1.6×10^{-12}	THG 1.064	35
pDHSSi		1.1×10^{-11}	THG 1.064	12
pDHSSi	LB	4×10^{-12}	THG 1.064	12
Polyacetylenes				
(CH)x	Shirakawa	1.3×10^{-9}	THG 1.907	38
		0.7×10^{-9}	1.442	38
		1.1×10^{-9}	1.362	38
		0.1×10^{-9}	0.826	38
(CH)x	Durham	2.7×10^{-8}	THG 1.907	39
pPA		5×10^{-11}	DFWM	43
Reference: Quartz		3.8×10^{-14}	THG 1.907	41

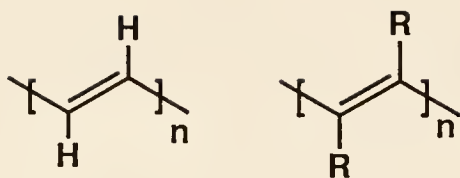


Figure 1-7. Polyacetylene and Substituted polyacetylene. R denotes various substituents. The backbone is in the *trans* configuration.

Polyacetylene has been widely studied for its electrical conducting properties.⁴² It is characterized by large π -electron delocalization along the backbone and as a consequence has a high molecular hyperpolarizability. However, the polymer is unstable to oxidation, insoluble, and difficult to process. Because of these reasons, much attention has been redirected to the substituted derivatives of polyacetylene.

Substituted polyacetylenes are characterized by lateral substituents including heteroatoms that confer new properties on the unsaturated backbone. A host of potential applications has been observed, other than materials for nonlinear optics^{43,44} They are usually soluble, amorphous, or semi-crystalline and are more stable to oxidation by air than, unsubstituted polyacetylene.⁴⁵ The effect of the side groups is to confer these new properties but at the same time they lower the conjugation efficiency. This lower conjugation efficiency can be associated with defects introduced in the polymer backbone during polymerization, e.g. saturated defects, conformational defects, etc.^{46,47}

The nonlinear optical properties of several *ortho*-substituted polyphenylacetylenes, pPA, have been studied by Wegner et al. using THG and DFWM techniques.⁴⁸ The bulkiness of the substituents was varied, which subsequently affected the conformation of the polymer giving rise to visible absorption properties.⁴⁹

Substituted Polyacetylenes

Compared to various vinyl polymers which are manufactured in large scale, ethynyl polymers are not. One of the reasons is the difficulty in synthesizing high polymers in good yields. Polymerization has often been attempted by using radical and ionic initiators in the past.^{50,51} In most cases, the products were linear oligomers in which the molecular weights were in the range of a few thousands. The formation of cyclotrimers was often observed. Thus it was rather difficult to synthesize polymers whose MWs' were higher than ten thousand. The polymers are also often composed of a mixture of configurations and conformations.

Acetylene selectively polymerizes in the presence of Ziegler catalysts, whose components have low Lewis acidity.⁴⁰ *Cis* polyacetylene forms at low temperature, and *trans* polyacetylene at high temperature.⁵² Likewise, Ziegler catalysts have been the most versatile catalysts for the polymerization of substituted acetylenes until the advent of Group 5 and 6 metal halide catalysts. Primary and sec-alkylacetylenes yield high MW polymers in the presence of Ziegler catalysts such as with a mixture of iron trisacetylacetone with triethylaluminum [Fe(acac)₃-EtAl(1:3)]. However, aromatic and heteroatom containing monosubstituted acetylenes produce mostly insoluble polymers and/or oligomers. Furthermore, no disubstituted acetylenes are known to polymerize with Ziegler catalysts.

The most widely studied monoacetylene to date has been the phenylacetylene, an analog of the vinyl monomer, styrene. The monomer produces only oligomers with number average molecular weight of a few thousand by use of conventional radical, cationic, or anionic initiators. Ziegler catalysts provide relatively higher molecular weight oligomers of

phenylacetylene, but a large fraction of the product is insoluble. In 1974, the first report on the polymerization of phenyl acetylenes using WCl_6 and MoCl_5 catalysts was published by Masuda and Higashimura.⁵³ Since then, various derivatives of this catalyst have been made and applied to a large number of monomers: mono- and disubstituted, hydrocarbon, and heteroatomic. The result of which is the large number of publications and reviews mainly by Masuda and Higashimura.⁵⁴

Group 5 and 6 catalysts can be classified according to their reactivities and monomer specificity. The first group of catalysts is, simply the respective metal chlorides, MoCl_5 and WCl_6 (Class I).⁵³ These catalysts are capable of polymerizing various monosubstituted acetylenes. In particular, they have been found to be excellent with phenylacetylenes. NbCl_5 and TaCl_5 have been known to produce cyclotrimerized products with phenylacetylene.⁵⁴ But with disubstituted acetylenes, they tend to give high MW products. The second type is equimolar mixtures of WCl_6 and MoCl_5 with an organometallic co-catalyst (Class II).¹⁸⁵ These catalysts polymerize not only monosubstituted but also disubstituted acetylenes. Ziegler catalysts can only polymerize *primary* or *secondary* monoalkylacetylenes. Class II catalysts can polymerize other structural isomers of a particular monoalkyne. Organometallics containing Group 4 and 5 main group metals are very effective as cocatalysts, e.g. tetraphenyltin (Ph_4Sn), triethylsilane (Et_3SiH), triphenylbismuth (Ph_3Bi). The third group of catalysts (Class III) is obtained by ultraviolet irradiation of a CCl_4 solution of metal hexacarbonyls [$\text{Mo}(\text{CO})_6\text{-CCl}_4\text{-}h\nu$, $\text{W}(\text{CO})_6\text{-CCl}_4\text{-}h\nu$].^{54,187} These catalysts polymerize various monosubstituted acetylenes and disubstituted acetylenes such as those in which one substituent is chlorine. This class is generally less active than the above two kinds of catalysts but

tends to provide polymers having higher MWs. Polymerization for this class proceeds only with UV irradiation and a halogen containing solvent.

Other Mo and W catalysts for polymerization that have been used are generally less reactive. The Fischer carbene and Casey's carbene have been found to give good yields.⁵⁴ Interestingly enough, Schrock's Lewis acid free molybdenum alkylidine catalyst has been found to polymerize monosubstituted acetylenes in good yield but not disubstituted acetylenes.⁵⁵ The reactions with this catalyst supports a reaction mechanism in which polymerization proceeds via the metal carbene.

The reaction mechanism involves an active specie: a complex having a metal-carbon double bond called a metal carbene which forms a ring structure. It has been shown many times that the metal carbenes mediate various reactions. Other than polymerization of acetylenes, W and Mo catalysts are also known to catalyze olefin metathesis. The scission of the C=C bond takes place with the result that an olefin having the substituents R and R' is converted to two olefins, one with only an R and the other R'. Another interesting case in particular, is with polymerizations involving ring opening metathesis polymerization (ROMP)⁵⁶ and acyclic diene metathesis (ADMET) polymerization.⁵⁷ In fact, a novel route to substituted polyacetylenes which does not use the monoacetylene monomer is the ROMP of cyclotetraene monomers. This has been the specialization of Grubbs' group at Caltech where they attach various substituents to the cyclooctatetraene monomer.⁵⁸ The use of open chain monomers to produce substituted polyacetylenes have been made by K. Wagener and D. Tao to give good yields and interesting chemistry.⁵⁵ All of these make use of the metal carbene intermediate as the active species.

The rationale for the metal carbene mechanism is as follows: First, there are many catalysts effective in olefin metathesis that are also effective with the polymerization of acetylenes. Second, acetylenes can be regarded as extreme members of cycloolefins, i.e. two membered rings in which the aliphatic chain of a cycloolefin is replaced with a carbon-carbon single bond.

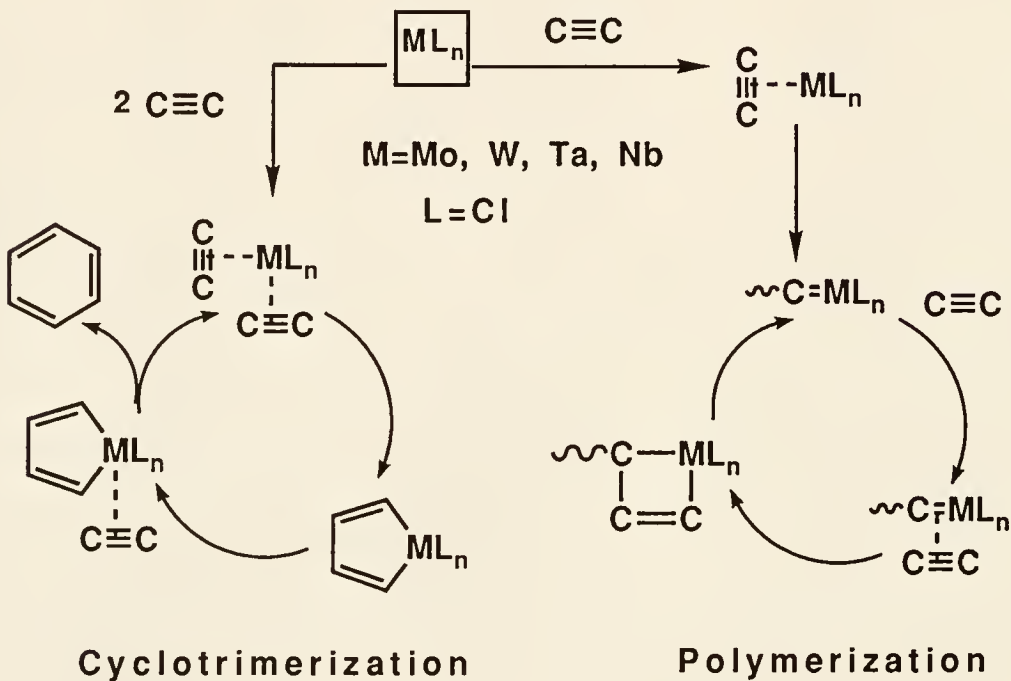


Figure 1-8. Mechanism of Polymerization and cyclotrimerization. The metal alkylidenes are the active species which forms a metallacyclobutene ring intermediate upon coordinating with the monomer.

Katz has demonstrated the validity of this mechanism using ^{13}C NMR and deuterated polymers.⁵⁹ In some cases, the metal carbene has been isolated. The conclusions are that the cleavage of two π bonds are involved with these catalysts whereas only one π bond is cleaved with Ziegler-Natta catalysts. These findings show that the polymerization of acetylenes by the W or Mo catalysts proceeds via the metal carbene mechanism, whereas that by the Ziegler catalyst involves a metal alkyl (insertion) mechanism.

Almost no information on the transfer and termination reactions in the polymerization of acetylenes by Group 5 and 6 transition metal catalysts has been obtained. This is important in that if an effective transfer agent can be found, polymers with controlled MW and well defined ends can be obtained.

The competing reaction between cyclotrimerization and polymerization is an interesting case in that suppression of cyclotrimerization leads to higher MWs. An important difference between the two is that for cyclotrimerization to occur, two acetylene monomers must coordinate simultaneously to the active species, while only one molecule must coordinate before polymerization should occur. Hence cyclotrimerization is prone to steric effects. An example is that 1-hexyne produces a mixture of cyclotrimer and polymer with Mo and W catalysts whereas *t*-butyl monoacetylene yields only high polymer.⁶⁰

The copolymerization ability using this catalyst is dependent on the coordinating ability of the monomers. In general, acetylenes are more reactive than olefins in a coordination reaction since the former have a stronger coordinating ability. For example, in the copolymerizaiton of phenylacetylene with styrene using $\text{WCl}_6\text{-Ph}_4\text{Sn}$ essentially only phenylacetylene polymerizes.⁶¹ With various acetylenes using W and Mo based catalysts, sterically less hindered acetylenes always show higher reactivity. This suggests that the propagation reaction consists of two stages, i.e. monomer coordination and reaction of the coordinated monomer with metal carbene, and that the relative reactivity of monomers in copolymerization is governed by the competitive coordination of the monomers.

As a result, the versatile Group 5 and 6 catalysts have been widely used for the polymerization of substituted polyacetylenes. With the view of using these materials for nonlinear optical properties, Wegner et al. have used several substituted phenylacetylenes using these catalysts to produce high MW

polymers with good absorption properties.²⁷ $\chi^{(3)}$ has been measured using spin cast films, and as outlined earlier, has a high value. Le Moigne et al. have extended this work to other derivatives, and sometimes with liquid crystalline properties.⁶² Their results have been oriented toward maximization of the conjugation length by controlling several aspects of the synthesis. Various derivatives are outlined as shown in Figure 1-9. Subsequently, their method of synthesis was used and studies were made in this dissertation on the film forming properties of these polymers.

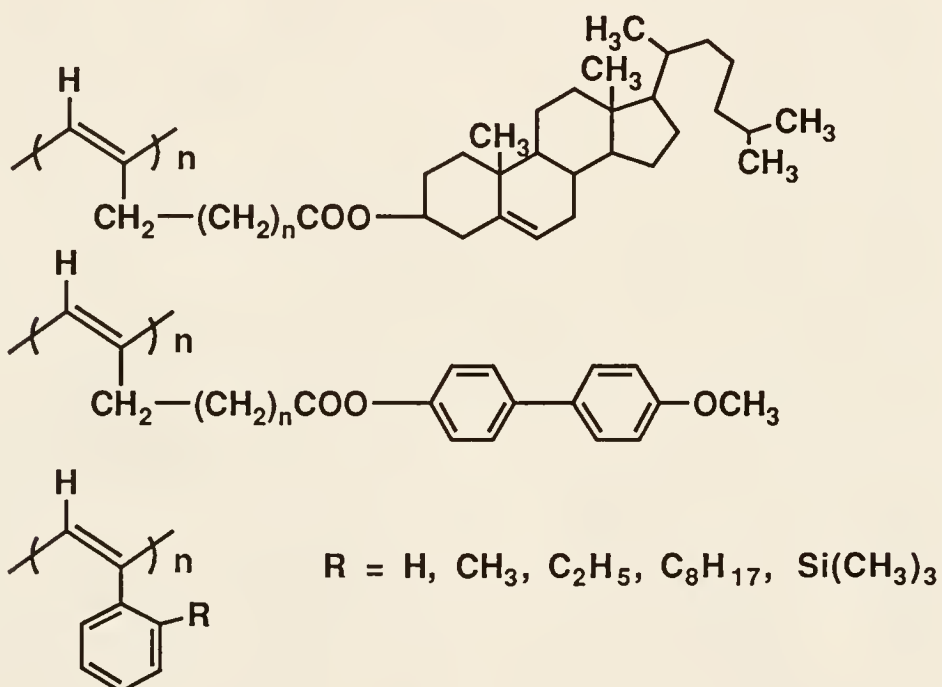


Figure 1-9. Cholesteryl and methoxybiphenyl esters of poly(ω -alkynoic esters) and *ortho* substituted poly(phenylacetylenes).

Cyclopolymerization of Unconjugated Diynes

Interestingly, Group 5 and 6 catalysts have also been found to be very effective with cyclopolymerization of unconjugated diynes to produce

substituted polyacetylenes. Cyclopolymerization is a mechanism which favors intramolecular cyclization first over intermolecular reaction in the propagation step of the polymer (alternating intra-intermolecular polymerization). Cyclopolymerization was extensively studied by G. B. Butler et al. of the University of Florida, who has been cited as the pioneer in cyclopolymerization.^{63,64} Most of the work done was on different types of α and ω dienes using a variety of initiators. Statistical and mechanistic arguments have been put forward to explain the occurrence of such polymerization. It has been found that the favorable formation of a six-membered ring together with the smaller decrease in activation entropy leads to a less energetic pathway.⁶⁵

In 1961, J.K. Stille reported the cyclopolymerization of 1,6-heptadiyne using Ziegler-Natta type catalysts to form polymers with cyclic recurring units in an alternating double and single bond backbone :⁶⁶

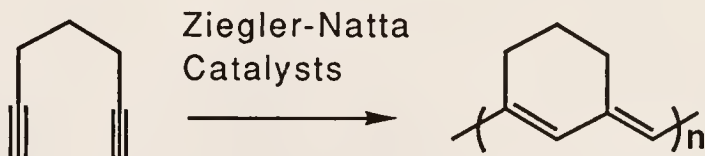


Figure 1-10. Cyclopolymerization of nonconjugated diynes by Ziegler-Natta catalysts.

Other structures were speculated as to the possible products formed with these reaction conditions.⁶⁷ In 1983, sparked by the interest to produce highly conducting polymers, H.W. Gibson et al. synthesized free-standing polymer films of 1,6-heptadiyne using homogeneous catalysts derived from $Ti(OC_4H_9-n)_4$ and $Al(C_2H_5)_3$.⁶⁸ A combination of spectroscopic, chemical techniques, and model compounds proved the structure as that initially reported by Stille. Other diynes such as 1,7-octadiyne and 1,8-nonadiyne gave predominantly

cross-linked products. Modest electrical conductivity values were obtained with these films, but they were not stable to oxidation by air for long periods of time.

Recently, a series of papers have come from S.K.Choi and coworkers on the cyclopolymerization of several diyne derivatives using the metathesis catalysts MoCl_5 and WCl_6 with several cocatalysts. Several derivatives are shown in Figure 1-11.^{69,70,71,72,73,74,75}

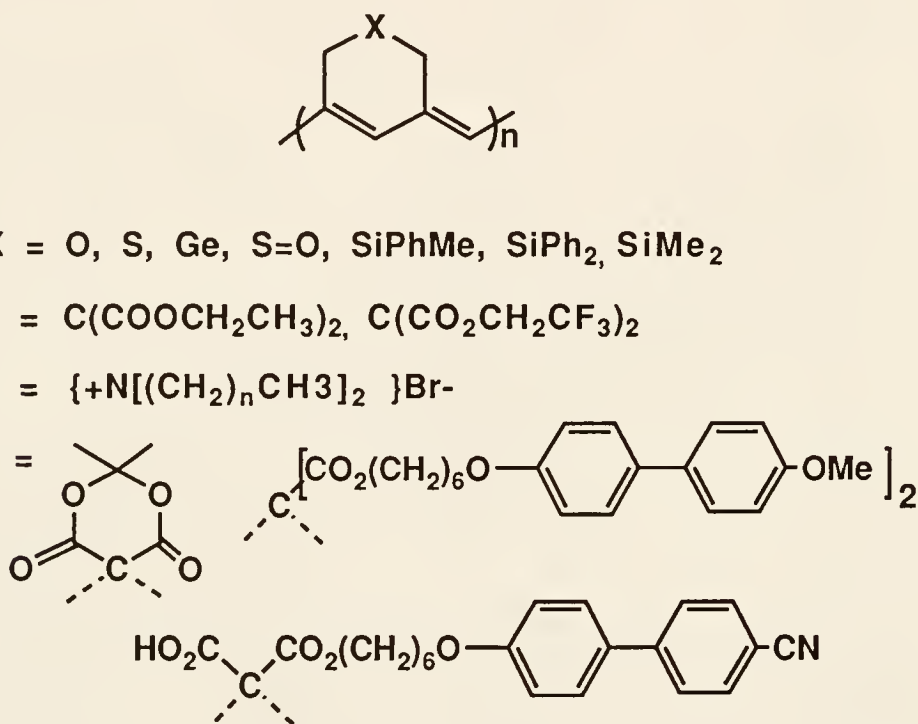


Figure 1-11. Cyclopolymerized nonconjugated diyne derivatives synthesized using Group 5 and 6 metal halide catalysts. X is represented by different groups.

The versatility of these type of polymerizations can be seen in the number of derivatives that have been polymerized since the methodology was introduced. Using standard Schlenck techniques under vacuum, high molecular weight polymers were obtained. These polymers are surprisingly stable for long periods of times, have high conjugation lengths, are soluble in

common polymer solvents (except for thioether and ether derivatives), and have high molecular weights of the order of 1×10^5 . The favorable formation of a six-membered ring allows cyclopolymerization. Propagation with this type of catalyst is generally thought to proceed via a metal carbene and metallacyclobutene intermediate similar to olefin metathesis as discussed earlier. Two types of monomer orientation have been proposed in which α -addition leads to the possibility of five-membered ring formation.⁷⁶

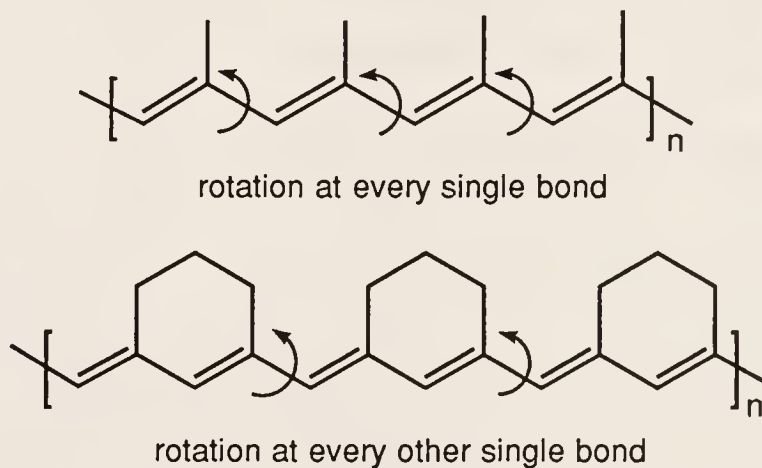


Figure 1-12. Statistical comparison of rotations in the main chain of substituted polyacetylenes for a regular polyenic and cyclopolymerized backbone.

Formation of these types of polymers is an important development toward control of conformation in substituted acetylenes. Alternating six-membered ring units gives a *trans* configuration that prevents isomerization to the *cis* form in the *endo* double bond and at the same time limits the conformational rotations possible for the chain resulting in *trans* polymers with higher conjugation efficiency (see Figure 1-12). Thus a more "controlled" backbone is observed, with longer conjugation lengths exhibited in the UV spectra.^{71,72}

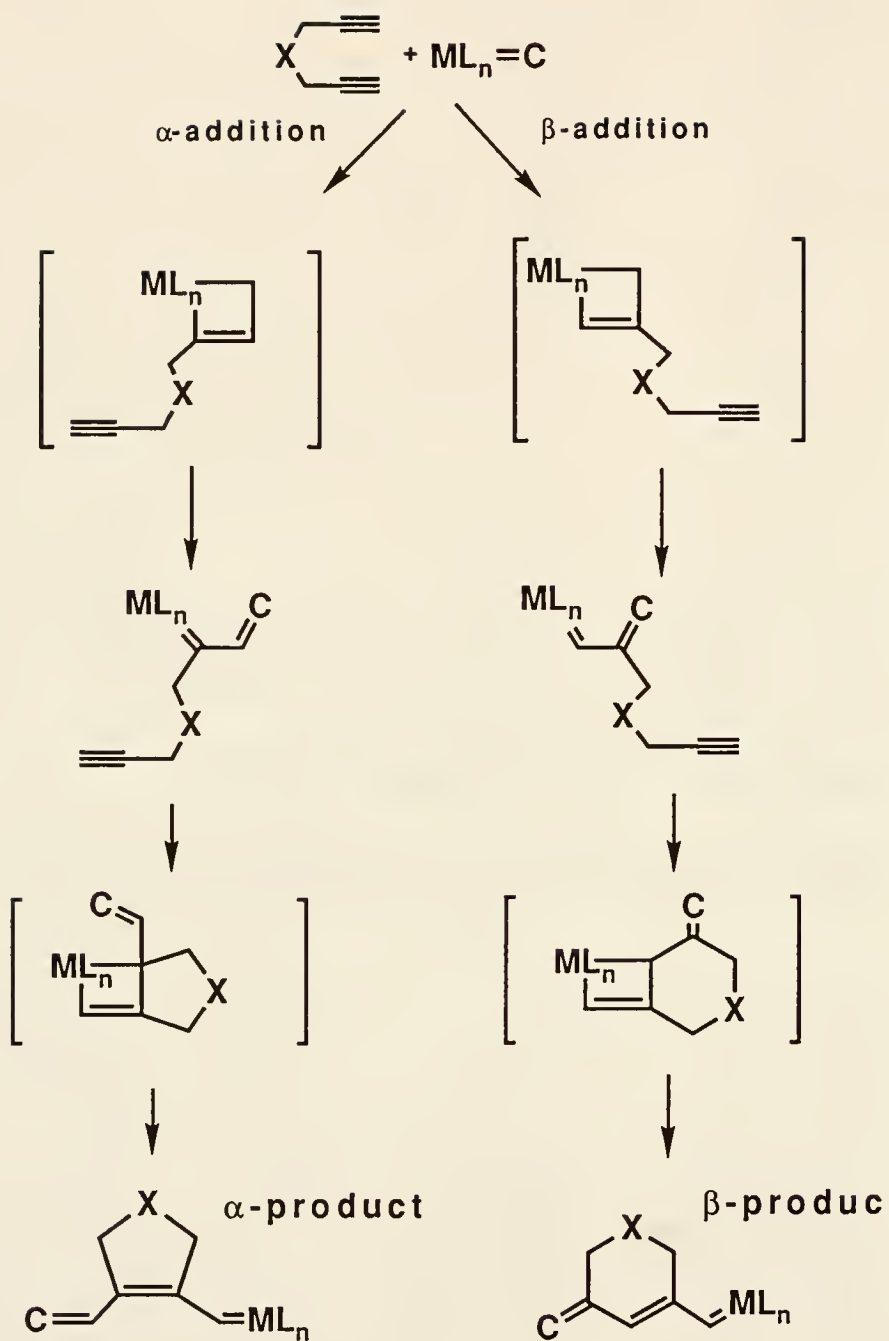


Figure 1-13. Mechanism of cyclopolymerization with Group 6 metal catalysts via the metallacyclobutene ring. α and β addition are possible with β -addition (six membered ring) commonly observed.

The Langmuir-Blodgett Technique

Thin films are required not only for application purposes but also to implement many fundamental optical measurements that are crucial in understanding the origin of nonlinearities in organics. Specially for conjugated polymers, with the absorption coefficients being very large (10^5 cm^{-1}), many optical measurements cannot be performed without thin films. For applications of course, molecular organization is required since the effective nonlinearity of a material is minimized unless the molecules are organized. Additionally, thin films are a prerequisite to applications in the guided wave geometry which is known to be the desired geometry in integrated optics. Because of all the above reasons, thin film organization of polymers has received extensive attention.

The Langmuir-Blodgett (LB) method is a technique for assembling ordered molecular multilayers from monolayers by vertical deposition on a substrate. Irving Langmuir, whose name is associated with the technique, did much to make the field into a fully developed science. However, many pioneers in the past, produced the significant advances that led to this development. Benjamin Franklin and Lord Rayleigh, are among the few famous men who contributed.^{77,78} Agnes Pockels and Katherine Blodgett were women beyond their time who pioneered the deposition methods that are now used routinely for LB film fabrication.^{79,80} Beginning in the late 1920s, significant work was published by Adam,⁸¹ Davies and Rideal,⁸² Crisp,⁸³ and Harkins,⁸⁴ together with Langmuir performed research which quantified the science and its physical and thermodynamic aspects . Gaines' book "Insoluble Monolayers at the Gas-liquid Interface" first published in 1967, has been the standard text for researchers for many years.⁸⁵ He is credited with extending Gibbs'

thermodynamic treatment to monolayers at surfaces. A period of renewed interest in Langmuir Blodgett films followed in the 1960s with the possible applications towards electronics miniaturization. Hans Kuhn, who is now being honored by associating the LB film technique as the Langmuir-Blodgett-Kuhn (LBK) technique, did much to apply the technique into novel and exciting application of thin films.⁸⁶ Langmuir-Blodgett research today is an interdisciplinary science with many prospects for device applications. Excellent overviews of this horizon were given by Roberts⁸⁷ and Ulman.⁸⁸ Major contributions in the literature have also been given by: Ringsdorf⁸⁹, Möbius⁹⁰, Mohwald⁹¹, Wegner⁹², and Lando⁹³ just to name a few, who have contributed to the growth in knowledge and technology of LB films.

The Monolayer Phenomena

The technique starts with an understanding of the delicate balance at the interface which is responsible for monolayer forming properties. From the three phases of matter; solid, liquid, gas, five groups of interfaces can be classified. The interface can be treated as a mathematical plane, in which adsorption of a third substance gives rise to a *surface excess concentration* that give it a definite thickness. The Langmuir-Blodgett Monolayer technique makes use of the air-water (gas-liquid) interface. Commonly, an *amphiphile* is a molecule that has two properties in a single molecule. Translated to the air-water interface, these are molecules that have both a hydrophobic and a hydrophilic group. A delicate balance of the hydrophilic group associating with water and the hydrophobic group pulling away from the subphase, produces the spreading properties of the amphiphile. This spreading force is often quantified by measuring the surface tension γ . Thermodynamically, it is defined as a

derivative of Gibbs free energy (G) with respect to the surface area (s) at a constant temperature (T), volume (V) and moles (n). It is given by the equation

$$\gamma = (\delta G / \delta s)_{T,V,n} \quad (1.7)$$

The various interfaces in an amphiphile contain specific surface energies defined by the surface tensions. The balance between these forces and the tendency toward minimization of the free energy, determine the spreading properties of a material.

A more common experimentally determined parameter is the surface pressure Π which is defined as follows:

$$\Pi = \gamma_0 - \gamma \quad (1.8)$$

The plot of Π versus mean molecular area (Mma) or simply Area, measured at constant temperature is referred to as the surface pressure-area isotherm. Such experiments are considered as two dimensional analogues of bulk/pressure volume isotherms with analogous treatment of phase transitions and compressibility less one dimension.⁹⁴

Langmuir-Blodgett Apparatus

The amphiphile is usually spread at the interface using a volatile solution to form a monolayer. A shallow trough, commonly made of teflon, holds a certain area of water. The purity of the water used is of utmost importance, not to mention the purity of the amphiphile. Movable barriers are responsible for controlling the area of the trough. The barrier is either of hydrophobic or hydrophilic materials, each having certain advantages and disadvantages. This two dimensional compression is responsible for pressure induced changes and

orientation of amphiphiles at the interface. The surface pressure changes are measured by a sensitive surface balance. Two types are available: either the Langmuir or the Wilhelmy plate balance. One is more effective than the other, depending on the viscosity of the amphiphile monolayer. The Wilhelmy plate method is the most common, which employs a rectangular plate dipping into the interface. The plate must have zero contact angle with one of the phases. Changes in the interfacial tension are measured by the vertical pull of the plate. The Langmuir Balance makes use of a floating barrier which measures the force directly exerted by the film, in relation to a clean surface. The result is the surface pressure-area isotherm, which is the standard measurement for describing monolayer behavior.

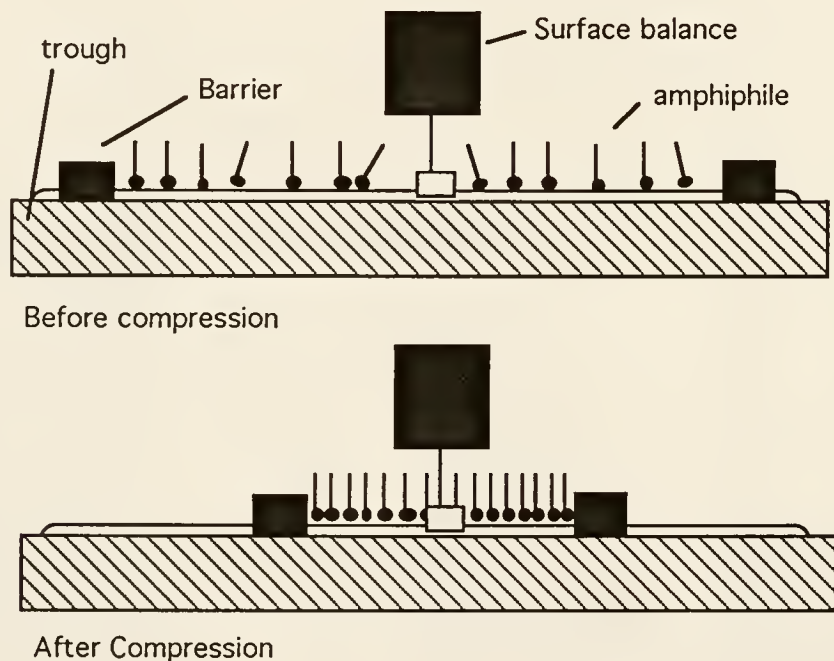


Figure 1-14. Schematic diagram of a monolayer compression of amphiphilic molecules spread at the air-water interface.

Several designs have been used by most researchers. Before the advent of commercially available apparatus, most of the troughs were "home

made". A circular design, called the Fromherz trough, and the constantly moving wall trough are variations to the common rectangular troughs with movable barriers.^{95,96} A commercial trough produced by KSV Instruments (Helsinki, Finland) is currently the most popular because of its modular design. The film balance used is based on the Verger-de Haas trough principle.⁹⁷ Different measuring devices can be attached to the mainframe and are all controlled by a software program that allows calibration and control of the parameters for measurement.

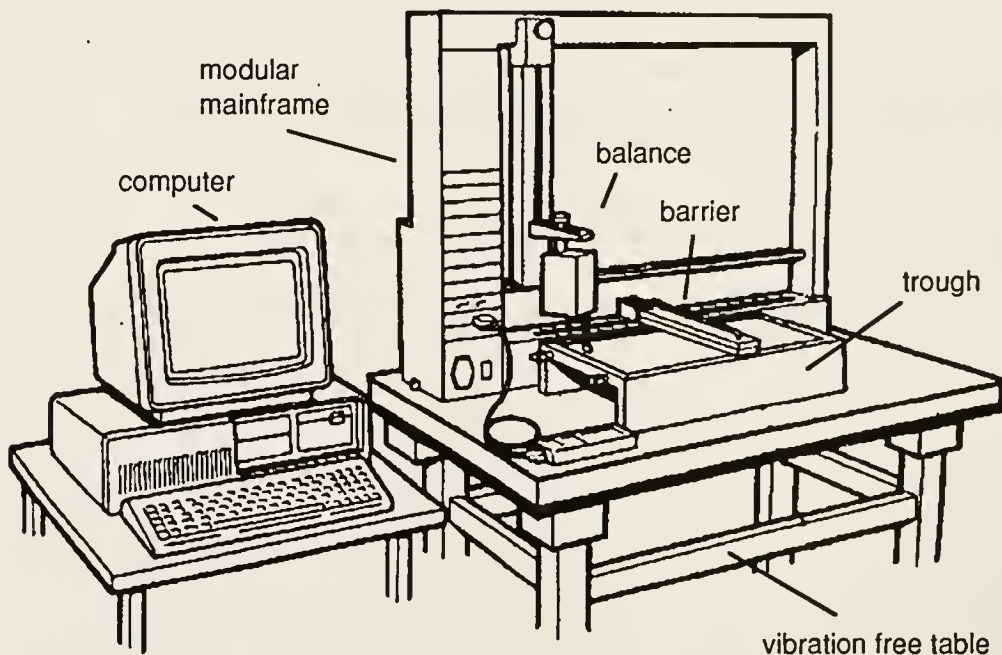


Figure 1-15. KSV 5000[®] LB Langmuir-Blodgett System with an IBM computer interface. The modular frame allows attachment of other surface analytical instruments such as a surface potentiometer.

In addition to the surface pressure-area isotherms, various surface analytical techniques have been utilized for investigations at the air-water interface. They range from surface potential measurements to delicate X-ray

synchrotron measurements. The following techniques have been important in particular for our investigations: surface potential, *in situ* UV-vis spectroscopy, Brewster angle microscopy, and relative reflectivity. A detailed treatment of these various surface analytical techniques will be given at the chapter on methodology (Chapter 2).

LB Vertical Deposition Technique

One result of being able to control monolayers is to deposit them into multilayer films by dipping. Two types are possible, the horizontal and the vertical technique. The horizontal method, developed both by Langmuir and Schaefer in 1938 is involves transferring the monolayer film to a horizontally positioned plate and then lifting the film off the subphase.⁹⁸ This technique is especially important for transferring very viscous films.

Vertical transfer, commonly called the Langmuir-Blodgett technique, was developed mainly by Katherine Blodgett. Various solid substrates are used and are generally of hydrophilic or hydrophobic surface. The most common treatment for hydrophobization being the use of alkylchlorosilanes. Transfer is usually achieved when the monolayer has greater attraction for the surface of the substrate than it has to the subphase. By compressing the monolayer at a specific surface pressure, the monolayers can be deposited at certain orientations. During transfer, the pressure is maintained constant by barrier movement, that is why isobaric stability is an important prerequisite for film deposition. Deposition data are collected in the form of the *transfer ratio*. The value is defined as the change in area of the monolayer at the water surface calculated by the barrier movement divided by the area of substrate that actually passes through the monolayer at the surface. Any area change at the film

surface is assumed to result from monolayer transfer onto the surface of the substrate. Complete transfer should yield a ratio of 1.0.

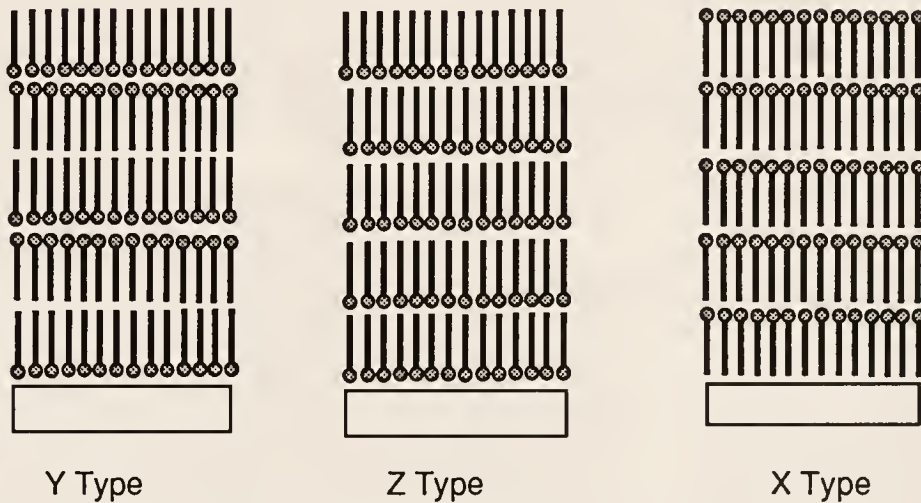


Figure 1-16. Different alternations and deposition modes in LB films.

Different deposition modes are expected because of the two way movement of the substrate in vertical dipping. They are classified as X, Y, Z deposition. Y-type being the most common, deposits layers in both the downstroke and upstroke whereas Z type deposits in the upstroke and X type on the downstroke.

The use of the alternate trough has allowed the formation of more intricate structures and even control of the deposition behavior of films. The design involves a two compartment trough with a common subphase area. A roller mechanism has been developed to deposit alternately, the disadvantage being the absence of a third compartment by which the substrate can pass before depositing the other film.⁹⁹ This has been solved with the addition of a third compartment incorporated in the KSV LB5000 Alternate Trough.

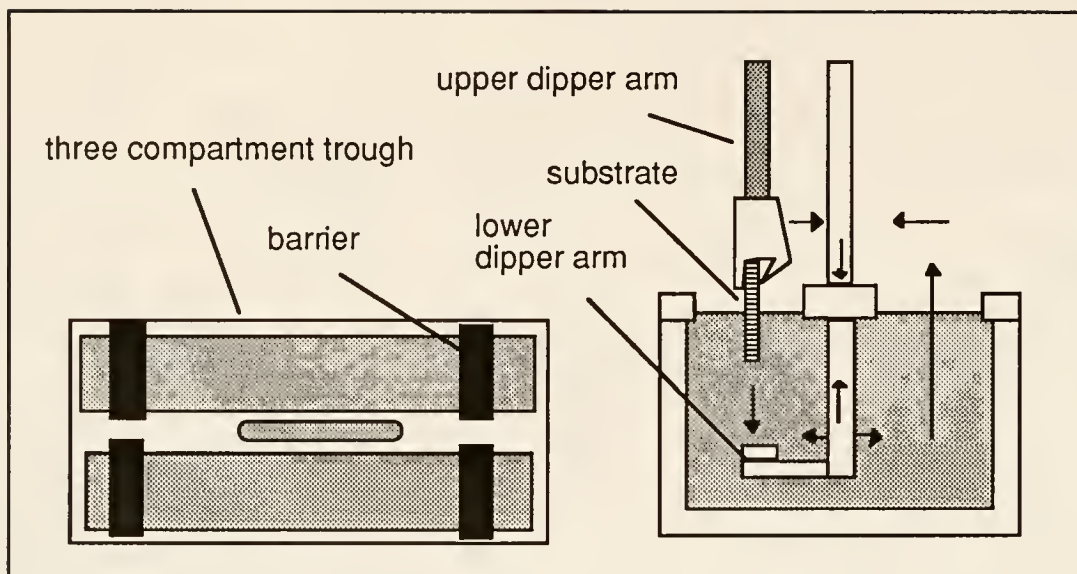


Figure 1-17. Schematic diagram of a three compartment trough (KSV Instruments) used for alternate deposition of layers. An upper arm and lower arm are utilized to cycle the substrate through the troughs.

Polymers at the Air-Water Interface

Polymers at dissimilar interfaces or polymer interfaces are a growing research area with numerous scientific, medical, and technological applications. Adhesives, peptide synthesis, synthetic membranes, flocculation, bio-materials, nonlinear, and opto-electronic materials, are some of the direct applications that are benefited by such research. The majority of research in the field of Langmuir Blodgett monolayers and multilayers however, has been on low molecular weight amphiphiles. As the inherent thermal and mechanical instability of LB films from low molecular weight amphiphiles has become a handicap for applications, current research is now being focused to films of organic polymers.¹⁰⁰ The two dominant approaches in this direction are to polymerize ordered monomers into their film structures or to spread preformed polymers.

Agnes Pockels was the first to spread polymeric films on water surfaces. In the 1890s she described measurements on films, "colophony" and "mastic," being just some of the substances that she investigated using a home made trough.¹⁰¹ In 1903, Devaux reported the spreading of the protein albumin.¹⁰² These initial observations predated then the concept of both polymers and monolayers. The first documentation of synthetic polymeric monolayers was made by Katz and Samwel in 1928, for poly(vinyl acetate) and poly(methylmethacrylate).¹⁰³ Polymers of hydroxydecanoic acid by a condensation-step process were studied by Harkins, Carman, and Ries in 1935.¹⁰⁴ An excellent review was published in 1946 by Crisp, who established a criteria for the interpretation of surface pressure and potential-area isotherm measurements.¹⁰⁵ He also attempted to categorize the monolayers based on viscosity and isothermal reversibility. Since then, a variety of synthetic polymers have been studied at the interface over the years such as : poly(vinylacetate), poly(acrylates) and poly(methacrylates), poly(vinyl fluoride), poly(vinylidene fluoride), and poly(dimethylsiloxane) have been investigated.^{106,107,108,109,110,111} Their behavior has been characterized on the basis of surface-pressure and surface potential area isotherms. These systems are able to form stable monolayer films on pure water, however, transfer to solid substrates often results in inhomogeneous films containing numerous defects.

Two classifications can be made based on the character of the π -A curves: *expanded* and *condensed* types. Expanded films are more compressible and exhibit a reversible collapse. Fowkes¹¹² offered a molecular interpretation distinguishing the two, suggesting that in expanded films, the polymer segments are miscible with water molecules in the surface layer, while in the condensed films the polymer chains are in contact and water is

substantially excluded. Measurements during compression and expansion cycles suggests categorization of spread polymer films according to their hysteresis behavior. Gaines used the terms; *reversible*, *reversible collapse*, *irreversible collapse*, and *rearrangements* to characterize surface pressure decay and curve compatibilities.¹¹³ A *reversible* behavior is one in which the cycle can be stopped with no decay in surface pressure, and the expansion curve reproduce the initial compression. In cases of *reversible collapse*, the collapsed film respreads when the available area is increased, and below the collapse pressure, the compression and expansion curves are again identical. In cases of *irreversible collapse*, once the film has collapsed, the material does not respread, although subsequent compressions-expansions limited to surface pressures below collapse are reversible. Lastly, *rearrangement* behavior is observed where the initial compression curve, bears little relation to subsequent compression and expansions.

Proteins are copolymers with a non-regular sequence of amino acids and are of uniform molecular weight. Interfacial properties are sensitive to the degree of polymerization (higher molecular weight materials generally become insoluble in water), which gives proteins an advantage in this respect. The Π -A curves of proteins tend to be similar and are typified by that of *bovine serum albumin*.¹¹⁴ For proteins, the approach to segmental equilibrium after compression or expansion of the monolayer is often sufficiently slow to be followed experimentally. The comparative slowness reflects the *high surface viscosity* in protein films, evidently arising from the need to break interchain H-bonds for flow to occur. The great stability of protein monolayers despite high solubility in the subphase, can be rationalized on the basis of this large value for the free energy of adsorption. However, as a protein monolayer is compressed to high pressures and increasing numbers of segments are

expelled from the interface, the free energy difference between the molecule in its adsorbed and solution states is progressively reduced. The probability of desorption which is negligible at $\pi=0$, attains values where its rate can be detected by the permanent decrease of area of the monolayer. It is also possible to calculate the free energy of adsorption from the Π -A curve of the protein.¹²⁰ A consequence of the effect of molecular size in desorption is that, in systems containing a mixture of proteins, the higher molecular weight proteins will tend to displace the smaller size proteins from the interface, other things being equal. Experimental evidence points very strongly to the α -helix or some closely related conformation being present at the air-water interface.¹¹⁵ The conformation of the polymer backbone is fully defined and its symmetry is such that it has no significant net dipole moment perpendicular to its axis. Furthermore, its rodlike nature imposes a high degree of order in the monolayer.

One way to improve the spreadability and orientation of these polymers is to polymerize well known amphiphilic monomeric units. As mentioned earlier, the first approach involved linking together monomer monolayers by polymerization at the air-water interface. The most popular of these are the poly(diacetylenes), polymerized either at the interface or after subsequent LB multilayers have been formed.^{17,92} Due to shrinkage and movement during polymerization, some structural problems arise in the films. Alkyl derivatives of Polyanilines have been successfully synthesized and characterized at the interface by Duran and co-workers.¹¹⁶ Usually, the polymerization reactions induce structural reorganizations which can induce defects in the multilayers, e.g. shrinkage. These problems can be minimized by appropriate molecular design. However, the control of the degree of polymerization, and the removal of unreacted monomers and side-products is not possible using this approach.

Polymerization research at the air-water interface continues as well as that of LB films. The spreading of preformed polymers still offers the most expedient way of producing well characterized polymer monolayers and multilayers free from structural defects.

The presence of defects in polymerized ordered monomers thus favors preformed polymers. To improve their ordering, the trend has been to make them more amphiphilic or orientable. One approach to this is to synthesize amphiphilic orientable functionalities and incorporate them either as side groups or at the mainchain of the polymer. Polymers studied usually fall into one of these categories:

- (1) Amphiphilic polymers, such as polymers of fatty acids, Poly(octadecylmethacrylate), poly(maleic-anhydride), poly(vinyl stearate), poly(octadecylacrylate);
- (2) Liquid crystalline polymers, the most common of which is the side chain liquid crystalline polymer (SCLP). The mesogenic part is attached to main chain via a flexible spacer;
- (3) Rod-like polymers, such as poly(silanes), poly(alkylglutamates), which have a rigid polymeric backbone with a flexible hydrophilic or hydrophobic backbone. The polymers of interest to this research are of the latter type.

Recently, Wegner et al. have studied a type of this polymer for NLO studies.^{12,100} Utilizing a rigid polysilane backbone, monolayers were deposited with high anisotropy of the polymeric chains. Well-ordered multilayers are formed with the long alkyl chains acting as bond solvents, fluidizing the monolayer.

Theory of Polymer Behavior at the Interface

Polymers show the same general types of behavior as small molecules. The compressibility of condensed films varies markedly with temperature and can be extremely low at the theta temperature (temperature in which there is ideal mixing between solvent and polymers). Mixed monolayers of compatible polymers can be formed as well as mixed monolayers of polymers and simple molecules.¹¹⁷ It is important to have a main polymer chain with hydrophilic groups regularly distributed at short intervals along it. Long sections without such groups, tend to form ill-defined loops clear of the water surface as described earlier. In general, there is much greater toleration of structural variation than with monomer systems. Not only completely nonpolar polymers [poly(ethylene), poly(propylene)] but also some very polar monomer units [nylon, Poly(acrylonitrile)] could not spread at the air-water interface. This would result in the formation of biphasic regions or microdomains similar to defects in the bulk.¹¹⁸ Presumably, the attractive forces between the chain segments are much larger than the hydration forces, and hence the spread state is less stable than a three-dimensional polymer aggregate.

In order to understand the behavior of polymers at the interface, it is necessary to define the free energy (ΔG_{total}) of the polymer at the interface. It appears that the surface free energy in this case is not an intrinsic characteristic, but corresponds to a notion of a "potential surface free energy depending on the environment."¹¹⁹ The conformation taken-up by a long chain flexible polymer molecule adsorbed at an interface illustrates the competing tendencies of energy minimization and entropy maximization via the well known Gibbs' free energy equation:

$$\Delta G = \Delta H - T\Delta S \quad (1.11)$$

ΔG is a summation of the individual free energy changes associated with the various segments or structural groupings of the polymer ($\Delta G_{\text{total}} = \sum_i \Delta G_i$). The behavior of a polymer molecule may be described in terms of a series of discrete segments, each segment containing on the average a certain number of monomer units. Three possible situations can occur depending on the enthalpy of the system as outlined by MacRitchie:¹²⁰

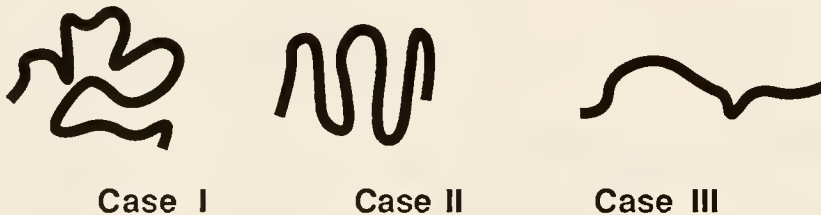


Figure 1-18. Various conformations of the polymer depending on the enthalpic behavior and its effect towards free energy minimization.

Case I *No absorption or emission of heat when the polymer molecule is introduced to the interface (i.e. $\Delta H = 0$)*. The enthalpy of interaction between polymer and subphase is equal to the polymer-polymer interaction. Molecular configuration is determined exclusively by entropy. The molecule will therefore adopt the conformation of greatest disorder, that of a *perfectly random coil* at the interface.

Case II *There is an absorption of heat when the polymer molecule is spread at the interface ($\Delta H=\text{positive}$)*. The molecules acquire energy from the environment and go to a higher potential energy state. The energy of interaction between polymer and subphase is higher than the sum of the polymer-polymer and subphase molecule interactions. To reduce this unfavorable enthalpy change, the polymer molecule “folds-

"up" to minimize its interactions with subphase molecules. This signifies an increase in order of the system, resisted by the universal drive to increase the disorder or entropy. The conformation taken up by the polymer molecule is one that, although not completely folded-up, is *more folded than a random coil*.

Case III *There is an emission of heat when the polymer molecule enters the interface (ΔH =negative).* Polymer-subphase molecule energy of interaction is less than the sum of the polymer-polymer and subphase-subphase molecule energies of interaction. ΔH is negative and polymer and subphase molecules decrease their potential energy when they approach each other. The polymer molecule will stretch out to increase interactions of its segments with subphase molecules. The conformation will be one that is *more stretched out than the random coil*. For a very large ΔH (magnitude), polymer molecules adopt a rigid rod configuration.

Temperature influences the entropic term of the free-energy since the entropy is multiplied by the temperature. As the temperature increases, the ordering caused by the enthalpy changes assume less significance and the disrupting effects of the thermal motion become more dominant.

Comparison with small molecules

Usually, monomers of most polymers do not have large non-polar and strong hydrophilic groups like typical small molecules possessing a long hydrocarbon chain and one or more strong polar groups. However, because a given polymer chain contains a large number of repeating monomeric units, its total free energy of adsorption ($n\Delta G_{\text{monomer}}$) per polymer chain (n = degree of

polymerization) can be very high even if $\Delta G_{\text{monomer}}$, the free energy per monomer unit is relatively small.¹²⁰ In addition, linear polymers are assumed to have a conformation in which the main chain backbone lies along the interface in contrast to the long axes of small molecules, which are normally assumed to be orthogonal to the surface. In reality, the possibility of chain entanglements in polymers are dominated by their spreading behavior.¹²¹ The polar segments predominantly interact with the aqueous phase and the non-polar ones with the non-aqueous phase, consistent with steric requirements. In this conformation, the chains have a certain flexibility that leads to an effect that is unique for polymer monolayers. As the monolayer is compressed, segments of the molecular chain, each consisting of a number of monomer units are *pushed out* of the interface into the adjacent bulk phases (see Figure 1-19).

Polymer relaxation and equilibrium at the interface

For each value of Π , there is an equilibrium between segments in the interface and in the adjacent phases. This depends on: (1) the interfacial pressure, (2) the nature and flexibility of the polymer, and (3) the compression of the subphase and the temperature.^{120,105,85} As the monolayer is compressed, the equilibrium shifts in favor of the displaced segments. As a result, the Π -A curves of polymers tend to show relatively high compressibility. The Π -A curves of polymers are relatively featureless. At low areas, Π -A curves of a sigmoid form are given by many polymers. The high compressibility in the low pressure regions arises largely from entropic effects associated with the large number of arrangements (configuration and conformation) formed by the mixing of flexible polymer segments and solvent molecules.¹¹³

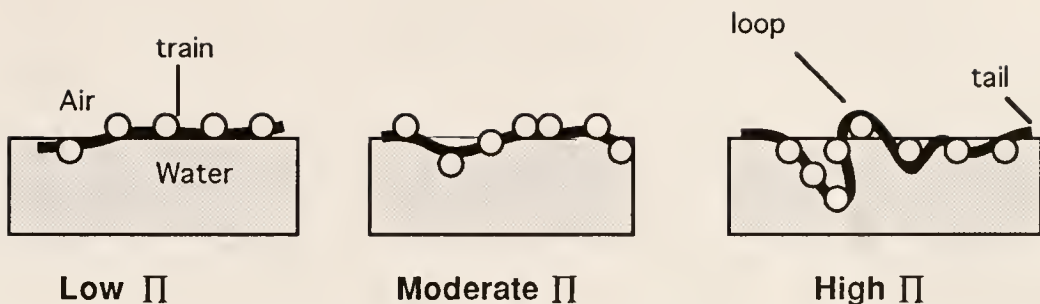


Figure 1-19. The Loop and Train model for polymer conformation depending on the surface pressure at various stages of compression at the air-water interface.

A statistical thermodynamic treatment of this effect for a completely unfolded monolayer was developed by Singer:¹²²

$$\Pi = (kT/A_o)\ln(1-A_o/A) + (kT/A_o)(t-1/t)(z/2)\ln((1-2A_o)/zA) \quad (1.12)$$

This equation, is based on the lattice theories of Huggins and Flory where t is the total number of segments per molecule, k is the equilibrium constant for segment-subphase interaction, A is the area available per segment, A_o is the limiting area available per segment, and z is the surface coordination number in the 2-D quasi lattice in the interface. For a completely rigid chain $z = 2$, and for a completely random chain $z = 4$. For very dilute polymer monolayers, the equation has been found to give good agreement with experimental results. Other contributions to equations of state for polymer monolayers take into account surface activity coefficients, partial solution of polymer chains in the subphase, intermolecular cohesion, and intermolecular repulsion.¹²³ At moderate interfacial pressures, polymer chains become close packed and the monolayer exhibits its lowest compressibility in this region. At higher pressures, the compressibility increases markedly again as segments of molecules are forced out of the interface (loops and tails), decreasing the proportion of attached segments (trains). The contributions of the loops and tails to the surface pressure is negligible compared to that of the trains.

Polymer structure and properties in general are time dependent.¹²⁴ Because of their relatively large size and high molecular weight, they rarely achieve true equilibrium, e.g. physical aging can take years. However, at aqueous interfaces, this equilibrium is sometimes observable within the time frame of experiment. The polarity of the aqueous phase provides a high interfacial energy driving force for orientation of polar phases, blocks, segments of the polymer towards the aqueous phase. In vacuum, air, or other non polar surfaces, the polymer chain orients its non-polar components towards the interface minimizing the interfacial energy. *Polymer relaxation* has been defined as a time dependent return to equilibrium of the system which has recently experienced a change in the constraints acting upon it. Each polymer chain has a particular motion frequency which is dependent on temperature and inertia of the participating segments. These chain motions are also usually dependent on the presence of a “free volume” between polymer chains.¹²⁵ Because the free volume in the polymers increases with temperature, *the relaxation times decrease, in general, with increasing temperature.*

Polymers and water

Polymer surface restructuring effects in response to a surrounding liquid phase are probably more pronounced in aqueous systems due to the unique hydrogen bonding and acid base characteristics of water. Studies suggest that the restructuring of a polymer in the presence of water corresponds to two stages:¹²⁶ After a first step of macromolecular chain movement, necessary in order that the hydrophilic part can appear in the surface, there is a second step of orientation of the polar groups at the interface which is accompanied by a rapid increase of the polar component of the surface free energy. There is an asymmetry of the force field at the interface. In contact with air, for instance, the

polymer chain segments orient in order to expose the hydrophobic group towards the gaseous phase and to bury the polar group inside the polymer. So the *surface appears hydrophobic*, in spite of the hydrophilic sites present in the matrix. In contact with water, we see the inverse: polymer segments reorient to adapt a conformation achieving minimal interfacial tension by exposing the hydrophilic parts. The ability to respond to changes depends on the mobility of the surface groups and segments. This is related to, but not the same as, the mobility of polymeric chains in the bulk

Interactions of polymers at the interface

Intermolecular forces of polymers at interfaces can be reduced into two phenomena: London dispersion forces and electron donor-acceptor (acid-base) interactions. H-Bonding is included in the latter, and dipole phenomena are usually negligibly small. Polymers that exhibit polar character can often be divided into acidic or basic, e.g. poly(methylmethacrylate) basic, post-chlorinated poly(vinylchloride) acidic. The liquid phase in this case is important in "controlling" the nature of interaction, e.g. a solvent that is more acidic than a third component (solid) is preferentially bound to a basic polymer.¹²⁷ Molecular weight studies have also been done to determine the effect of chain length on these type of interactions.¹²⁸

Langmuir-Blodgett Films and Materials for Nonlinear optics

The requirements of organic materials for nonlinear optics dictate that high anisotropies and thin film structures are important for maximizing their properties. In this respect, the LB technique has been widely employed as a means of fabricating interesting structures. Early work has focused mostly on

small molecule amphiphiles with applications as materials exhibiting second order effects. The requirements, being a non-centrosymmetric structure, are largely fulfilled by the orientation of the amphiphiles at the interface and at the same time the deposition of various configurations preventing centrosymmetry to the whole multilayer. Since the inherent instability of these small molecule systems has been discussed previously, the trend now is the use of polymers. The design of spread polymers incorporates these active materials as side chain groups appended to an inactive mainchain. Rare still is to find LB films of polymers with applications for third order effects. Most of the polymers studied in the past have applications for electrical conductivity. To the author's knowledge, no one has examined monolayer and multilayer LB thin films of substituted polyacetylenes. Although these polymers are prime candidates for such materials, usually the method employed for film preparation has been film casting²⁷ or epitaxial vacuum deposition.²²

Summary and Overview of the Dissertation

The principal area of interest is the air-water interface and its influence in ordering. The principal polymers of interest are substituted polyacetylenes. The structural requirements of the monomer and polymers, characterization, behavior at the interface, and orientation are presented. Indirectly, the results of these studies should be useful towards improving the properties of polymers with nonlinear optical properties. The use of the Langmuir-Blodgett technique is critical as outlined earlier for device requirements and fundamental studies of such materials. The study of these polymers comprises both the synthetic aspect in which the configurational and conformational behavior is studied. The major part of this dissertation though, is in addressing the Langmuir monolayer

film behavior of substituted polyacetylenes as a class of polymers. Once stable and well characterized films of these polymers are formed, they may be transferred to solid substrates in order to form highly ordered films with defined thickness. It is expected that this approach will differ substantially from bulk or cast films, in the degree of ordering, control, and applicability. This should result in various new physical properties of polymeric thin films.

The approach to highly ordered substituted polyacetylenes can be divided into two pathways:

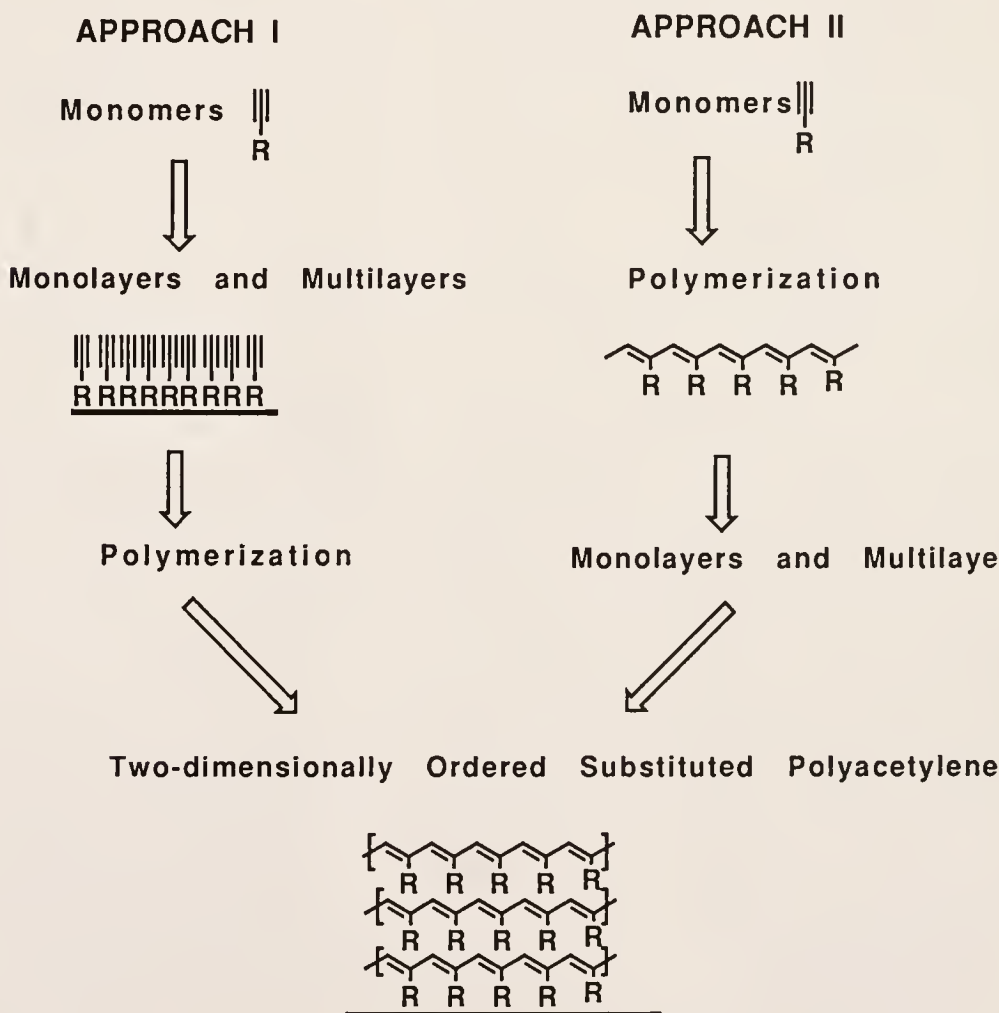


Figure 1-20. Schematic diagram of the twofold approach to two-dimensionally ordered substituted polyacetylenes.

Ordered monomer approach: Monomers will be ordered as films and polymerized. This can be done by restricting the monomers to two dimensions using the Langmuir technique. Multilayers will be deposited on a substrate. Polymerization can be done *in situ* or with the thin films.

Preformed polymer approach: Polymers will be synthesized in solution or in bulk. Their behavior at the air-water interface will be studied in order to control molecular conformation and ordering. Thin films can be subsequently built-up using the LB technique.

Eventually, the preformed polymer approach is dealt with in detail as the more promising approach. The other approach will be studied further by another doctoral student, Mr. M.J. Roberts.

This chapter has introduced the development of materials for nonlinear optical applications, the important aspects of this type of polymers, the Langmuir-Blodgett technique, and the behavior of polymers at the interface. This background and literature review is necessary to develop a complete appreciation of the science described herein.

Chapter 2 gives details of the synthetic procedure and the experimental apparatus used in the investigation. An extended description of the various surface analytical techniques is given.

In Chapter 3, investigations on the behavior and polymerizability of liquid crystalline monomeric monoacetylene amphiphiles is discussed. LB films of the monomers are built-up and characterized. Subsequently, these multilayers are polymerized by γ -irradiation and the results are discussed.

In Chapter 4, the second approach, a series of poly(ethynylbenzoate) polymers are investigated. The configuration and conformational behavior as well as catalyst effects are discussed. The film behavior of the polymer are then detailed. An interesting result is the importance of the alkyl chain in fluidizing

the monolayer. A variety of monolayer analytical techniques proves its worth in these investigations.

In Chapter 5, the configurational improvement of the poly(diethyldipropargylmalonate) is discussed. Then the monolayer film studies are described in terms of film fluidity. Comparison between high and low MW derivatives is highlighted in terms of monolayer properties. Interesting LB film depositions leading to multilayer structures are subsequently made.

Lastly, Chapter 6 contains the important comparisons between the different approaches and types of polymers.

CHAPTER 2

EXPERIMENTAL

Materials

All materials used for synthesis of monomers and polymers were obtained from Aldrich Chemical Company unless otherwise specified. Starting materials of reagent grade purity were used without further purification. TLC and ^1H NMR were employed to verify the purity of compounds. Reagent grade solvents were used for the reactions. Anhydrous solvents were prepared usually by distillation with calcium hydride or sodium. The solvents used for the polymerization were freshly distilled by vacuum to the reaction vessel (Schlenck tube).

Monomers and Polymers

Monoacetylenic Liquid Crystalline Monomers

The monoacetylenic monomers used in this study denoted as compounds I, II, III, were obtained from Dr. A. Blumstein and coworkers (University of Massachusetts at Lowell). These belong to a series of liquid crystals that have different length alkyl chains between the mesogen and the acetylene group. Samples with eight carbon long chains were used for this study. In addition, several amphiphiles (IV and V) used for blend studies were obtained from Dr. W. Ford and Dr. A. Schuster of Oklahoma State University and Max Planck Institute in Mainz, respectively. The detailed synthesis of the liquid crystalline monomers are described elsewhere.^{143,129} In general, the

monomers were synthesized by the condensation of acetylenic chloride and mesogenic alcohol. The undecynoic acid was purchased from Farchan Laboratory. The schematic diagram of the reaction is shown below:

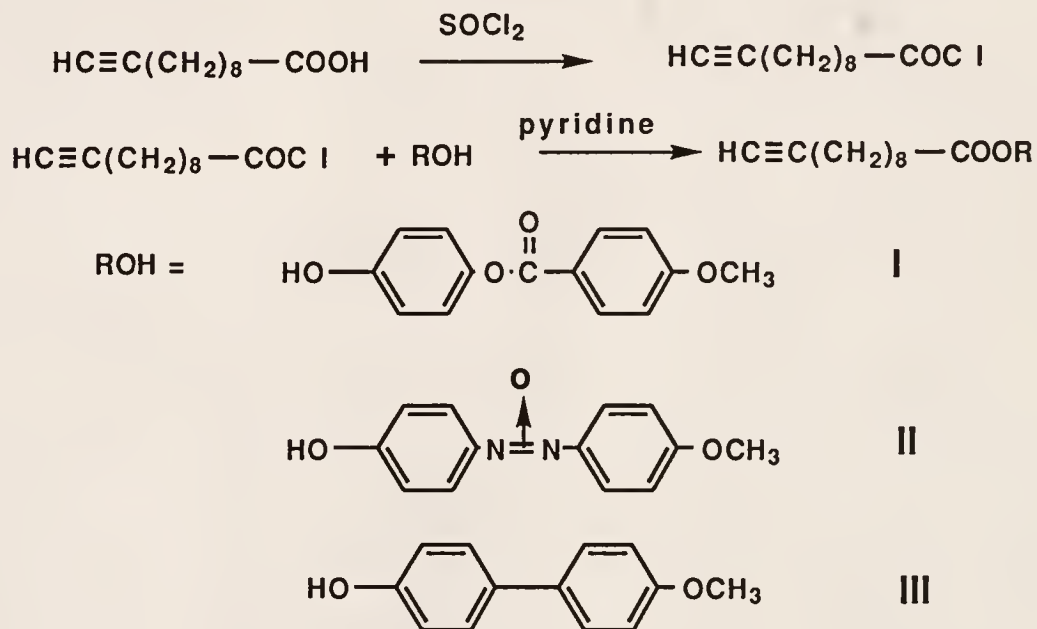


Figure 2-1. Esterification of the undecynoic acid chloride with the mesogenic alcohols to produce compounds I, II, and III.

Polyethynylbenzoate Polymers

The polyethynylbenzoate alkyl and phenyl esters were synthesized by A. Hilberer from Dr. J. Le Moigne's group in Strasbourg, France. These include: Polymers 1 and 2, and the different alkyl chain derivatives PPAC-n where n=1,2,4,8,16 carbons. Polymer 1 is denoted alternatively as PPAC-16. Details of the synthesis are described elsewhere.⁴⁷ The scheme of the monomer syntheses is shown below (Figure 2-2). In general, dehydrating condensation was employed effectively using dicyclohexylcarbodiimide (DCC) and dimethylaminopyridine (DMAP) to esterify the bromobenzoic acid with the linear alcohols to high yields. A palladium coupling reaction using

trimethylsilylacetylene (TMSA) and a palladium (II) acetate (PdAc_2) - triphenylphosphine (PPh_3) was employed to introduce the acetylene group. Removal of the trimethylsilyl group was facilitated by tetrabutylammoniumfluoride (TBAF). ^1H NMR, ^{13}C NMR, IR, and elemental analysis were used to elucidate and verify the structure, with good results. Polymerization of the monomers proceeded as described in Figure 2-3.

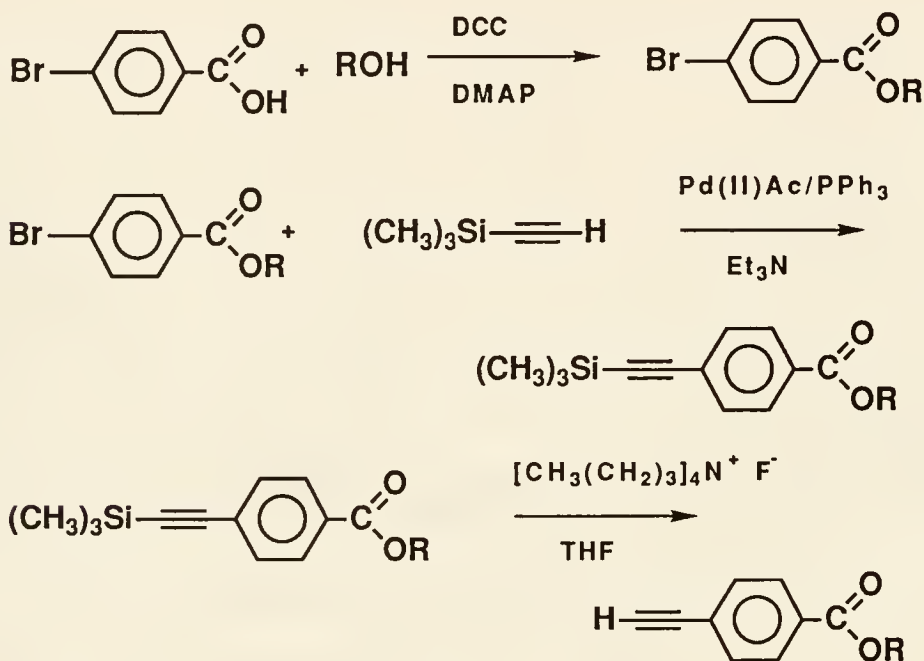


Figure 2-2. Synthetic scheme for the monomers of Polymer 1, 2, and the PPAC-n series. In general, R is either any of the homologous alkyl chains or the phenyl.

Monomer synthesis

The monomer for Polymer 3 was obtained by the prior synthesis of alkoxyphenols from hydroquinone and the corresponding linear alkyl bromide in cyclohexanone. The alkoxyphenol was then used for esterification with bromobenzoic acid. A series of even alkyl chain lengths was synthesized in good yields. The typical synthesis of the monomer is described as follows:

A mixture of the alkylbromide (16 mmol.), the hydroquinone (32-64 mmol.), and potassium carbonate (64 mmol.) was refluxed for sixteen hours in cyclohexanone. The reaction solution was filtered. The filtrate was concentrated, and then recrystallized from ethanol, to yield the *p*-alkoxyphenol.¹³⁰ The esterification of the *p*-bromobenzoic acid and the *p*-alkoxyphenol was carried by dehydrating condensation using DCC.¹³¹ To 8 mmol. of *p*-alkoxyphenol in 40 ml. methylene chloride with 100 mg of DMAP was added 8 mmol. of 1,4-bromobenzoic acid. The solution was initially stirred at 0°C to which DCC was slowly added and urea precipitated. The mixture was stirred at 20°C for 3 hours and the precipitated urea filtered off. The filtrate was evaporated under vacuum and the residue was redissolved in methylene chloride in order to filter the insoluble urea. The organic solution was successively washed with aqueous solutions of HCl, NaHCO₃, and pure water, and finally dried. The solvent was removed and chromatography of the residue was done on a SiO₂ column with CHCl₃ as eluent. Crystallization in methanol/methylene chloride gave white platelets of the esterified product.

The bromo derivative was then reacted with trimethylsilylacetylene (TMSA) to subsequently produce an ethynylated product.¹³² To a deaerated solution of the (17 mmol) bromo derivative in 50 ml of anhydrous triethylamine, 34 mmol of TMSA was added dropwise. Catalyst, palladium(II)acetate, (5 mg) was then added together with 50 mg triphenylphosphine. The mixture was refluxed for 24 hours, then cooled and filtered to remove the hydrobromide salt. The orange brown filtrate was concentrated, mixed with 200 ml of aqueous sodium bicarbonate, and then extracted with dichloromethane (3 x 50 ml). The organic fractions were combined, dried over magnesium sulfate, and concentrated to yield an oil. The residue was taken up in methylene chloride and passed through a column of silica with a mixture of methylene chloride and

pentane. The eluent was concentrated and further purified by column chromatography. The final product was a yellowish solid.

Different chain lengths from the series were obtained in good yield and the structure was elucidated using common organic spectroscopic characterization techniques. The data shown below for the ten carbon alkyl chain length derivative is taken as typical for the rest of the monomers with differences only on the alkyl regions of the spectra.

Monomer, *p*-decanoxyphenyl-*p*-ethynylbenzoate: Yellowish solid, yield = 78%; m.p. 74.35 °C; IR (KBr pellet) 3240 cm⁻¹ (m, sharp, acetylenic C-H stretching), and 610 cm⁻¹ (m, acetylenic C-H bending), 1740 cm⁻¹ (s, carbonyl ester); ¹H NMR (CDCl₃) 3.25 ppm (s, acetylenic proton), 8.2-7.6 ppm (s, 4H aromatic benzoate), 7.2-6.9 (s, 4H aromatic phenol). ¹³C NMR (CDCl₃) 80 and 88 ppm (acetylenic α and β), 164.88 ppm (m, carbonyl carbon), 157-115 ppm (m, 8C aromatic); Analysis, Calc. C: 79.4, H: 7.9, O:12.7. Found. C: 79.1, H: 8.0, O: 12.9.

Table 2-1. Elemental Analysis of the monomers with calculated and actual values.

Alkyl Chain Length of Derivative	Calculated C%, H%, O%	Observed C%, H%, O%
8	78.9, 7.4, 13.7	78.6, 7.6, 13.8
10	79.4, 7.9, 12.7	79.1, 8.0, 12.9
12	79.8, 8.4, 11.8	79.8, 8.5, 11.7
14	80.2, 8.7, 11.1	79.2, 8.8, 12
16	80.5, 9.1, 10.4	81.1, 12.18, 6.72
18	80.8, 9.4, 9.8	78.9, 9.3, 11.8

Elemental analysis of the monomers show good correlation with the calculated values for the structures with different alkyl chain lengths. The data are summarized in Table 2-1.

Polymerization was done for these monomers using the Schlenck tube technique. The apparatus and set-up used was similar to that of the other polyethynylbenzoate derivatives and the description below can be taken as typical. Figure 2-4 shows a schematic diagram of the polymerization set-up in which the whole system, under vacuum, was purged with N₂ gas. All glass apparatus was cleaned and flamed or oven dried prior to use. Dry box handling technique was used to introduce the catalyst and the solid monomer in the reaction vessel.

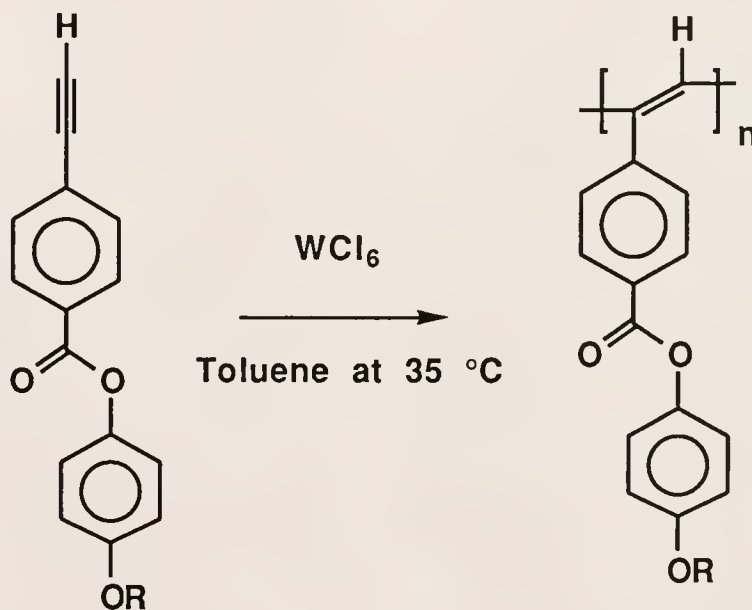


Figure 2-3. Polymerization of the monomer with WCl₆ in toluene using the Schlenck tube technique. R = 8, 10, 12 carbons polymerized successfully.

Typical polymerization

Monomer (250 mg) and catalyst (5.8 mg) were placed in a clean and dry reaction vessel under argon. Fresh dry solvent (toluene) was introduced to the

reaction vessel by evaporation to make an approximately 1.0M solution. The polymerization was carried out at 30°C for 24 hours. The product was recovered in methylene chloride and poured into a large excess (150 ml) of methanol. The precipitant was then redissolved in THF and passed through a silica column to remove the catalyst. The eluent was then concentrated and reprecipitated in methanol, then oven dried and weighed.

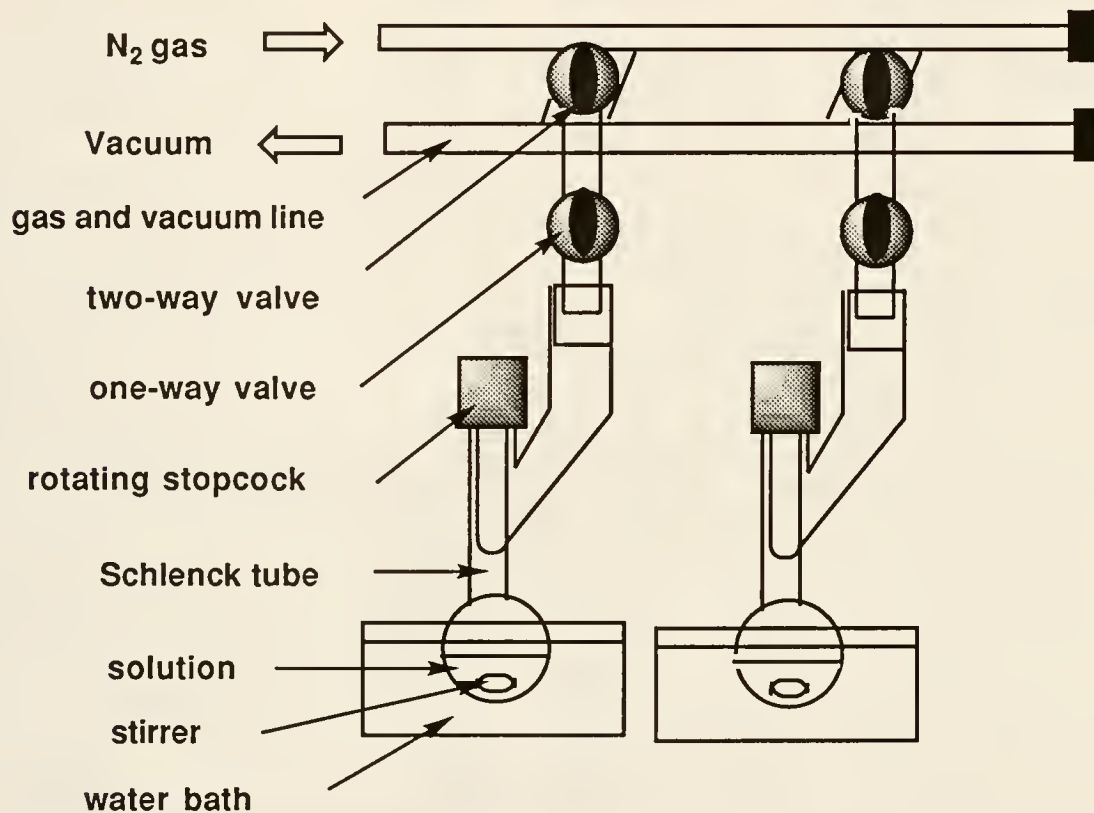


Figure 2-4. Polymerization set-up under N₂ gas and vacuum line. Monomer and catalyst was introduced to the tube under dry box conditions prior to polymerization.

Polymer of *p*-decanoxyphenyl-*p*-ethynylbenzoate: A reddish brown product was obtained with 89% yield. IR (KBr) 1600 cm⁻¹ (m, sharp polyenic double bonds), 1265 cm⁻¹ (=C-H in plane deformation), disappearance of 3240 cm⁻¹ peak (acetylenic C-H stretching), 922 and 970 cm⁻¹ (=C-H out of plane

deformation); ^1H NMR (CDCl_3) disappearance of 3.25 ppm resonance (s, acetylenic proton), 7.2-6.5 ppm (b, ethylenic protons); ^{13}C NMR disappearance of 80.4 and 82.7 ppm (acetylenic α and β), 135-125 ppm (b, ethylenic carbons with phenylene and cyclohexadiene C=C carbons); Analysis, calc; C:79.2, H:8.1 Found; C:79.1 H:8.1.

Only polymers from 10,12, and 14 carbon derivatives were obtained. No further reactions were run however since the goal of producing a lateral substituent variant for the series was achieved. The polymer with a 12 carbon derivative gave similar NMR, IR, and UV spectral observations with the 10 carbon derivative except for the alkyl region. The ^{13}C NMR of the 14-carbon derivative showed a small resonance at 0.2 ppm signifying the presence of the trimethylsilyl groups in the polymer. This residue came from the incomplete conversion of the monomer by the removal of the trimethylsilyl protecting group. This could account for the discrepancy between the calculated and observed value in the elemental analysis. Despite drying of the polymer for a long time, this peak was not removed and therefore is probably associated with the polymer backbone (trimethylsilane or trimethyl-silylacetylenes are volatile). This would mean that some disubstituted acetylenes were copolymerized with the monomer resulting in a more irregular polymer. Some saturated defects are observed in the 4.1-3.5 ppm region in the ^1H NMR and between 60 to 30 in the ^{13}C NMR. This derivative was not used for comparison with the other polymers.

Synthesis of Poly(diethyldipropargylmalonate)

Monomer preparation

The monomer diethylhepta-1,6-diyne-4,4-dicarboxylate, was prepared according to a literature procedure.⁷⁴ The following procedure was used:

diethylmalonate (6.75 g = 1 equiv.) was added to previously dried ethanol (100 ml) containing sodium ethoxide in ice bath. The sodium ethoxide was prepared from 3.0 g of sodium in ethanol. After 5 min., propargyl bromide (10.5 g = 2 equiv.) was slowly added to the stirred suspension, and the mixture heated under reflux for 6 hours. The reaction was stopped and alcohol was removed under pressure. The product was diluted in water and petroleum ether was added to precipitate the product. The product was recovered by filtration, and dried to get a 75 % yield. m.p. was at 45 °C (lit. 45.5 °C). It had the following spectral properties: IR (KBr) 3300 cm⁻¹ (m, \equiv C-H stretching), 1740 cm⁻¹ (carbonyl ester); ¹H NMR (200 MHz CDCl₃) 1.28 ppm (t, 6H), 2.1 ppm(s, 2H), 3 ppm (s, 4H), 4.3 ppm (q, 4 H). ¹³C NMR: 15 ppm (CH₃), 60.8 ppm(CH₂ of CH₂C \equiv C), 72 ppm (\equiv C-H), 81.6 ppm (C \equiv C), 171 ppm (carbonyl C), Analysis, calc; C:66, H:6.7,O:27.3 Found; C:65.5 H:6.8, O: 27 .7

Typical polymerization

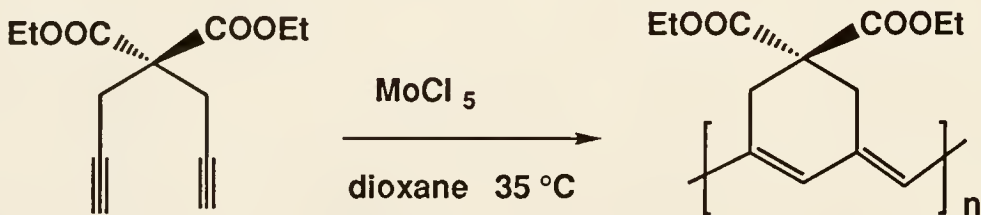


Figure 2-5. Polymerization of diethyldipropargylmalonate using MoCl₅ catalyst in dioxane solution.

Monomer (250 mg) and catalyst (5.8 mg) were placed in a clean and dry reaction vessel under argon. Fresh dry solvent (dioxane) was introduced to the reaction vessel by evaporation to make an approximately 0.1 M solution (varied). The polymerization was carried out at 25°C (35 °C) for 24 hours

(varied). The product was recovered in anhydrous methylene chloride and poured into a large excess (150 ml) of methanol. The precipitate was then redissolved in THF and passed through a silica column to remove the catalyst. The eluent was then concentrated under vacuum and reprecipitated in methanol, then oven dried. The yield was determined by gravimetry.

Table 2-2. Summary of polymerization yields and conditions. Reaction was done at 35 °C for the high MW polymer derivatives and at 25 °C for the low MW polymers.

Polymer	Ct./Mo ratio (mole)	Conc. in [M] ±0.02	Time rxn. (hrs)	Total% Conver sion	sol. %	insol.%
pDDM1H	1:50	0.07	24	88 %	100	0
pDDM2H	1:50	0.15	24	63 %	95	5
pDDM3H	1:50	0.30	24	70 %	86	14
pDDM25	1:25	0.15	24	66 %	85	15
pDDM1L	1:50	0.12	1	40%	87	13
pDDM2L	1:50	0.12	3	45%	100	0
pDDM3L	1:50	0.12	12	55%	89	11
pDDM4L	1:50	0.12	18	68%	100	0

Variations on the procedure were made to change the parameters of the reaction. For different concentrations, the solvent introduced was measured on graduations in the Schlenck tube within ± 0.2 M uncertainty. Catalyst ratio was controlled by weighing the right amount of catalyst at the dry box stage to obtain a 1/25 and 1/50 catalyst/monomer ratio. The time of polymerization was

controlled simply by stopping the reaction at the desired point and using separate tubes. Table 2-2 summarizes the yield and parameters of polymerization.

The following spectral properties were taken as typical for the high MW polymer and the low MW polymer groups respectively. No noticeable differences in the spectral properties were observed and the elemental analysis is tabulated separately.

Poly(diethyldipropargylmalonate), pDDM3H: A black amorphous solid was obtained with a 70 % yield. UV = 550 nm (purple solution), IR (KBr) 1600cm⁻¹ (m, sharp polyenic double bonds), 1250 cm⁻¹ (=C-H in plane deformation), 1727 cm⁻¹ (carbonyl), disappearance of 3300 cm⁻¹ peak (acetylenic C-H stretching), 925 and 970 cm⁻¹ (=C-H out of plane deformation); ¹H NMR (CDCl₃) disappearance of 2.1 ppm resonance (acetylenic proton), 7.0-6.4 ppm (broad, ethylenic proton), ¹³C NMR 14 ppm (methyl C), 41 ppm (ring methylene C) disappearance of 72.4 and 81.2 ppm (acetylenic α and β), 123.2 ppm and 138 ppm(s, polyenic carbons), 171 ppm (s, carbonyl);

Poly(diethyldipropargylmalonate), pDDM1L: A black amorphous solid was obtained with a 40 % yield. UV= 546 nm (purple solution), IR (KBr) 1610cm⁻¹ (m, sharp polyenic double bonds), 1250 cm⁻¹(=C-H in plane deformation), 1725 cm⁻¹ (carbonyl), disappearance of 3315 cm⁻¹ peak (acetylenic C-H stretching), 930 and 990 cm⁻¹ (=C-H out of plane deformation); ¹H NMR (CDCl₃) disappearance of 2.1 ppm resonance (acetylenic proton), 6.7 ppm (sharp, ethylenic protons), ¹³C NMR 14.8 ppm (methyl C), 41.5 ppm (ring methylene C) disappearance of 72.4 and 81.2 ppm (acetylenic α and β), 124 ppm and 137.6 ppm (s, polyenic carbons), 172 ppm (s, carbonyl).

Several very small peaks were observed at 41, 57, 123,137 and 172 ppm (usually adjacent to the larger peaks) which were not previously reported.

This may be indicative of small amounts of five membered ring units on the polymer backbone as reported in the literature.¹³³ No attempt was made though to systematically study the parameters which control the formation of this ring. In any case, these are not expected to significantly affect the configuration as well as the conformation of the conjugated sequences .

Table 2-3. Elemental Analysis of the polymeric products obtained from the soluble fractions of the polymers.

Polymer	C %	H %	O %	Total
calculated C ₁₃ H ₁₁ O ₄	66.0	6.7	27.3	100
pDDM1H	65.1	6.8	27.0	98.9
pDDM2H	65.6	5.5	27.3	98.4
pDDM3H	65.5	6.5	27.0	99.0
pDDM25	62.8	7.2	27.0	97.0
pDDM1L	65.6	6.2	27.0	98.8
pDDM2L	64.8	6.7	26.8	98.3
pDDM3L	65.6	6.7	26.5	98.8
pDDM4L	65.0	7.0	26.4	98.4

General Instrumentation

¹³C NMR and ¹H NMR spectra were recorded on a Bruker AC200F spectrometer system operating at (¹H) 200 and (¹³C) 60 MHz. Deuterated chloroform (CDCl₃) was used as solvent and all chemical shifts reported are internally referenced to this. (¹³C) spectra were run typically between 12-14 hrs acquisition time. Infrared Spectra of the powder-pressed pellets in KBr were

recorded on a Perkin Elmer 983. UV spectra were recorded on a Perkin-Elmer UV/VIS/NIR Lambda 9 spectrophotometer and/or Shimadzu UV 210-PC UV-vis scanning spectrophotometer in spectro grade methylene chloride, THF in solution (10^{-4} - 10^{-5} M), and on a quartz plate for the cast film.

The reaction set-up for polymerization was attached to a high vacuum (10^{-5} mmHg) and N₂ gas line, separated by a two way high vacuum valve (Figure 2-4). Specially constructed Schlenck tubes (50 - 75 ml) with a high vacuum valve was used. Monomer and catalyst was weighed and introduced to the tube in a glove box under Argon.

Differential Scanning Calorimetry (DSC) and Thermogravimetric Analysis (TGA) were performed on a Perkin Elmer 7 Series Thermal Analysis System and/or DSC 7 Thermal Analysis System in aluminum pans with a heating and cooling rate of 10 °C/min. DSC samples (10-20 mg) were analyzed with liquid nitrogen as coolant under a helium or nitrogen flow rate of 25 mL/min. TGA samples were performed under nitrogen with a flow rate of 50 ml/min. and program heating from 50 to 700 °C at a rate of 10 °C/min. Optical observations were obtained with a Leitz Orthoplan or Nikon Diaphot optical polarizing microscope equipped with a Mettler FP52 hot stage and FP80 Central Processor.

Elemental analyses were performed by the analytical services group (Mr. M. Keyser) of the Institut Charles Sadron in Strasbourg, France.

For molecular weight determination, Gel Permeation Chromatography (GPC) method was used. Data was collected using a Waters Associate Liquid Chromatograph apparatus equipped with a U6K injector and differential refractometer and a Perkin Elmer LC-75 ultraviolet (UV) spectrophotometric detector. Two Phenomenex 7.8 mm x 30 cm Phenogel 5 consecutive linear cross-linked polystyrene gel columns were used. The eluting solvent was

HPLC grade tetrahydrofuran (THF) at a flow rate of 1.0 mL/min. Polymer samples were dissolved in THF (0.5 to .05 % w/v) and filtered (~50 µm) before being injected (10-40 µL) to the sample injection port. The retention times were calibrated using polystyrene standards (Scientific Polymer Products Inc.). The following narrow molecular weight polystyrene standards were used with a polydispersity $M_w/M_n \leq 1.06$: $M_w = 650000, 142000, 79000, 59500, 47500, 30700, 12200, 7820, 1940$. The Millennium 2010® data collection and analysis software system running on a 386 IBM PC computer was used for calibration curve calculation and peak analysis.

Langmuir-Blodgett Technique

Langmuir Monolayer Film Studies

For the materials studied at the air-water interface, spreading solutions were prepared using spectro grade chloroform or methylene chloride (Kodak® or Fisher® ACS grade) at 0.2-1.0 mg/ml concentrations. Volumes of 50 to 200 ml were spread using a Hamilton gas tight microsyringe with an uncertainty of $\pm 1\%$. The solution was delivered dropwise, allowing time for evaporation of solvent. The water used was of excellent purity (ion resistivity of 18 MΩ) and was purified by deionization (Continental Water Systems), followed by the Millipore Milli-Q® Plus 5-bowl filtering system.

Data was collected using the KSV LB5000® modular Langmuir-Blodgett System (KSV Instruments Helsinki, Finland) in a clean dust free environment. The trough is made of teflon with channels underneath to allow for circulation of cooling/heating liquid from a temperature bath. Temperature was controlled with a deviation of $\pm 0.5^{\circ}\text{C}$ using a Neslab® refrigerating and heating circulating bath. A teflon or nylon barrier was used for controlling the surface area by

symmetrical compression. A surface balance using the Wilhelmy plate method (platinum or paper) was used to record the surface pressure. Isotherm, mean molecular area-time, surface pressure-time plots were recorded with the version 4.4 KSV software package installed in an IBM-PC AT computer interface. The monolayers were compressed with a speed of 1 to 3 $\text{\AA}^2/[\text{molecule (repeat unit)} \times \text{min}]$. and were considered reproducible only if a range of $\pm 1 \text{ \AA}^2/\text{molecule(repeat unit)}$ in area deviation were observed. All isotherms were run a minimum of two times. The mean molecular area (Mma) refers to the average surface area/molecule or area/repeat unit in the case of polymers. To determine the stability of a monolayer, the following procedures were used. First, the monolayer was compressed until it reached a given surface pressure and the barrier was stopped. The surface pressure changes were then monitored as a function of time. In the second method, the mean molecular area of the compound or polymer was monitored as a function of time while keeping the applied surface pressure constant. The applied surface pressure was kept constant by computer control of the barrier movement.

Langmuir-Blodgett film deposition

A KSV LB5000 dipping trough was used for conventional vertical deposition. Precise dipping movement was performed by a computer controlled mechanical dipping arm attached to the mainframe. For alternate dipping, a three well compartment trough was used together with a 180° angle moving mechanical dipper/arm. Films were deposited on specially prepared glass, quartz plates, and silicon wafers. The dipping speed was maintained at speeds of 1.0 to 10.0 mm/min. in both directions. The dipping motion was delayed at the top of its travel for either 5 or 10 minutes to allow time for the previously

deposited layer to dry in the air. The transfer ratio and surface pressure were monitored and recorded during the dipping process.

For alternate deposition, the KSV 5000 Alternate Deposition System was used. The dipping procedure is the same as above, with two monolayer films maintained at constant pressures simultaneously. Delay time, dipping speed, and cycle sequence (trough 0, 1, and 2) were controlled by programming.

The glass and quartz plates were cleaned using the following procedure: the plates were immersed in a detergent solution and sonicated for 10 minutes and then placed in a solution consisting of a 1:1:3 mixture containing NH₄OH, H₂O₂, and Milli-Q® water respectively. The plates in the solution were then heated for 30 minutes at 80 °C. Alternatively, a solution of Chromerge® in concentrated sulfuric acid was prepared and the substrate soaked for several hours. Hydrophobization of substrates was done using a standard technique which involves placing the clean substrate sequentially in each of the following solvents: CH₃OH, CHCl₃ / CH₃OH, CHCl₃. This is done at 15 minute intervals in a sonicating bath. The substrate is then placed in a mixture of 70 ml pure decalin, 10 ml chloroform, 20 ml carbon tetrachloride, and 2 vol % octadecyltrichlorosilane and sonicated for 2 hours. The plates are then sonicated for 10 minutes on the reverse order of solvents mentioned above.

UV spectra of the deposited multilayers were obtained using a specially constructed sample holder on a Perkin-Elmer UV/VIS/NIR Lambda 9 spectrophotometer.

X-ray diffraction of the liquid crystalline monomer LB Films was taken using a GE XRD-5 diffractometer at 35kV and 30 mA using Cu K α (1.54 Å) radiation with a scan rate of 0.4 deg./min. Measurements were done with the assistance of Prof. Blanchard of the Department of Geology, University of Florida. Low angle X-ray diffraction for the poly(diethyldipropargylmalonate)

and stearic acid films was performed by Dr. Jing Fei Ma of Prof. Nagler's research group, Department of Physics, University of Florida. A Rigaku 18-kW rotating anode diffractometer with a Cu K α line, at $\lambda = 1.54 \text{ \AA}$ passed through a graphite monochromator. The diffracted X-ray beam was passed through a graphite analyzer before detection.

FTIR-ATR measurements were performed by Mr. Houston Byrd of Prof. Talham's research group, Department of Chemistry, University of Florida. The spectra were recorded with a Mattson Instruments Research Series-1 Fourier Transform infrared (FTIR) spectrometer using a narrow-band mercury cadmium telluride detector. A Harrick TMP stage was used for the ATR experiments. Polarized FTIR-ATR spectra was taken with s- and p-polarized light. All spectra consist of 1000 scans at 2.0 cm^{-1} resolution.

Surface Analytical techniques at the air-water Interface

In addition to the use of the surface balance for surface pressure-area isotherm measurements, several analytical techniques were used to investigate the surface properties of spread monolayers. A brief background is described for each technique and then the specifications of the apparatus as well as the measurement procedures are described:

Surface potentiometer

Next to the surface-pressure area isotherm, the most useful tool for characterizing the air-water interface is the surface potentiometer. The surface potential is defined as the change in phase boundary potential produced by an interfacial film. The measured quantity is the difference between the potential at the air-water interface, with and without a monolayer. The Helmholtz equation relates the potential to changes in the surface dipole moment, μ :¹³⁴

$$\Delta\mu / A = \epsilon_0 \Delta V \quad (2.1)$$

where A is the area per molecule, ΔV the surface potential, and ϵ_0 is the permittivity constant in vacuum. Further discussion is given in Appendix C. Two methods are generally used, the ionizing electrode method and the vibrating plate (condenser) method. The first method makes use of an air-electrode mounted a few millimeters above the surface and incorporates a small radioactive source.¹²⁰ This ionizes the gap between the air electrode and the surface thereby making it conducting.

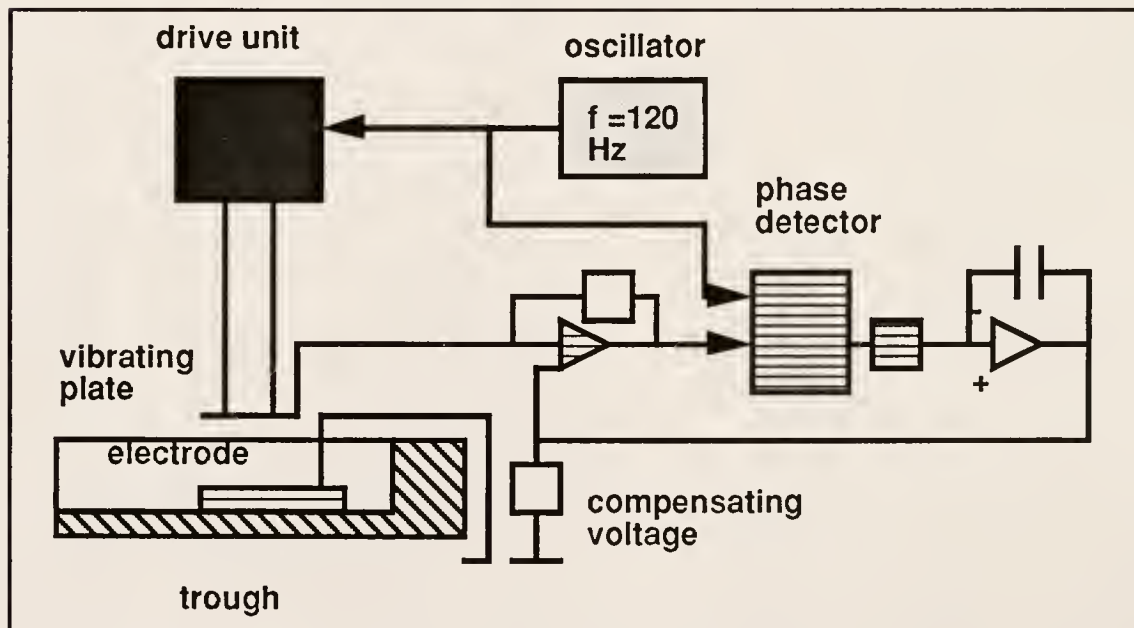


Figure 2-6. Surface Potentiometer set-up (vibrating plate method) showing the schematic diagram of the compensating voltage circuitry. Diameter of the vibrating plate and electrode is 4 cm.

The other method is a capacitance method. An alternating current is generated by the small amplitude vibration of metal plate at a certain frequency (about 80-120 Hz).¹²⁰ This results from the potential difference between the

plates producing a capacitance that induces AC current into the circuit. The plate is attached to a voice coil of a loudspeaker and is located as close as possible to the interface without disturbing it. The alternating current is amplified and detected by a phase detector. The phase detector gives a DC current output which charges the following feedback capacitor until the compensating voltage equals the surface potential and no currents occur. This potential can be plotted as a function of the mean molecular area to produce the typical surface potential-area isotherm.

A KSV 5000 SP module with a measuring range of ± 10 V with a ± 5 mV precision was used to measure the surface potential at the air-water interface. Based on the vibrating plate method, an alternating current is generated by the small amplitude vibration of a metal plate at frequencies of about 80-120 Hz. Another metal plate electrode is placed underneath the subphase at a distance of 1-2 cm from the upper plate. Calibration was done using the software calibration program and an adjustable DC-power supply or battery. The potential was set to zero for the air/water subphase, just before the monolayer is spread.

UV-vis spectroscopy at the interface

In situ measurements of UV-visible absorption spectra can be made at the interface by using the appropriate set-up.⁸⁷ Simultaneous recording of surface-absorption-area and pressure-area relationships provide insight into the orientation and arrangement of molecules at the interface. The presence of changes in both wavelength and absorption can be measured in situ with changes in surface area by compression of the monolayer. The result is a three dimensional plot containing the axes of surface area, wavelength and absorbance. Wavelength shifts in compression can be used to determine the

presence of molecular aggregations by π - π^* interactions as well as changes in the conjugated sequences of absorbing amphiphiles. As light passes through a monolayer, it is either reflected, absorbed or transmitted. The portion of light that is absorbed is detected by a detector which gives the spectral changes.

The set-up, shown below, makes use of optical fibers to direct light as well as to detect the transmitted light. Light channeled from a Xe arc lamp source is first passed through the monolayer. This is in turn reflected by a mirror beneath the water subphase which causes the transmitted light to pass through the monolayer for the second time. The light is then detected by the other optic fiber and channeled through a photodiode array detector. The photocurrent output is in turn converted to a voltage, amplified and converted by an analog to digital converter into a series of digitized readings that generates a spectra in a computer interface. To maximize resolution and spectral range, the wavelength sensitivity can be varied by a holographic or ruled grating to the desired blaze wavelength with the detector optics.

In this study, in-situ UV-Vis spectroscopy was performed using an Oriel Instaspec III Spectroscopy system. A modified KSV trough (minitrough) was used with a special attachment for holding the optical fibers as well as in fixing the mirror underneath the subphase. A Xe Arc lamp light source with a spectral range of 190-900 (UV to near IR) was used, coupled to a quartz optical fiber bundle. The exit plane of the bundle was set horizontally at 3 cm above the water surface. A plano-convex mirror was placed at 5 mm underneath the subphase (parallel to the water subphase) to reflect the transmitted beam. A nitrogen gas and cooling bath cooled the Multispec® photodiode array detector of 1024 elements. Cooling increases the dynamic range of the PDA detector.

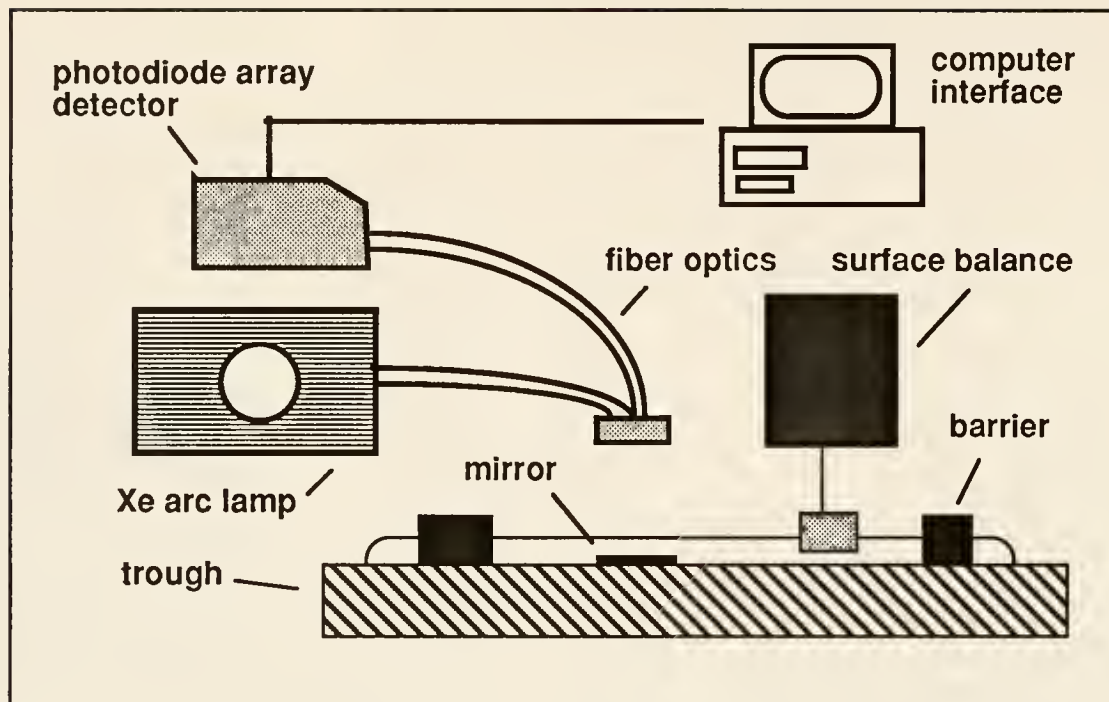


Figure 2-7. Schematic diagram of an in situ UV-Vis Spectroscopy set-up for measurements at the air-water interface. The photodiode array detector is cooled with N₂ gas and a circulating cooling bath

Gratings of 2400 and 400 lines/mm were used together with combinations of blaze wavelength with ranges from 250-750nm. The choice of the grating/blaze wavelength combination is based on proximity to the absorption peak of interest. The grating with higher number of lines/mm gives a smaller spectral range but greater resolution. The grating with the closest blaze wavelength to the desired absorption peak was chosen. A scanning frequency and integration time of 1 spectra/10-40 seconds and 1 second, respectively, were used for the measurements. Exposure time (0.5 - 1 sec.) was controlled (to below the saturation level) via an automated shutter mechanism interfaced to the computer. Correction was made for shot noise (photon noise), electrical noise, and dark current noise prior to data acquisition. This was done by taking a reference reading at the the interface without the monolayer (before

spreading) and a background reading with the shutter off prior to the actual measurements. The data acquisition cycle of the spectrometer was timed to coincide with events in the monolayer e.g. compression, isobaric creep measurements, etc. Data is stored in the computer and retrieved at the end of the cycle. Absorption spectra and three dimensional UV-vis/time or area plots were generated using the Instaspec III peak analysis software program.

Brewster angle microscopy and reflectivity measurements

Brewster angle microscopy allows the direct observation of monolayer morphology without the complication of added probe molecules since contrast is dependent upon differences in the refractive indexes of pure components rather than on emission by excitation of added chromophores. Brewster angle microscopy or BAM is based on a simple principle of optics. When p-polarized light is directed at an interface of two materials, with refractive indices n_1 and n_2 where $n_1 > n_2$, reflected light intensity is zero at an angle which is called the Brewster angle and defined as

$$\tan (\alpha) = n_2 / n_1 \quad (2.2)$$

When a film possessing a refractive index n different from that of n_2 , is introduced to the surface, light is reflected. The Brewster angle microscope images are light reflected from the interface. Such changes in refractive index at the interface are caused by differences in density, orientation and aggregation in pure films and phase separation in mixed films are seen as intensity changes in the BAM image. An advantage of this technique is that contrast is obtained without the addition of foreign molecules. Therefore the concern for miscibility of a fluorescent probe and its possible effect on monolayer behavior is eliminated.

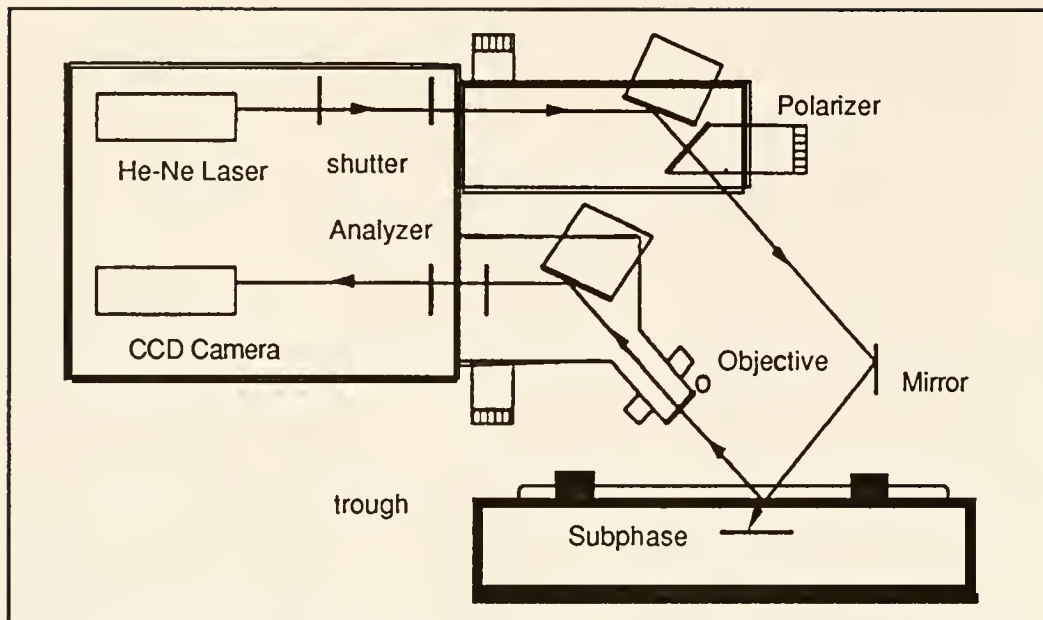


Figure 2-8. Brewster Angle Microscope set-up showing the path of laser light reflected through a set of mirrors. A polarizer-analyzer system is used for polarized microscopy. Images are observed through an external video monitor. An auxiliary integration unit can be attached.

The Brewster Angle Microscopy(BAM) used was a BAM-1® from Nanofilm Technologie GmbH (Goettingen, Germany). A 5 mW He-Ne laser light set at p-polarization was used to illuminate the images. The angle of incidence was set initially at 53° and then adjusted to minimize the reflected intensity of the clean water surface prior to the spreading of each film.

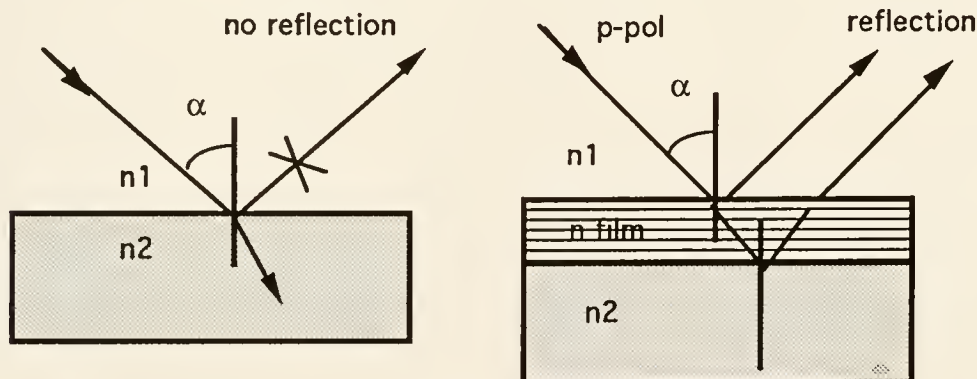


Figure 2-9. Schematic diagram of the Brewster angle phenomena in optical media of different refractive indices.

The images are observed on a video monitor from which recordings were made on a VHS video cassette recorder. Frame grabbing of images was done using a Sun Sparc station with commercially available imaging processor software.

Relative reflectivity data were obtained from the images in two ways: An auxiliary video integration unit VIU1® also from Nanofilm Technologie was attached to the control module of the microscope, in which integration of the pixels are automatically given as DC output. The plots are recorded in an X-Y plotter or as voltage changes from a multimeter. Calibration is made between the air/water interface (zero reflection), and a fully saturated image. The other method involved integration of the image pixels using a software program in a SUN Sparc station (VideoPix®, Sun Microsystems Inc. 640 x 480 pixels in 256 gray scales). Data are plotted as a ratio of intensity (air-monolayer-water)/intensity (air-water).

CHAPTER 3

APPROACH I: POLYMERIZATION OF ORDERED MONOMERS

Introduction

Liquid Crystalline Monomers at the Interface

Liquid crystals are extensively used in both passive and active display devices. The function of such devices comes from the ability of the liquid crystalline molecules to self organize at a number of intermediary states between the isotropic liquid and the organized solid state.¹³⁵ Liquid crystals are generally classified as either thermotropic or lyotropic in behavior. Thermotropic liquid crystals have thermodynamically stable, temperature dependent intermediary states that are called mesophases, the most common of which is the nematic phase (N). Others such as the cholesteric (Ch) and the smectic phases (S) are characterized by higher dimensional order and sometimes chirality.¹³⁶ Control of these phases is brought about by systematic variations in the shape and interactions between the molecules. The classical shape is that of a stiff rod-like moiety (called the mesogen) with a flexible chain attached to one or both ends of the moiety giving it a high aspect ratio (length:width).

The use of liquid crystalline structures in making Langmuir-Blodgett films is a step towards better morphological control. Considering the fact that many liquid crystalline compounds are amphiphilic in nature, it would seem inevitable that these self-organizing systems would be investigated confined to a semi-

two-dimensional water surface. Ringsdorf et al. have synthesized, spread, and transferred a variety of liquid crystalline molecules and polymers starting two decades ago.¹³⁷ Much research since then, has been explored with a wide range of fields covering both investigation techniques and materials research. The number of articles appearing in journals such as *Langmuir* and *Thin Solid Films* attests to this growth. In principle, the presence of polar groups especially in the mesogenic moiety and the hydrophobic nature of the flexible chain orients the molecule. The presence of π - π interactions between phenyl rings increases intralayer interactions.¹³⁸ Interesting multilayer architectures have been built up with liquid crystalline amphiphiles. However, there is a lack of device applicability at present due to intrinsic instability. The disadvantage, is the subsequent rearrangements brought about by mechanical or thermal stress on the multilayers with time. This lack of temporal stability within LB films of liquid crystalline amphiphiles points towards polymerization as a means of retaining this order. It has been shown that polymerization of monomer crystals proceeds with high rates and low overall activation energies.¹³⁹ In 1964, G.M.J. Schmidt and collaborators, enunciated the topochemical principle of reactions in the solid state.¹⁴⁰ This concept emphasized that groups undergoing reaction in the solid state should be close to 4-4.5 Å in distance and that reactivity is greater in the ordered lattice than at defects. The field has become immensely popular with the solid state polymerizations of LB films of diacetylenic monomers by G. Wegner and collaborators beginning in 1969.^{141,92} The advantages of polymerization of ordered monomers lies not only in the topological control but also in stabilizing the ordered structures in multilayers. These often result in enhanced mechanical and thermal stability of multilayers.

Objectives

To date, while much study has been confined to polymerizations of diacetylenic amphiphiles, little work has been done on liquid crystalline monoacetylenes. Previous work with liquid crystalline monoacetylenic amphiphiles has been done most notably by three research groups: Le Moigne and coworkers have synthesized a number of liquid crystalline substituted acetylenes (including compound III) and have succeeded in polymerizing a few of these acetylenes in the bulk using metathesis Group 6 catalysts and γ -irradiation in the bulk (albeit to low yield).¹⁴² Blumstein and coworkers, who have synthesized the liquid crystalline acetylenes used in this study, have found low bulk polymerization yields using γ -irradiation.¹⁴³ Also Ogawa has attempted to polymerize amphiphilic alkyl substituted acetylene monomers in LB films using X-ray and KrF excimer laser light.¹⁴⁴ Each of these workers reported low yields for polymerization of these types of monomers. Recently, liquid crystalline monoacetylenes have also been polymerized successfully with Ziegler-Natta and metathesis catalysts to high yields by H. Shirakawa and coworkers.¹⁴⁵

In this study, three substituted acetylene compounds, which are known to form nematic liquid crystalline phases in the bulk (Table 3-I), were chosen to see if they would form Langmuir films (insoluble monolayers at the air-water interface). It is hoped that greater order will be induced by the mesogenic groups when coupled with amphiphilic interactions at the water surface. In principle, the increased intralayer ordering should position the acetylene group ideally for polymerization. The liquid crystallinity restricts the orientation of the monomer normal to the surface while the Langmuir-Blodgett technique constrains the monomer to the surface. Thus, the interest in Langmuir film

formation lies in the possibility of polymerizing a highly oriented monomer as multilayers deposited on a substrate (Langmuir-Blodgett film). This chapter will mainly focus on polymerization of these ordered monomers and constitutes the Approach I route for highly ordered substituted polyacetylenes.

Bulk Characteristics of the Monomers

The monoacteylenic monomers (I, II, III) used in this study were obtained from Blumstein and co-workers (University of Massachusetts at Lowell). In addition, several amphiphiles used for blend studies (IV and V) were obtained from W. Ford and A. Schuster (Oklahoma State University and Max Planck Institute in Mainz).

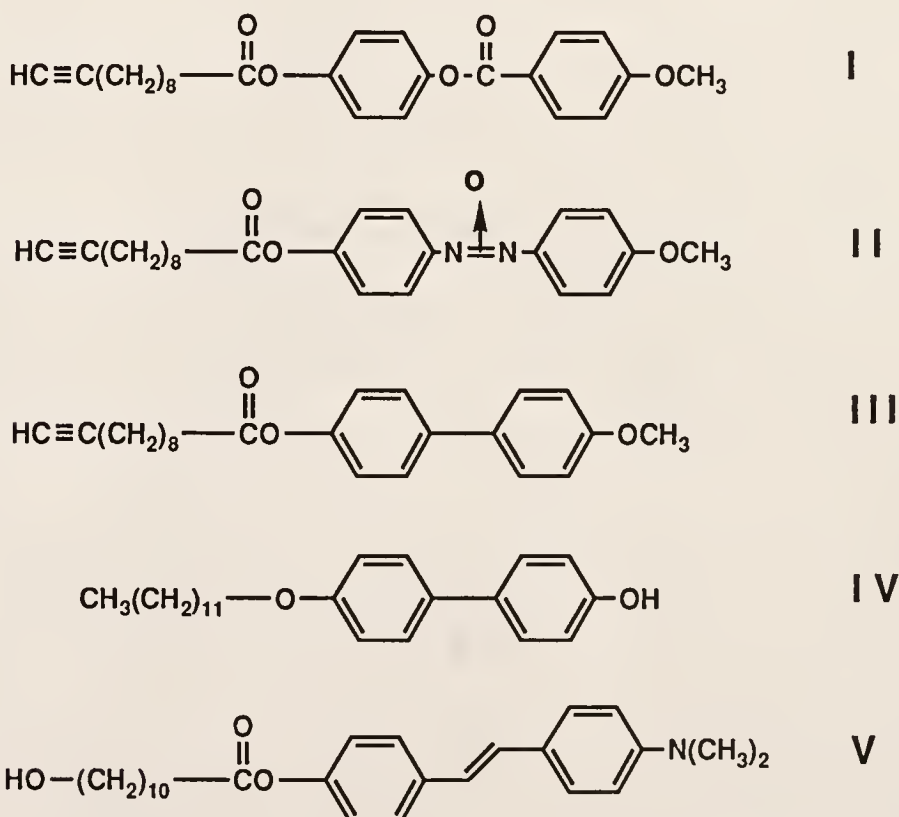


Figure 3-1. Chemical structure of Compounds I, II, III and the interactants IV and V.

The study of compound III was mainly done by another doctoral thesis candidate M.J. Roberts and references to this work will be confined to parts which are relevant for understanding the overall behavior of this class of monomers.

The detailed synthesis of the monomers is described elsewhere.¹⁴³ In general, the monomers were synthesized by the condensation of acetylenic chloride and mesogenic alcohol. The schematic diagram of the reaction is shown below:

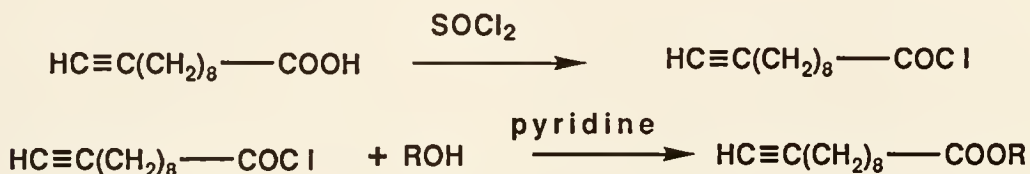


Figure 3-2. General synthetic route for the monomers. Shorter alkynoic acid derivatives have also been synthesized by Blumstein et al.

Table 3-1. Thermotropic behavior of the liquid crystalline monomers in bulk as determined by Blumstein and coworkers.

Compound	Heating	Cooling
I	C 38.38 N N 71.93 I	I 67.32 N N 42.19 C
II	C 96.23 N N 102.97 I	I 97.24 N N 75.83 C
III	C 76.71 I	I 65.56 N N 52.01 C

Table 3-1 shows the transition temperatures of the compounds upon heating and cooling as observed by optical microscopy and DSC. From the table, it can be seen that both compounds I and II show enantiotropic behavior while III shows a monotropic behavior. All mesophases obtained with these monomers are nematic with characteristic "schlieren" textures, as observed by optical microscopy. Small transition enthalpies ΔH_{IN} (typically 0.2 - 0.4 cal/g) and entropies ΔS_{NI} of 0.3-0.4 show "classical," i.e. noncybotactic nematics. Based on these results, the following order in promoting liquid crystallinity can be assigned:

$$\text{II} > \text{I} > \text{III}$$

Langmuir Monolayer Film Studies

Surface Pressure-Area Isotherms

Plots of surface pressure versus mean molecular area as shown in Figure 3-3, were done for both compounds under study. For compounds I and II, at ambient temperature, the surface pressure onset occurred at mean molecular areas (Mma) of 16 \AA^2 and the apparent collapse pressures were very low. Two transitions were observed for compound I, at $\Pi = 8$ and 20 mN/m . All the isotherms were reproducible within $\pm 1 \text{ \AA}^2/\text{molecule}$ in area.

The monolayers were observed to be viscous as evidenced by the deflection of the Wilhelmy plate especially on a one barrier trough compression. Even though the isotherms were very reproducible, consideration of the chemical structure of the monomers suggests that this onset is too small to correspond to the formation of a true two dimensional monolayer. Both monomers consequently showed poor hysteresis behavior in monolayer compression and expansion cycles.

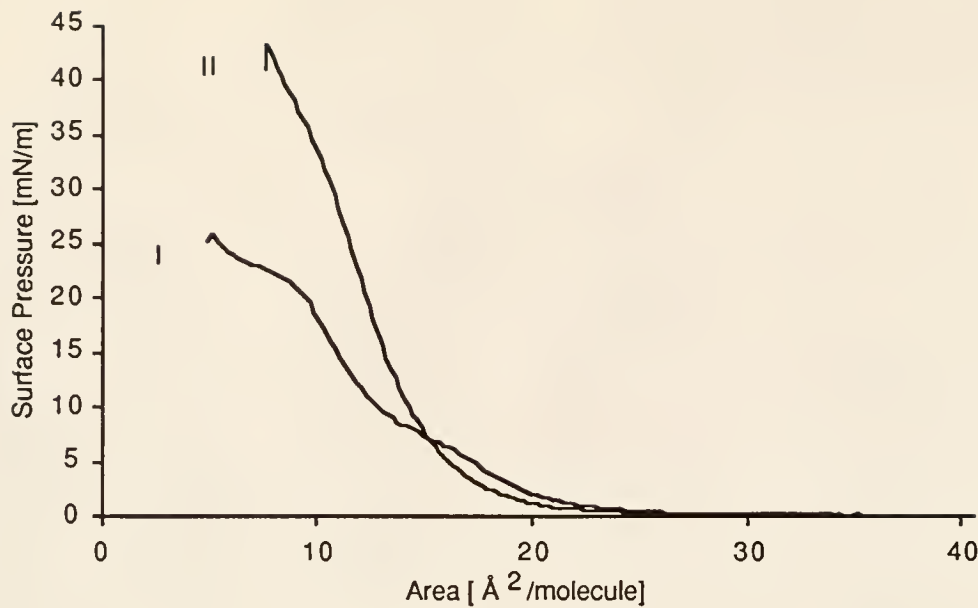


Figure 3-3. Isotherms of pure compounds I and II at 25 °C and compression speed of 3.5 Å²/(molecule x min). Note the two inflection points observed for the isotherm of compound I.

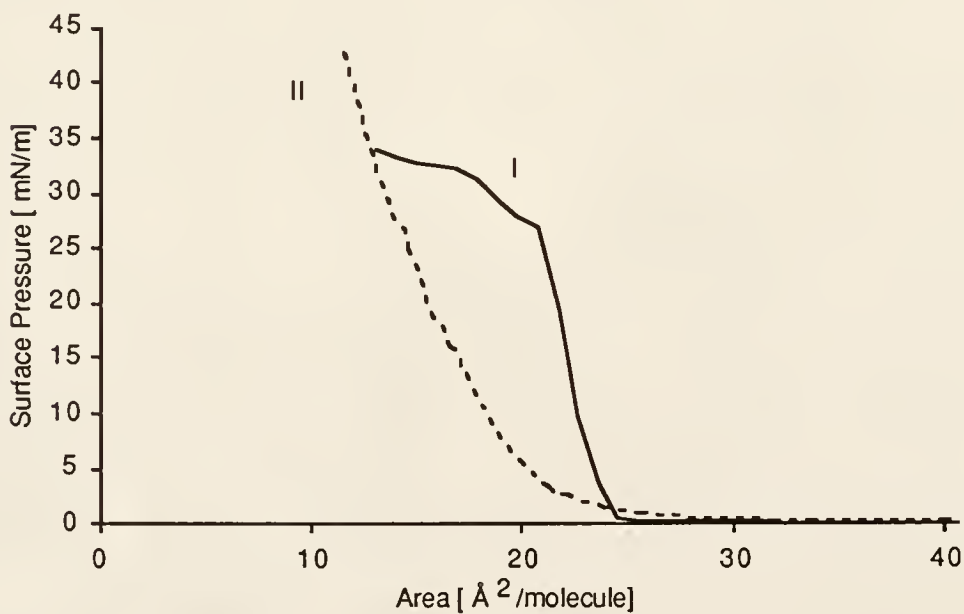


Figure 3-4. Monolayer behavior at lower temperature (16 °C) for compounds I and II. Note the change in area (Mma) and the shift of the inflection points for compound I

Figure 3-4 shows isotherms recorded at lower temperatures for the two monomers. It is apparent that at lower temperatures, greater onset M_{ma} (higher than 20 Å²) values are obtained and the collapse pressure increased substantially. This exothermic behavior is accompanied by an increase in the Π for both transitions of compound I which shifts from the shoulders at 8 and 20 mN/m to distinct inflection points at 25 and 30 mN/m respectively at 16 °C. The onset M_{ma} values are more reasonable in view of the chemical structure of the monomers.

Stability of the monolayer.

For good deposition of the liquid crystal on a substrate, the formation of a stable monolayer is essential. A monolayer is considered stable when it displays a steady M_{ma} at constant surface pressure over a large time scale. Stability studies versus time showed that the films of compounds I and II are not stable over long periods of time (>30% loss in 10 minutes) at 16 °C and 15 mN/m, although they show better hysteresis as compared to higher temperatures and are reproducible. In general, the lower temperature runs were characterized by more reasonable M_{ma} values in the condensed phase region and more stable monolayers, but not stable enough for multilayer depositions.

In order to improve the stability of compounds I and II, two approaches were explored: the effect of repeated expansion and compression, and the effect of mixing other compounds which could act as "stabilizers".

After repeated expansion and compression of the films, an increase in the stability over time is observed for compounds I and II. One drawback of this approach though, is the apparent loss of material due to dissolution,

evaporation, or changes in ordering (e.g. crystallization, local bilayer formation, etc.) over an extended period of time. It takes five cycles of expansion and compression to produce a reasonably stable film even at low temperatures. Another drawback is the decrease in Mma and collapse pressure values after expanding and compressing.

Several experiments were also performed on mixtures of the compounds. Mixing the monomers with either compound IV or V often increased the stability of the resulting monolayer film. However, since polymerization of the acetylenic compounds is desired, the amount of the "monolayer stabilizer" has to be minimized. Isobaric creep measurements showed that blending of compound I or II with 9 mol% of compound V was sufficient to stabilize the films. The isotherms did not follow the additivity rule for the above compositions, which is indicative of miscibility.⁸⁵ Initially, compound IV was used for both I and II. Even at 50 mol % of the stabilizing compound the resulting film was not stable and apparently no real mixing occurred. When compound V was used as a stabilizer with I and II, a minimum of only 9 mol % was necessary to produce a stable film.

The combination of I or II and V produces a stable film. This behavior might be due to a greater degree of intermolecular π -orbital overlap between the aromatic rings of the mesogenic groups.^{146,138,147} In general, much higher Mma values were obtained for the condensed phases of the compounds in blends with compound IV and V. The stability of compounds I and II with compound V at constant Mma was greater than that found for pure I and II.

A similar study using stearic acid with compounds I and II gave analogous results to blends with IV. In general, by varying the mole ratio of the mixtures and careful choice of "interactant" one can have the stability characteristic of a more stable compound. No detailed mixing studies were

done, in particular to higher ratios (results in less reactive functional groups per area) as the use of the interactant was minimized to that of stabilizing the monolayer.

Brewster Angle Microscopy

Brewster angle microscopy of compounds I and II were done at both ambient and low temperatures. As has been observed from the isotherm measurements, no true monolayers were observed with the pure compounds. At high areas, before the onset pressure rise to the condensed phase of the isotherm, small domains or aggregates were observed "floating" within the field of view of the microscope. This is a clear indication of the nonhomogeneous nature of the monolayer at high areas. As spread, the liquid crystalline materials tend to form local aggregates which form a very viscous film upon compression. The aggregates were observed to be birefringent by the use of an analyzer rotated at 10°/min. The nonuniform intensity within the domains signify the different local tilt angles of the molecules within the domain. Both Compounds I and II exhibited this behavior but the formation of larger and more uniform domains is stronger with compound II. At lower areas, the domains are observed to fuse together forming a homogeneous film, again more evident with compound II. Compression beyond the collapse pressure results in a heterophase film for compound I. This phenomenon was similar in both ambient and low temperatures. No pictures were taken of the mixed Langmuir film due to lack of material.

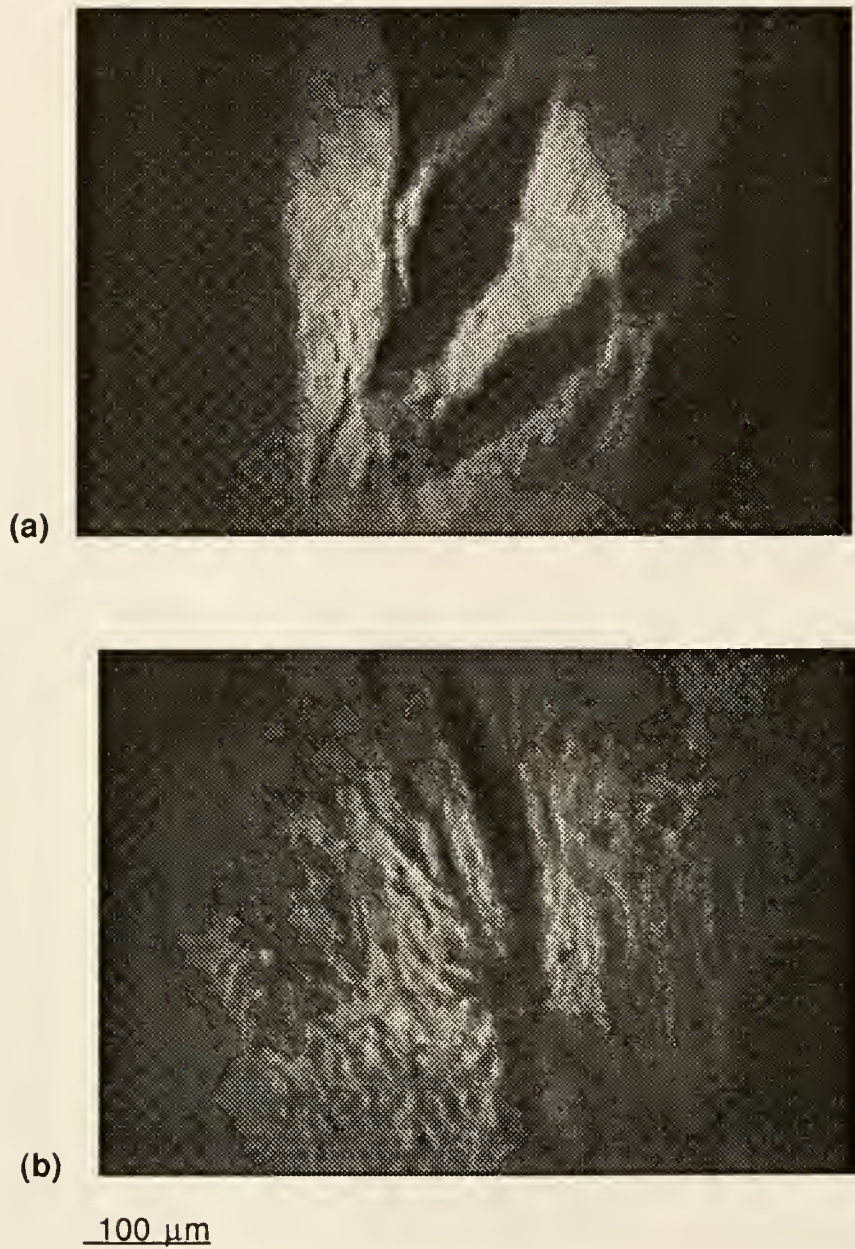
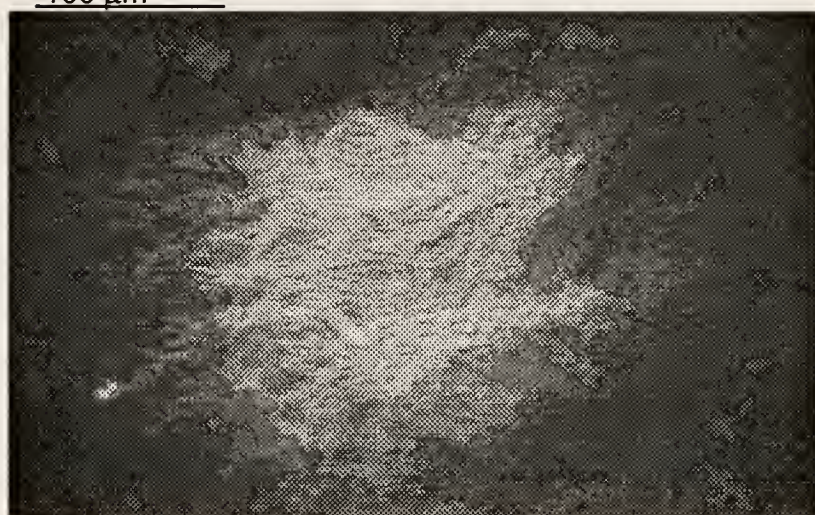


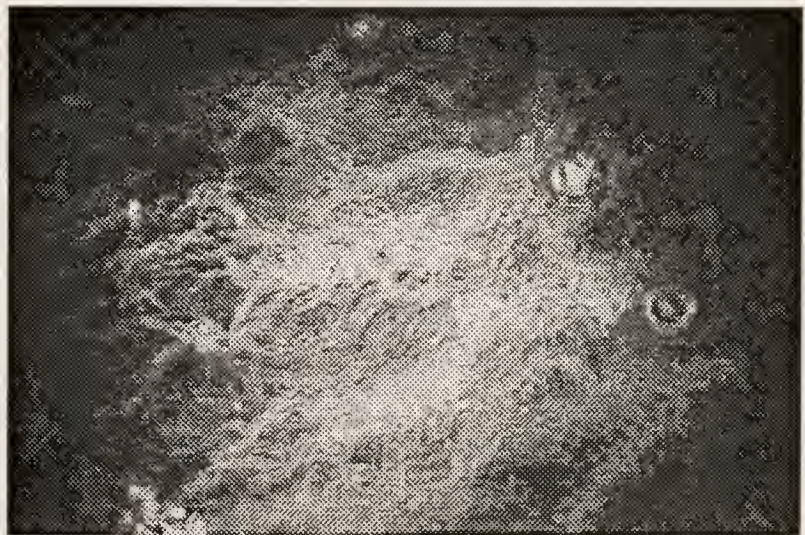
Figure 3-5. Brewster Angle Microscope pictures of Compound I at 11°C
(a) 40 \AA^2 , (b) 30 \AA^2 , (c) 25 \AA^2 , (d) 23 \AA^2 , (e) 22 \AA^2 /molecule
(refer to isotherm in Figure 3-4)



(c)

100 μm

(d)



(e)

Figure 3-5 (continued)

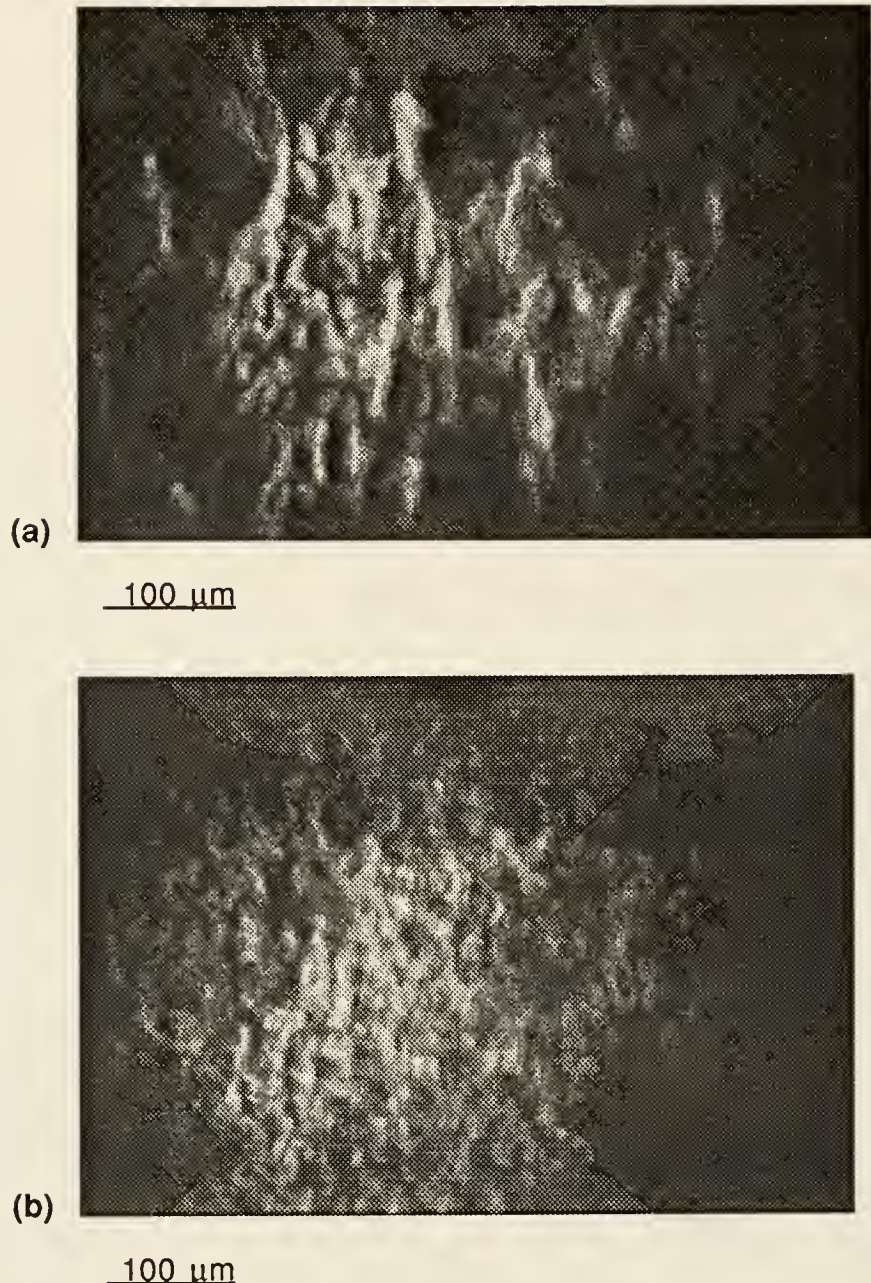
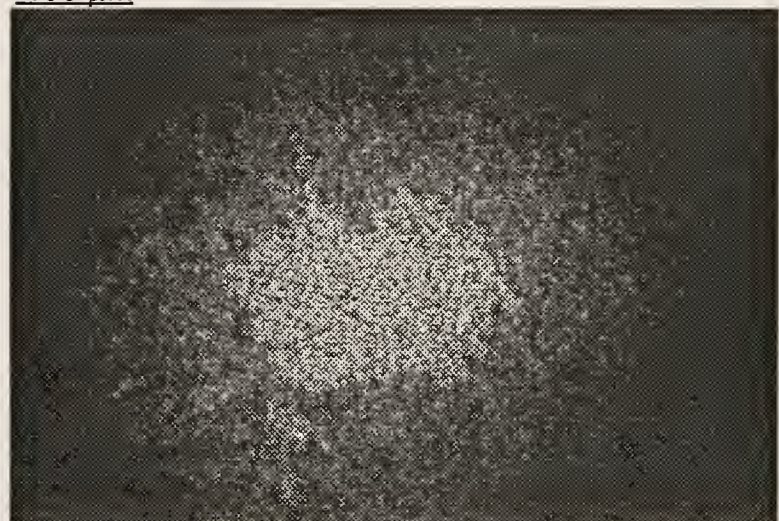


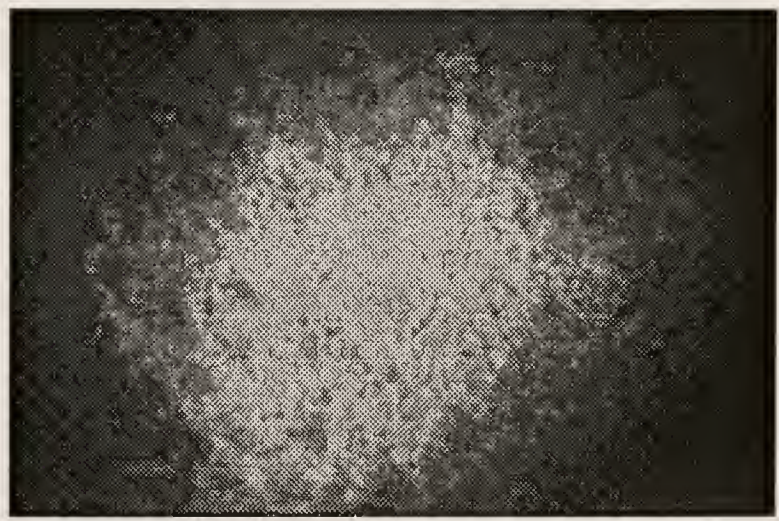
Figure 3-6. Brewster Angle Microscope pictures of Compound II at 11°C
(a) 40 \AA^2 , (b) 30 \AA^2 , (c) 20 \AA^2 , (d) 15 \AA^2 , (e) 12 \AA^2 /molecule areas.
(refer to isotherm in Figure 3-4)



(c)

100 μm

(d)



(e)

Figure 3-6 (continued)

Analysis of Results

The amphiphilic nature of the monomer is in competition with the interaction of the monomers with each other. This serves as a driving force towards the formation of domains of the monomer as initially spread at the interface (positive ΔH). It was necessary to break up this domain formation in order to orient the reactive acetylene group for polymerization. The nature of the amphiphile based on the results is that of a stronger van der Waals interaction between the molecules themselves. Some mesogenic moieties can be presumed to predominantly lay flat at the interface with the alkyl part free to rotate as long as the acetylene group (which is slightly polar due to the electron rich π -cloud) is not hydrated by water molecules.^{147,138} Some molecules would also be not adsorbed at all. The observed mean molecular area supports this observation since a lower apparent area indicates less molecules are adsorbed per Mma than calculated. This indicates that some of the molecules are laying flat on each other or are actually forming three dimensional domains. In this case, the effect of lowering the temperature seems to result in forming more order within the domains with preference towards orthogonal orientation. This is consistent with the higher mean molecular area observed at lower temperatures. Nevertheless the film still remained unstable for deposition. The Brewster Angle Microscopy (BAM) pictures verified a nonfluid ordered birefringent layer for the pure compound as spread in both ambient and low temperatures. Larger, but more homogeneous domains are observed to form at lower temperatures. It is possible that the difference in size and increased ordering at lower temperatures is brought about by the spreading solution (chloroform), remaining longer at the interface. This would then increase local

ordering and allow the formation of much larger domains due to slow evaporation of solvent. Thus, greater ordering is induced at lower temperatures.

The problem of stability was partially solved by blending with a minimal amount of amphiphilic interactant. In this case, the surfactant properties of the interactant amphiphile are enough to induce stability in the monolayer. This is also reflected in the non-additivity of the isotherms.⁸⁵ The resulting film had better Langmuir monolayer film properties in which LB films were subsequently built. No detailed mixture studies were done, since the only interest was to allow the deposition of the monolayer to substrates. And since only a minimal amount was used, it was regarded as not enough to effectively hinder polymerization.

LB Film Deposition and Characterization

Deposition

Multilayers of stable blends of both compounds were successfully deposited on quartz substrates at low temperatures. Transfer of the monolayers was done at an applied surface pressure of 15 mN/m for the blends I + V and II + V since peeling off is observed at lower surface pressures and the film is not adequately stable at higher surface pressures. During the depositions, the transfer ratio was recorded. The transfer ratio (TR) gives an indication of the quality of the dipping process and ideally should be unity. It is found that Z-type films (upstroke) were formed for the blends of all three compounds using both hydrophilic and hydrophobic quartz substrates with the exception of II + V blend. A maximum of 28 layers was deposited for the II + V blend and 32 layers for the I + V blend. The blend II + V tends toward a Y-type deposition after the first 3 Z-type layers are deposited on a hydrophilic substrate. The blend I + V begins as

a Y-type and trends toward a Z-type deposition after the first two layers on a hydrophobic substrate. Two deposition attempts were made for both and the observations were confirmed.

UV Spectra of LB Films

No absorption bands were observed below 200 nm due to the absorption of air at this range so that the $\pi-\pi^*$ transition of the acetylenic moiety is not observed by UV (normally at 173 nm). Absorptions between 240 to 260 nm for the forbidden transitions of the benzene rings in the mesogenic group are observed. The band observed at the 320 nm region for compound II is due to the azoxy chromophore conjugated to two benzene rings.

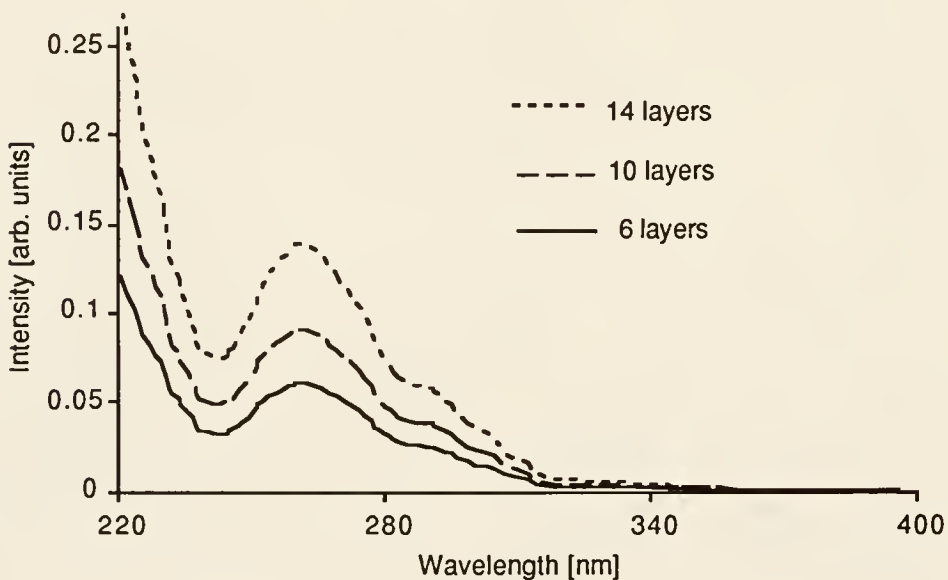


Figure 3-7 .UV of I + V LB Film showing additive effect of putting more layers on the substrate.

No significant difference was observed between the spectra of the pure compounds and the blends since only a minimal amount of the "stabilizer" was

added relative to the pure compound. In general, the absorption spectra of the multilayers shows the additive effect of increasing the multilayers on increasing the intensity of the absorbance. No polarized UV-vis spectra set-up was employed.

X-ray of LB Films

Langmuir Blodgett films of I + V (32 layers) and II + V (28 layers) blends gave Bragg reflections in the X-ray diffractometer from which d-spacings (layer thickness) were calculated. These reflections are attributed to the stacking period of the layers. There was a correlation observed between the dipping behavior of the blends and the observed layer thickness as calculated from the diffractogram.

For blend I + V, a first order reflection was observed at an angle of 3.3 degrees. No peak corresponding to twice the d-spacing was observed at smaller angles. This corresponded to a layer thickness of 26.7 Å for the monolayers deposited at the substrate which is consistent with a unidirectional z-type deposition (head to tail packing) as observed for blend I + V. The difference from the calculated length of the molecule of approximately 30 Å could be attributed to tilting of the molecule. Other models could also be made which could account for kinks, dipole repulsions, and interdigitation along the long molecular axis.

For blend II + V, two reflections were observed in the small angle region at angles of 1.58 and 3.32 degrees and strong and medium intensities respectively. These reflections corresponded to the first and second order reflections of a stacking period of 55.86 Å. This is again consistent to the observed dipping behavior of blend II which would correspond to a Y-type head

to head or tail to tail packing of the monolayers. Since the calculated thickness of a straight molecule was 30 Å, this could also correspond to a certain extent of tilting or overlap on the part of the monolayers. Tilting is plausible as the Mma for the blend of II + V at deposition was 28 Å² compared to an ideal packing of 22-25 Å² for compounds of this type. The absence of second order peak for I + V and higher order peaks for both blends shows the lack of long range ordering within the multilayers. However, it is not known if these reflections were simply not observed due to limitations in the instrument as no measurements were made using small-angle X-ray scattering (SAXS) with a rotating anode source.

Polymerization of LB Films

Polymerization

Two methods were explored to polymerize the monomer blends. The first method involved irradiating the monolayer on the trough under air or nitrogen atmosphere. The other was by irradiation of the LB film.

Monolayer polymerization attempt at the air-water interface

Polymerization at the air-water interface was attempted, analogous to polymerization of diacetylenes.¹⁴⁸ A high pressure quartz mercury vapor arc lamp was used with a spectral range of 189 nm-400 nm (Hanovia Utility Model lamp, 100 watts, U-shaped quartz mercury arc tube). The procedure used for both blend films (I+V and II+V) is as follows:¹⁴⁹ The monolayer was first compressed to the desired pressure (5 and 15 mN/m) and equilibrated for 30 minutes. The change in Mma with time was recorded for another 30 minutes. The film was then exposed to the UV lamp at the desired exposure time (5, 10, and 15 min. for three different trials) and the change in Mma vs. time was

likewise recorded. No noticeable change was observed with the slope of the Mma vs. time as compared to unexposed film. Likewise, expansion and recompression after the exposure also did not show any noticeable difference from a similar procedure with the unexposed film.¹⁵⁰ Collecting the monolayer film by suction filtration and redissolving in chloroform followed by UV-vis analysis gave the same UV-vis spectra as the monomer. Since the presence of oxygen could limit the polymerization in air, for the next attempt, the whole set-up was enclosed in a plastic glove bag with a constant stream of N₂ gas passed to maintain a positive pressure. Maintaining the film at a pressure of 10 mN/m for both films, the results were evaluated using similar procedures described earlier. No polymer was again obtained using this set-up. From here on no further attempts were made to polymerize the monolayer film at the air-water interface. More detailed studies of this in-situ polymerization of monoacetylene monomers will be continued by another graduate student, M.J. Roberts for his dissertation.

Polymerization of LB Films

In the second method, the Langmuir-Blodgett monomer films were exposed to a ⁶⁰Co γ -ray source. All the blend films of I, II, and III were exposed to γ -irradiation with an approximate dosage of 160 Mrad (assistance in set-up provided by Dr. Hanrahan, Department of Chemistry). Decolorization was observed on the quartz slides typical of exposure to γ -irradiation. Molecular weight of the polymers were analyzed by Gel Permeation Chromatography (GPC) calibrated with polystyrene standards from 6200 - 65,000 g/mol in THF.

The GPC data showed that the deposited III + IV blend reacted to give 21% conversion. A bimodal peak showed a large amount of oligomers with approximately 10 repeat units long, along with very much smaller portions of

high molecular weight polymer. Using the same conditions with the II + V blend, two polymerization attempts were made with 20% and 1% conversion respectively with an average number of repeat units of 54 ($M_n = 22,600$ $M_w/M_n = 2.4$). For the I+V blend, only monomer with some degradation products was found with both trials.

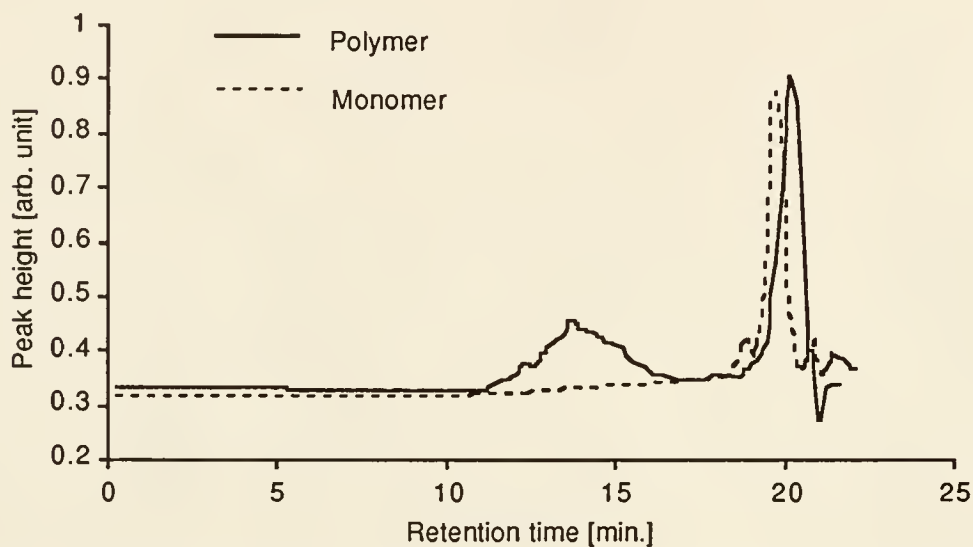


Figure 3-8. Gel Permeation Chromatography of polymerized II + V Film using polystyrene standard for calibration. The monomer peak is shown for comparison.

The difference in reactivity is not clear although X-ray investigations show slightly better ordering of the II+V blend film with the presence of two Bragg peaks. In general, the percent conversion is higher than that found with bulk polymerization for II and III monomers. Not enough material though was collected for NMR spectroscopy, which would have determined the microstructure of the backbone as well as any degradation products.

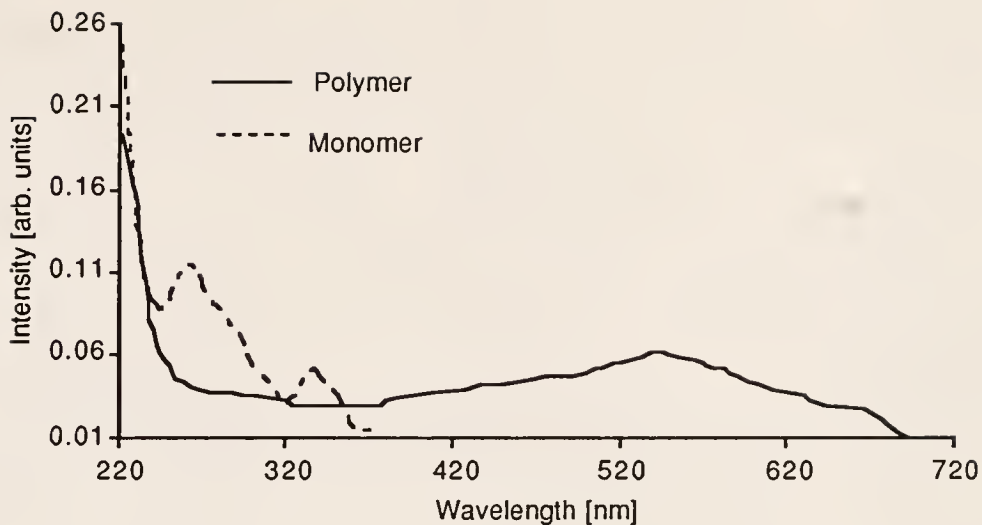


Figure 3-9. UV-vis spectra of the II + V LB film before and after polymerization

Examination of the UV-vis spectra of the II + V multilayer after irradiation showed a broad peak at the 550 nm with a range of 300-700 nm in the base. No peaks were observed though at the 320 nm region as in the UV-vis of the original monomer blend LB film. This could be indicative of a degradation reaction which destroyed the azoxy chromophore in the process. The spectra of the I + V LB film was not significantly different from that of the original.

Analysis of Results

The polymerization at the air-water interface was largely limited by experimental set-up and availability of the right light source. It is known that polydiacetylenes are readily formed by UV-light irradiation of the diacetylene monomer at the interface.¹⁵¹ The favorable condition is due to the higher wavelength absorbance of the reactive diacetylene group. In comparison, the monoacetylene functional group has an absorption of 187 nm near the vacuum-

UV range. It was hoped that a broad spectrum UV-light source will be capable of reaching down to the minimum excitation wavelength for acetylene or generate a radical initiator.¹⁵² However, due to absorption of air, the amount of light that reaches the monolayer below 200 nm is always minimized. Furthermore, the effect of oxygen (positive or negative) is unknown. The use of high energy light source such as X-ray or KrF excimer laser light is not possible with our Langmuir trough set-up.¹⁵³ Much is needed to be done to maximize the possibilities of this approach. No further approach was taken with regards to this direction. However, this initial approach has shown the limitations and possible directions towards realizing polymerization of monoacetylenes at the interface. The most viable approach may be that of chemical modification on the functional group by the attachment of moieties that will increase the wavelength absorbance of the functional group, e.g. attachment of a phenyl or anthracene ring to the acetylene.¹⁵⁴ Another is the use of photosensitizing agents that are capable of providing initiators for the polymerization of acetylene.¹⁵⁵

The polymerization of LB films proved to be more successful although the results were not conclusive for the I + V blend since no polymer was obtained with two attempts. On the other hand, with the II + V blend, a 21% conversion was observed with a UV-vis λ -max of 550 nm indicating the formation of the conjugated double bond. The disappearance of the absorption band at 320 nm indicated secondary reactions which could only mean the loss of the azoxy group and other absorbing groups with the polymerization. The absorption at 550 nm is particularly significant in contrast to earlier work on ω -tricosynoic acid which gave only a small absorbance change.¹⁵³ It is not apparent why the II + V blends gave a 21% conversion whereas the I + V blend did not. The most obvious difference being on the order observe with X-ray and the type of

deposition. In principle, the II + V blend forming a Y-type film will have the opportunity for greater contact between functional group. The head to head type of deposition allow interdigitation of the head groups giving a greater density of functional groups. Likewise, polymerization of the III + IV blend was also successful. The III + IV film being more inherently stable than the two could have better orientation of the functional group so that even with a Z type deposition, it gives a comparable degree of conversion as the Y-type II+V blend. It is possible that this greater order is a direct consequence of stability owing to a more favorable conformation of the phenyl rings.¹³⁸ These results, show the potential of this approach with this class of monomers.

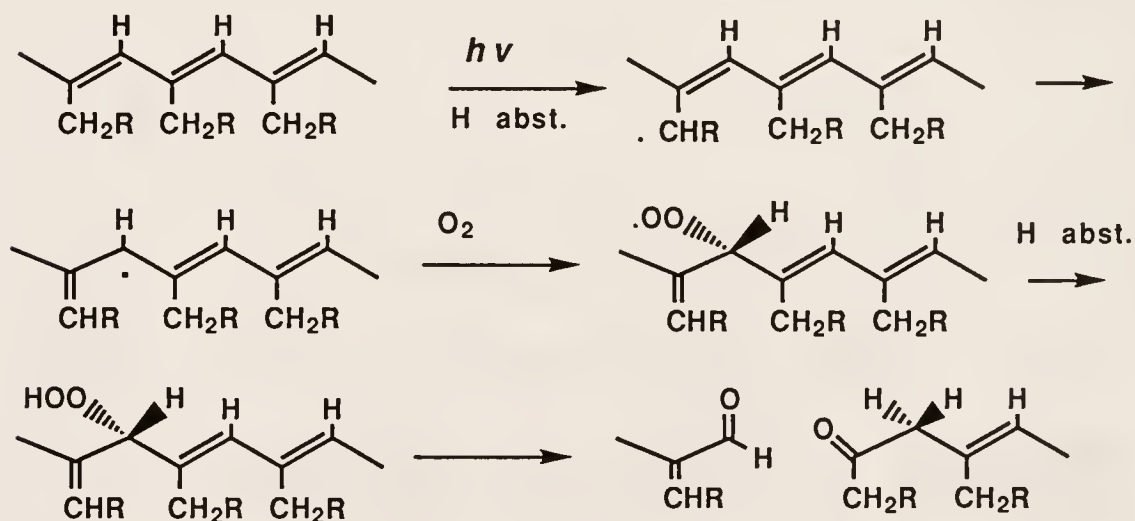


Figure 3-10. Possible mechanism of polymer backbone degradation with the formation of allylic radical and the presence of oxygen.

The possible effect of oxygen on the reaction and the subsequent secondary reactions within the mesogenic group could have limited the yield for the reaction. The effect of radical oxygen on the polyacetylene double bond has been investigated previously.¹⁵⁶ Main chain scission and cross-linking are possible depending on the nature of the substituent.¹⁵⁷ Figure 3-10 shows

a possible degradation mechanism. This involves the main-chain scission at the allylic position by UV irradiation and formation of an allylic radical. A double bond rearrangement transfers the radical into the main chain. This leads to the formation of a hydroperoxide by reaction with oxygen with the radical and subsequent formation of the carbonyl groups (via dioxatane ring formation). Another variation is direct excitation of the double bond in the main chain especially for polyacetylenes without the allylic hydrogen.

The formation of other reactive species could also possibly explain the lack of polymeric products after the air-water interface reaction. Since ozone can be formed readily with UV-light interacting with oxygen in the air and near the subphase, this could react with double bonds (ozonolysis), effectively disrupting the formation of any polymer.¹⁵⁴ The limiting effect of the domain size and shape in the polymerization is also unknown. This may be the case with the polymerization of the II+V blend which on one occasion gave 21 % and the other 1%. The variable size and shape would lead to much less than ideal orientation of the monomers for polymerization. It is possible that the monomers, although not oriented with the long axis orthogonal to the interface, would have domains that allow for enough local distance and orientation to let the functional groups react within a domain. The effect of the added order to the domain by the spreading at the interface, can be compared to the polymerization in bulk of the same monomer. Bulk polymerization of the isotropic liquid state only gave 2% conversion as reported by Blumstein and coworkers using the same dosage of γ -radiation.¹⁴³ This indicates the added order in the domain is induced by spreading at the interface as compared to bulk three dimensional domains. Other characterization techniques to determine the extent and resulting tacticity of the reaction was not done for lack of material.

Summary

This work has shown that it is possible to polymerize ordered LB multilayers of the monoacetylene monomer to form substituted polyacetylenes. The liquid crystalline monoacetylene allowed ordering of the monolayer at lower temperatures and with the use of an interactant. LB film deposition was possible for such monolayers with good stacking properties and sufficient lateral ordering. While polymeric products are formed as shown by UV and GPC, degradation of the side groups probably occurred because of the high energy mode of initiation. Better polymerization geometries and functional groups are therefore needed in order to maximize the technique. This could possibly be done by chemical modification of the reactive functional group and the use of reactive initiators that are easily formed at ordinary conditions.¹⁵⁸ Further investigations in this approach will be carried out by M.J. Roberts for his dissertation work. The next chapters will then be focused on the preformed polymer approach for substituted polyacetylene films.

CHAPTER 4

APPROACH II A : POLY(ETHYNYLBENZOATE ESTER) POLYMERS

Introduction: Design of Polymers

The semi-rigid nature of the double bond-single bond polymer backbone confers unusual properties which allows the possibility of conformational changes leading to a more planar and conjugated structure. To date, most studies have been made on the chain dynamics of flexible main chain type polymers at the air-water interface.^{113,100} In this study, the Langmuir film behavior of a series of substituted polyacetylenes shown in Figure 4-1 was investigated at the air-water interface in order to study the effect on the local conformational behavior of each polymer with a view towards enhancing the planarity of the main chain. In addition, a series of polymers similar to Polymer 1, with different alkyl chain lengths, were studied to observe film behavior dependence with chain length. The stiffness and length of the lateral substituent is increased systematically by a combination of phenyl and alkyl groups. Long alkyl side chains are expected to decouple polymer-polymer interactions and thus aid in solubility. The polar carboxylic groups are expected to facilitate hydrophilic interactions with water.^{159,105} In principle, the right balance of substituents should give the desired monolayer behavior. Complimentary to the Approach I study in Chapter 3, this and the following chapter concentrate on the manipulation of preformed polymers at the air-water interface towards ordered structures.

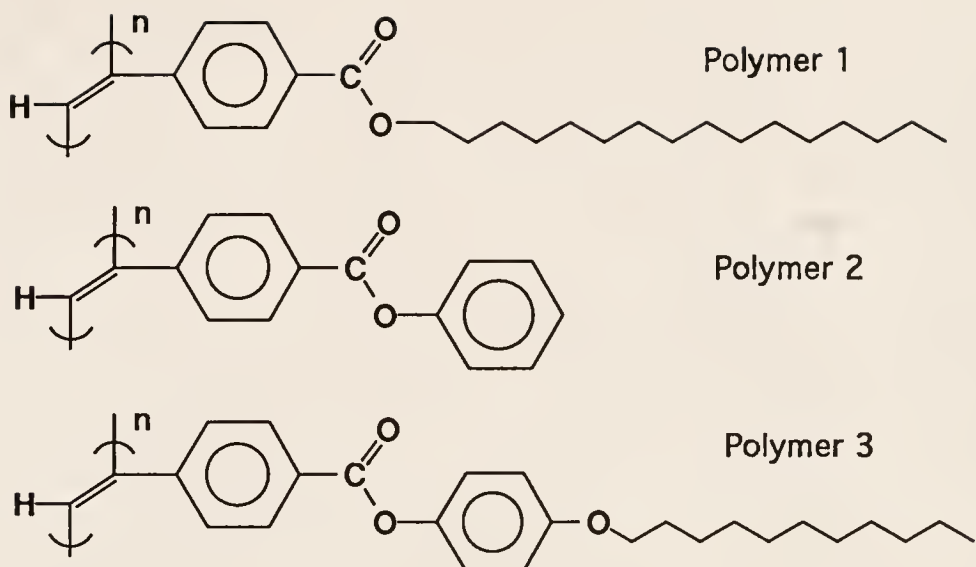


Figure 4-1. Poly(ethynylbenzoate) polymers: Polymer 1, poly(hexadecyl-*p*-ethynylbenzoate); Polymer 2, poly(phenyl-*p*-ethynylbenzoate; Polymer 3, poly(*p*'-decyloxyphenyl-*p*-ethynylbenzoate)

The polymers shown above were synthesized from a series of esters of *p*-ethynylbenzoate prepared using the metathesis catalyst WCl₆. These polymers were prepared in an effort to observe substituent effects on the "stiffness," microstructure, and conjugation efficiency of the polymer backbone. Comparison was made between polymers with alkyl, phenyl, and alkoxyphenyl groups attached to the *p*-ethynylbenzoate. The synthesis and physical properties of these polymers will be described. The results will be discussed in terms of the configuration and conformation adopted by the polymer in the bulk and monolayer films. Lateral substitution is therefore expected to influence the conformation of the polymer at the air-water interface. The Langmuir technique can induce the polymeric chains to form highly ordered anisotropic films by confining them to a quasi two-dimensional conformation.¹⁶⁰ At the same time, more planar local conformation should be induced by the lateral pressure during compression and the conjugation length should be increased.

Synthesis of Monomers and Polymers

Figure 4-2 shows the synthetic route used for the preparation of the homologous series of p-ethynylbenzoate esters with p-alkoxyphenols of different chain lengths. The phenyl and alkyl substituted material were prepared in the same manner:⁴⁷

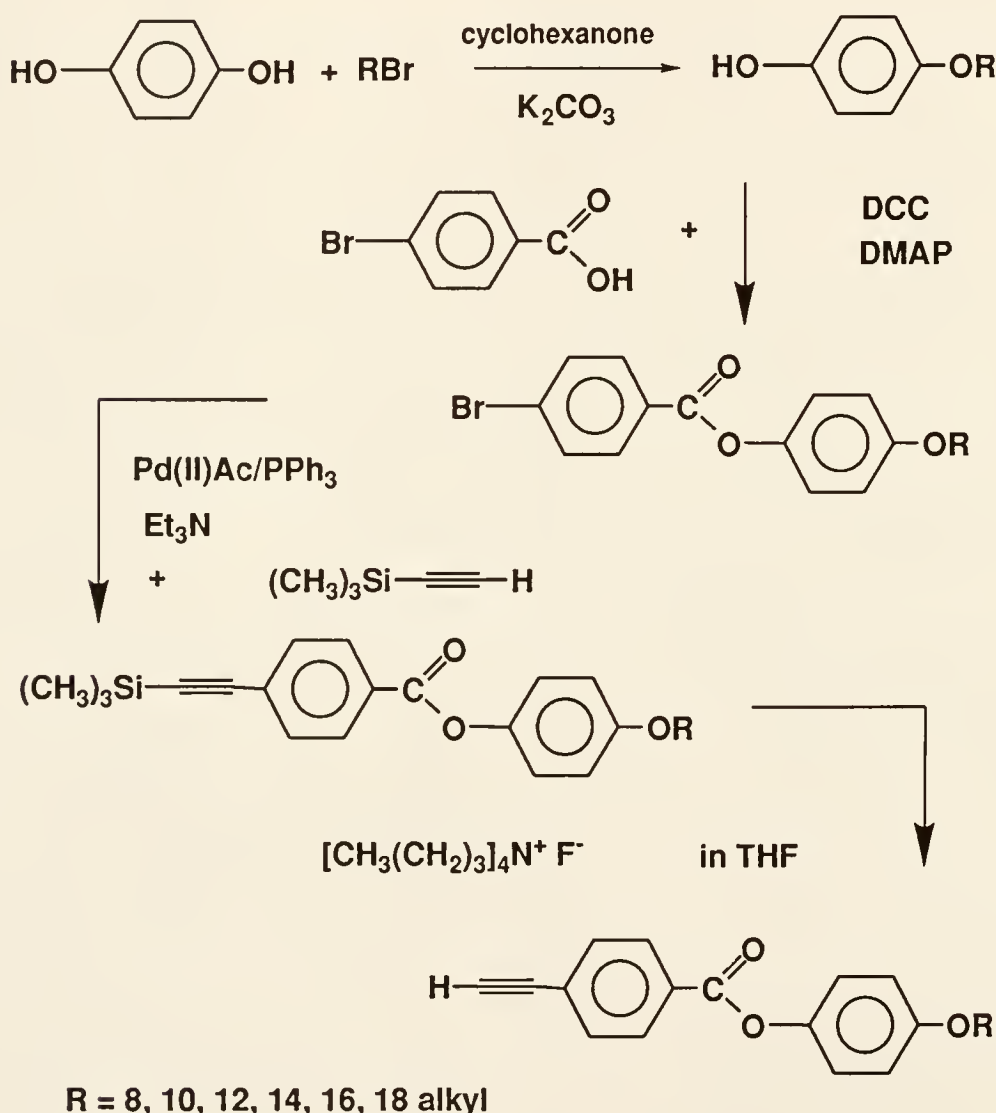


Figure 4-2. Synthetic scheme for the synthesis of the monomers utilizing a palladium coupling reaction to attach the acetylene to the phenyl ring.

The phenols were synthesized from the base-catalyzed reaction of hydroquinone and alkylbromide in cyclohexanone. This was followed by esterification of the purified product with p-bromobenzoic acid using dicyclohexylcarbodiimide (DCC) and 4-N-dimethylaminopyridine (DMAP) in methylene chloride.¹³¹ The resulting ester was then reacted with trimethylsilylacetylene (TMSA) using a Pd(II)Ac/PPh₃ catalyst system in triethylamine to produce an ethynyl benzoate derivative with a silyl group attached. The silyl group was subsequently removed by using tetrabutylammonium fluoride in THF.¹³²

The purified products were yellowish solids and were soluble in a range of organic solvents depending on the alkyl chain length. Elemental analysis results were in good agreement with calculated values for the proposed structures (see Experimental Section). DSC and optical microscopy revealed no thermotropic liquid crystalline phases in all the monomers that were synthesized. These monomers will be further investigated for the polymerization of Langmuir-Blodgett films similar to the work in Chapter 3. This will be undertaken by another doctoral thesis student, M. J. Roberts and will not be included in this work.

The polymerization was done with a WCl₆ metal halide catalyst in dry toluene using standard Schlenck techniques under a nitrogen atmosphere;⁵³ The same catalyst system was utilized in preparation of the other *p*-ethynylbenzoate esters shown in Figure 4-2. Only the monomers with alkyl chain lengths of 10, 12, and 14 carbons gave high MW polymers the rest gave low MW oligomers with low yields. The polymerization yields for the high MW polymers averaged around 90%. The polymers were highly soluble in common organic solvents such as chloroform, toluene, THF and formed red-colored solutions. The polymers were insoluble in methanol, which was used to

precipitate the product. Gel Permeation Chromatography using polystyrene as a standard and THF as eluent gave apparent molecular weight values summarized in Table 4-1.

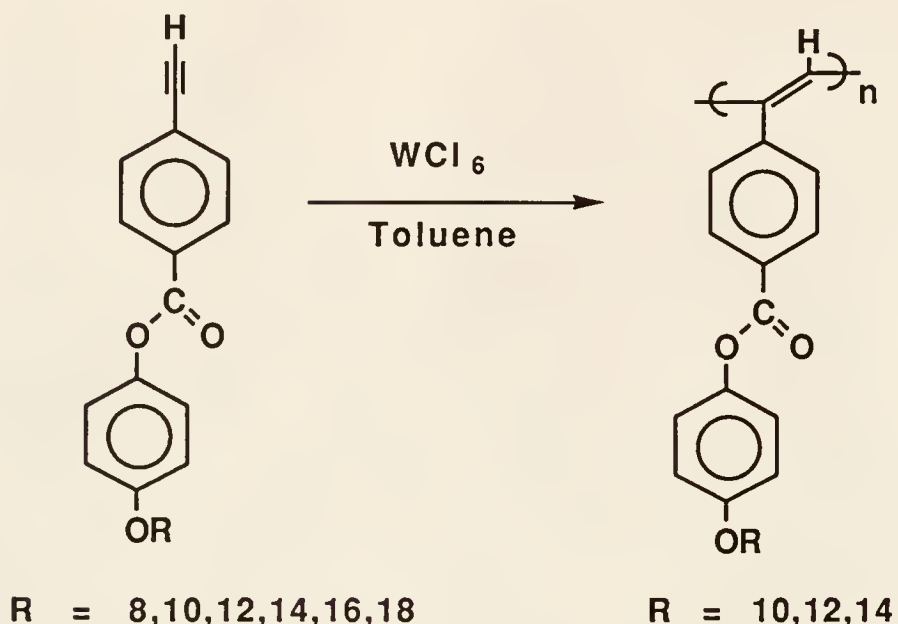


Figure 4-3. Polymerization under N_2 at 35°C using vacuum Schlenck technique.

Table 4-1. Molecular weight of polymers determined by Gel Permeation Chromatography using narrow molecular weight polystyrene standards in THF.

Polymer with Alkyl Chain (R)	Molecular Weight Mw	Polydispersity Mw/Mn	Percent Yield
10	66,500	1.48	89%
12	43,400	1.70	95%
14	82,600	1.69	78%

Details of the molecular weight determination are given in Chapter 2. Elemental analysis was in good agreement with calculated values except for

the 14 carbon derivative (see Experimental Section). Since the 10 and 12 carbon derivatives are very similar in their structure and spectroscopic properties (only a difference of two methylene units), the data on the 12 carbon derivative will be taken as typical. The 14 carbon derivative data will not be included due to the inconclusive elemental analysis (see Experimental Section). The details of the synthesis of Polymers 1 and 2 are reported elsewhere.^{47,37} In general, the products appeared as reddish brown amorphous solids.

Structural Characterization

The UV visible spectra of the polymers (10,12,14 carbon derivatives) in solutions were taken using methylene chloride as solvent. An onset was observed at the 600 nm region and a shoulder around 450 nm for all the polymers. Polymer 3 showed two peaks at 240 and 280 nm corresponding to the phenyl group adjacent to the polymer backbone and to the alkoxy chain respectively. For the same concentration, the *p*-ethynylbenzoate esters of alkyl (Polymer 1) and phenyl (Polymer 2) show similar spectra with higher intensities at the shoulder region and a single peak maxima at 250 nm instead. For all three polymers, a transparent red film of good optical quality can be obtained by casting from a concentrated solution. No significant differences in wavelengths were observed between their solutions and cast films.

The ¹H NMR spectra of the 12 carbon *p*-alkoxyphenyl ester derivative (Polymer 3) is characterized by the disappearance of the peak at 3.3 ppm (terminal acetylenic proton) and the appearance of a broad peak at 7.2 - 6.5 ppm corresponding to the formation of double bonds. This broad peak is due to

a distribution of different conformations of the *cis* or *trans* isomers and peaks of the phenylene protons.¹⁶¹

IR spectra reveals an intense absorption at the 1600 cm⁻¹ region indicating the formation of double bonds. This is coupled by the disappearance of peaks at the 3300 and 2100 cm⁻¹ region which are attributed to the acetylenic group of the monomer (see Experimental Section).

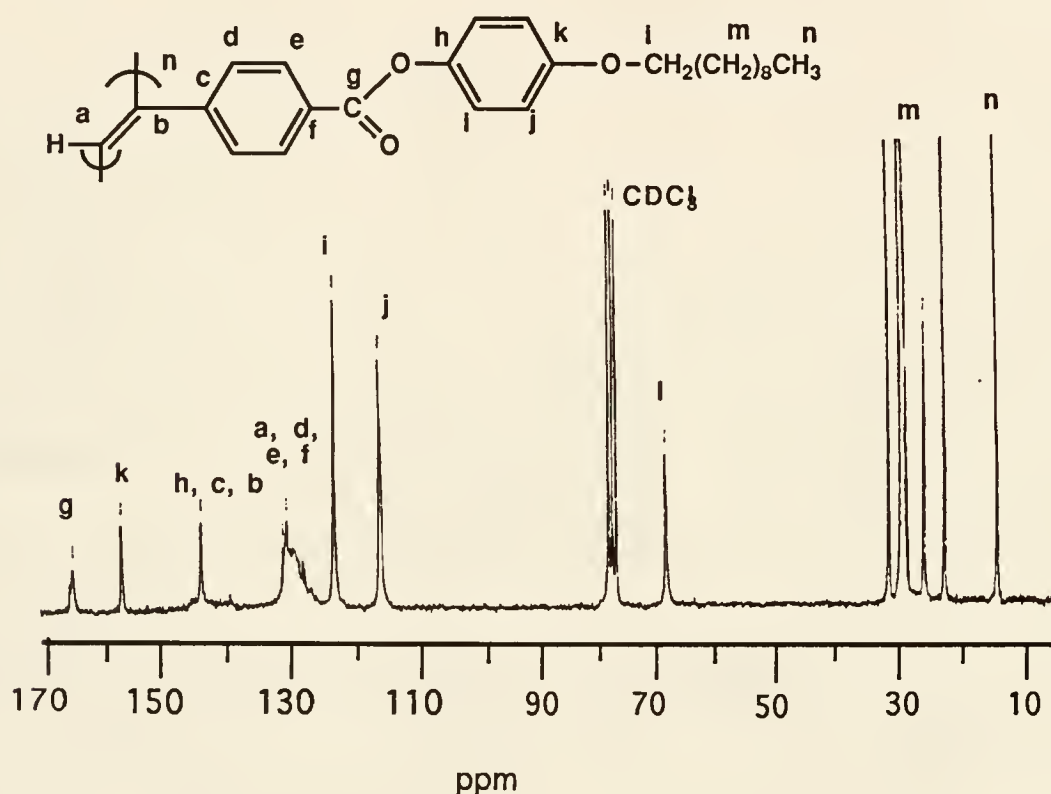


Figure 4-4. ^{13}C NMR spectra of the *p*-alkoxyphenylester derivative (Polymer 3). Also see peak assignment in Chapter 2 (see section on polyethynylbenzoate polymers)

Figure 4-4 gives the ^{13}C NMR spectra of the 12 carbon *p*-alkoxyphenyl ester derivative. The polymer is characterized by the disappearance of the acetylenic carbons at 83 and 80 ppm compared to the monomer. The broad resonance at the 125 to 135 ppm region indicates the formation of the double

bonds. This region is highly important for distinguishing between isomers of substituted polyacetylenes.^{161,162,163,164} The broad peak likely arises from a distribution of conformational and configurational sequences of the polymer (Appendix B). Two resonances are associated with the *cis* and *trans* content of the polymer according to Percec, et al.: the resonances at 132 ppm are for *cis* and 126 for *trans*.¹⁶³

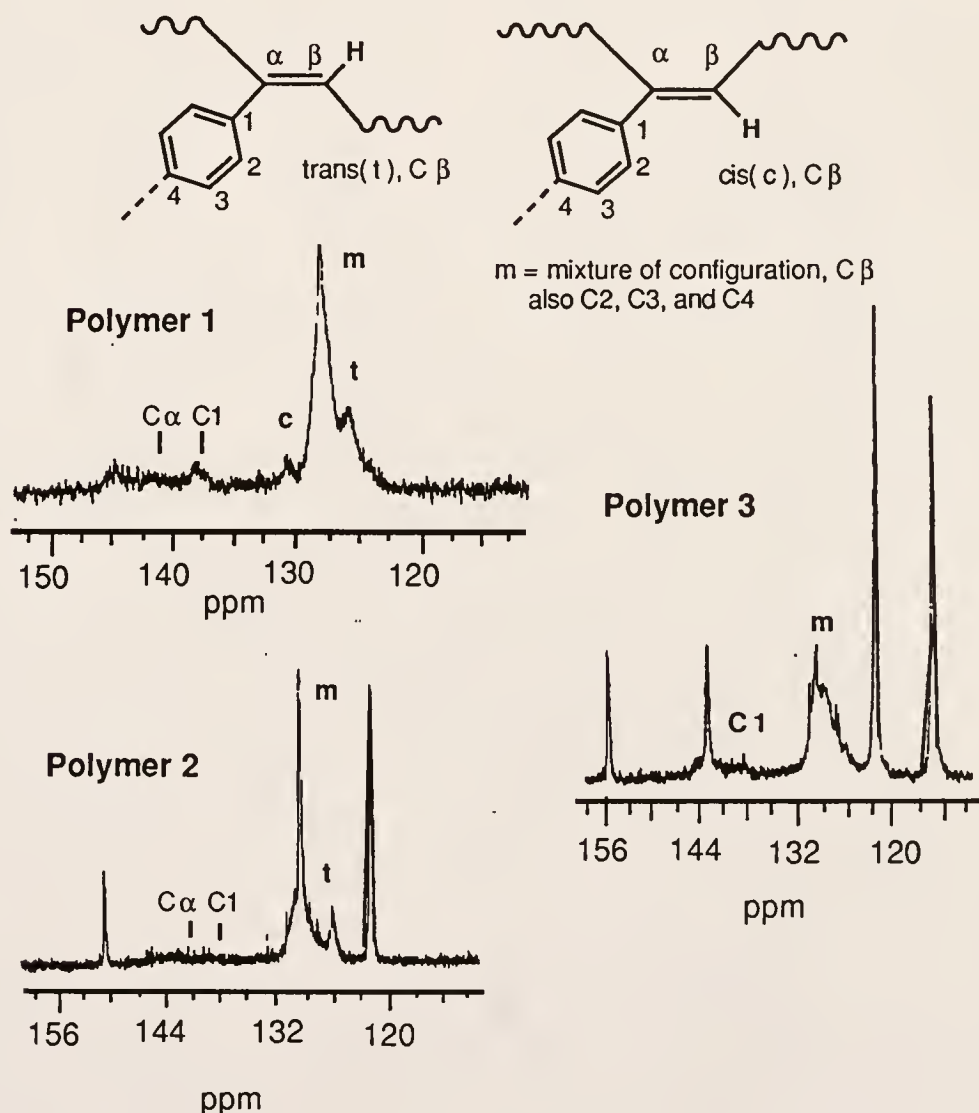


Figure 4-5. ^{13}C NMR of Polymers 1, 2, and 3 in expanded view for the region of interest (120-132:tertiary carbons and 135-147:quaternary carbons).

Figure 4-5 shows a comparison of the ^{13}C NMR spectra of the polyenic part of the three different polymers. Upon close examination several important points can be observed:

First, for the alkyl derivative, the *trans* content at 126 ppm (tertiary carbon β [$\text{C}\beta$] to the phenyl ring), is larger than the *cis*. This was confirmed by observation of the resonance Raman spectra of Polymer 1 at double bond stretching frequencies of 1525 and 1499 cm^{-1} (described elsewhere).⁴⁷ For the phenyl derivative, no *cis* peak is observed at 132 ppm, and for the alkoxyphenyl derivative, no *trans* or *cis* peaks can be clearly assigned.

Second, a broadening is observed at the 130-127 ppm region which could signify a large distribution of conformations. This distribution is a result of the non-planar conformations adopted by the chain and the low average chain length of purely *cis* and *trans* sequences. However, the influence of the NMR relaxation time on the magnitude of this intensity is uncertain. Nevertheless, close observation of the two tertiary peaks provide a measurement of the degree of pure *trans* and *cis* sequences in the backbone. A trend towards lower content of *trans* sequences may be observed as substitution goes from alkyl to phenyl and alkoxyphenyl groups, presumably due to increased steric interaction. In general, this leads to a lower ratio of *trans* to *cis* content. The peak also consists of contributions from both the phenylene carbons of the *p*-ethynylbenzoate as well as the ethylenic carbons of 1,3-cyclohexadiene defects.¹⁶³

Third, generally, the quaternary carbons have weaker signals than the tertiary carbons.¹⁶⁵ The resonances become weaker for the *p*-alkoxyphenyl derivative (Polymer 3). The lack or weakness of resonances in this region is an indication of the absence of cyclohexadiene defects. Again the effect of relaxation time on the resonance intensity is uncertain. Nevertheless, this result

is consistent with the decrease in the backbiting side reaction in the presence of the more sterically hindered alkoxyphenol substituent which leads to cyclohexadiene defects.

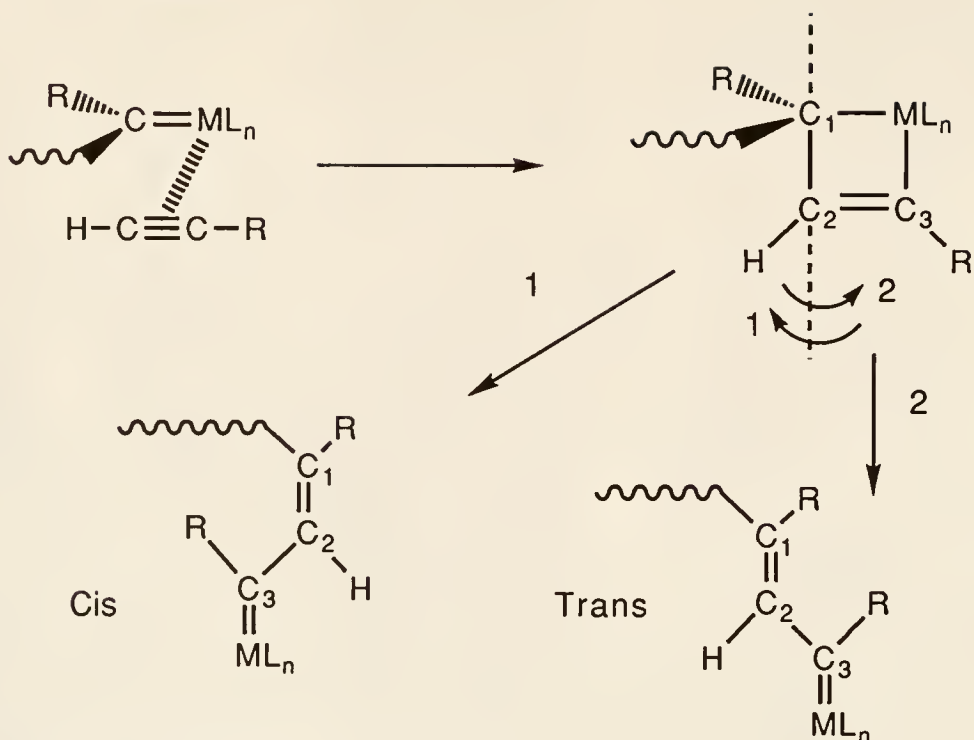
DSC measurements were made on the *p*-alkoxyphenyl derivatives. These showed no transitions for chain lengths of 10 and 12 carbons. An isotropic structure was also indicated by optical microscopy measurements as a function of temperature. The DSC results indicate that these polymers are much more disordered than those with alkoxybenzoate side chains, where a first order side chain melting transition is seen for 8 carbon and 16 carbon homologues (designated as PPAC-8 and PPAC-16).

Analysis of Characterization Data

The polymers synthesized are composed of a mixture of configurations and conformations with a higher *trans* ratio as indicated by NMR, Raman, and IR spectroscopy. Since the same catalysts and the same polymerization conditions were used for all three polymers, the above differences are clearly substituent effects. Recently, molecular mechanics and molecular dynamics calculations also indicated that the polyacetylenic backbone conformation and configuration should be substituent dependent.¹⁶⁶ This would mean that the size of the substituent should influence the backbone microstructure with other variables controlled.

The above effect may arise from the interaction of the substituent with the catalyst during the polymerization propagation. In a mechanism proposed by Katz and Percec, the propagation occurs through a metallacyclobutene intermediate.^{59,165} This planar intermediate then undergoes ring scission in which the C₁ - C₂ bond rotates around its axis to form a coplanar double bond.

(a) Head to tail addition



(b) Head to head addition

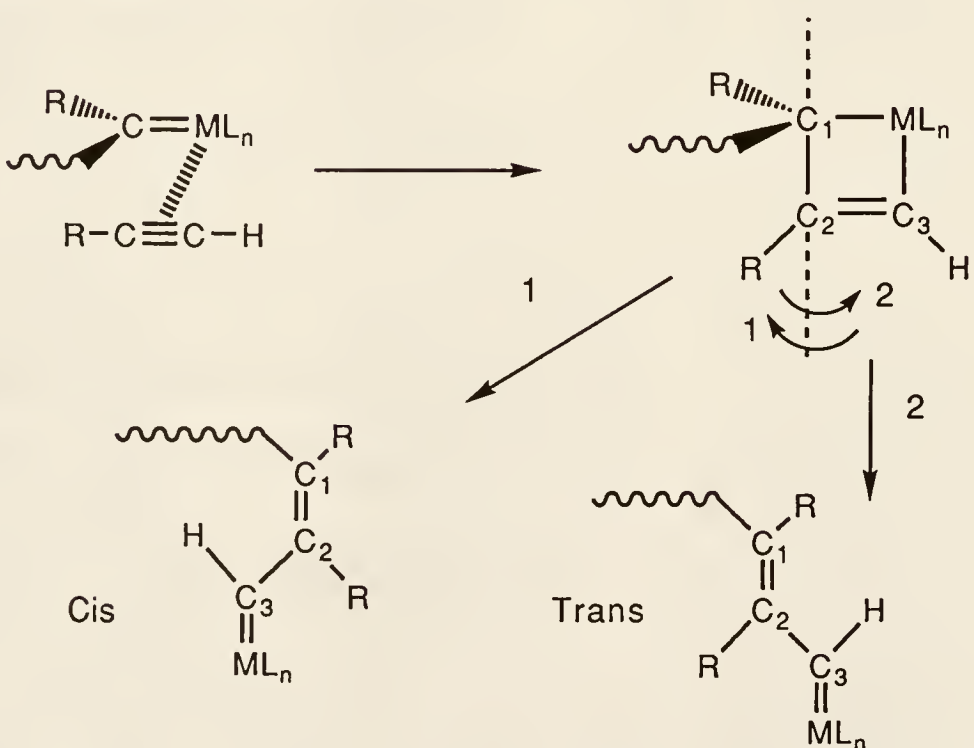


Figure 4-6. Mechanism of configurational effects with the metal halide catalyst via the formation of a metallocyclobutene ring: (a) head to tail
(b) head to head (tail to tail) placement.

This rotation *determines* the polymer configuration, though other mechanisms are possible (Appendix B). The C₁ - C₂ bond will rotate in such a way that will minimize steric interaction if necessary between the substituent of the chain and the coordinated metal. Thus a *cis* or a *trans* product is obtained depending on the nature of the interaction. Because these monomers are substituted, both head-to-head and head-to-tail configurations are possible at the growing chain end. The *cis* or *trans* content may be determined by the change in conformation at the terminal repeat unit upon cleavage of the metallocyclobutene ring as shown in Figure 4-6. In the case of head-to-head placement, both *cis* or *trans* configurations are possible (Figure 4-6b). In the case of head-to-tail placement, Figure 4-6a indicates that the conformation (2) resulting in *trans* configuration should be sterically hindered and unfavorable. Head-to-tail *cis* configuration is possible, however.

The above mechanism shows the effect of possible orientations and monomer placement on the growing polymer chain. Subsequent molecular geometry relaxations of the polymer would allow for changes in conformation due to rotations about single bonds. These rotations result in a planar or non-planar conformation for a given configurational sequence. Both configurational and conformational effects could account for the broad peaks observed in the spectra. To further understand the effect of configurational sequences on planarity, molecular modeling was performed on the phenyl-*p*-ethynyl benzoate polymer (Polymer 2). Sequences involving head-to-head and head-to-tail placements having *cis-cisoidal*, *cis-transoidal*, *trans-cisoidal*, and *trans-transoidal* configurations were modeled (see Appendix B for nomenclature). All sequences with the exception of the head-to-head trans-transoidal combination resulted in non-planar conformations due to van der Waals interactions.³⁷ Figure 4-7 schematically shows the results obtained for the head-to-head

placement *trans-transoidal* combination. This can only be possible in an alternating head to head and tail to tail placement of the monomer so as to allow the proper distance between each phenyl ring and prevent steric interaction.

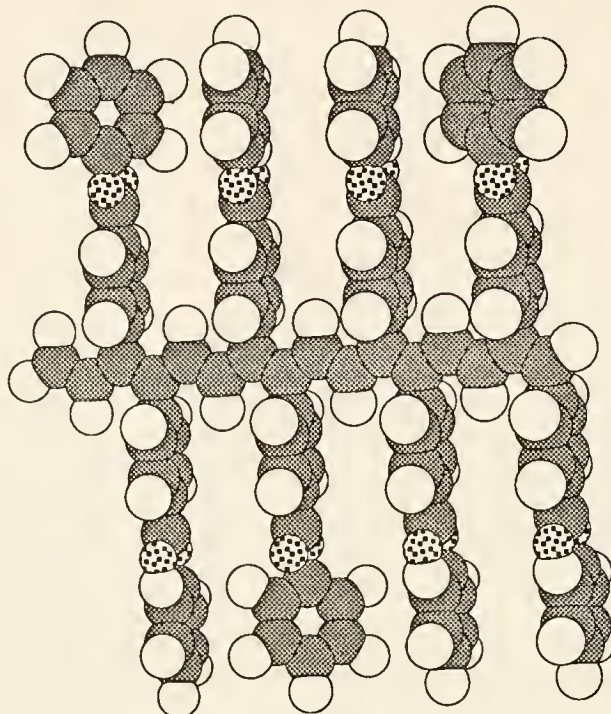


Figure 4-7. Corey-Pauling-Koltun (CPK) modeling of a head to head *trans-transoidal* configuration of Polymer 2 (8 repeat units). Pattern code: solid gray shade -carbon, white - hydrogen, and dotted - oxygen.

For the series of polymers, the effect with this particular catalyst is to decrease the *trans* content as the stiffness of the lateral substituent is increased. It also results in the formation of less pure configurational sequences along the series. Thus, polymerization using the metathesis catalyst WCl_6 is not specific towards formation of a highly planar chain. This implies that in order to obtain highly planar substituted polyacetylenes, a more configurationally specific catalyst than WCl_6 is needed. It also implies that the appropriate lateral substituents in the correct configuration may be an interesting means to increase the long term conformational stability of the polyacetylene backbone.

Monolayer Studies

With the important structural and chemical characteristics of the polymers analyzed, attention is now turned to the film-forming properties for this class of polymers. With the eventual objective of forming multilayer structures, the effect of pressure induced changes on the polymer conformation as well as film properties at the air-water interface in general, was studied using the Langmuir-Blodgett trough technique. As earlier mentioned, LB film properties of the monomers will be investigated separately by another doctoral thesis student. The results and discussions for the polymers are presented below.

Surface Pressure-Area Isotherm

Representative isotherms of the polymers and one of the monomers are shown in Figure 4-8. Only the monomer of poly(*p*'-dodecanoxyphenyl-*p*-ethynylbenzoate) gave a stable monolayer with an onset pressure increase at 33\AA^2 and a collapse pressure of 60 mN/m. The polymer has an abnormally lower limiting area (A_0) compared to its monomer. The isotherms of the phenyl (Polymer 2) and alkoxyphenyl (Polymer 3) derivatives are almost similar in shape and have low compressibility with an onset pressure increase at 20 and 23\AA^2 . Polymer 1, on the other hand, has an onset of 37\AA^2 with a plateau region between 17 to 32\AA^2 . It exhibited a much lower collapse pressure (10mN/m) compared to the alkoxyphenyl and phenyl derivatives which are at 55 and 52 mN/m respectively.

Measurements during compression-expansion cycles showed irreversible behavior for both Polymers 2 and 3.¹¹³ Subsequent expansion and compression of their monolayers gave isotherms with little resemblance to the initial compression curve. The polymer with the alkyl chain (Polymer 1) on

the other hand showed reversible behavior at the region below 10 mN/m pressure and an irreversible behavior at pressures higher than this. The polymers were subjected to different compression rates. In general, the limiting area (A_0) was observed to decrease with decreasing compression rate. This is a common behavior observed with polymers, and could be attributed to relaxation at the surface with slower compression speeds.⁸⁵

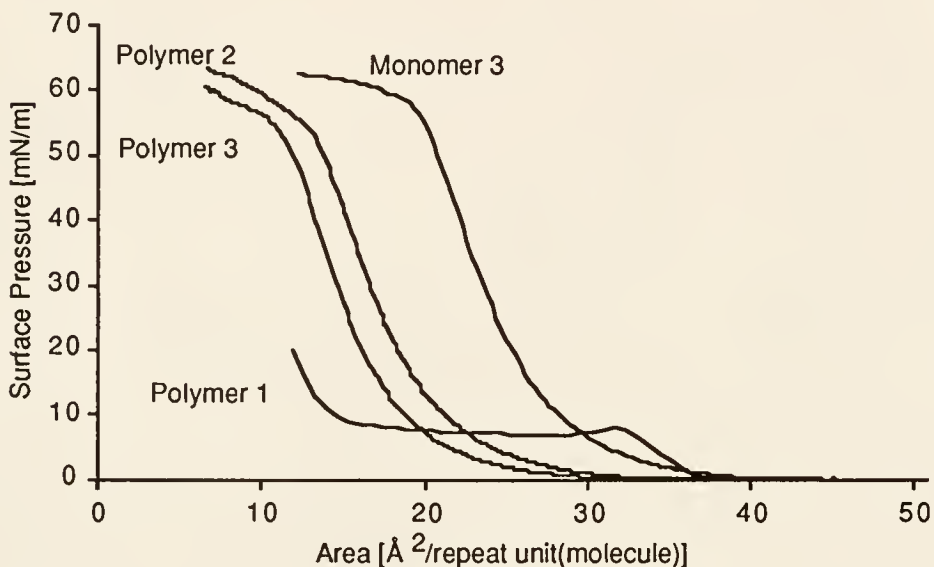


Figure 4-8. Isotherms of Polymers 1, 2, 3 at 25 °C and compression rates of 3.5 Å²/(repeat unit x minute).

With most polymers studied as Langmuir films, the measured Mma corresponds to the monomer repeat unit area assuming that the polymer backbone lies flat on the surface with any substituents packed perpendicular to the surface (ΔH is negative).^{105,120} With the mesogen-like substituent attached directly to the semi-rigid main chain, the packing of the chains will be influenced considerably by the orientation of this group. In principle, the substituents, if positioned normal to the water surface, would give low Mma, and

if parallel, would give considerably higher values. This is an ideal situation wherein the main assumption is that the alkyl side chains do not affect backbone conformation considerably. As discussed above, the configuration of these polymers determined by ^{13}C NMR spectroscopy has been identified as a mixture of non-planar *cis-transoidal*, (or *trans-cisoidal*) and *cis-cisoidal*. Small conjugated segments give rise to absorption in the visible region of the spectrum. Due to this mixture of configurations and the bulky side chains, the polymers are expected to form irregular helicoidal conformations. This would indicate that certain segments of the polymer will be out of the air-water interface as part of the helix turn.¹¹⁵ As such, the polymer chains will be hindered from close packing.

In view of the lower area of the monomer monolayer compared to the polymer, the occurrence of such conformations in the monolayer is most likely. The mean molecular area (Mma) of the polymer monolayer suggests that the chains lie neither orthogonal nor flat at the interface at an orientation in between. This means that statistically, at any given area, all the substituents are not totally adsorbed but certain segments are situated above the interface (loops).¹⁶⁷ Compression brings about an increase in the distribution of these loops, increasing the overfilm region which eventually leads to collapse. Thus, the polymers maintain their helicoidal and planar sequences even at the air-water interface consistent with that observed in ^{13}C NMR data in CDCl_3 solution. Well defined parameters such as monolayer thickness, in plane anisotropy, periodicity of the helix turn would need to be quantified however, in order to directly define absolute conformational behavior. This can only be done with appropriate techniques, e.g. neutron reflection, X-ray fluorescence, ellipsometry, etc.^{168,169,170} At best, only relative comparisons between the

conformational behavior of the polymers can be made at this point and in the succeeding discussions.

Typical of polymer monolayers, no sharp transitions are observed with these polymers except for Polymer 1.¹¹³ For this polymer, the reversibility of the curve before the first transition might be attributed to van der Waals interaction between the alkyl chains.¹⁰⁵ This can be visualized as the side chains being lifted in or out of the water upon expansion and compression. Subsequently, the region after the first transition is attributed to a biphasic regime containing domains of close packed phenyl (stiff) parts of the substituent. The irreversibility can be explained by a rearrangement of the polymer backbone as a result of intermolecular interaction between the stiff phenyl rings directly attached to the polymer. These observations are consistent with the surface potential measurements shown below.

Surface Potential

The surface potential in general increased with increased compression and did not necessarily follow the curve of the isotherm as shown in Figure 4-9. For the series of polymers, the largest $\Delta V/\text{\AA}^2$ was observed with Polymer 1 at all temperatures. The onset surface potential rise was about 5 \AA^2 in advance of the onset surface pressure rise. By the time the surface pressure started to increase, the rise in potential was essentially complete. Polymers 2 and 3 showed a smaller change in ΔV upon compression and have a similar behavior at different temperatures. However, with the Polymer 3 surface potential diagram, a noticeable feature is the change in slope at an area of 28 \AA^2 . This does not correspond to any noticeable transition in the isotherm of the polymer. The surface potential curve for Polymer 1 also showed a reversible behavior at

pressures below the first transition and irreversibility at higher pressures. The rise in ΔV is also essentially complete by the time the first transition is finished. The slope remains flat onwards, indicating the lesser role of the phenyl rings in affecting ΔV .

From the plot in Figure 4-8, it can be seen that Polymer 3 does not have any sharp transitions in the surface pressure isotherm, but the slope change in the surface potential diagram may reveal a structural transition consistent with that of Polymer 1, in which the initial rise in slope can be attributed to interaction between the alkyl side chains of the polymer.¹⁷⁶

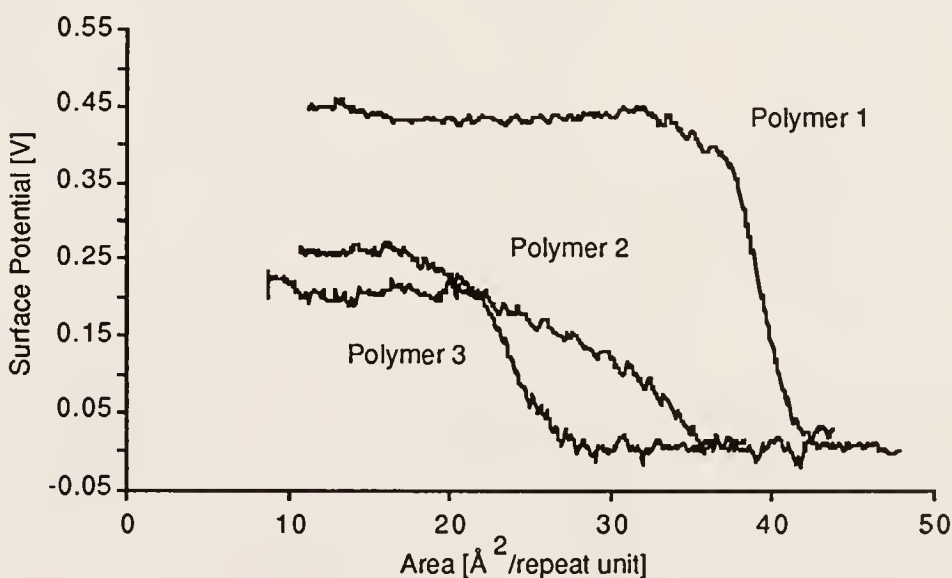


Figure 4-9. Surface Potential-Area isotherms of the polymers taken at room temperature (25 °C) with a compression rate of 3.5 Å²/(repeat unit x min.). See figure 4-8 for comparison with respective Π -A isotherms.

Polymer 2, by comparison, did not have any significant transitions in the surface pressure and surface potential isotherms. Thus, alkyl side chains influence the observed transitions in both the isotherm and the surface potential measurements depending on the proximity to polymeric backbone. The

presence of a stiff phenylbenzoate substituent between the alkyl chain and the polymer decouples this effect as in the case of Polymer 3.

Isobaric Creep Stability

Isobaric creep measurements done to study polymer behavior at a constant surface pressure of 5 mN/m are shown in Figure 4-10. Polymers 1 and 3 had a decrease in area of about 1 Å² and Polymer 2 decreased by 2 Å² within 30 minutes. At various temperatures, the phenyl derivative showed the least deviation from this behavior while Polymer 1 tended toward increased instability at higher temperatures. However, at higher pressures, the differences in temperature dependence were not so evident.

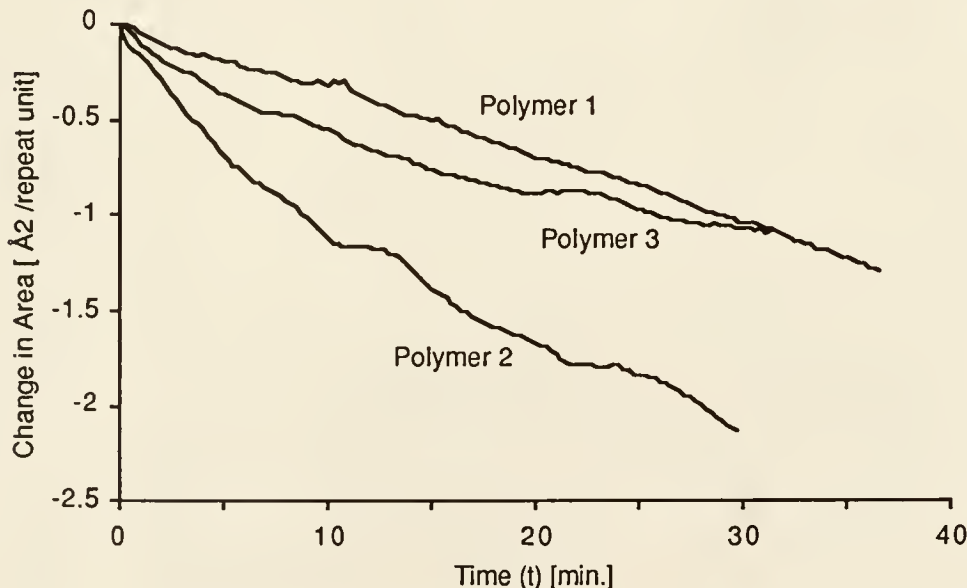


Figure 4-10. Isobaric creep stability at 25 °C for Polymers 1, 2, 3 at $\Pi = 5 \text{ mN/m}$.

Considering the weak hydrophilicity of the ester groups, the decay in area with time at constant pressure can be attributed mainly to a rearrangement

of the phenyl and alkyl components of the substituents to accommodate the compressive stress.¹²⁰ Reasonable monolayer stability is indicated by the small decrease in surface area over time. This is an important prerequisite for multilayer depositions (LB films) to substrates, where experiments may last for several hours. It seems that the presence of the alkyl chain has an important role in enhancing stability, possibly due to an increased intralayer van der Waals interaction. This is seen in the greater decay with time for Polymer 2, which did not have any alkyl chain. However, thermal effects are in favor of the phenyl ring substituent which may have important consequences in the overall thermal stability for applications purposes. At higher surface pressures, all the polymers show similar behavior. At this point, the backbone mobility would be primarily dependent on the stiff phenyl rings directly attached to the polymer.

Temperature Dependence

In general, as the temperature increased, the mean molecular area (Mma) also increased. The biggest shift with temperature among the three was observed with Polymer 1. The shift with Polymer 3 at a higher temperature (36°C) was significant in view of the A_0 being comparable to the value observed with the monomer at room temperature as shown in Figure 4-11. The collapse pressure in general decreased as the temperature increased. Only a minimal change was observed with Polymer 2.

These results show that the shift in the mean molecular area is also dependent on the presence of the alkyl chains. The smallest variation with temperature is observed with Polymer 2. The increase in Mma lead to more expanded films. This would indicate increase in the surface area as a result of increased thermal motion. Significantly, the similarity in area between Polymer

3 and its corresponding monomer at higher temperatures would indicate a packing arrangement approaching that of a more regular conformation.

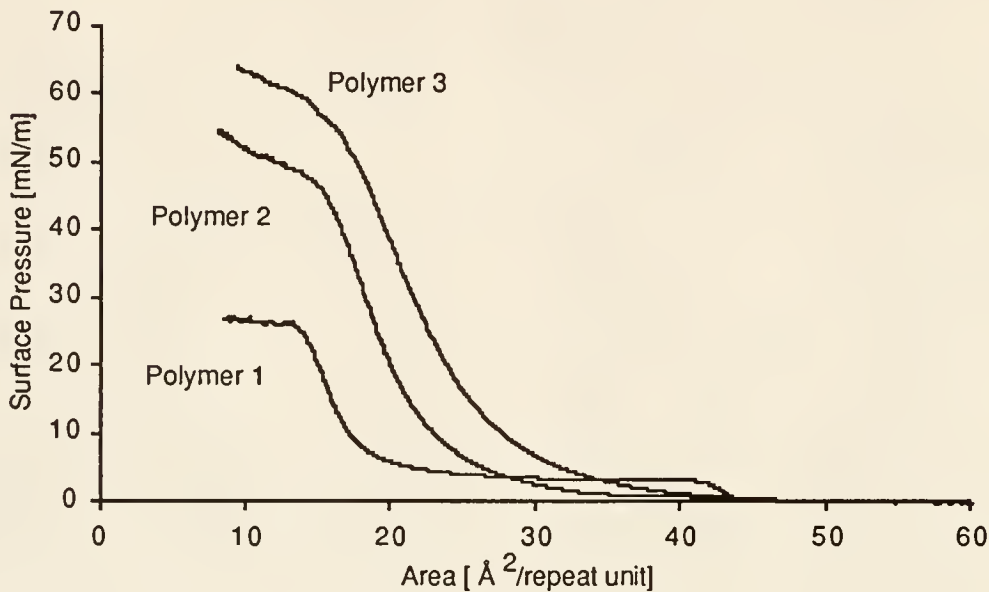


Figure 4-11. Surface pressure-area isotherms of Polymers 1, 2, and 3 taken at 36 °C. Speed of compression is 3 Å²/(repeat unit x min.). Compare with isotherms in Figure 4-8.

For Polymer 1, the decrease in the collapse pressure and increase in onset π -A rise with increasing temperature suggests an endothermic process. This is brought about by the lowering of the energy needed to collapse the film with increasing temperature.¹⁷¹

UV-Vis Measurements

The UV-Vis spectra of the polymers were observed *in situ* to determine the changes in orientation and conjugation length upon compression. Plots of the spectra are shown in Figure 4.12. No significant λ_{max} shift in the 300 nm region was observed for all three polymers. However, at the 450 nm shoulder,

Polymer 1 showed a red shift of order 30 nm coincident with the onset rise of the surface pressure isotherm. No shifts were observed for Polymers 2 and 3. To determine the relative change in intensity for the two peaks (300 and 450 nm), the ratio of their intensities were plotted as a function of change in area per molecule (Mma). The results are shown in Figure 4-12.

Also the polymers at room temperature showed no significant red or blue shift at the 300 nm region with compression. Since the region at 300 nm is important for observing the presence of aggregation between the mesogen-like part of the substituent, the absence of any shift is indicative of the lack of lateral intramolecular and intermolecular ordering of the phenyl rings even with compression.^{138,147} This is consistent with the observed configuration by NMR in which steric interaction prevents plane stacking of the lateral substituents in solution.

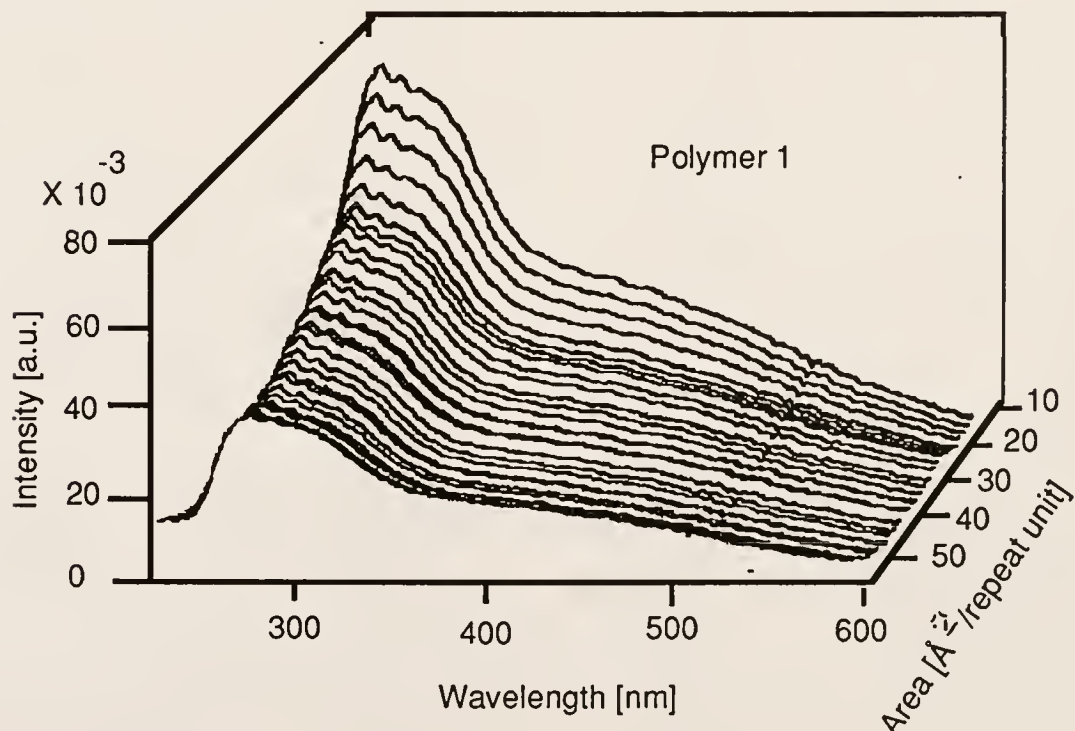


Figure 4-12. Surface plots of UV-vis spectra at 25 °C for (a) Polymer 1, (b) Polymer 2, and (c) Polymer 3 on compression at $3 \text{ \AA}^2/(\text{repeat unit} \times \text{min.})$. Scan rate is at 1 spectra/15 seconds with 1 sec exposure time.

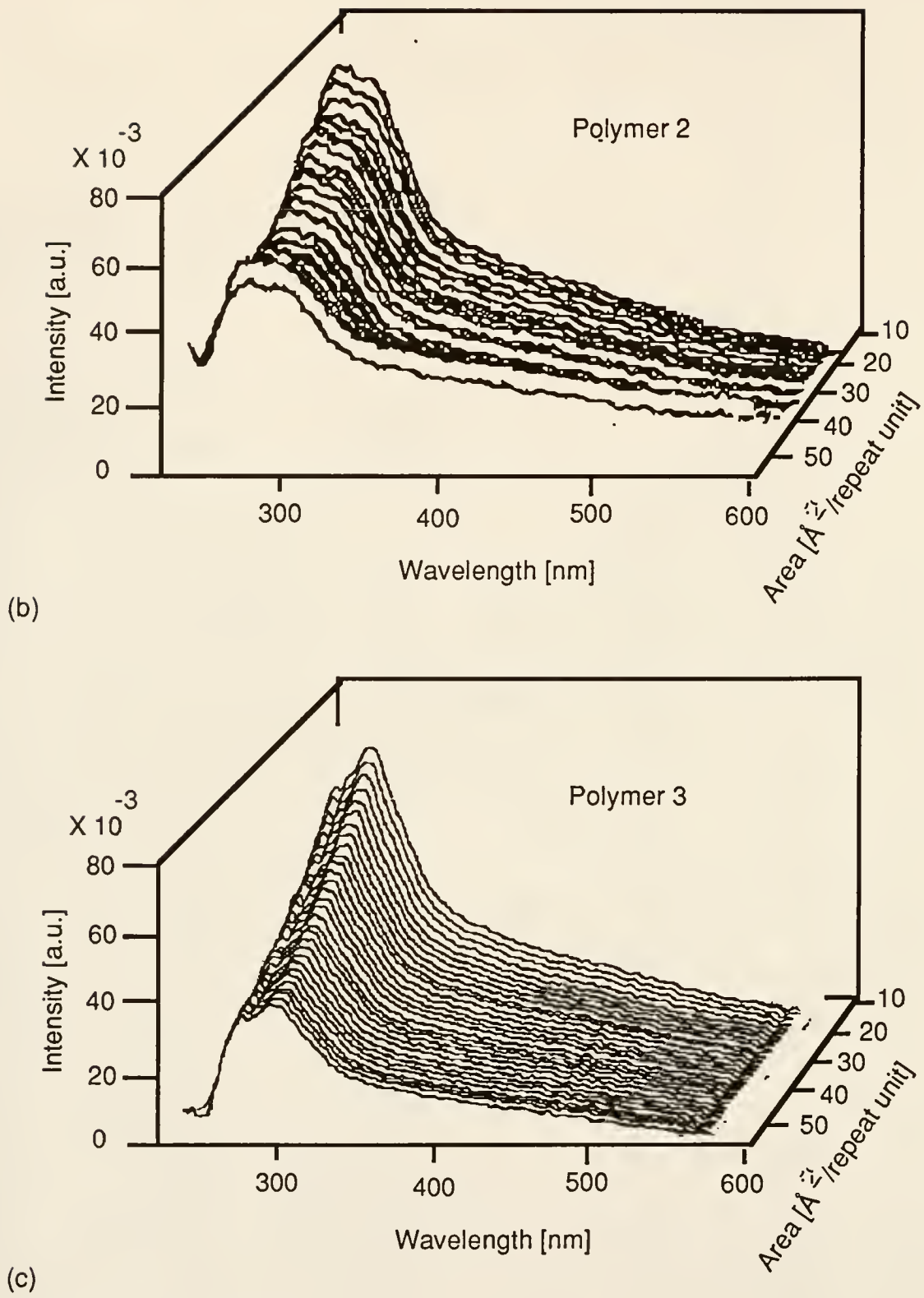


Figure 4-12 (continued)

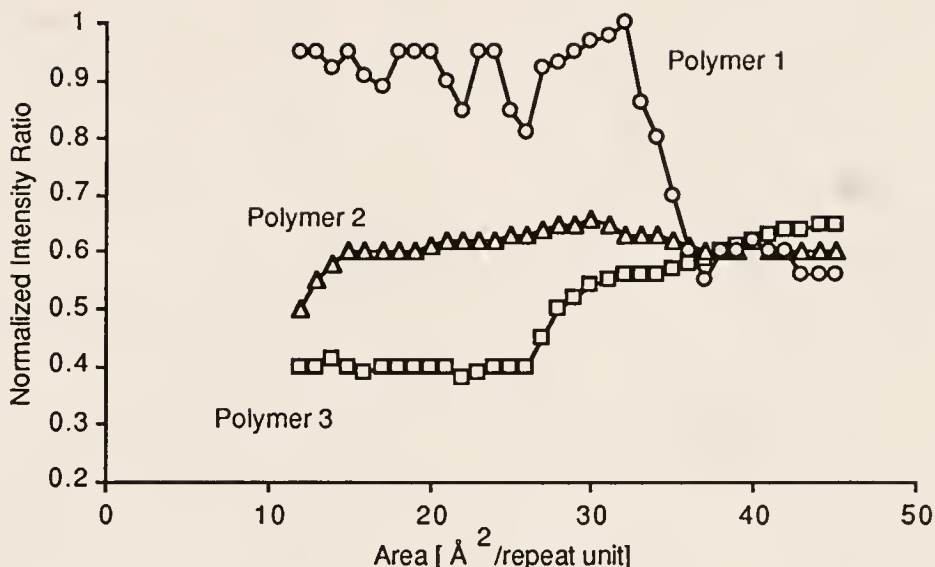


Figure 4-13. Absorbance intensity ratio for 450 and 300 nm peaks ($I_{450}/300$) of Polymers 1, 2, and 3 with an uncertainty of ± 0.05 on the normalized intensity ratio units.

The observed red shift for Polymer 1 at the 450 nm region could be brought about by the greater amenability of the polymer to changes in the local conformation. The absence of a second phenyl ring lateral to the backbone gives a less stiff substituent compared to Polymers 2 and 3. The presence of the alkyl chain would also allow for conformational changes due to van der Waals interactions as observed earlier with the reversibility of the surface pressure and surface potential curves.

The absorbance was observed to increase with compression for all three polymers. In order to distinguish the increases due to concentration effects from increases due to changes in local chain planarity, the ratio of peak maxima at 450 and 300 nm was taken for all the polymers. An increasing value would mean an increase in concentration of conjugated sequences in the backbone brought about by conformational changes. As shown in Figure 4-13,

compression for Polymer 1 resulted in an increase in ratio with compression, leveling off coincident with the onset of the surface pressure isotherm. Polymer 2 showed a decreasing ratio with compression which leveled off at the onset of the surface pressure isotherm. For Polymer 3, the ratio also decreased with compression but a small increase was observed prior to the onset of the surface pressure which then decreased and leveled off. These data again point to greater conformational changes associated with Polymer 1 consistent with the structure. The increase with Polymer 3 can be explained by the effect of the alkyl chains on the conformation of the polymers at the gaseous region. The subsequent decrease in Polymer 3 as well as the decrease in Polymer 2 may be due to the onset of the helicoidal conformation as discussed above. This shows that the limiting conjugation length that can be achieved is determined mainly by the type of substituent that is employed. For Polymers 2 and 3 the limiting conjugation length is set at the outset of the initial polymerization conditions. Little conformational changes can be expected due to the stiff lateral substituent. For Polymer 1, compression results in an increase of the conjugated sequences due to rotations about single bonds since the phenyl substituent is not as sterically hindered as the phenylbenzoate of Polymers 2 and 3. The role of the alkyl chain at the other end of the substituent can be observed for both Polymers 1 and 3 as in the gaseous phase.

Thus, UV-vis absorption spectra in the monolayer indicate pressure induced local conformational changes on segments of the backbone. These changes are highly substituent dependent. The red shift in λ_{max} at 450 nm with compression and the increase in the intensity ratio shows the importance of the lateral substituent in influencing conformational changes. Changes in local chain anisotropy will be investigated in the future using cross-polarizers with the UV-Vis spectra measurements.

Poly(ethynylbenzoate alkyl esters); Alkyl Chain Length

As observed above, the effect of the increasing stiffness of the substituent resulted in the formation of less configurationally pure polymers with the result that only local conformational changes can be observed at the interface. An important result that is evident from the above studies, is the presence of the alkyl chain at the tail of the substituent. This apparently decouples the polymer-polymer interactions thereby resulting in better monolayer behavior. In the following study, initiative was taken to investigate the effect of the alkyl chain length in decoupling these polymer-polymer interactions. A homologous series of poly(alkyl-*p*-ethynylbenzoate esters) including Polymer 1, was previously synthesized in which the alkyl chain length was systematically varied. The schematic representation for the polymer series is shown in Figure 4-14.

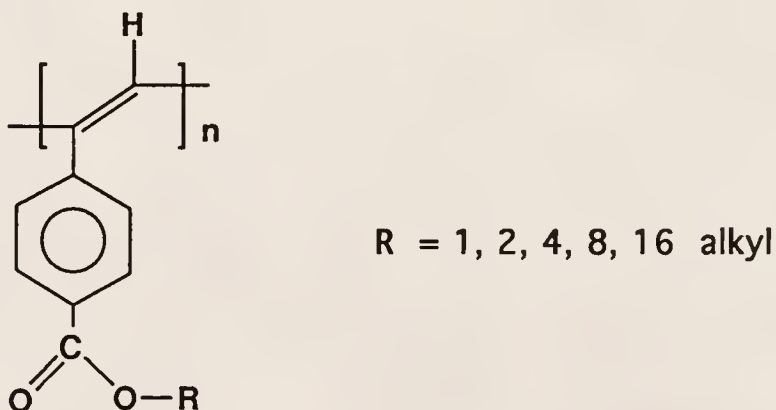


Figure 4-14. Poly(alkylethynylbenzoate) homologous series synthesized using the same procedure as Polymer 1 and 2 with varying alkyl chain length. Numbers denote the number of carbons in the alkyl group, R.

The synthesis and characterization of these polymers was done in a similar manner as Polymer 1 by A. Hilberer. The full description of the properties and synthesis is described elsewhere.^{37,47} In general, the polymers consist of a distribution of *cis* and *trans* configurations as determined

by NMR and Raman spectroscopy. No chain length dependence on this configuration distribution was observed. A summary of the important properties are described below:

Table 4-2. Summary of Molecular weight analysis by Light scattering technique and Gel Permeation Chromatography in THF using a polystyrene calibration curve.⁴⁷

Polymer	Mol. Wt. by LS	Mol. Wt. by SEC	Polydisp. Mw/Mn	α of $[\eta] = KM^\alpha$
PPAC-1	71,400	39,700	2.52	0.92
PPAC-2	79,200	47,000	2.75	0.92
PPAC-4	78,300	46,000	1.79	0.92
PPAC-8	55,700	31,700	2.82	0.92
PPAC-16	131,000	79,300	1.6	0.92

The Mark-Houwink coefficient α as obtained from intrinsic viscosity evaluation by universal calibration gave an average value of 0.92, regardless of the chain length. All the polymers were stable up to 330 °C in both air and nitrogen as examined by thermogravimetric analysis (TGA). Differential scanning calorimetry (DSC) showed the following thermal transitions: PPAC-16 , 26 °C, $\Delta H = 10.8 \times 10^{-2}$ J/mole and PPAC-8, 75°C, $\Delta H = 6.6 \times 10^{-2}$ J/mole. Optical Microscopy revealed no birefringence, but a strong chain length dependent softening point. By X-ray diffraction analysis: PPAC-8 at 120 °C, gave a broad diffraction ring in the small angle region and a diffusion band in the wide angle region. The average d-spacing corresponding to the small angle reflection is 24 Å. The small angle diffraction band disappeared at 160°C. The polymers could therefore be characterized as showing semi-

crystalline properties. The apparent lack of glass transition could be related to the high backbone stiffness. The chain stiffness or flexibility should also determine the packing behavior of the polymer. The carboxylic groups were expected to facilitate hydrophilic interactions with water. The main difference between these polymers would therefore be mainly on the length of the alkyl chain.

These polymers exhibited third order non-linear optical properties on the order of 10^{-12} esu (1.6×10^{-11} calc.) as determined by THG (Third Harmonic Generation) on solution cast thin films.^{47,61}

Isotherm Measurements

Compressional isotherms of the polymers at room temperature (25°C) are shown in Figure 4-15. The isotherms are reproducible within 1 Å² with compression speeds not higher than 6 Å²/repeat unit x min. Likewise, little change in the shape or slope, especially at the overfilm region is observed with different speeds. Changes with different concentrations of spreading solution is observed for the small chain length polymers. No strong inflection points or biphasic regions are observed other than the collapse. All the isotherms, except for PPAC-16 (initially called Polymer 1), show low compressibility as compared to most polymers spread at the interface. The Polymer PPAC-16 has an onset area higher than the rest of the polymers with a collapse pressure of 7 mN/m. PPAC-8 has a lower collapse than the other short chain derivatives, but the extrapolated Mma at zero pressure lies within the same area as the other derivatives. In general, the collapse pressure increased the smaller the alkyl chain length.

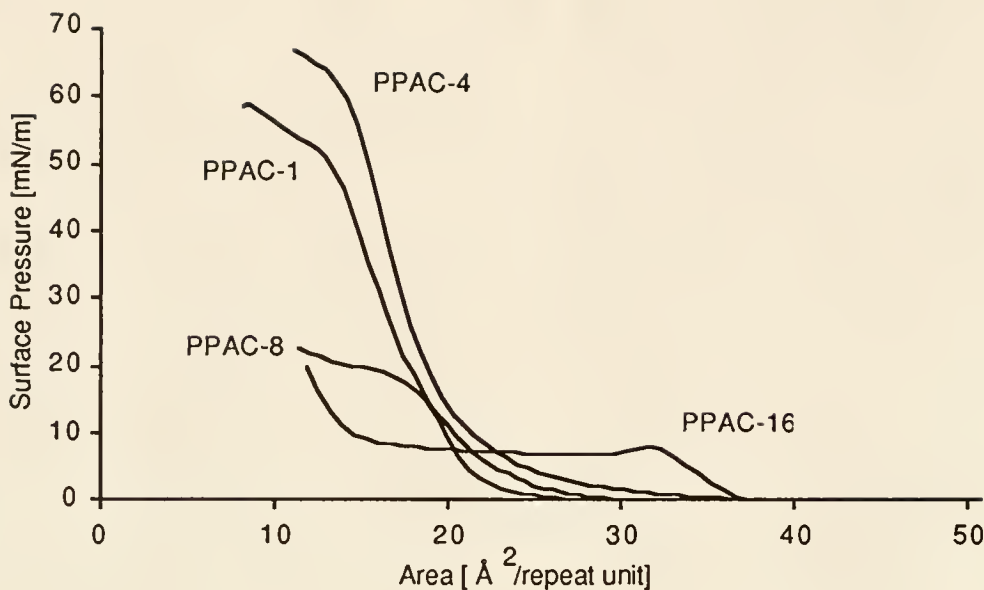


Figure 4-15. Surface Pressure area isotherms for the PPAC-n series at 25 °C and 3 Å²/(repeat unit x min.) compression rate.

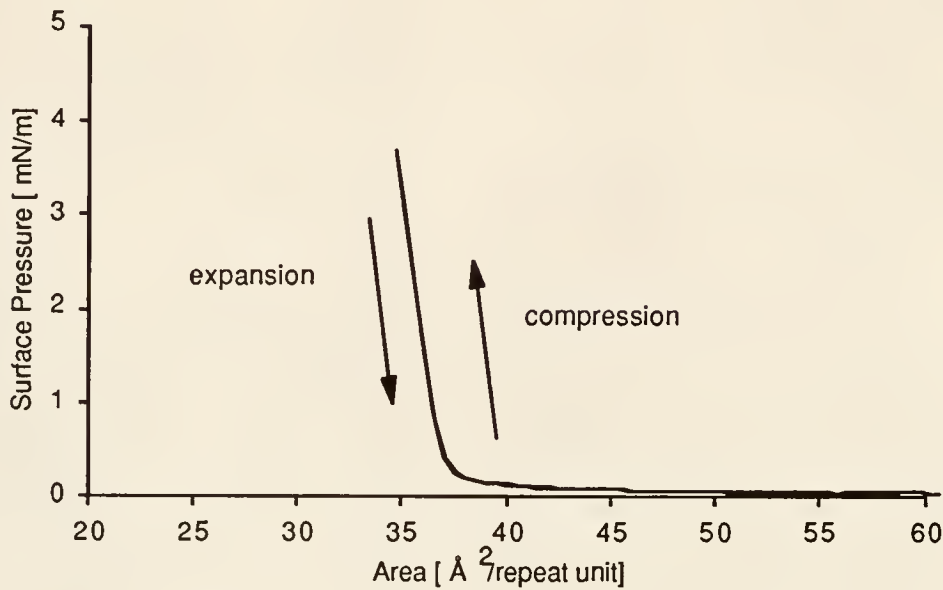
With the phenyl ester attached directly to the semi-rigid main chain, the packing of the chains will be influenced considerably by the orientation of this group. The main difference of these polymers with the previous ones is the lack of a stiff substituent other than the phenyl ring. The alkyl chain therefore is expected to more directly affect the polymer backbone in comparison to Polymer 3. Like the previous polymers, the configuration of these polymers as determined by ¹³C NMR spectroscopy has been identified as a mixture of non-planar *cis-transoidal* and *trans-cisoidal* with small conjugated segments giving rise to absorption in the visible region of the spectrum. Due to this mixture of configurations, the polymers are expected to form irregular helicoidal structures, in maintaining their configuration. This indicates that certain segments of the polymer will be out of the air-water interface as part of the helix turn (for an ideal helix) of the semi-rigid backbone. In view of the lower area observed, the

occurrence of this configuration in the monolayer is again most likely. This configuration should result in the presence of a free volume within the polymer that is not filled up with substituents.¹²⁵ It is relevant that PPAC-8 shows a lower collapse pressure than the lower alkyl chain derivatives. This indicates that the transition to the overfilm region is affected by the presence of a longer alkyl chain.

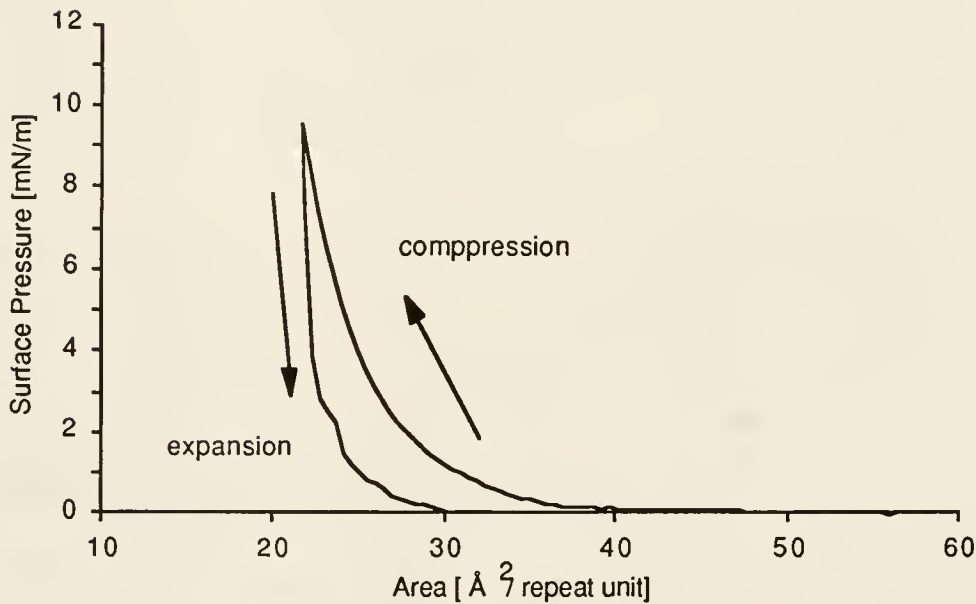
Hysteresis.

Compression-expansion cycle studies showed a *rearrangement* type of behavior as classified by Gaines for the smaller chain length derivatives (see classifications in Chapter 1, section on Polymers at the Air-Water Interface).¹¹³ This was observed when subsequent expansion and compression of the monolayer gave little resemblance to the initial compression curve at various pressures along the isotherms. However, at higher temperatures, PPAC-8 showed improved hysteresis behavior. PPAC-16 gave *reversible* behavior at all temperatures. This reversibility of the curve could be attributed to van der Waals interaction between the alkyl chains as previously studied. This might be due to the side chains being lifted in or out of the water upon expansion and compression. The irreversibility observed with the other polymers could be explained by a rearrangement on the polymer backbone as a result of intermolecular interaction between the stiff phenyl rings directly attached to the polymer. As mentioned above, the free volume around the chain (as a result of spreading conditions, e.g. when the solvent evaporates) allowed for greater interaction at lower areas or higher pressures. This resulted in the formation of larger domains, where small domains either created by the spreading conditions or concentrations are fused together. At high pressures,

rearrangements would tend to be dominated by the polymer backbone, producing irreversible conformations, thus different monolayer behavior upon expansion.



(a)



(b)

Figure 4-16. Hysteresis behavior (one cycle) of (a) PPAC-16 and (b) PPAC-1 at 25 °C and compression-expansion rate of 3 Å²/(repeat unit x min.), note expanded scale in (b).

Temperature Dependence

The isotherms of the polymers were measured at different subphase temperatures (Figure 4-17). The most evident difference among the polymers was the area and pressure dependence of PPAC-16. In general, for this polymer, as the temperature increased the mean molecular area (Mma) increased and the collapse pressure decreased. Likewise, the collapse pressure for PPAC-8 decreased with increasing temperature but the area (Mma) remained relatively the same. Little change was observed for the shorter chain derivatives (typified by PPAC-1).

Figure 4.18 shows $-d\pi/dT$ plot for the three polymers, showing a negative dependence (endothermic behavior) for PPAC-16 and PPAC-8. This shows that the presence of the alkyl chain facilitates the transition to the overfilm region and is highly temperature dependent. However, the increasing Mma for PPAC-16 is possibly a phenomena of side chain melting at the interface with increasing temperature, in which thermal motion governs the behavior of the alkyl chains instead of adsorption.¹⁷⁹ This results in a greater separation of the polymer chains as a result of increased decoupling. For PPAC-8 it seems that the increased energy in the form of heat does not affect the alkyl chains considerably as the area did not change that much. This means, that the transition to the overfilm region is mostly dominated by the alkyl chain, whereas compressional properties of the monolayer are dominated by the backbone. These data indicate that the transition to the overfilm region is mainly entropy dependent, since temperature affects the transition to a more disordered state and this transition appears to be independent of compression speed.¹⁷²

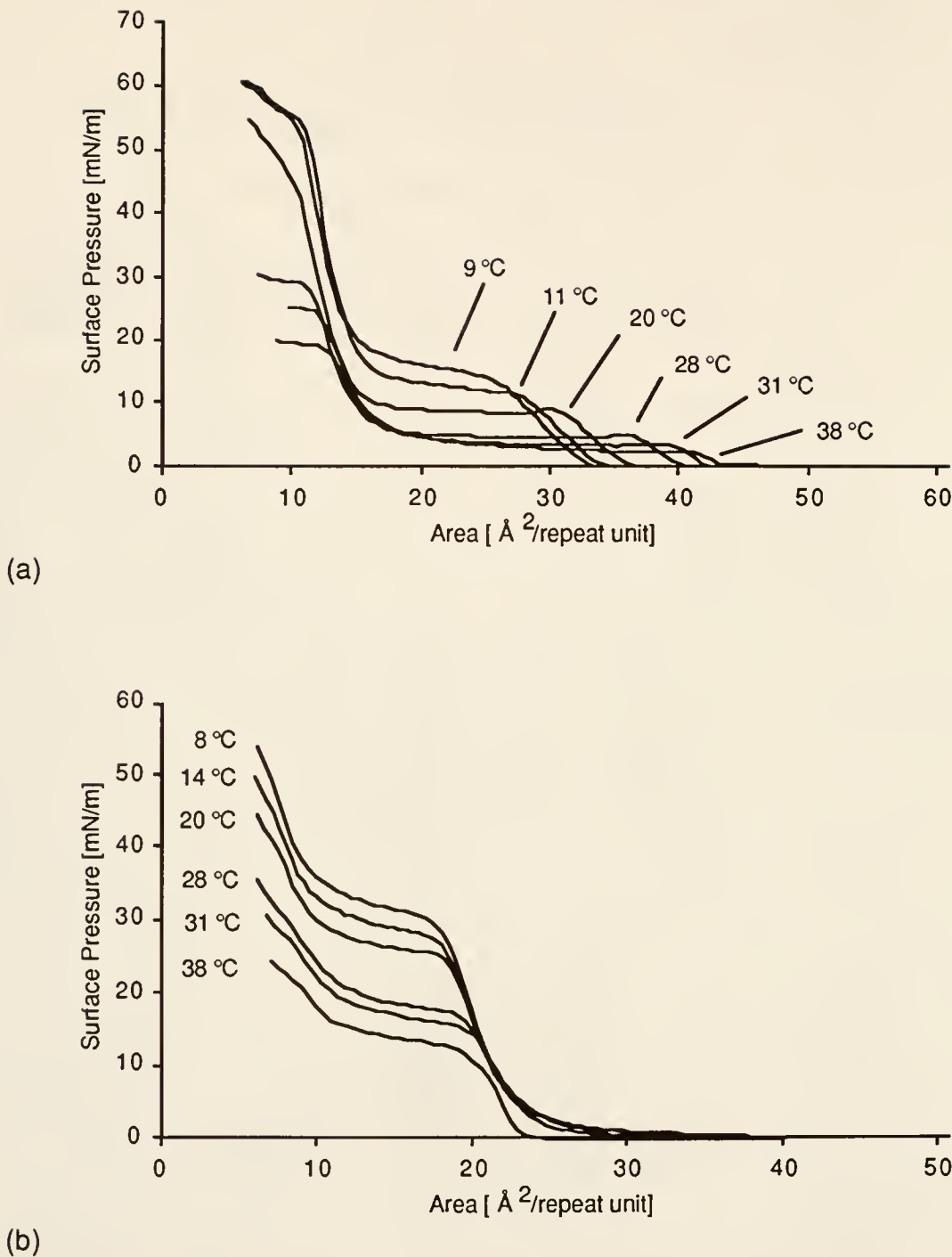


Figure 4-17. Isotherms for (a) PPAC-16, (b) PPAC-8, and (c) PPAC-1 taken at different temperatures with a similar compression rate of $2 \text{ Å}^2/(\text{repeat unit} \times \text{min.})$. Temperature is within $\pm 0.5^\circ\text{C}$ deviation.

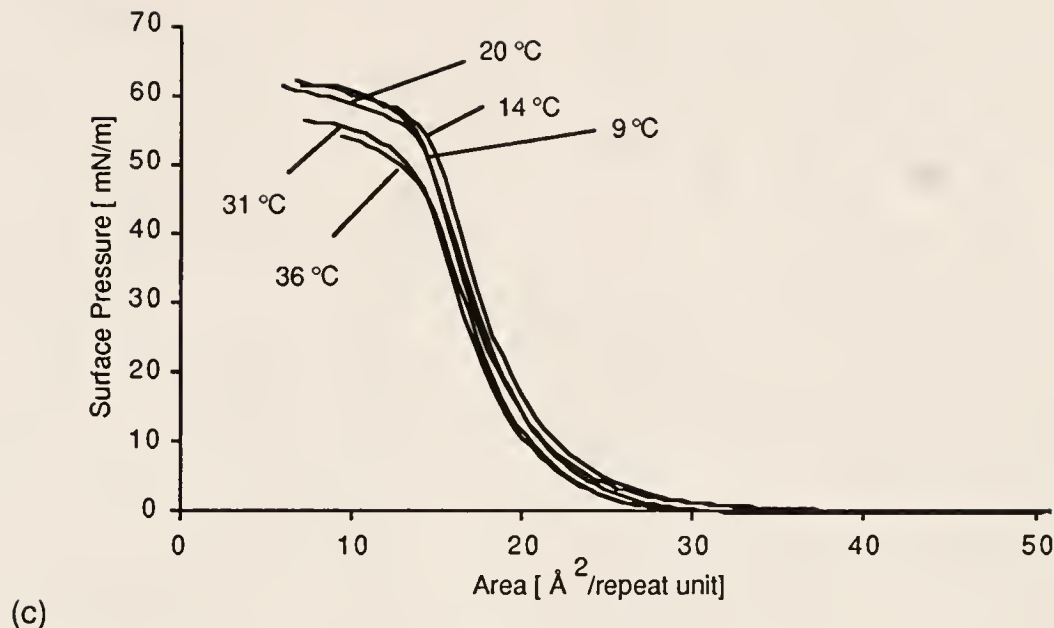


Figure 4-17 (continued)

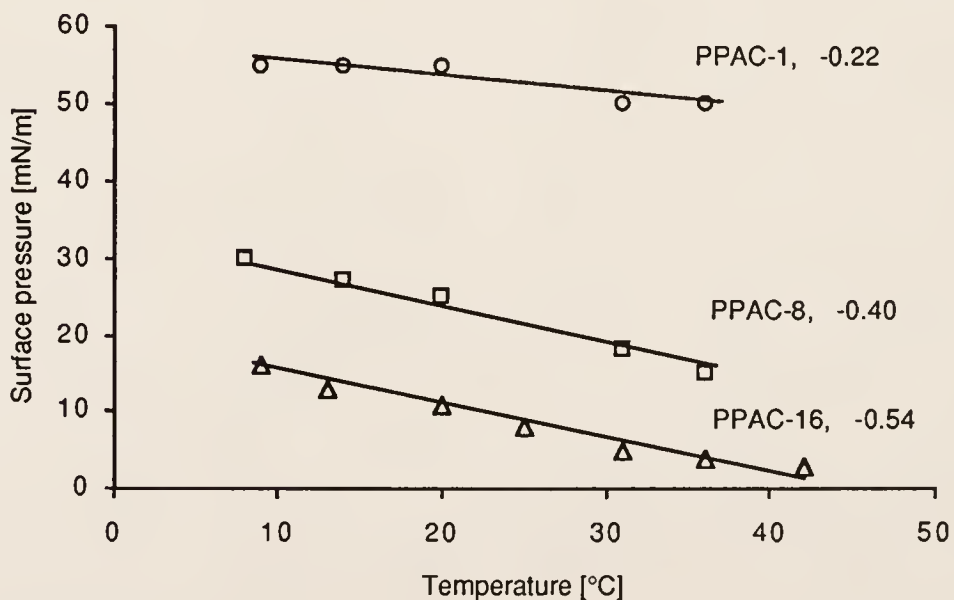


Figure 4-18. Plot of $-d\Pi/dT$ for polymers PPAC-1, 8, and 16. The values for the surface pressure Π correspond to the collapse pressures of the isotherms. The numbers given above represent the slope (m) of the curves and was determined by least squares method ($\text{mN/m } ^\circ\text{C}$).

Surface Potential Measurements

Investigation of the surface potential behavior of the polymers showed some interesting differences. Although it was not possible to determine exactly the orientations of the apparent surface dipoles (considering the myriad of conformations and configurations are possible for polymers, gross assumptions have to be made)¹⁷³ comparison of behavior between the various polymers could be made. Moreover, correlation with measurements from other surface analytical techniques were found to be complementary. PPAC-1 and PPAC-4 showed a gradual monotonic increase in potential starting from a high area, up to the low compressibility region (steep slope of the Π -A isotherm). The surface potential became relatively flat onwards. Various spreading concentrations tend to change the slope, but the net value of the potential change remained the same. On the other hand, a steep rise of the potential, about 5 \AA^2 in advance of the surface pressure rise was seen for PPAC-16, and a similar behavior less reproducibly with PPAC-8. Beyond the collapse, the potential remained relatively flat for PPAC-16, and a gradual decrease was observed with PPAC-8.

A more sensitive parameter would be the observed changes in the apparent surface dipole moment. This was calculated from the Helmholtz equation (proportional to the product of the area and ΔV) as shown in Chapter 2 and in detail in Appendix C.¹⁷⁴ The surface dipole moment curves were divided into three regions. As shown in Figure 4-19, with the same spreading concentration, PPAC-1 and PPAC-4 showed a reproducible monotonic increase in the surface dipole at the high area region (region I). This increase was attributed mainly to concentration effects rather than net dipole reorientation (phase changes) as verified by Brewster angle microscopy (discussed in detail in the next section). Domains of the polymer were observed

to fuse together as the surface area decreased. Good reproducibility indicated that the surface dipole moment (potential) does not vary with the domain size since the area scanned by the potentiometer is of order cm^2 while the domain sizes are of the order of $\mu\text{m}^2 \cdot \text{mm}^2$. Thus, the dipole moment measured was an average over a wide area much larger than the domain sizes. This also indicated that this smooth region in the Π -A isotherm curve could not be associated with a true liquid expanded phase.¹¹³

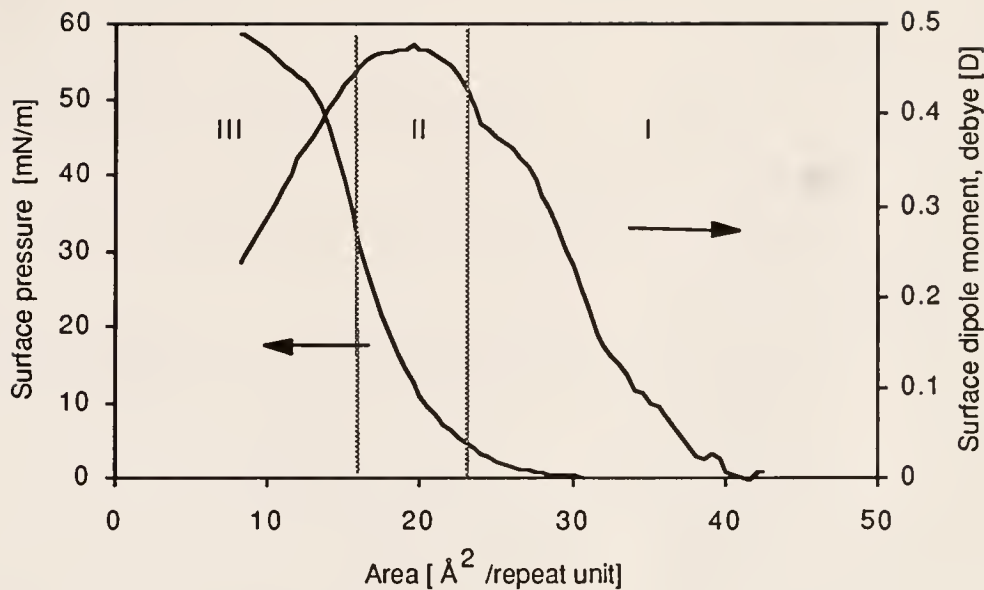
For PPAC-16 and PPAC-8, a steep dipole increase was observed in advance of the surface pressure. That the steep rise was not just the result of the presence of the monolayer front for PPAC-16 was also verified by (BAM) Brewster Angle Microscopy.¹⁷⁵ Moreover, this onset had good reproducibility even with different spreading concentrations. For the PPAC-8, a variability of 2 \AA^2 was observed for the onset rise with various spreading concentrations. Considering the difference in behavior between the short alkyl chain derivatives, this may be indicative of a phase transition (liquid expanded) not observed with the Π -A isotherm at higher surface areas.¹¹³ For all the polymers, the contributions to the dipole will come mainly from the following functional groups:^{105,174}

- (i) The terminal methyl group of the alkyl chain.
- (ii) The carbonyl ester functionality
- (iii) The water subphase molecules immediately beneath the monolayer.

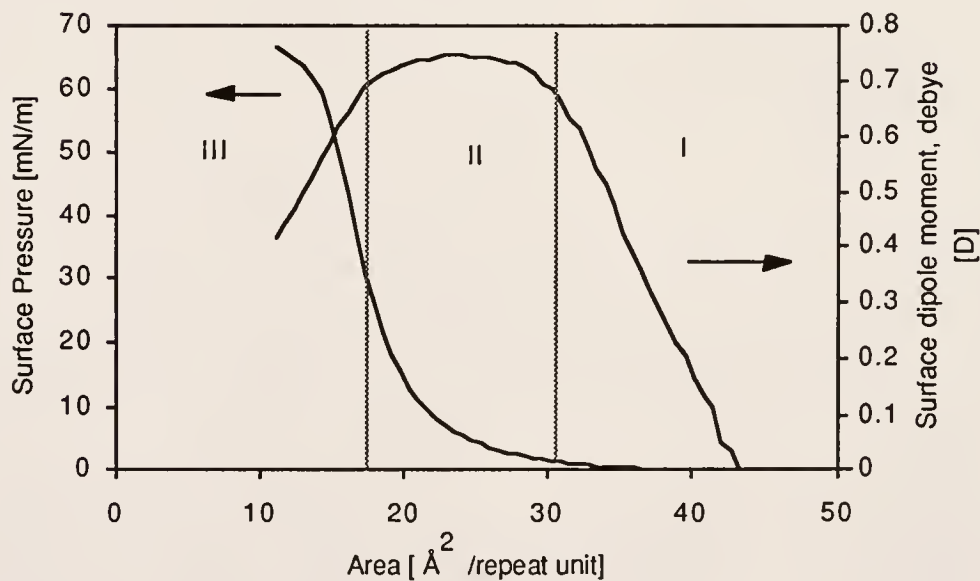
Since the longer alkyl chains extend laterally further from the backbone, they would be the first to "feel" the interaction with the other chains. Therefore, a transition represented by a steep rise in advance of the Π -A isotherm can be attributed to a positive contribution from these groups. This would represent a lifting up of the alkyl chains towards an increasing normal position at the interface resulting in a positive dipole contribution (terminal methyl group

directed from water to air). The longer alkyl chains would be less adsorbed at the interface and would therefore be more mobile to reorient with compression. According to Mobius et al. independent of the number of carbons in the hydrophobic chain, a large contribution to the surface dipole ($0.35 \pm 0.01D$) arises from the terminal methyl group oriented perpendicular from the surface plane.¹⁷⁶

For PPAC-1, PPAC-4, and PPAC-16 a relatively flat region on the surface dipole (region II) was observed. However, there was a difference in that this flat region corresponded to a high compressibility region below collapse in the PPAC-4 Π -A curve (less evidently for PPAC-1). On the other hand for PPAC-16, this flat region extended from the low compressibility (high pressure) to the collapse point of the curve. This means that even prior to the low compressibility area of the monolayer the films of PPAC-4 and PPAC-1 are relatively condensed and showed little dipole reorientations compared to PPAC-16. This was again found to be consistent with results in BAM measurements, in which a homogeneous film was already observed at this area for PPAC-4 and PPAC-1. As was discussed earlier, this occurred as the small domains at high areas had fused together to form a single film. Although the film appeared homogeneous in the microscope, it probably has different local film densities of polymer or aqueous rich phases (a homogeneous heterophase film). Nevertheless, this means that the flat region is not associated with small domains but rather with a condensed phase (less dense than at lower areas) of the film. It is also likely that at these areas, the shorter alkyl chains associate more strongly since the short range forces bringing the ester dipole doublets and the forces between the backbone will be greater when the side chain is short. This would explain the relatively flat region of the curve observed.

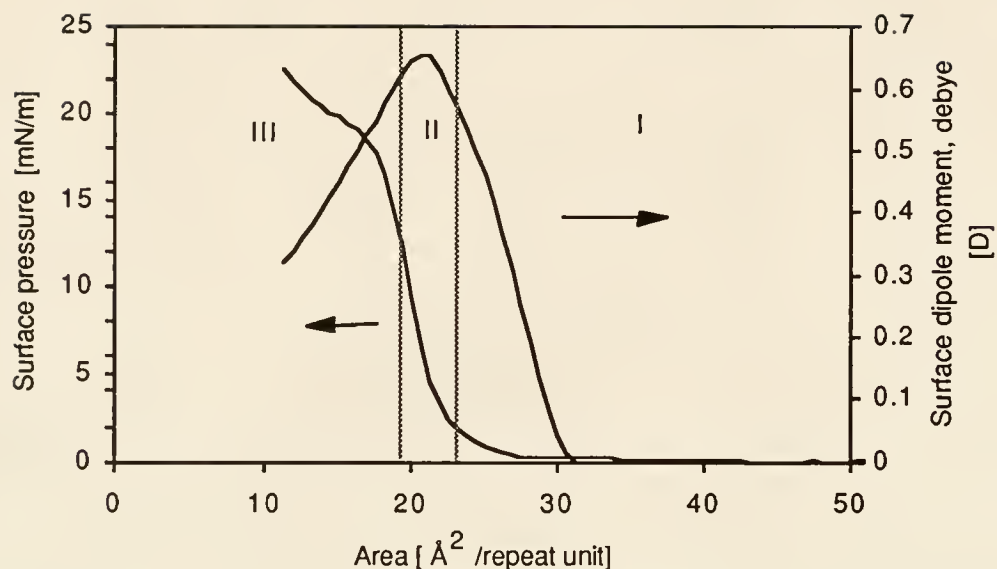


(a)

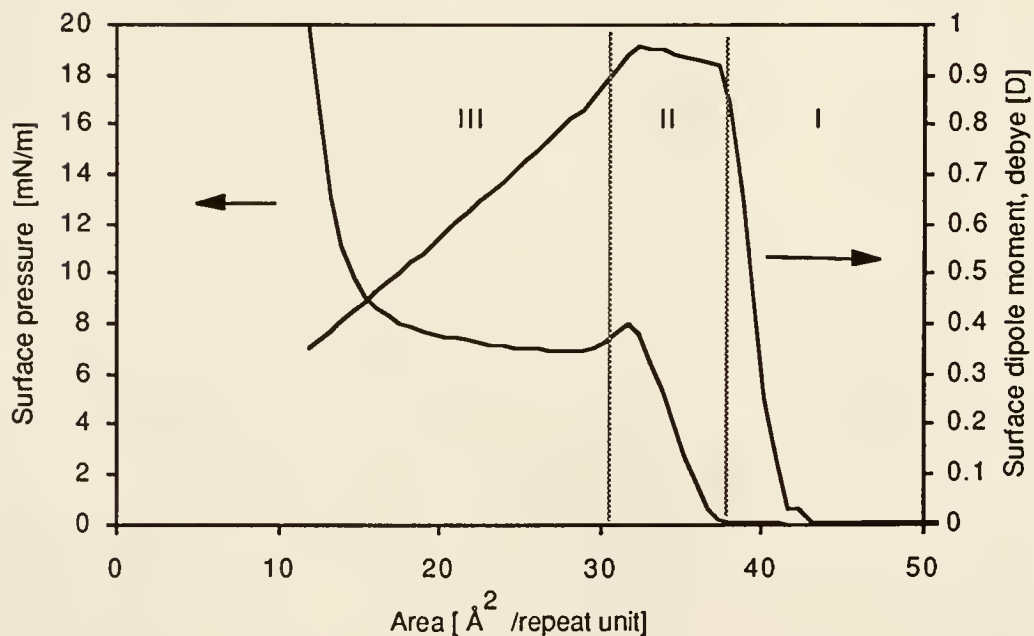


(b)

Figure 4-19. Surface Dipole Moment-area plots for (a) PPAC-1, (b) PPAC-4, (c) PPAC-8, and (d) PPAC-16 at 25 °C with compression rate of $3 \text{\AA}^2/(\text{repeat unit} \times \text{min.})$. Reproducibility of the isotherms on similar spreading conditions is within $\pm 1 \text{\AA}^2$ and $\pm 0.02 \text{ D}$



(c)



(d)

Figure 4-19 (continued)

It must be mentioned that although the shorter chain derivatives tend to form domains as spread, microstructural changes are still possible as the area is decreased since the domain density is expected to increase with increasing lateral pressure due to compression.¹²⁰ For PPAC-16 , this flat region represents little surface dipole contribution from both the terminal methyl group and the carbonyl functionality in the polymer.¹⁰⁵ This may be associated with changes in the packing density of the other carbons in the chain with increasing van der Waals interaction, but with little dipole contribution. PPAC-8 showed no flatness at this region but rather proceeded to decrease right away (region III).

At lower surface areas (region III) most of the contributions to the apparent surface dipole could be expected to come from the carbonyl group which is nearer to the backbone. The decrease in dipole at this overfilm region could be associated mostly with a reorientation of the carbonyl towards negative dipole contribution resulting in decrease in the apparent surface dipole.^{105,173} This is reasonable for two reasons: the low surface areas would significantly restrict the mobility of the alkyl chain because of increased van der Waals interaction. Secondly, the polymer backbones will be much closer with each other because of the high pressure environment. Although it would not be possible to assign specific orientations by vectorial summation of the contributing dipoles, this region would represent a highly compressed state (collapse) for all the polymers.^{177 113,105}

For PPAC-8, the steep decrease (region II-III) immediately after the maximum increase in surface dipole signified a balance between the contribution of the carbonyl group and the alkyl chain to the surface dipole. This would mean that at the event in which the methyl group contribution was about to peak (similar to PPAC-16), the negative dipole contribution of the carbonyl group ensues, resulting in the immediate decrease in the surface dipole.¹⁷⁶

The absence of the flat region could signify the immediate transition to a highly compressed state without a liquid condensed phase.

Brewster Angle Microscopy

To correlate the changes in the Π -A and V-A isotherms directly with the morphology of the polymers at the interface, Brewster angle microscopy measurements using a *BAM-1* microscope system from Nanofilm Technologie were made.¹⁷⁸ The images were generally recorded with the same compression conditions as the surface pressure and potential isotherms. Representative images of the films were taken at various areas in the isotherm (Figure 4-20, 4-21, and 4-22) and references can be made on the plots of Figure 4-15 and 4-19 for the corresponding surface pressure and surface potential behavior.

What is immediately evident from these images is that at high areas, the short alkyl chain derivatives PPAC-1 and PPAC-4 formed flakes or glass-like domains at the interface. These domains are not deformable. The size of these flakes vary with the concentration of the spreading solutions. A heterophase domain image at higher concentrations is observed, where the different shades of gray indicate the various thicknesses within the domain. At lower areas with compression, a homogeneous film is observed. For PPAC-8 the same phenomena can be observed. On the other hand, highly deformable foam-like domains are observed for the PPAC-16 at high areas. The monolayer is fluid and a statistical distribution of holes are observed. The kinetics and thermodynamics of this foam formation were not investigated further though.

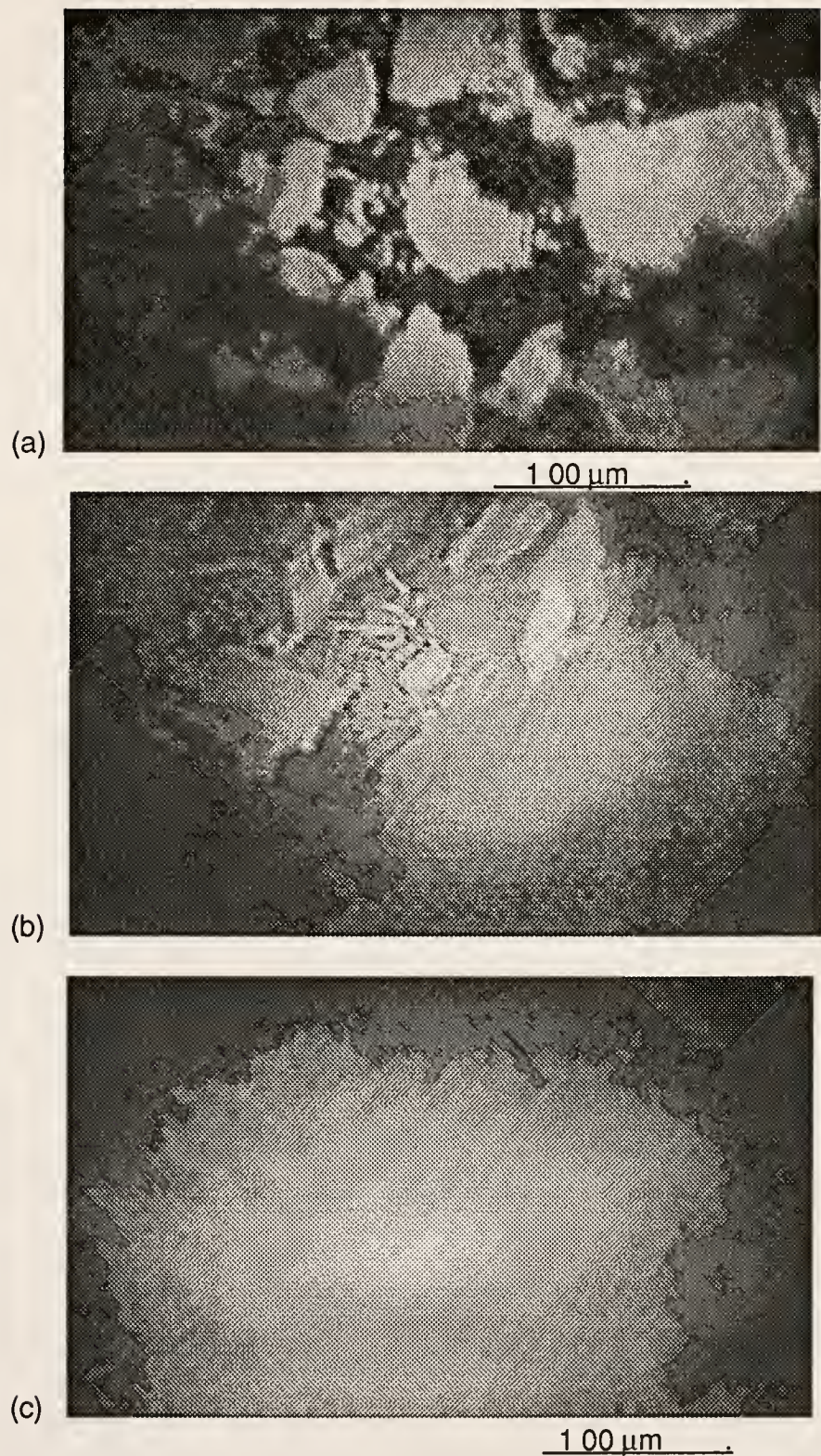


Figure 4-20. BAM images of PPAC-1 at 25 °C, with cross-polarizers set at 90°.
Refer to Figure 4-15 for surface-pressure area isotherm. Images taken at corresponding areas of: (a) 50, (b) 35, (c) 19 Å²/(repeat unit)

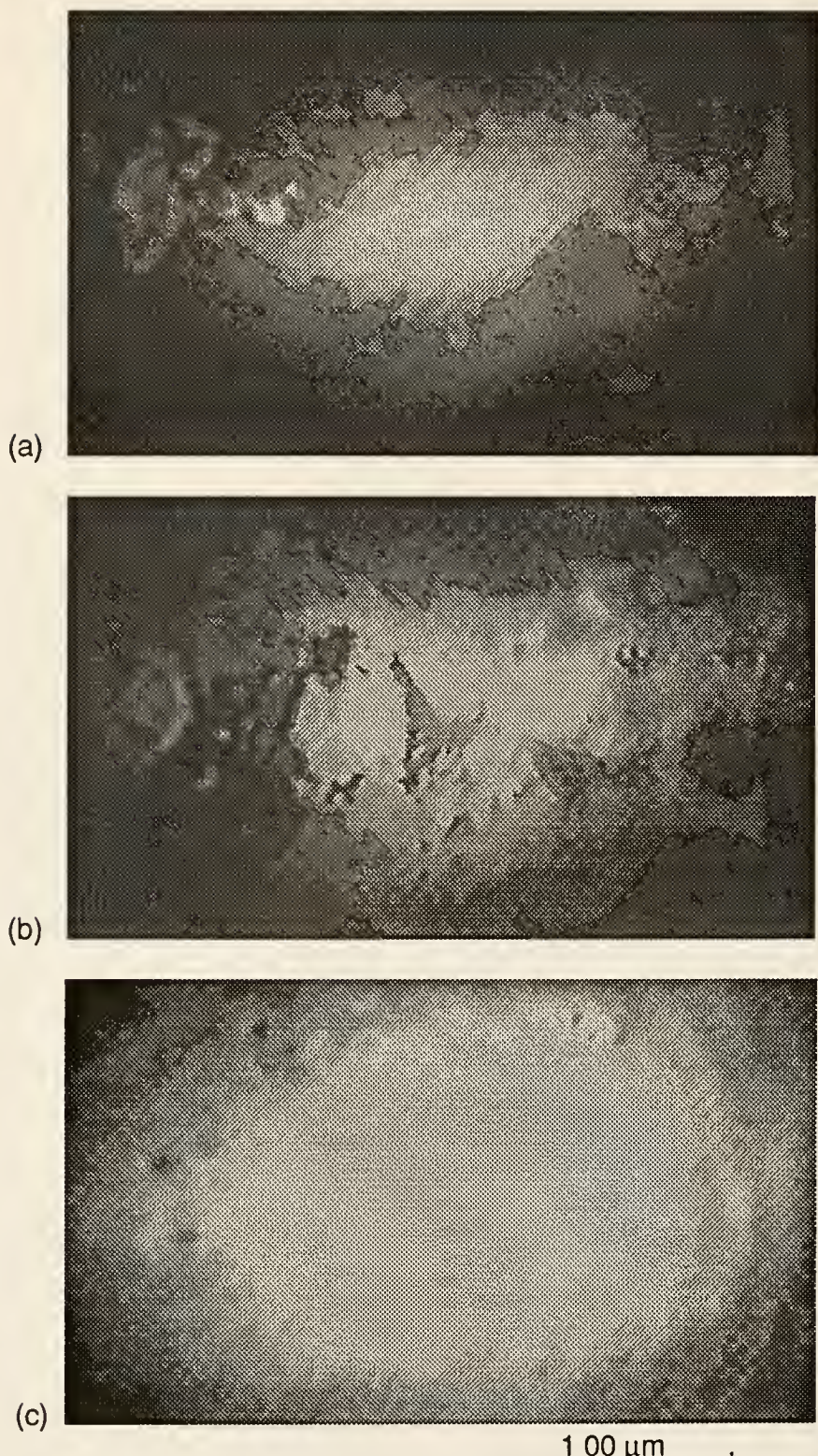


Figure 4-21. BAM images of PPAC-8 at 25 °C, with cross-polarizers set at 90°. Refer to Figure 4-15 for surface-pressure area isotherm. Images taken at corresponding areas of: (a) 50, (b) 32, (c) 20 Å²/(repeat unit)

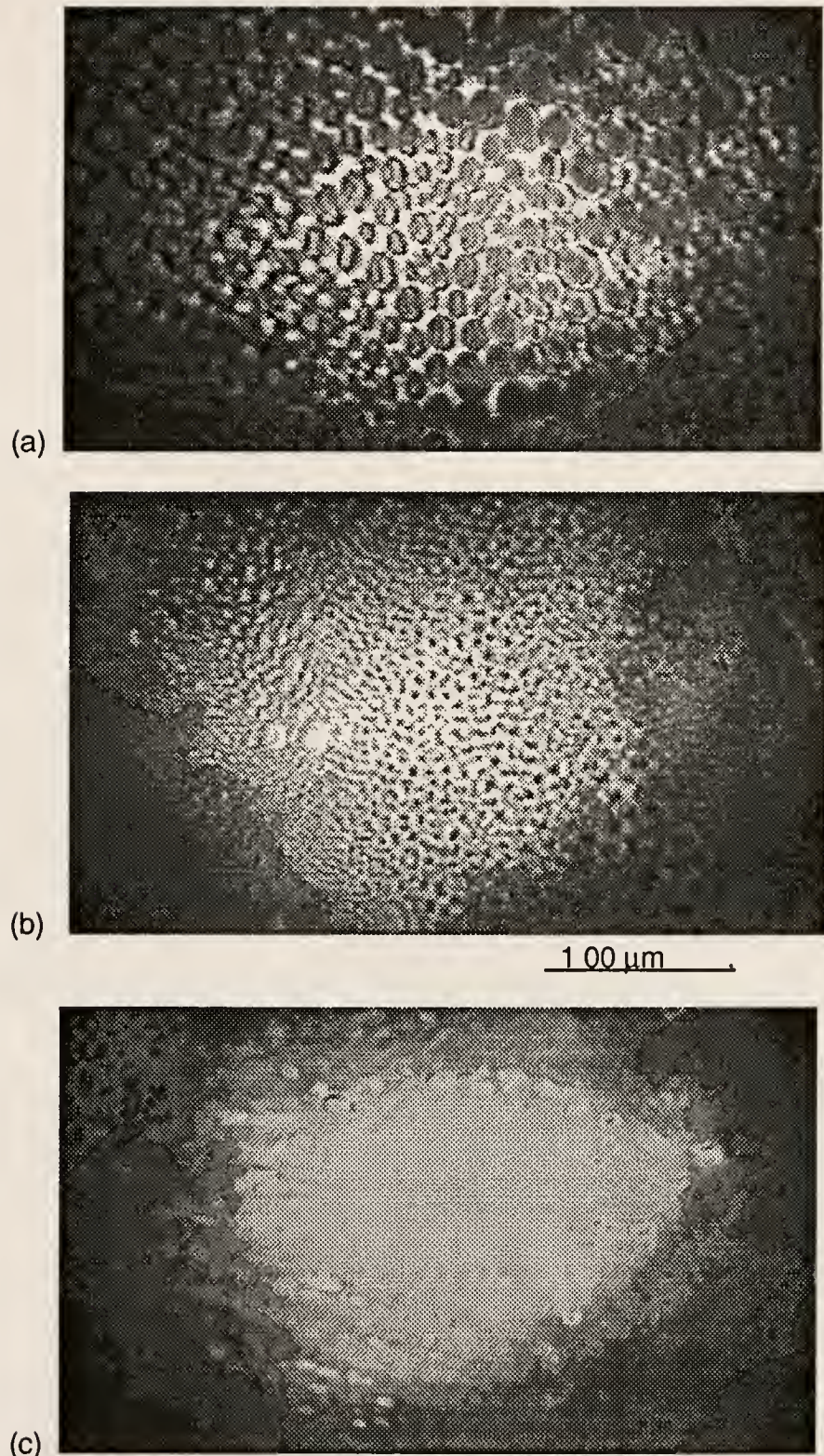


Figure 4-22. BAM images of PPAC-16 at 25 °C, with cross-polarizers set at 90°. Refer to Figure 4-15 for surface-pressure area isotherm. Images taken at corresponding areas of: (a) 50, (b) 43, (c) 30 Å²/(repeat unit)

These results are somehow consistent with the π -A isotherm behavior. PPAC-1 and 4 forms what appears to be highly viscous films with some concentration dependence. From the BAM images, it is seen that the polymer is actually "precipitated" out during spreading, the size of the domains being dependent on concentration and spreading method. These domains tend to "fuse" together with compression (high pressure environment) where the domain boundaries are in contact with each other. Therefore, despite the initial formation of domains, a homogeneous heterophase film is formed up to the overfilm region especially with dilute spreading concentrations. It is expected that at this stage, pressure due to compression will have a considerable effect on the density of the monolayer. Since the polymer domains can be regarded as "isolated islands" upon spreading, pressure due to compression will have little effect at high areas. However, once the domains have been fused, the effect of pressure will be directed to the film itself, rather than the interface region as a whole. As discussed earlier, the surface dipole measurements reveal little of these domain formation as the surface potential is measured over a wide surface area relative to the domain size. However, at low areas, the surface dipole moment measurements is a reflection of changes in the monolayer density. This is observed with the negative surface dipole effect for the polymers at lower areas (region III) as discussed earlier.

PPAC-16, forms foam like domains that are highly deformable with little concentration dependence. The fluid nature of the monolayer suggests the role played by the attached alkyl chains as "bond solvent" to the polymer backbone. We suppose that this difference in morphology is brought about by the influence of the side chain acting as an internal plasticizer.^{179,105} Thus the polymer-polymer interaction is decoupled by the long alkyl chain derivative leading to a fluid monolayer. At the overfilm region, a transition to the bilayer domain is

observed by the formation of "white streaks" which are perpendicular to the direction of compression. These observed white regions within the domain are thought to be nucleation bands for the transition to the bilayer or multilayer region.

For PPAC-8, the formation of flakes at the interface despite a different surface potential (dipole) behavior than PPAC-1 and PPAC-4 is surprising. Moreover, the observed changes in the surface potential (dipole) for PPAC-8 did show some concentration dependence. As discussed earlier, the surface dipole changes at high areas are mainly associated with concentration effects. Since the film is observed to be relatively homogeneous near the surface potential (dipole) onset, this may indicate that the apparent increase in the dipole is essentially a phenomenon of the monolayer film and not the domains. This is in contrast to the short chain derivatives which exhibited the increase in surface dipole while the domains were still fusing together. Therefore the surface dipole behavior as discussed earlier may be more related to the phenomena of PPAC-16, than to the short chain derivatives.

Deposition of LB films

LB Film deposition (vertical dipping) was tried on the polymers of these series using glass and quartz substrates. No deposition was made for Polymers 2 and 3 since their monolayer behavior was observed to be similar to the shorter alkyl chain derivatives. Hydrophobization of the slides was done according to the procedure in Chapter 2. Hydrophobic slides were used for the experiment. The dipping speed, waiting time, and surface pressure were varied in order to maximize dipping conditions.

The result is that PPAC-1,4, and 8 did not deposit with the vertical dipping method. On the other hand, PPAC-16 deposits well only on the downstroke (X-type) but with partial removal in the upstroke. To circumvent this difficulty, alternate dipping was employed to get better deposition ratios. The result is shown in Figure 4-23.

To enhance the deposition properties of the other polymers, blends with stearic acid (SA) and the polymer were made.¹⁸⁰ A polymer:stearic acid ratio of 4:1 and 1:1 was used. These monolayer films resulted in z-type films for PPAC-1(1:1) and x-type films for PPAC-8 (1:1 and 4:1) respectively. However, the miscibility of the polymers and stearic acid e.g. domain distribution and phase separation was unknown.

To verify the monolayer mixing properties, surface pressure isotherms and Brewster Angle microscopy was used. The surface pressure-area isotherms with stearic acid are shown in Figure 4-24. Comparison of the mean molecular areas with their respective molar ratios, show that the PPAC-1 blend at both 1:4 and 1:1 were additive, meaning they could behave as an ideal solution, but were probably immiscible.

This immiscibility was in fact observed with the Brewster angle microscope, in which separate domains are observed especially at high areas, where the stearic acid is usually fluid (Figures 4-26, 4-27, and 4-28). The polymer appeared as irregularly shaped domains with a lighter contrast as compared to the stearic acid domains. For PPAC-8 blends, the isotherm areas showed a slight negative deviation observed at 1:1 while the 4:1 blend was additive. From the BAM pictures, this behavior seem to be correlated by the more fluid 1:1 mixture as compared to the 4:1. However, at high pressures (near the collapse point), the appearance of randomly distributed white streaks with the PPAC-8:SA 1:1 mixture may indicate phase separation at these

conditions. This means that a compromise on the blending properties of the polymer and stearic acid is reached at a definite pressure below collapse.

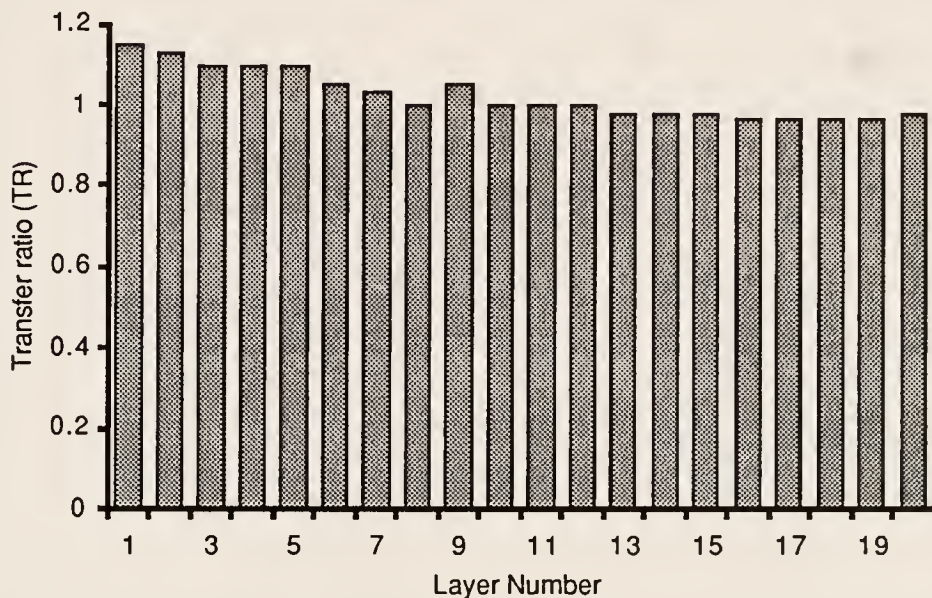


Figure 4-23. Dipping data for PPAC-16 using the alternate tough deposited on the downstroke mode (x-type) at 25 °C, $\Pi = 6 \text{ mN/m}$, and rate of 10 mm/min.

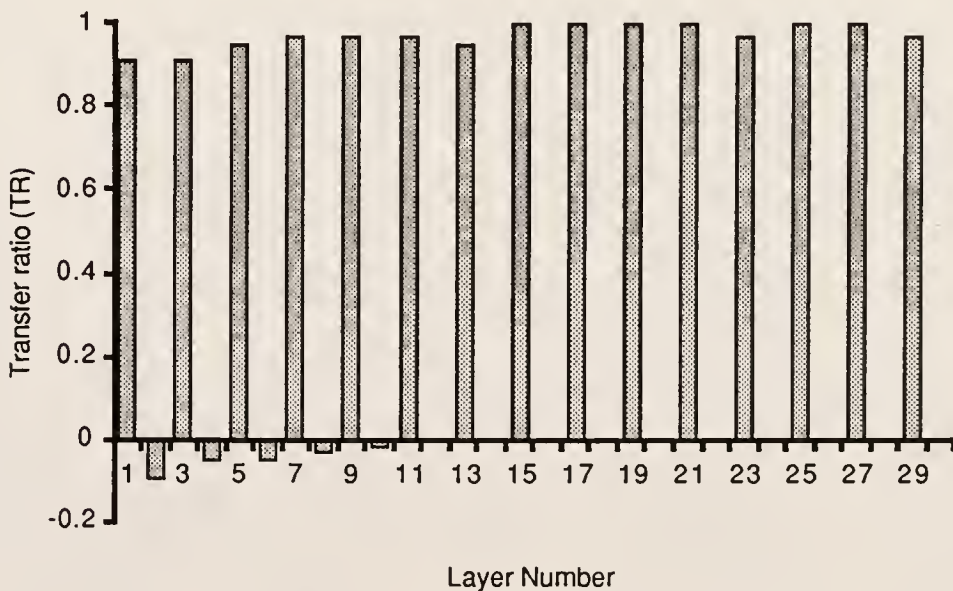
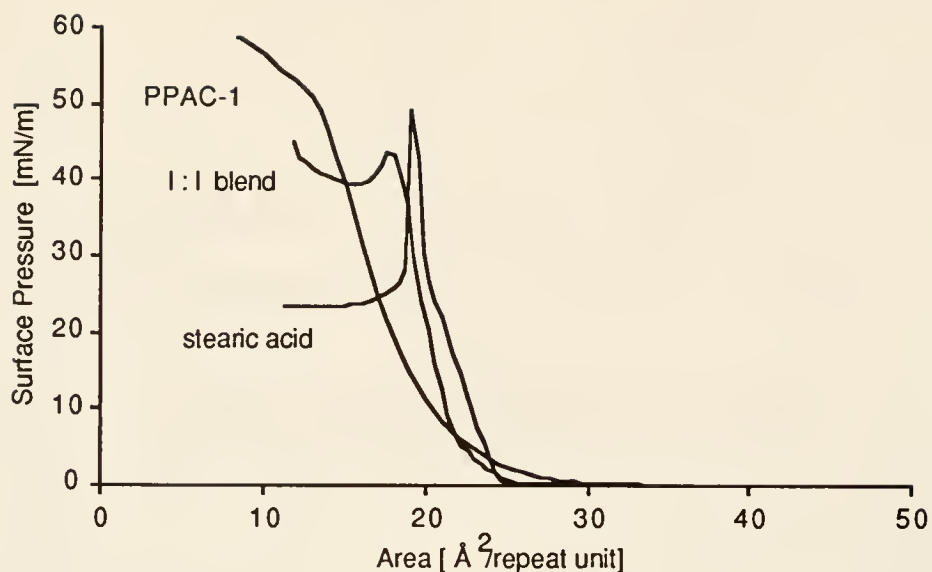
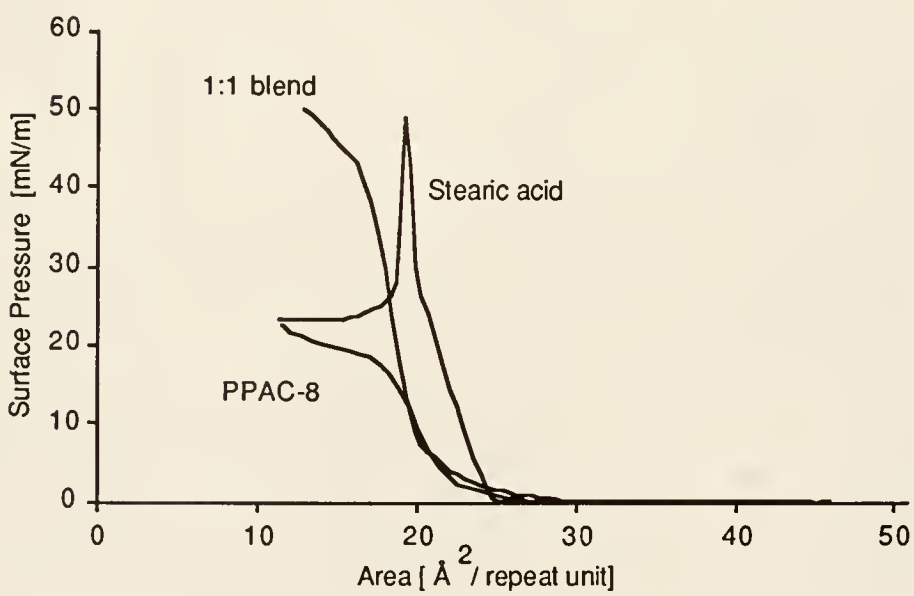


Figure 4-24. Deposition ratios for blend of PPAC-8:SA 1:1 on a conventional trough a 25 °C, $\Pi=19 \text{ mN/m}$, and 10 mm/min speed. (Note: odd number of layers represent downstroke indicating x-type deposition)

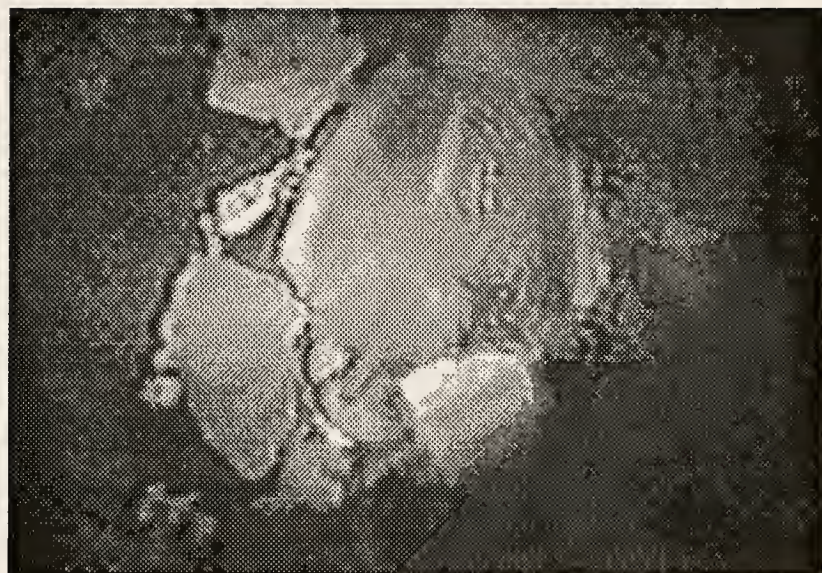


(a)



(b)

Figure 4-25. Surface-pressure - area isotherms for (a) PPAC-1:SA, 1:1blend and (b) PPAC-8:SA, 1:1 blend at 25 ° C and 3 $\text{\AA}^2/(\text{repeat unit} \times \text{min.})$ compression rate.



(a)

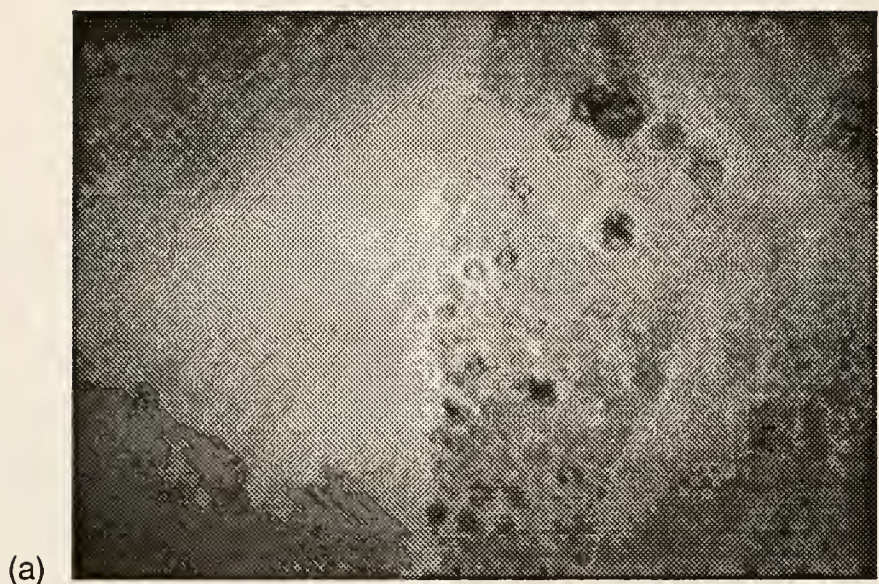
1 00 μm .



(b)

1 00 μm .

Figure 4-26. Brewster angle microscopy for Blends of PPAC-1 and stearic acid at 25 °C with cross polarizers set at 90°. Refer to Figure 4-25 for Π -A isotherm: (a) PPAC-1:SA ,1:1 blend , 25 \AA^2 /(rep.unit) and (b) PPAC-1:SA 4:1 blend, 25 \AA^2 /(rep.unit).



(a)

1 00 μm .



(b)

1 00 μm .

Figure 4-27. Brewster angle microscope images for PPAC-8:SA 4:1 blend taken at 25 °C. The pictures correspond to (a) 30 and (b) 22 $\text{\AA}^2/(\text{repeat unit})$

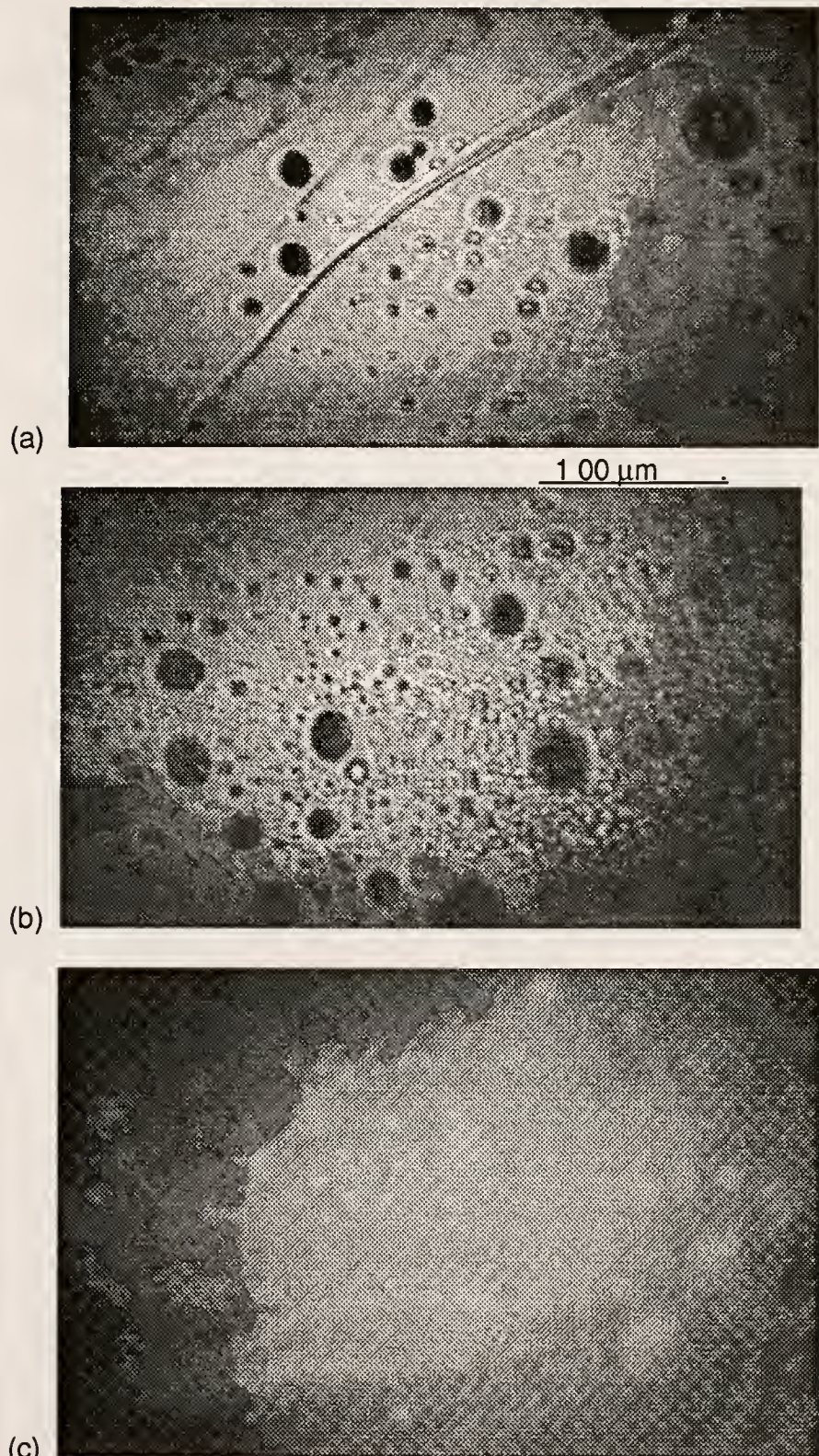


Figure 4-28. BAM images of PPAC-8:SA 1:1 blend at 25 °C. Refer to Figure 4-25 for the isotherm. Images correspond to areas: (a) 30, (b) 27, (c) 19, (d) 18 Å²/(repeat unit).

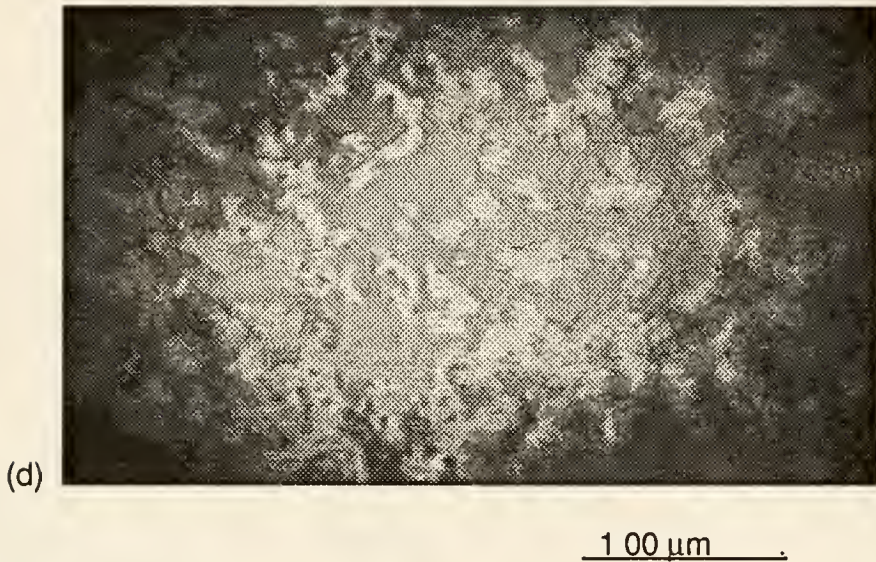


Figure 4-28 (continued)

100 μm.

These results show that only PPAC-16 is inherently depositable to substrates and that blending is necessary for good deposition of PPAC-8. Although, films are formed for PPAC-1, the nature of the film behavior, suggests that no long range ordering is observed and that good deposition of this films is a consequence of monolayer stabilization and plasticization by stearic acid alone and not through a favorable polymer-stearic acid interaction. On the other hand, for PPAC-8 at the 1:1 ratio, good miscibility (at a pressure below the collapse) is observed in the quality of the film and therefore a favorable interaction with the stearic acid is observed.

Summary

This study has shown that the different substituents played an important role in determining the local conformational behavior of the polymers and their chain microstructure. The higher *trans/cis* ratio is a consequence of a substituent effect and the type of catalyst used. Computer modeling of the configurations suggested that the *trans-transoidal*, head to head placement

combination, is the only configuration capable of giving substituted polyacetylenes free from steric interaction between the substituents. Regiospecific catalysts (as alternate mechanisms to chain addition) should play an important role achieving this configuration in the synthesis of these polymers. During formation, the polymers essentially retain their configuration and conformation. The substituents are "locked in" by the backbone configuration, the degree of which is dependent on the stiffness of the substituent and presence of flexible side chains.

The semi-rigid nature of the backbone and the role of the substituent is further observed at the air-water interface. The configuration and conformation is essentially retained at the interface. The stiff substituent contributed little to enhancing film forming properties but appeared to amplify the role of the alkyl chain attached to it. The effect though, of longer alkyl chain length tended to enhance the positive spreading properties of the polymers. This behavior can be discussed in terms of the balance between polymer-polymer interchain attraction and subphase hydration of the carbonyl groups. The consequence of the shorter chain length results in stronger cohesive forces between the polymer chains. That is the polymer-polymer interaction is favorable compared to the polymer-subphase interaction. The ester group is not favorably hydrated and the hydrophilic character seems weak, compared to the hydrophobicity. This is in contrast to the well-known behavior of esters attached to the polymer backbone of a series of polymethacrylates.¹⁸¹ The basic difference in behavior, therefore lies mainly in the character of the backbone.

The value of α which is calculated using the Mark Houwink equation is found to be equal to 0.92 for all these polymers regardless of the chain length. The parameter α is a measure of chain stiffness and has a range of 2.0 for a rigid polymer backbone and 0.6 for a flexible type.¹⁸² This means that the

polymer backbone is indeed of a semi-rigid type. Rigidity of the polymer backbone is therefore a contributing factor that gives rise to these polymers' conformational behavior at the interface. The fact that the value of α for all polymers is similar suggests that this semi-rigidity is brought about mainly by the phenyl part of the substituent, regardless of the alkyl side chain length. This behavior holds true for the solution properties in a non-theta solvent. However, marked differences in behavior were observed for these polymers at the air-water interface. It seems that the alkyl chains have greater freedom to interact because of the lack of solvent molecules to solvate the chains. The result is that PPAC-8 and PPAC-16, the longer chain length derivatives among the series showed better monolayer behavior at the interface. The monolayer properties of the PPAC-8 polymer approaches that of the PPAC-16 specially at higher temperatures but is not as fluid as the latter. These results are consistent with the observed transitions with the DSC in which at room temperature the PPAC-16 chains are already melted, while they did not melt until 75 °C for the PPAC-8 derivative.

The deposition of the polymers on to substrates, likewise emphasizes the importance of the long alkyl chain length. PPAC-16 is able to deposit with good deposition ratios, especially in the downstroke mode (x-type). The formation of domains, as observed with BAM for the shorter chain length derivatives, prevent the polymers from having a greater attraction to the substrate than the subphase. However, blending with stearic acid results in better deposition properties, but good film quality is only realizable with the PPAC-8 derivative, which as mentioned earlier, approaches the PPAC-16 behavior. This however demonstrates the ability of this polymers to form good multilayer film structures by the LB film deposition technique.

CHAPTER 5

APPROACH II(B): POLY(DIETHYLDIPROPARGYLMALONATE) HIGH AND LOW MOLECULAR WEIGHT POLYMERS WITH IMPROVED CONFIGURATION

Introduction

The conformational behavior of the substituted polyacetylene backbone is limited by the rotations of the single bond.¹⁶⁶ In the previous study of polyethynylbenzoate polymers, it was shown that configuration is an important limiting factor in both the length of the conjugated segment and the monolayer behavior.^{183,47} To investigate a polymer with improved configuration, a cyclopolymerized substituted polyacetylene was synthesized as shown in Figure 5-1. The improved *trans-transoidal* configuration is due to the presence of a cyclohexene ring for every repeat unit, limiting rotations to the external single bond. The ring essentially locks the internal single bond from further rotations that can lead to helicoidal structures (conformational defects).¹²⁵ This is observed in the red shifted absorbance spectra (ave. 550 nm) for this class of polymers as compared to the previously studied substituted polyacetylenes.⁷⁴

At the same time, the molecular weight of the polymer was controlled. It has been found that high molecular weight polymers (average of 50 repeat units and more) have a tendency for increased chemical, configurational, and conformational defects.^{37,47} For the substituted polyacetylenes, these defects result in a lowering of the effective conjugated sequences (see Appendix B).⁹

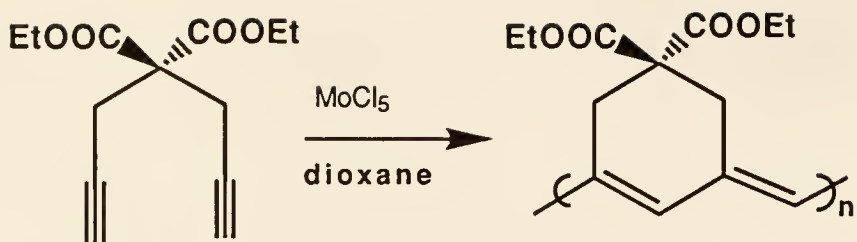


Figure 5-1. Polymerization of diethyldipropargylmalonate by metathesis catalyst MoCl_5 in dioxane under N_2 gas.

The diethyldipropargylmalonate monomer is a nonconjugated 1,6 diyne monomer. Cyclopolymerization of the monomer has been done previously by S.K. Choi and coworkers using the metathesis catalyst MoCl_5 in dioxane.⁷⁴ The use of this catalyst system resulted in the formation of high MW products of the order of 100,000 with an average polydispersity of 2. Previous work has also been done to cyclopolymerize the malonate derivatives using Schrock's Lewis acid free molybdenum alkylidene catalyst in solution.⁷⁶ A mechanism approaching that of living polymerization was proposed and low polydispersity polymers were obtained. Their results indicate that with controlled monomer feed, the desired MW can be achieved. The exact role of the Group 5 and 6 metathesis catalysts and the nature of the substituents attached to the acetylene is not known though. Schrock's group has proposed the formation of small amounts of five membered rings via α -addition using their catalyst.^{133,76}

In this research, we have sought to control the MW of the polymer by varying the polymerization conditions, in particular by limiting the time of polymerization.¹⁸² Other variables such as the monomer/catalyst ratio and the solution concentration were also explored. The main objective being to obtain a low and high molecular weight polymer for comparative studies. The monomer used was synthesized using common organic reactions and the synthetic route according to the literature.¹⁸⁴ The monomer was functionalized

considering that the presence of a good hydrophilic group should provide a better balance for the hydration of polymer monolayers at the air-water interface. In the present synthetic method, such functionalization is somewhat complicated by the sensitivity of the catalyst towards heteroatoms like N, O, and S which are common atoms in hydrophilic moieties. The ethyl ester group though, while not too destructive to the catalyst, was chosen as a starting point because it has sufficient hydrophilic character for polymer monolayers.^{105,74}

The behavior of the polymer at the air-water interface was studied by the Langmuir-Blodgett monolayer technique. It is important to characterize fully the monolayer film behavior. Not only is it useful for latter multilayer deposition, but it also gives an insight to film morphology and integrity as a whole. Thus, a number of surface analytical methods were used to characterize the monolayer behavior. Comparison was made for both molecular weight derivatives. Then detailed compression-expansion cycle studies were made to further characterize the contribution of the ester groups and polymer backbone on chain conformation and film behavior. Interesting conformational dynamics of the polymer backbone were observed by UV-vis spectroscopy and correlated with the other measurements. The low molecular weight derivative had an overall better monolayer behavior than the high molecular weight polymer. The differences and behavior of the polymers are discussed in terms of the functional groups in the repeat unit structure and the intermolecular forces involved. A theoretical representation of the conformational dynamics of the conjugated backbone is also discussed. Successful deposition of both polymers was made using the vertical deposition technique. LB films up to 30 layers on glass and silicon substrates gave an average transfer ratio of 1.0 ± 0.05 . For the low molecular weight derivative, interesting alternating superlattice structures were made with stearic acid.

Synthesis of the Polymer

As in the previous study, polymerization of the monomer was done under N₂ gas using the Schlenck tube technique. The monomer had been initially synthesized with good purity as determined by ¹H NMR, ¹³C NMR, IR, and elemental analysis. Details of the synthesis are found in the experimental section of this work.

Three different experimental conditions were varied: time of polymerization, monomer catalyst ratio, and solution concentration. Reactions were carried out at room temperature (25 °C) for the low MW polymers and 35 °C for the high MW derivatives. No comprehensive attempt was made to study in detail the effect of the polymerization conditions on conversion, MW distribution, and degree of polymerization. The primary objective being to obtain a high and low molecular weight polymer of sufficient purity for LB film studies. The results are summarized in Table 5-1.

A black amorphous product is obtained by precipitation from methanol. The polymer is readily soluble in common organic solvents such as THF and chloroform to form a purple colored solution. Small insoluble fractions were isolated which would indicate the presence of some cross-linked products. No further characterization on the extent of crosslinking was possible as the amount of insoluble material was so small compared to the soluble product. The polymer is stable in air and in solution for long periods of time, consistent with literature findings. Films of good optical quality can be prepared by film casting on a glass substrate. Characterization of the polymers was done using ¹H NMR, ¹³C NMR, FT-IR and UV-Vis spectroscopies. Elemental analysis confirmed a low ash content which indicated little left-over catalyst. In general, no large differences in the structural characteristics of the polymers were

observed except for the molecular weight. Representative data of the high and low molecular weight polymers are as follows:

Table 5-1. Summary of results for polymerization of the malonate derivative with different conditions.

Polymer	Cat/Mo ratio (mole ratio)	Conc. in [M] ±0.02	Time of rxn [hour]	% Conv. *	color	UV-vis $\lambda_{\text{max}}(\epsilon_{\text{max}})$ nm($M^{-1}cm^{-1}$)
pDDM1H	1:50	0.07	24	88 %	purple	550 (6790)
pDDM2H	1:50	0.15	24	63 %	purple	550 (7850)
pDDM3H	1:50	0.30	24	70 %	purple	550 (9320)
pDDM25	1:25	0.15	24	66 %	purple	545 (5960)
pDDM1L	1:50	0.12	1	40%	purple	546 (6680)
pDDM2L	1:50	0.12	3	45%	purple	542 (8123)
pDDM3L	1:50	0.12	12	55%	purple	548 (6550)
pDDM4L	1:50	0.12	18	68%	purple	551(6300)

* Global yield. Some insoluble fraction was obtained possibly due to cross-linked products. Look at Table 2-2 in experimental section for complete data.

Representative NMR spectra of the monomer and high and low molecular weight polymer derivatives are shown in Figure 5-2 and 5-3. A broad trimodal resonance band of 6.4 to 7 ppm observed with the ^1H NMR, can be assigned to the conjugated double bond hydrogens of the polymer backbone. The peak at 6.7 ppm is observed to be consistently sharper with the low molecular weight derivatives. The disappearance of the resonance peak at 2.1 ppm and the broadening of the other peaks relative to the monomer spectra are all indicative of polymerization.

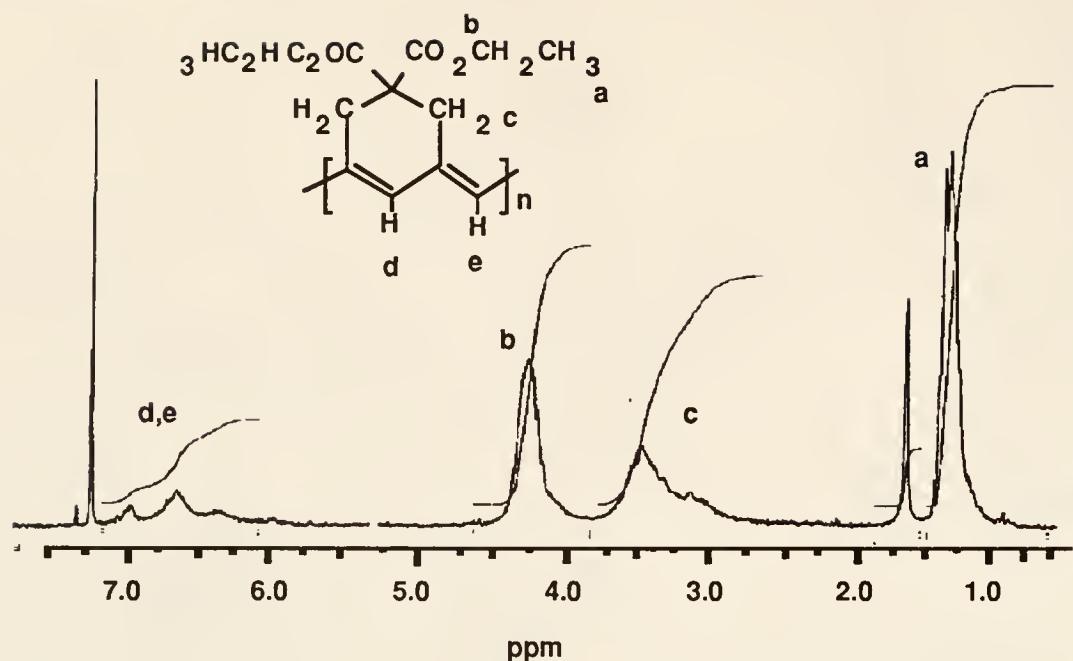
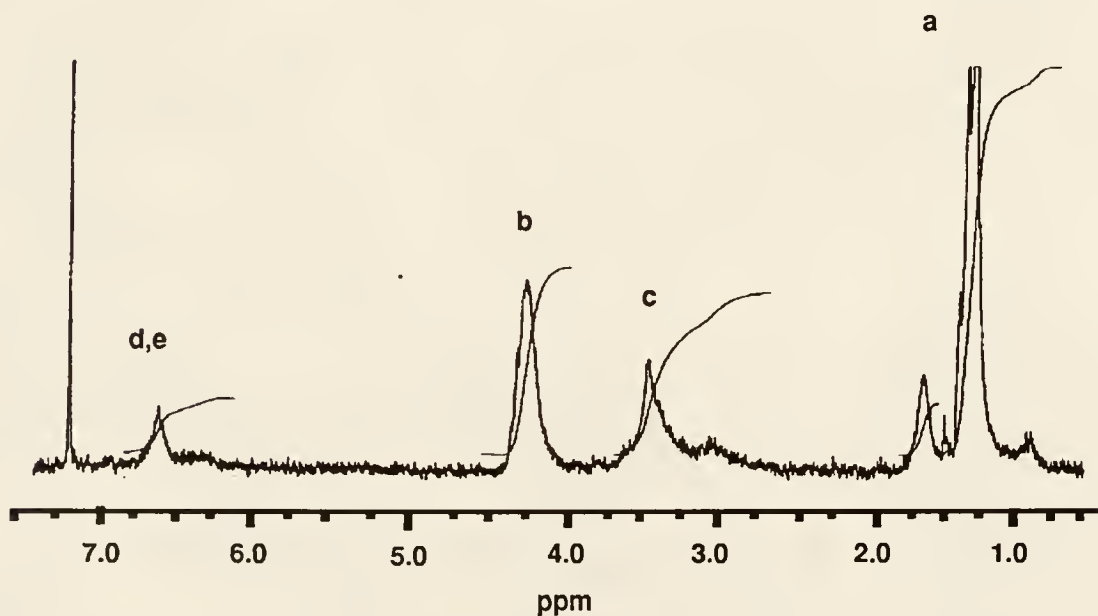
(a) ^1H NMR pDDM3H(b) ^1H NMR pDDM1L

Figure 5-2. ^1H NMR spectra of (a) high (pDDM3H) and (b) low (pDDM1L) molecular weight polymer in CDCl_3 .

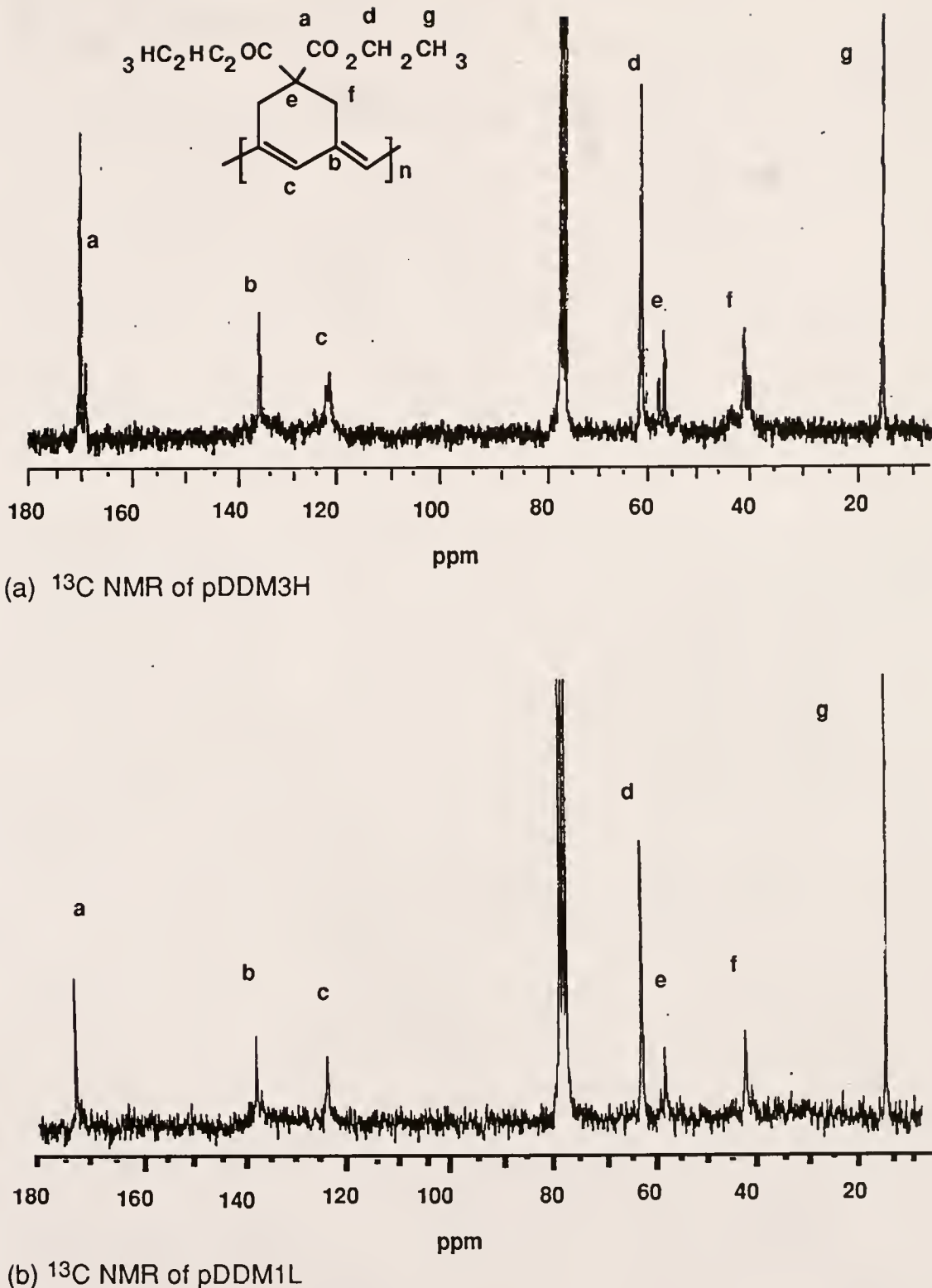


Figure 5-3. ^{13}C NMR Spectra of (a) high (pDDM3H) and (b) low (pDDM1L) molecular weight polymer. The peaks observed were consistent with those in the literature.⁷⁴

In the ^{13}C NMR, two peaks at 123 and 137 ppm can be assigned to the conjugated double bond and a peak at 172 ppm is due to the carbonyl carbon. The rest of the peaks can be assigned to the structure of the polymer repeat unit. All the values agree well with those found in the literature.

The IR spectra showed the conjugated carbon-carbon double bond stretching at 1600 cm^{-1} and the polyenic C-H out of plane bending vibrations at 970 cm^{-1} . A peak at 1015 cm^{-1} is assigned to a *trans* polyenic configuration. No peak was observed at 740 cm^{-1} , which is usually assigned to a *cis* configuration. Likewise, no acetylenic hydrogen at 3300 cm^{-1} was observed. For the UV-vis spectra, the $\pi-\pi^*$ absorption is observed in the visible region of the spectrum (300-650 nm) with a maximum at 545 nm (see Figure 5-4). Not much difference was observed between the UV-vis spectra of low and high MW derivatives. Likewise the spectra from a cast film was similar to that in solution.

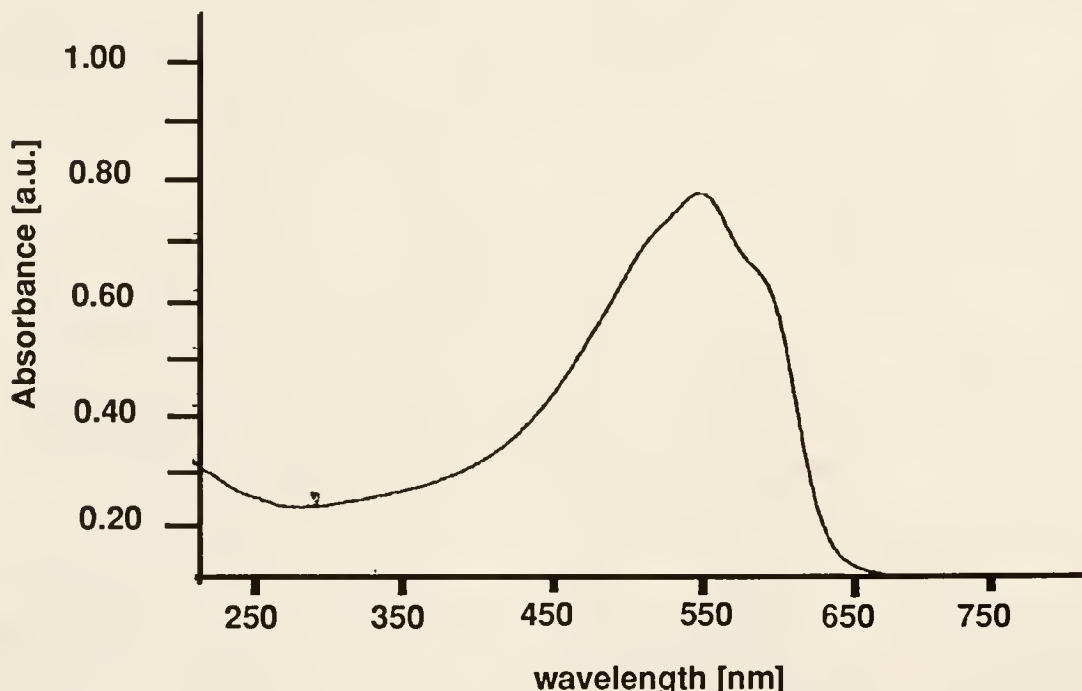


Figure 5-4. Representative UV vis-spectra in CHCl_3 (pDDM1L) low molecular weight polymer. No noticeable difference in peak shape or absorption maximum was observed with high MW polymers.

The molar extinction coefficient, ϵ_{max} , values, were taken from CHCl₃ solutions of the polymers. The observed values were typical of most substituted polyacetylenes.^{185,186,187,43} No apparent trend between MW and ϵ_{max} is observable though.

In contrast to the previously studied poly(ethynylbenzoate) polymers, the absorption spectra is characterized by a longer wavelength and a narrower band width. Using the model developed by Kuhn relating the length of the conjugated sequences and the UV-visible absorption maxima, the absorption band would put it near the convergence limit of 30 to 45 carbon average length of the polyene conjugated sequences.^{188,189} This absorbance behavior was verified more recently by Cohen with calculations for a series of conjugated polyenes.¹⁹⁰ Their treatment was even extended to predicting the nonlinear optical hyperpolarizability dependence on the conjugation length.

All the spectroscopic analyses show that the polymer was indeed formed. The relative molecular weights of the polymers were then obtained by GPC. A linear calibration curve of narrow weight polystyrene standards was used in a MW range from 1900 to 650,000 in MW. THF was used as a solvent and the samples were prepared with a range of 0.5 to 0.05 wt. %. A summary of the results are shown in Table 5-2.

GPC data show that there is a tendency for the polymer to give high MW fractions (observed from the appearance of the sharp peak), the more dilute the polymerization solution. The difference is probably due to the polymer chains remaining longer in solution and thus, the conversion to higher MW is achieved.^{191,182} This was not unfounded as the solution was observed to became gel-like and viscous with the more concentrated solutions especially near the end of the reaction. This high MW fraction is represented by a narrow peak with the range of 200,000- 350,000 g/mol.

Table 5-2. Molecular weight determination by Gel Permeation Chromatography (GPC) using a polystyrene calibration curve.

Polymer	Molecular Weight	Mw/Mn	Peak shape	UV-vis
pDDM1H	158,000	- *	bimodal	550
pDDM2H	89,857	1.786	near unimodal	550
pDDM3H	79,170	1.810	near unimodal	550
pDDM25	25,339	2.318	bimodal	545
pDDM1L	20,748	2.254	unimodal	546
pDDM2L	23,776	2.158	unimodal	542
pDDM3L	54,697	3.125	bimodal	548
pDDM4L	55,228	3.287	bimodal	551

* A narrow peak representing 20% of the eluted band represents a high MW fraction of $\approx 300,000$ is observed. Therefore, the calculated polydispersity may not represent the true distribution.

For the different times of polymerization, a broad peak is observed at 14 minutes elution time with a large polydispersity and a small peak at an elution time of 11 minutes is observed to grow the longer the reaction time. This represents a bimodal distribution of molecular weights in which lower MW polymers can be isolated at lower reaction times. The presence of the high MW peak was initially observed at 3 hours of polymerization time, and would grow significantly at 18 hours. Extrapolation to 24 hours reaction time gave the high MW peak as that of the pDDM2H sample.

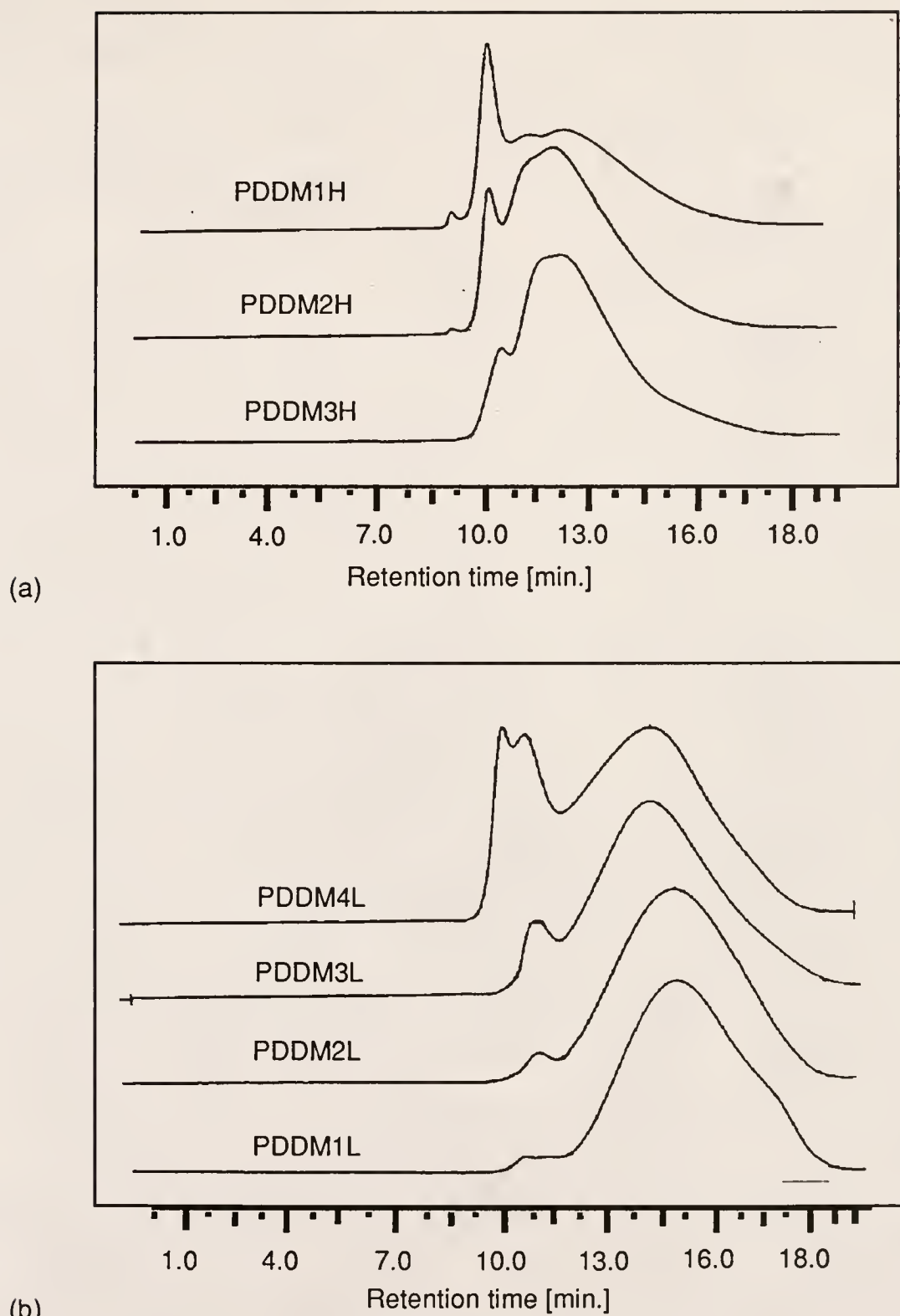


Figure 5-5. GPC or SEC Chromatogram of (a) high and (b) low MW polymers in THF using narrow MW polystyrene standards. Flow rate of 1.0 ml/min.

Longer reaction times lead to higher percent conversion for the lower MW series.^{192,193} Within the first hour of reaction, the average polymer MW of $\approx 20,000$ is formed. The presence of a high MW fraction is observed to increase with time.¹⁸⁶ Since the reaction temperature is lower than the usual reaction temperature of 35 °C, this would tend to lower the polymerization rate.⁵⁴ The slower rate in this case is an advantage in obtaining a low MW derivative.

All the polymers have higher degrees of polymerization than calculated from the monomer catalyst ratio. This is consistent with previous studies in which the rate of propagation is relatively faster than the rate of initiation for this catalyst system.⁷² For the higher amount of catalyst (pDDM25), a mixture of mostly low and high MW fractions is isolated, giving a broad polydispersity. Thus, lower MW polymers can be isolated at early times in the reaction. High MW polymer is obtained with longer reaction times and more diluted reaction mixture. The overall conversion of monomer to polymer increases with reaction time. The polydispersity is broad though compared to polymers obtained using Schrock's Lewis acid free molybdenum alkylidene catalyst. They have shown that the monomer/catalyst ratio was important in controlling the MW of the polymer using their catalyst.^{133,76} In this case, high MW polymers tend to give better polydispersity values using the present catalysts. Thus a low and high MW derivative were obtained to be used for comparative monolayer studies at the air-water interface.

Thermogravimetric Analysis

Thermogravimetric analysis of the polymer was done under N₂ gas in order to preclude the possibility of backbone oxidation in the weight loss. Figure 5-6 shows the TGA data for both the high and low MW polymer

derivatives of pDDM. The onset of weight loss for the high polymer is observed to begin at 305 °C and ends at 376 °C with 80% weight loss. On the other hand, the low MW polymer comprises a two step weight loss with a slow loss from 100 to 296 °C and a rapid loss from 296 to 365 °C with 75% loss. The initial weight loss may be attributed to gradual lost of CO₂, followed by polymer decomposition at higher temperatures.^{74,69} Thus, the results show the inherent stability of these polymers towards elevated temperatures. The high MW polymer as expected, showed better stability as compared to the low MW polymer.⁸²

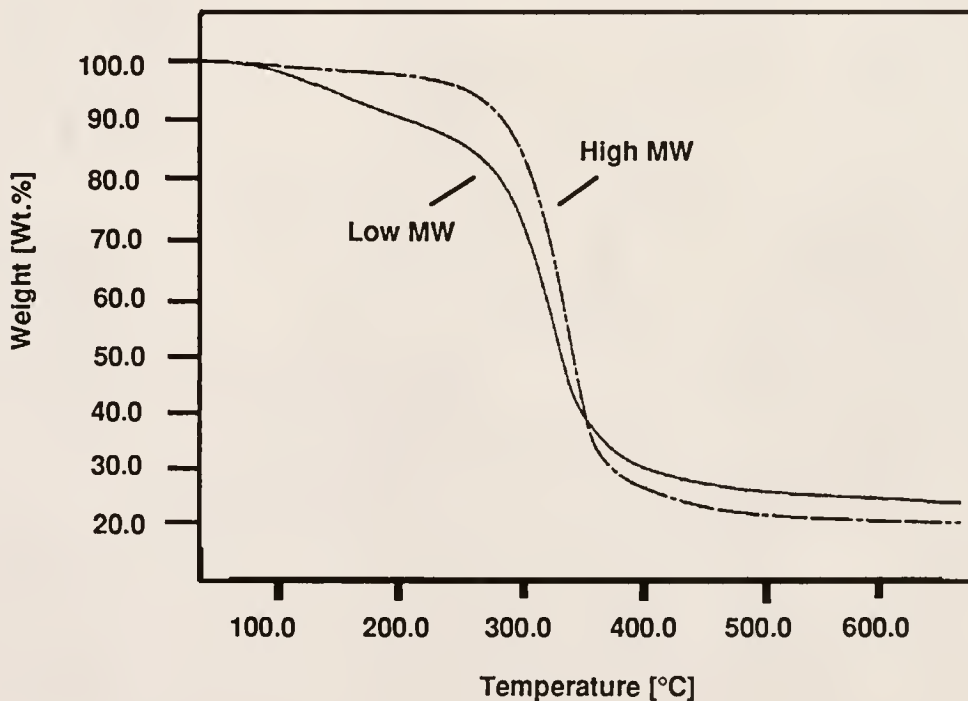


Figure 5-6. Thermogravimetric analysis (TGA) data for high and low MW polymer at 10 °C/min heating rate in N₂. Notice the expected difference in temperature stability between low and high MW derivatives.

Langmuir-Blodgett Film InvestigationsLangmuir Film Studies: Monolayer Structure and Orientation

For the Langmuir Film studies, two representative polymers from the high and low MW groups were chosen in order to compare their respective behavior at the interface: pDDM1L for the low molecular weight and the pDDM3H for the high molecular weight derivatives. The polymers were chosen because they had better polydispersity than the other derivatives of their respective molecular weight groups. With the structure of the polymers being the same, the dynamics of the low and high MW fractions are expected to be different at the interface and LB film.

Surface-pressure area isotherm.

The compressional isotherm of the polymers at room temperature are shown in Figure 5-7. Typical of polymers, no sharp transitions were observed.¹¹³ The pressure onset at the beginning of the isotherms are 55 and 48 Å²/(repeat unit [molecule]) for the high and low MW polymers respectively. The compression speed for these isotherms was at 3 Å²/(repeat unit x min); isotherms were reproducible within 1Å². Likewise, the high MW polymer has a higher collapse pressure than the low MW one, appearing in the isotherm as a change in slope at 32 mN/m and 45 mN/m for the low and high MW respectively. The area at which this change occurs is approximately the same, 22 Å²/(repeat unit) for both polymers. The high MW polymer showed some dependence on the spreading solution concentration especially between very dilute and concentrated solutions. It also showed some viscous nature, especially on a single barrier compression.

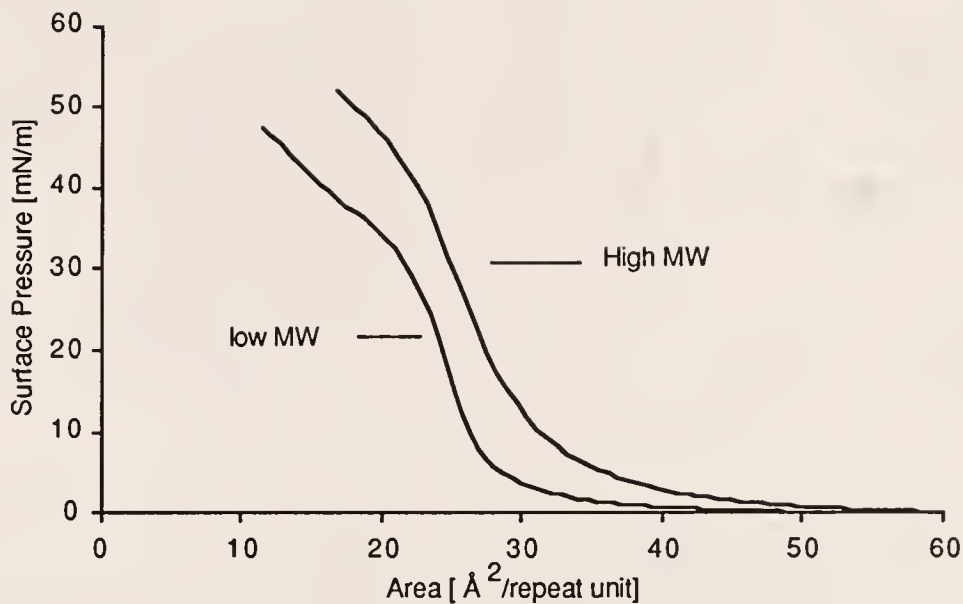


Figure 5-7. Surface Pressure-area Isotherms at 25 °C compressed with a speed of 3 Å²/(repeat unit x min.).

Both polymers exhibited compression rate dependence. This dependence is observed as a slight increase in compressibility and transition pressure to the overfilm region with increasing rate. The differences between the low and high MW polymers shown in Figure 5-7, however, persist even with different compression speeds. The greater compressibility observed in the isotherm at higher areas is consistent with entropically associated pressure changes.¹⁹⁴ Compression at different speeds brings about geometric constraints on the polymer conformation which prevents it from reforming to a lower energy conformation at the given time of observation.¹⁹⁵ The as-spread conformation tends to be kinetically trapped, causing the pressure build-up even at high areas. Thus, the variability of the slope is observed with different speeds. To obtain an isotherm free from the kinetics of compression, a stepwise equilibrium isotherm was measured for both polymers.⁸⁵ This zero speed curve was obtained by stepwise compression of the monolayer to a desired

area, followed by a relaxation of the pressure to a constant value. The isotherm which took several hours to record, is shown in Figure 5-8.

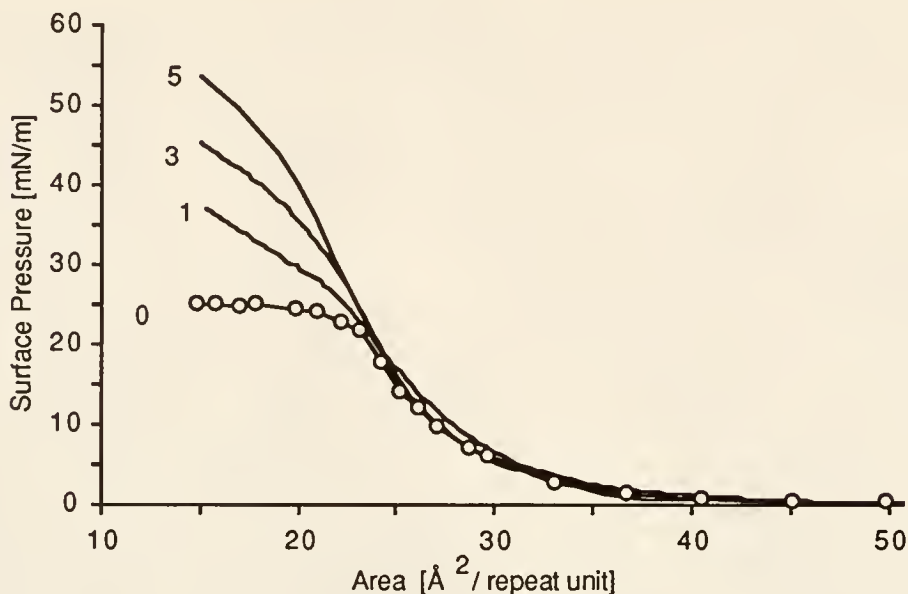


Figure 5-8. Step-wise equilibrium isotherm of low MW polymer, together with isotherms taken at various speeds. All were reproducible within 1 \AA^2 and were taken at 24°C . Note: numbers before the curves, indicate the rate of compression in $\text{\AA}^2/(\text{repeat unit} \times \text{min.})$)

Meaningful limiting area (A_0) values can be obtained by extrapolation of the low compressibility region to zero pressure. The repeat unit is defined as the cyclohexene ring, including the conjugated exo double bond. Accounting for the van der Waals radius, the theoretical value calculated from the area of the ring lying flat at the surface is 42 \AA^2 and 24 \AA^2 when it is orthogonal.¹⁰⁵ These values assume that the ester groups are hydrated and at the subphase. The observed limiting area (A_0) for both polymers, is in between the two values calculated for a repeat unit. This suggests that the conformation adopted by the polymer at the interface is statistically in between a planar and orthogonal orientation. Furthermore the low MW polymer seems to have adopted a more

orthogonal conformation to the interface at lower areas. A good analogy for the conformation is that of a "ribbon-like" structure, in which relatively planar segments are separated by conformational twists along the chain.³⁷

The collapse of the film occurs within the same area, but the transition pressure is higher for the high MW than the low MW polymer. The higher collapse is indicative of a more condensed film in which the overfilm transition is energetically higher.¹⁹⁶ This difference in intrinsic compressibility is further observed beyond the collapse point. For the step-equilibrium isotherm, the slope is relatively steeper for the high MW polymer, indicating higher pressures are needed to continuously deform the monolayer to the bulk phase. The fact that the isotherm is free from the kinetics of compression means that the property is inherent to the monolayer film. It should be noted that the term collapse here does not necessarily refer to the formation of the bilayer but a region in which the polymer chain has a tendency to "buckle-up".^{197,120} Due to the pressure of compression, this results in the formation of loops and tails at this overfilm region resulting in a change in the compressibility, and hence the slope.¹²⁰ That this overfilm region is a result of a homogeneous desorption process is also shown in the gradual change in the reflectivity curve (Figure 5-16) which is discussed in much detail later.

The effect of kinetics on the monolayer compression curve is also observed with surface pressure decay at constant area. As observed above, reducing the compression speed results in allowing partial relaxation of the film so that the curve approaches that of the zero speed isotherm. Faster speeds tend to kinetically trap the conformation as initially spread, which results in higher pressures due to reduced freedom to relax to a favorable conformation. This can be observed in a constant area stability measurements below collapse, where faster decay of the surface pressure with time is observed with

higher compression speeds. The above was evident only in the first 5 minutes, as the pressure remained stable onwards. With constant pressure measurements, both monolayers exhibited good isobaric creep stability for long periods of time at pressures below collapse. A surface area decay of less than 1 \AA^2 from 30 min. to 1 hour was observed at $\Pi=10 \text{ mN/m}$, suggesting sufficient film stability for LB film deposition. At pressures beyond the collapse, significant decrease in area is observed with time, e.g. 2 \AA^2 in the first 15 min. at $\Pi=35 \text{ mN/m}$, indicating much relaxation.

Temperature dependent isotherm measurements show that both films have a tendency to have lower collapse pressures with increased temperature. This effect is more pronounced with the low MW polymer as shown in Figure 5-9 where the collapse point became lower as the temperature increased. The change in the isotherm shape with temperature shows an endothermic behavior for the low MW polymer, where the increase in temperature aids in the transition to the overfilm region.¹⁷² This means that kinetically dependent transition phases should be facilitated at lower pressures if the temperature is raised. The fact that the isotherm shape below the collapse hardly changed for the different temperature isotherms indicate that this region is of greater equilibrium than the overfilm region.

Though the high MW polymer exhibited little dependence towards both compression speed (kinetics) and temperature (thermodynamics), the low MW exhibited strong dependence for both. What is surprising, is that the nature of change is almost similar and centered at the collapse transition and the region beyond. This means that the measured surface pressure beyond the collapse has both a thermodynamic and kinetic component.¹⁹⁸ It also shows the sensitive fluid nature of the low MW polymer as compared to the insensitive high MW polymer.

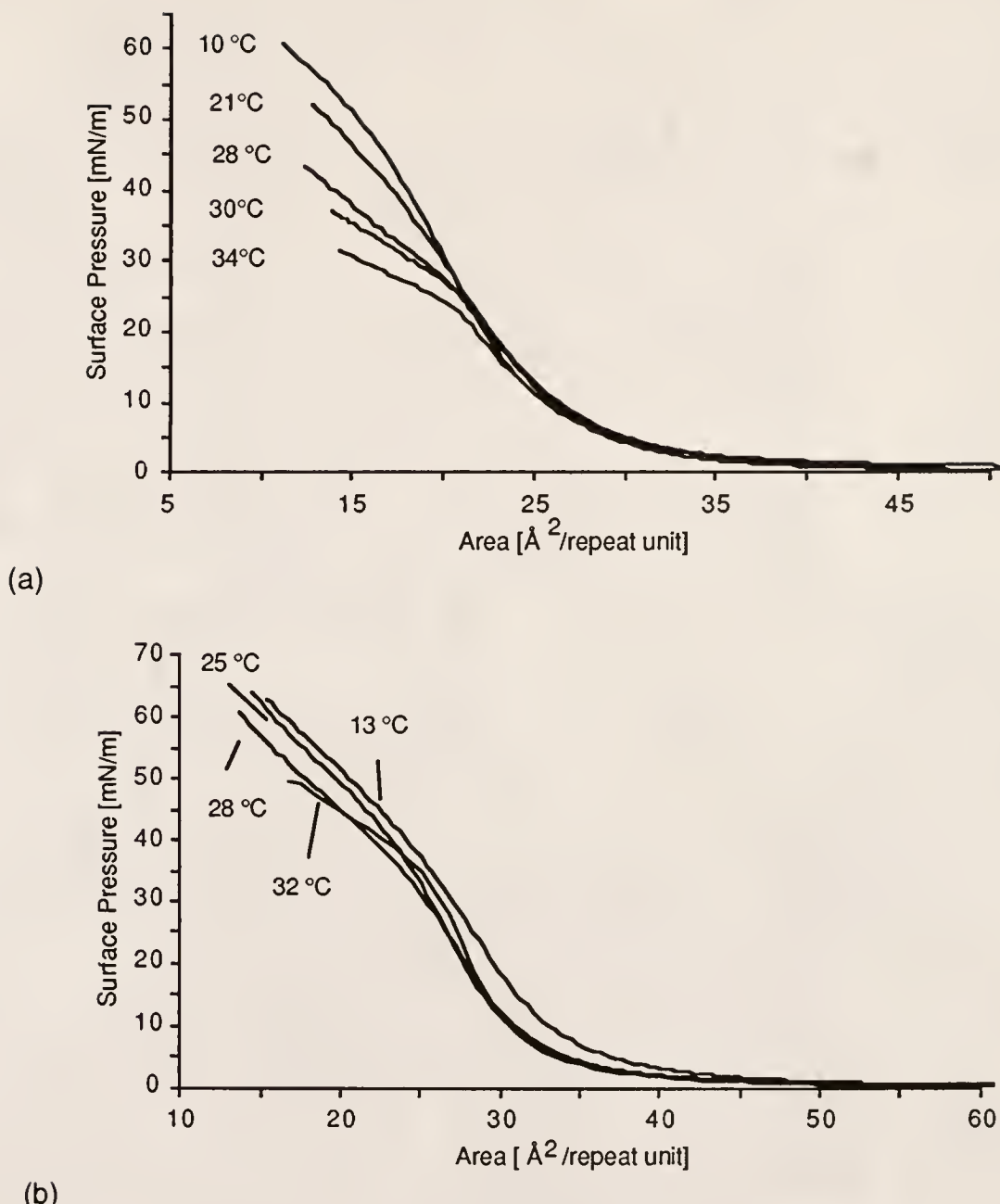


Figure 5-9. Surface pressure-area measurements at different temperatures compressed at $3 \text{\AA}^2/\text{repeat unit} \times \text{min}$. (a) Low MW polymer and (b) high MW polymer

The measurement of step-equilibrium isotherms at different temperatures and the use of the modified Clausius-Clapeyron equation should quantify this collapse transition behavior.¹⁹⁹ Recently, the thermodynamic and kinetic

components of the relaxation time beyond collapse has been quantified for a liquid crystalline side chain polymer monolayer by Duran and coworkers.²⁰⁰

Surface potential isotherms.

The surface potential in general, increased with compression but did not necessarily follow the curve of the isotherm as shown in Figure 5-10. The onset increase in surface potential starts at 20 \AA^2 in advance of the steep rise in the surface pressure isotherm. Higher areas (greater than 60 \AA^2) show fluctuations possibly due to the coexistence of high and low film density domains for the high MW and low MW polymers respectively.²⁰¹ The increase progresses up to the collapse area for both isotherms. At the collapse pressure onset, the surface potential curve becomes relatively flat. The net change is observed to be slightly higher for the high MW polymer.

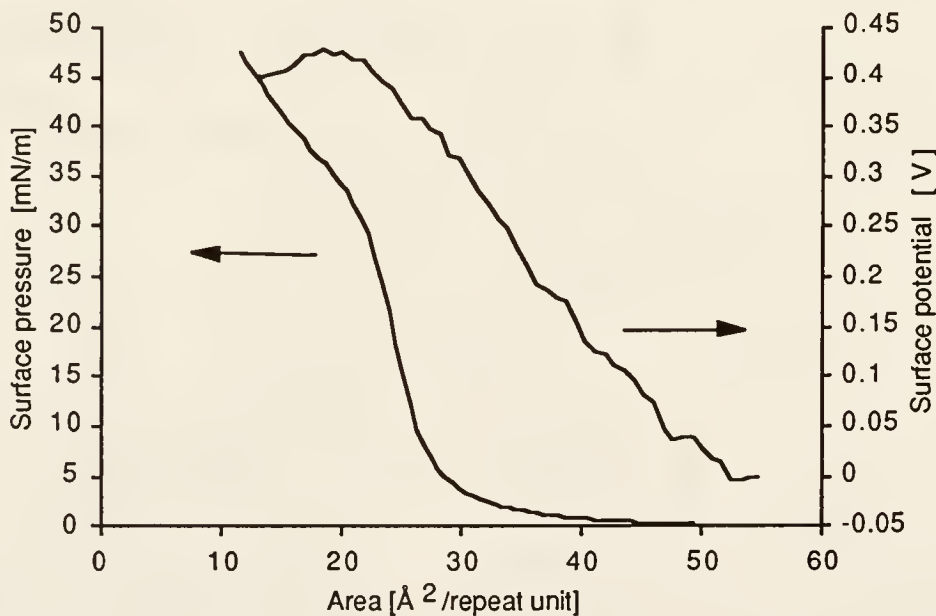
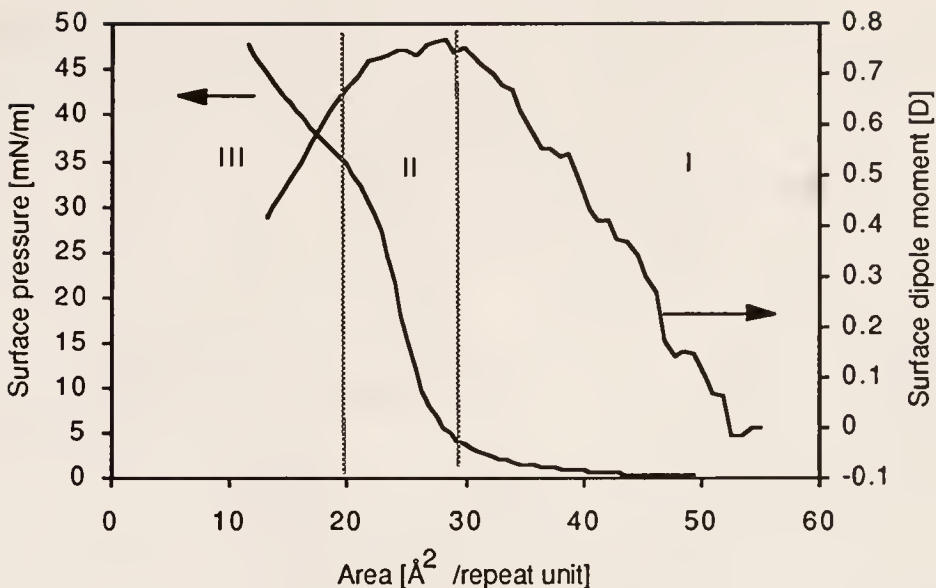
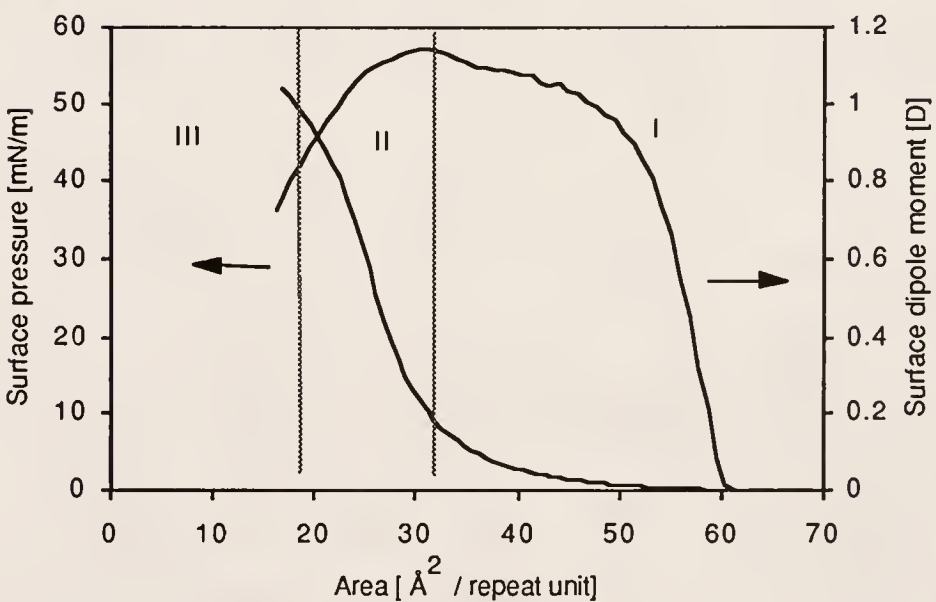


Figure 5-10. Surface potential isotherm for low MW polymer at 25°C and $3 \text{ \AA}^2/(\text{repeat unit} \times \text{min.})$ compression rate.



(a)



(b)

Figure 5-11. Surface dipole moment-area isotherms for (a) low MW and (b) high MW polymers at 25 °C and 3 $\text{\AA}^2/(\text{repeat unit} \times \text{min.})$ compression rate.

At first, the difference in the surface potential is not evident for both polymers. Both show a near linear increase in potential up to the collapse point. Increasing net positive potential value can be attributed to two reasons:^{176,120}

- (i) increase in concentration of the charge density detected by the plate electrodes
- (ii) reorientation of the net dipole towards the subphase direction.

That the net change from zero to collapse pressure is higher for the high MW polymer is simply a consequence of higher repeat unit density on the film domains. A more visible aspect of the orientation change in both polymers is the change in the mean surface dipole moment/ repeat unit with compression (Figure 5-11). This is calculated from the surface potential isotherm and the change in Mma using the Helmholtz equation for the dipole moment density:

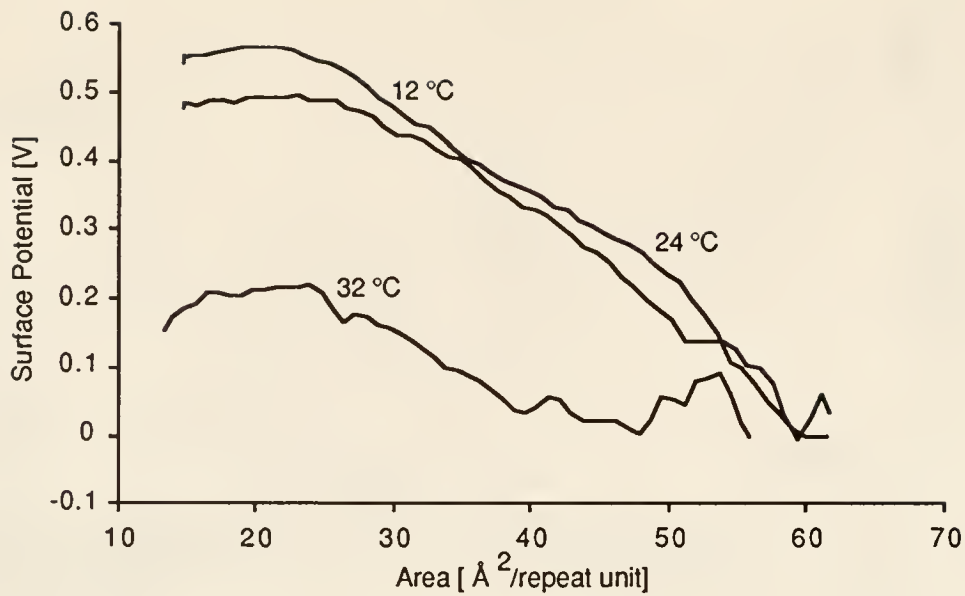
$$\Delta\mu = \epsilon_0 \Delta V A . \quad (5.1)$$

given the experimental data of the mean area per molecule and the surface potential ΔV , as well as the permittivity of the vacuum ϵ_0 (see Appendix C).^{202,134} Using a vibrating plate (condensor) method, ΔV is measured as $\Delta V = V_m - V_{w-a}$ where V_m is the surface potential of the air/monolayer/water interface and V_{w-a} is the surface potential of the clean air/water interface.

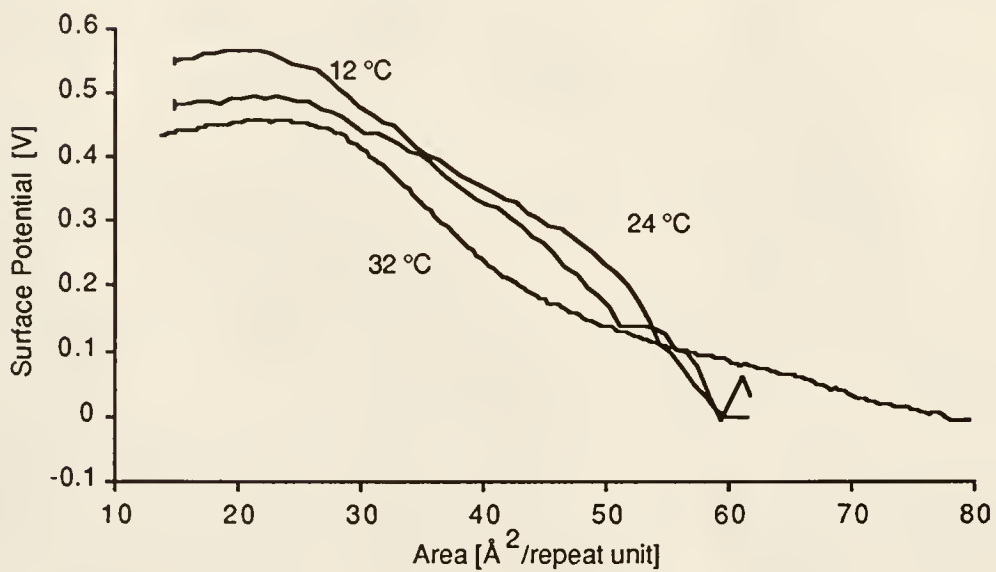
The curves show that the high polymer isotherm has a relatively flat region in the curve coincident with the onset rise in surface pressure (regions I to II). This is in contrast to the low MW polymer which showed a sharp change in the slope at the region also coincident with the onset rise in surface-pressure (regions I to II). Furthermore, along region I, the high MW polymer showed a steep rise in the dipole, whereas the low MW polymer showed a more gradual increase with limiting area. These net surface dipole changes are therefore

directly related to pressure induced changes on the monolayer. The steep rise for the high MW polymer may represent the monolayer front as detected by the plate.²⁰³ On the other hand, the gradual increase in the dipole moment for the low MW is indicative of homogeneous dipole reorientation with compression, a further evidence of film fluidity. Beyond the collapse (region III), both polymers showed similar decreasing behavior.

These differences in behavior are indicative of less dynamic carbonyl dipole reorientations for the high polymer occurring during compression.²⁰⁴ A three parameter model according to Demchak and Fort, suggests that contributions to the net dipole change, come mainly from the hydrated hydrophilic head group, hydrocarbon methyl group, and the water subphase.²⁰⁵ The contribution coming from the carbonyl moiety of two ester side groups is given a value of 1.8D (2×0.9 D/carbonyl).²⁰⁶ The methyl groups of the two esters on the other hand, have a value of 0.6 D (2×0.3 D/methyl group).¹⁷⁶ The contribution of water is considered negligible at -0.06 D.²⁰⁷ These values have been recently verified by Taylor and Mobius and their respective coworkers.^{208, 209} The larger magnitude of the ester group means that its contribution to the net dipole is greater. The high MW polymer showed a higher net increase in the dipole than the low MW polymer overall. Other than a net increase in the concentration of the repeat units during compression, greater amount of unhydrated methyl groups (pointing to the air) are expected to contribute to the rise in both dipole and potential. This is not unreasonable as stronger cohesive forces in the chain (both van der Waals and dipole) are facilitated by unhydrated methyl groups out of the subphase.^{105,176}



(a)



(b)

Figure 5-12. Surface potential isotherms taken at various constant temperatures for both polymers: (a) low MW polymer(b) high MW polymer. Speed of compression was at $3 \text{ \AA}^2/(\text{repeat unit} \times \text{min.})$ temperature within $\pm 0.5^\circ\text{C}$

Compression beyond collapse results in a decrease in the surface dipole moment. The decrease at the overfilm region is consistent with the formation of loops and tails, with the ester groups reorienting the carbonyl dipole away from the water subphase into the air.¹⁷⁷ The increase in reflectivity (Figure 5-16) intensity, which signifies an increase in the net film thickness at this region, together with decrease in surface pressure confirms this event.

The effect of temperature on the V-A isotherm is to lower the net change in potential from onset to collapse (Figure 5-12). This behavior is exhibited by both polymers with the slope almost remaining the same for the high MW derivative especially at the low compressibility region. Fluctuations at higher areas are also observed, which may represent the passing in and out of domains especially for the high MW polymer.¹⁷⁴

This means that with the as-spread polymers, introducing heat results in increased average kinetic energy which distorts the polymer's as-spread conformation.^{210,198} It would have been expected that the onset surface potential reading should be higher if hydration (solubility) of the ester groups is facilitated by heat. However, it seems that the opposite mechanism is in effect, in that the polymer is distorted to more disordered conformations results because of the increased kinetic energy.²¹¹ These analyses are not unfounded. In the first place, the ester group is not a strongly hydrophilic group as compared to, e.g. acids.²¹² The hydrophobic backbone would remain semi-rigid and immiscible, but the lateral groups like the cyclohexene ring and the ester groups would have a tendency for increased thermal motion. This thermal motion would be more predominant than the hydrating forces on the carbonyl group by water, thereby forcing the distortion of the backbone.²¹³ This is not surprising since the transition to the disordered collapse region is aided by

increasing temperature. The surface tension, γ , dependence with temperature, T, is governed by the relationship:^{120,85}

$$dS = -(d\gamma/dT) \quad (5.2)$$

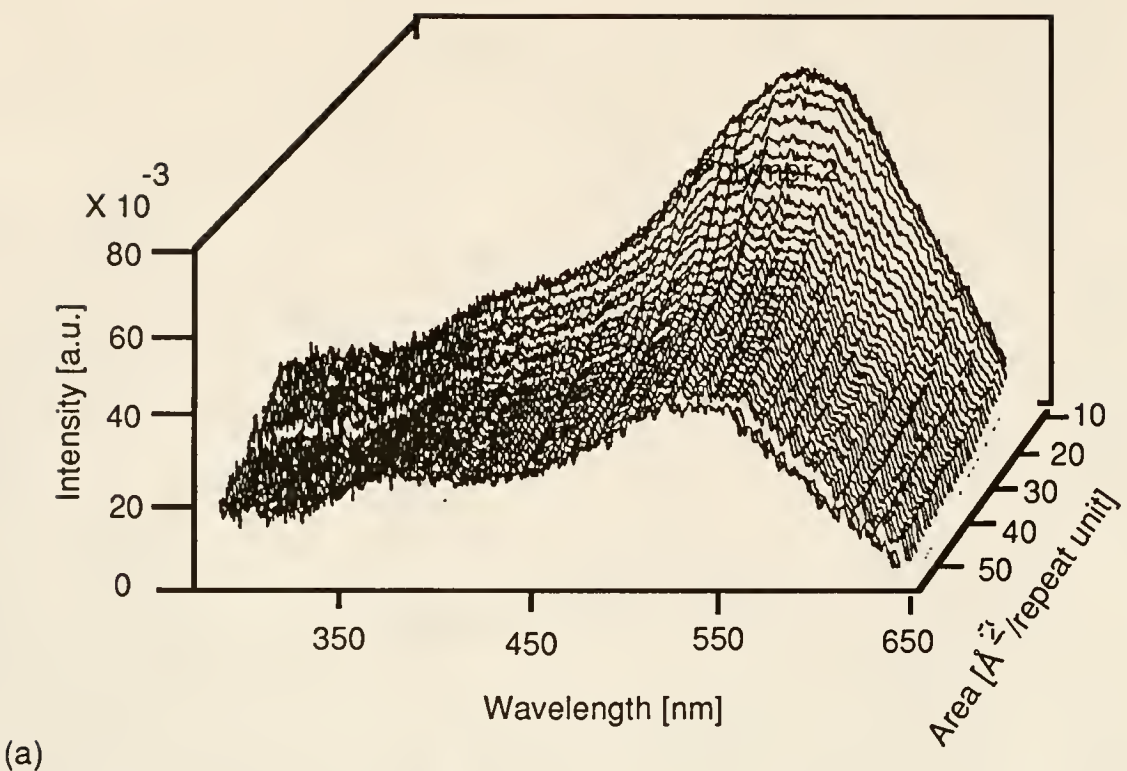
which is actually the surface entropic term (simply called entropy if γ is denoted as G, the Gibbs free energy). That is, as the temperature rises, the ordering effects caused by enthalpy, e.g. hydration, assume less significance, and the disrupting effects of thermal motion become more dominant. Qualitatively, this would indicate a distortion of the surface dipoles prior to compression with the result that less net dipole reorientations are observed with compression. These distortions would have a tendency to remove ester groups from the interface, preventing effective screening by water molecules.¹⁷⁶ The polymer chain acquires energy from the environment in the form of heat and goes to a higher disordered potential energy state. The contribution of reorientations in the water subphase molecules should be minimal even with increased temperature, i.e. effective H-bonding reformation ("flickering cluster" model).^{214,207} The effective contribution though would have been important in the presence of an ionized hydrophilic head group.²¹⁵

UV-vis measurements at the air-water interface

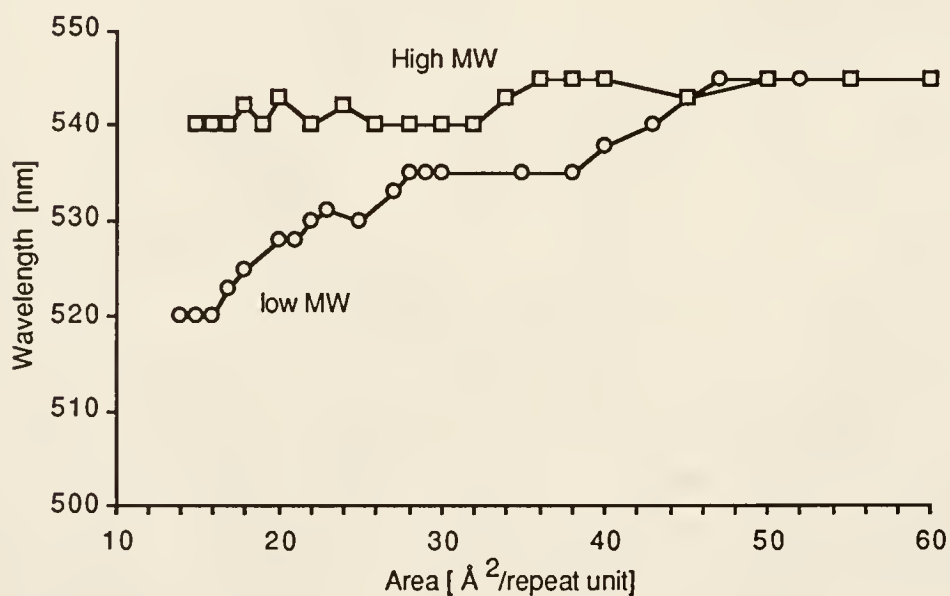
In situ spectroscopic observations of the monolayers were done based on the set-up as described in the experimental section. The change in wavelength maxima as well as absorption intensity was observed for both polymers. Two gratings were used (400 and 750 nm blaze wavelengths with 400 and 650 lines/mm respectively) to cross-reference the absorption maxima of the polymer at 545 ± 5 nm. Using the same spectrometer, the spectra of the

polymer was taken from a CHCl₃ solution in a quartz cell. The spectra was observed to be the same as that at the air-water interface, signifying the absence of any strong solvatochromic effects.²¹⁶ However, the effect on the value of the molar extinction coefficient was unknown, due to lack of data on absolute film thickness and beam path length.

For the high polymer, compression of the monolayer film did not produce a significant shift in the wavelength maxima even beyond the collapse point. However, a slight blue shift is observed with the low MW one of the order of 20 nm. Compression for the low MW polymer at different speeds resulted in variable slopes but the spectra remained blue shifted no more than 20 nm. The absorption intensity also increased nonlinearly with compression, consistent with increasing polymer concentration within the field of view of the UV light spot.^{217,218} This shows that the ribbon-like conjugated backbone of the low MW polymer is more amenable to pressure induced changes, especially at the overfilm region. This correlates well with the surface pressure and surface potential isotherm behavior. The overfilm region being characterized by "loops" should induce conformational defects that decrease the conjugation of the planar sequences. Since the UV-vis absorption properties are a direct measure of the polymer backbone behavior, this means that the conjugated sequences are affected grossly at the overfilm region for the low MW polymer. If true, this is direct evidence of in situ conformational changes in a substituted polyacetylene backbone as a result of compression.²¹⁸ Further analysis of these conformational changes will be discussed in detail with the compression-expansion cycle studies.



(a)



(b)

Figure 5-13. The three dimensional spectra for (a) pDDM1L is typical of the absorption spectra behavior with compression, i.e. increasing absorbance at lower limiting areas. (b). shows the plots of the change in λ_{\max} with the area for both polymers.

To observe possible pre-hydration effects of the polymer, up to 2 hours waiting time was allowed before a spread film of the low MW polymer was compressed. No significant difference in the λ_{\max} behavior was noticeable, compared to shorter waiting times. Likewise, compression of the monolayer at slow speeds did not produce any noticeable difference. These results suggests that no conformational changes are observable even with higher areas and slower speeds, at least within the time of observation.¹⁹⁵ The conformation of the as-spread film at higher areas in the interface is little influenced with time, though the detailed kinetic and thermodynamic relationships are unknown.

Brewster angle microscopy (BAM)

Although the above measurements provide insight into the degree of interaction and areas occupied the polymers within the monolayer, they cannot be related to any morphological features such as crystallization, aggregation or anisotropy. The morphology of the polymer film was directly observed at the air-water interface by Brewster Angle Microscopy or BAM. Images were taken from several spread films to make sure that the observed images are not just local phenomena. The analyzer, placed in front of the CCD camera was set at 90° so that the intensity changes reflect the extent of ordering.

The low MW polymer forms a liquid expanded film which flows with compression to form a homogeneous surface. The film remained featureless over the whole compression range. To test the deformability of the film, mechanical agitation was induced by the use of a stirring rod. After agitation, the monolayer reformed to its homogeneous state. This demonstrates the fluid nature of the low MW polymer film. Since a change in refractive index by the introduction of a third optical medium increases the optical density, the reflection intensity should increase. Qualitatively, this is observed in the images

in which the intensity increased with compression, reflecting increase in film density. The use of cross polarizers did not show any birefringence in the film, indicating an isotropic phase with the absence of any local domain anisotropies or crystallinity. This particular feature in film morphology is important for possible applications of the polymer as third order nonlinear optical material.⁶

In contrast, for the high MW polymer, condensed domains of various sizes were observed with the microscope even at high areas. These are also characterized by variable brightness within the domain, indicating some local optical density variations. The domains had a tendency to be smaller with the use of less concentrated spreading solutions. After mechanical agitation of the monolayer, the domains did not change in shape or size, indicating they were undeformable. Compression of the monolayer produced a homogeneous heterophase film, with the fused domain boundaries slightly visible. The reflectivity intensity also increased with compression. The use of cross polarizers also did not produce any birefringence in the film, indicating the absence of any local anisotropies or crystallinity within the domain. Thus, these domains are largely amorphous and insoluble to the water subphase.

These results clearly showed the striking differences in monolayer film structure for a high and low MW derivative of polyDDM. This correlates well with the other measurements with film compression. Whereas the low MW gave a uniform fluid film, the high polymer gave a viscous film made up of condensed domains floating on the surface. This observation for the high polymer is consistent with the concentration dependent spreading conditions where smaller domains change the compression properties.

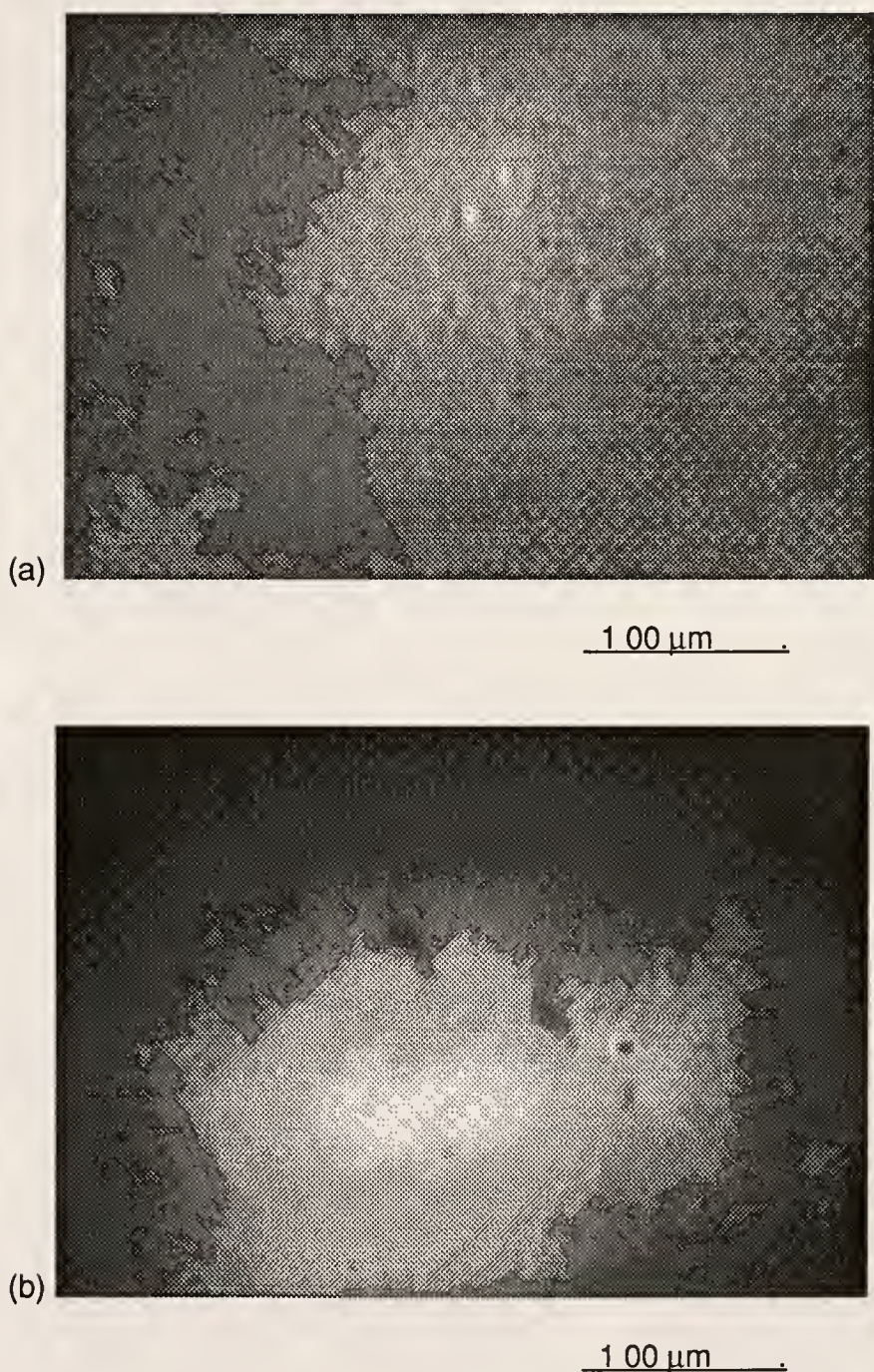
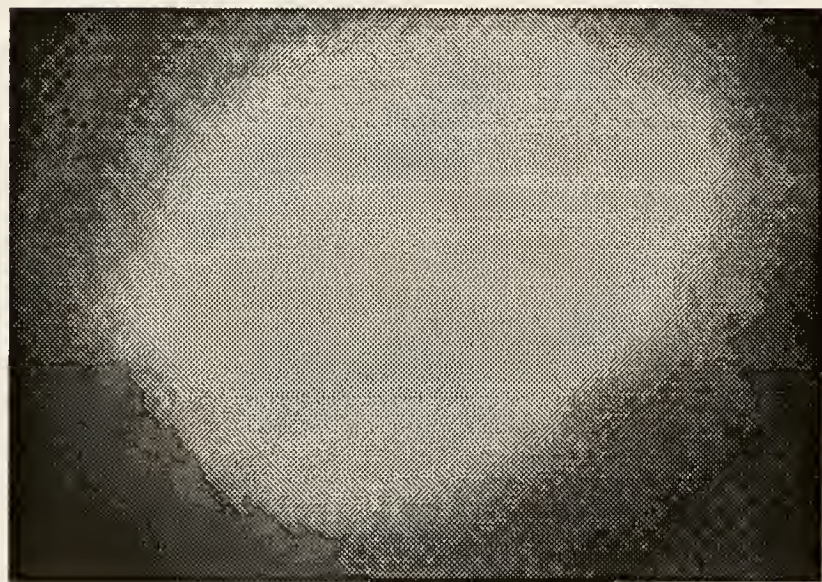


Figure 5-14. BAM images of low MW polyDDM at the air-water interface, 25°C
The images were taken from the following areas (a) 40, (b) 30, (c) 27,
(d) 25 Å²/(repeat unit). Cross-polarizers set at 90°.



(c)

1 00 μm .

(d)

1 00 μm .

Figure 5-14 (continued)

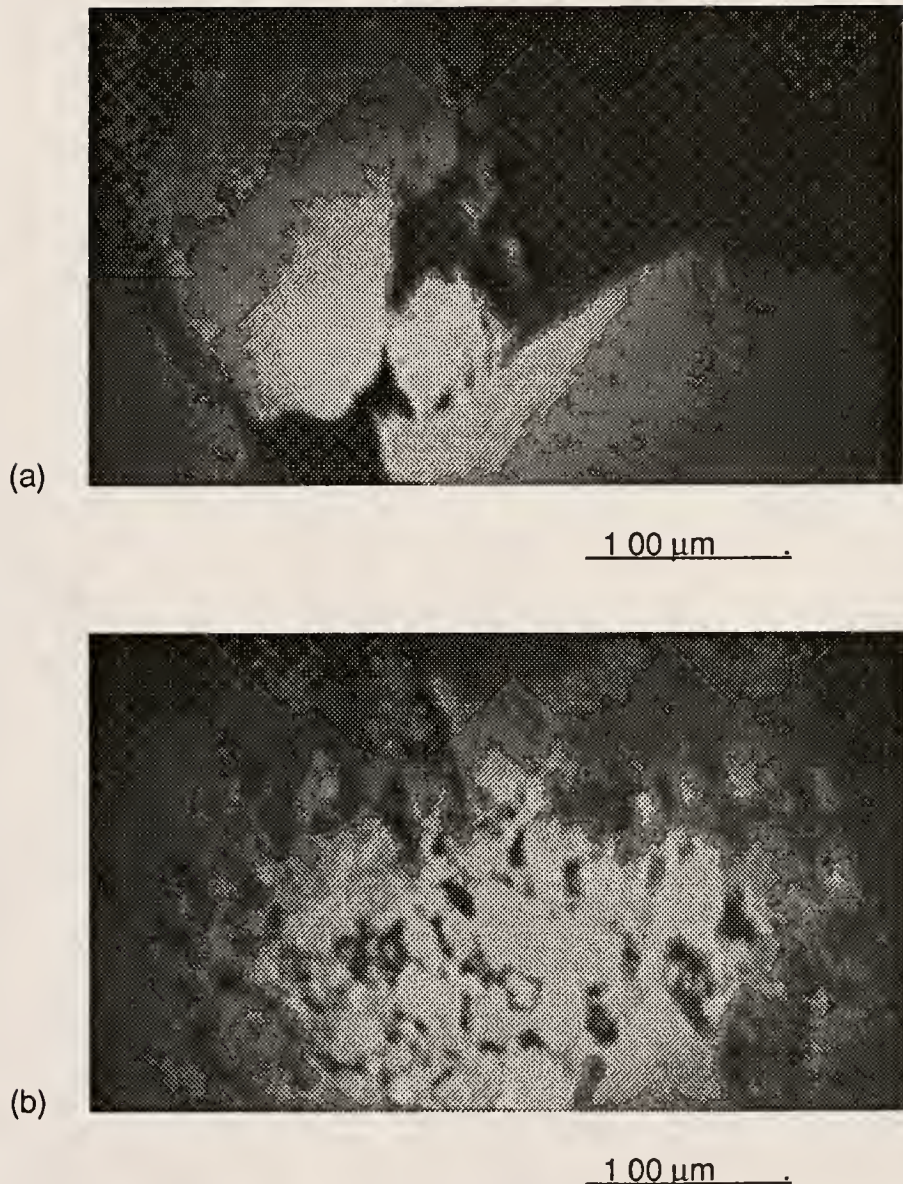


Figure 5-15. BAM images of high MW polyDDM at the air-water interface, 25°C
The images were taken from the following areas (a) 60, (b) 50, (c) 47,
(d) 45 (e) 27 Å²/(repeat unit). Cross-polarizers set at 90°.

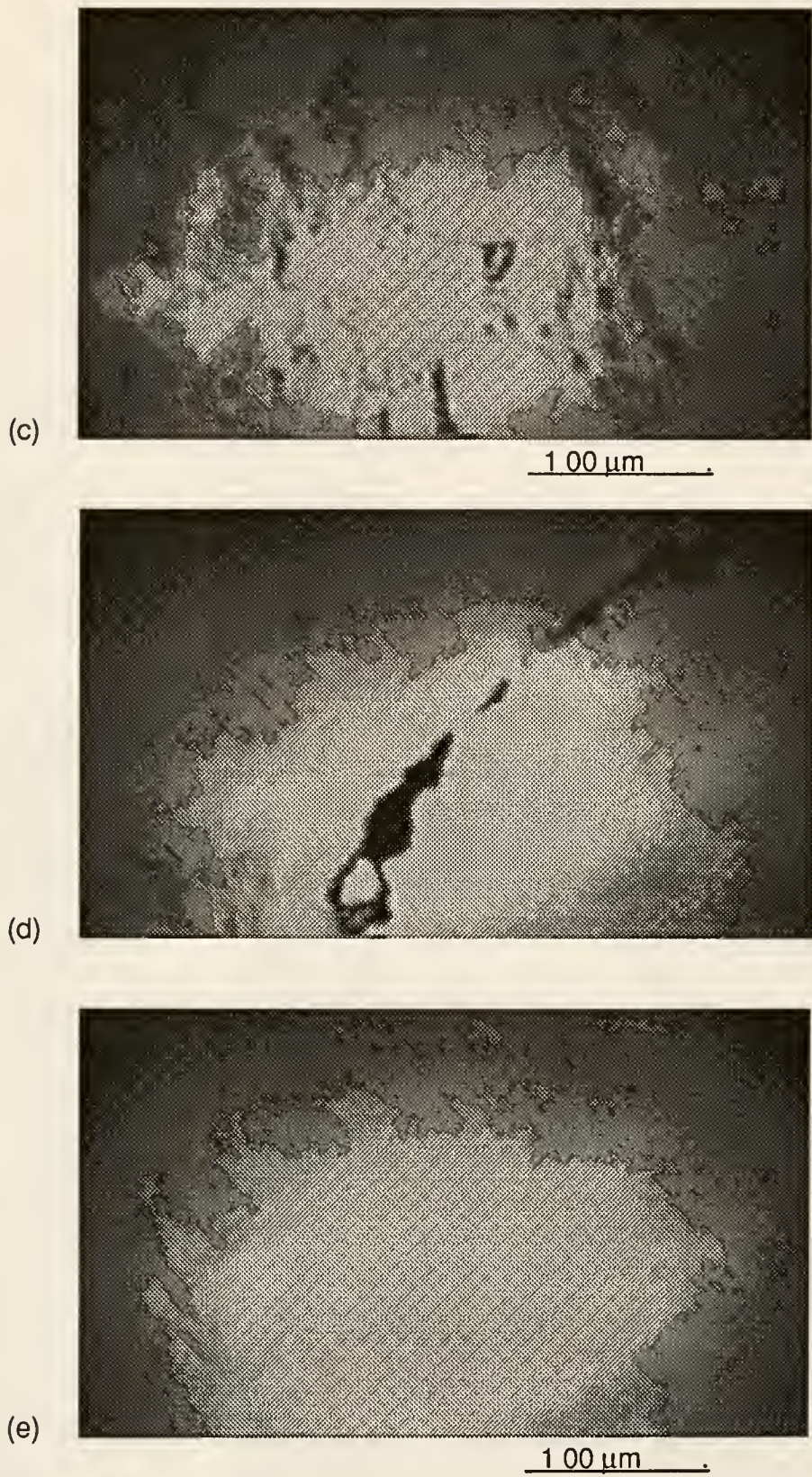


Figure 5-15 (continued)

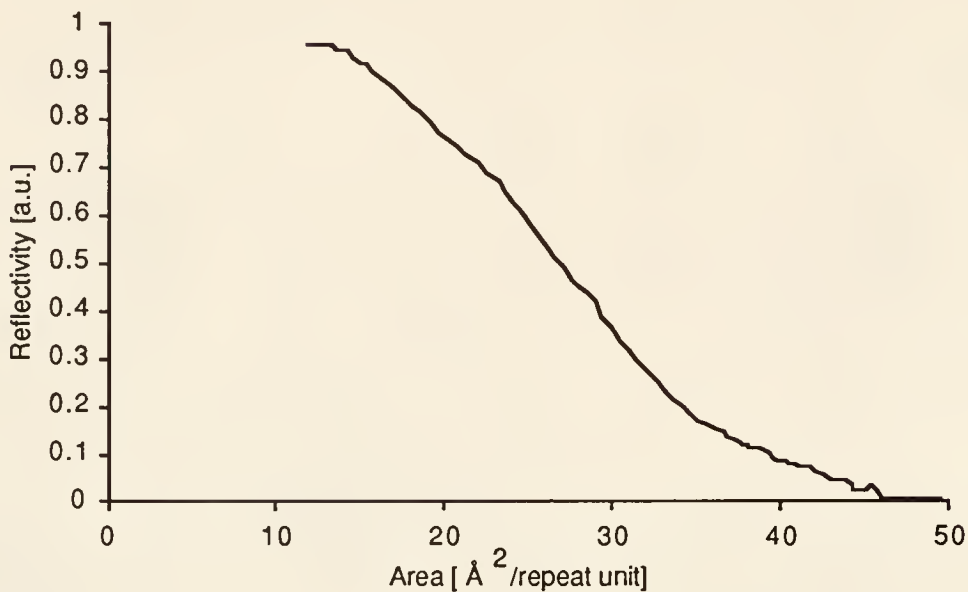
Relative Reflectivity

The best way to obtain absolute thickness of the monolayer film is by ellipsometry.²¹⁹ Changes in the refractive index which results in increasing optical density, give important insights on the conformational changes from planar to helicoidal structures.²²⁰ However, it is also possible to obtain relative thickness changes in the monolayer film by reflectivity intensity data. This is done by integration of the pixels from the intensity changes of the BAM images with compression.²²¹

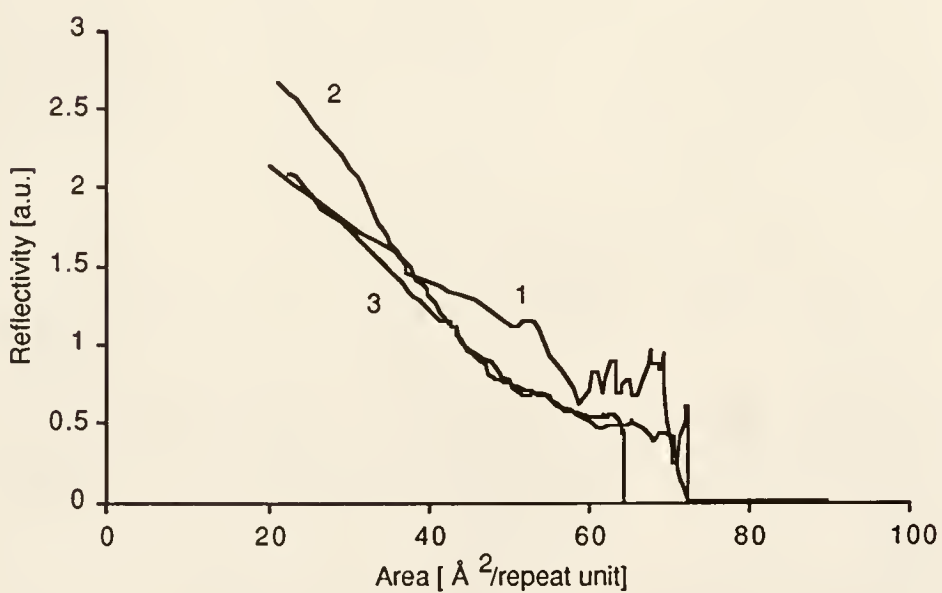
The reflectivity intensity plot was derived from the ratio of reflectivity intensity of the air/monolayer/water over the reflectivity intensity of air/water. At the same time, the gain of the video image was set constant. For the low MW polymer, the reflectivity increased monotonically with compression. The intensity was measured over various constant gain ranges and showed good reproducibility. On the other hand, the reflectivity for the high MW showed variability in the rise of the curve, showing much fluctuations at higher areas but tended to be uniform at lower areas. It also showed an onset rise at areas much higher than that observed with the surface pressure. Different trials showed that the curves did not coincide with each other and that the fluctuations can be correlated with the passing in and out of the domains on the view field. Reflectivity data also showed the variability of spreading conditions with the high polymer.

As mentioned earlier, the reflectivity curve for the low MW polymer, gave a gradual nonlinear increase with compression. The absence of any abrupt changes indicated that this transition to the overfilm region is a smooth homogeneous process. The relative thickness increasing gradually is consistent with equilibrium being shifted to the more loose coil structures in the film, which are gradually formed and removed from the monolayer at small

areas.¹²⁰ Gradually, with compression, the rest of the polymer chain is deformed to the bulk phase, grossly altering the compressibility of the monolayer.



(a)



(b)

Figure 5-16. Reflectivity Data for both polymers taken from the BAM images by video integration of pixels. (a) low MW and (b) high MW. Numbers in figure (b) represent successive trials using different films each time.

Analysis of Results

These measurements have shown the kinetic as well as thermodynamic aspects of the monolayer structure upon compression. A direct consequence of lower MW is better spreading properties as well as more dynamic orientational changes at the interface. The film homogeneity is an important aspect for the future processability of these type of polymers for nonlinear optical materials.⁶ What is interesting is to further differentiate the contribution of each functional group on the polymer conformation, namely: the ester side group, the ring, and the polymer backbone. Since the presence of the ester groups induces hydrophilicity to the otherwise hydrophobic polymer, the dipole forces acting on this group have an effect on the polymer conformation. There are three main possibilities of interaction for the carbonyl ester:

- (i) Dipole interactions with inter chain esters
- (ii) Dipole interactions with intra chain esters
- (iii) Hydration of the ester group by the water subphase

A first analysis of the monolayer behavior of polymers with ester sidegroups was made by Crisp.¹⁰⁵ Considering that there are two ester units per repeat unit, the polymer backbone can be considered to be in an ester matrix. The ester dipole interactions being dominant can be considered a continuous phase in an otherwise heterogeneous monolayer constitution (matrix--other phases contained within a continuous phase). Strong dipole interactions between the carbonyl groups both intra and intermolecularly will be a strong factor as well as van der Waals forces along the hydrophobic regions of the long chain. Differences are therefore expected in the behavior of a low and high MW derivative at the air-water interface.

The high MW polymer forms condensed films at the air-water interface. This is a consequence of greater cohesive forces (intercatenary and intracatenary forces) between polymer chains as against the polymer chain and the subphase. At the interface, the polymer chain is expected to have the lowest energy conformation with minimum interchain distance as determined by the van der Waals radii. For long polymeric chains at the air-water interface, geometric constraints limit the chain dynamics mostly to microstructural rearrangements i.e. short range interactions. This limits the entropy imposed on the two dimensional coils as a consequence of reduced number of available conformations.¹⁹⁴ Since the pDDM polymer has a hydrophobic (insoluble) and semi-rigid backbone, the chains have a tendency to reduce the internal excluded volume (intramolecular) so as to minimize subphase interaction (hydrophobic effect).^{125,126,222} However, the intralayer attraction with other polymer chains at the interface tends to increase the external excluded volume (intermolecular). Since the geometric constraints for a long polymer chain are greater, the balance is achieved only by maintaining the as-spread conformation. Thus, the high MW polymers forms macroscopically insoluble domains when spread at the interface. Alternatively, the strong cohesive forces can be explained by a strong dipole interaction between the ester groups. Assuming that the observed area per repeat unit corresponds to the polymer backbone lying flat at the surface, the observed limiting area correlates to the ring and ester groups being more laterally oriented to the surface (see above discussion on surface pressure-area isotherms). This means that a strong inter- and intra- molecular dipole interaction exists between the chains preventing the water subphase from readily hydrating the ester groups of the polymer chain. This stronger polymer-polymer interaction gives the high polymer a positive

enthalpy ($+\Delta H$) behavior which favors the formation of domains upon spreading, thus effectively "locking" the as-spread conformation.

For the lower MW polymer the different behavior is brought about by increasing contribution of short range forces, i.e. the hydration forces are able to compete with the dipole interactions of the esters. This gives the polymer a higher probability of orienting the plane of the conjugated backbone, normal to the surface. From the smaller limiting area of the surface pressure-area isotherm (see above discussion on surface pressure-area isotherms) this is probably the case. Because of less geometrical constraints on a smaller chain, greater conformational freedom allows better hydration of the ester groups. This counteracts the tendency for the strong van der Waals interaction in the hydrophobic backbone. This results in increased internal excluded volume (brought about by hydration) and decreased external excluded volume (from the lower limiting area). This balance allows the polymer to spread well at the interface. The result is that the low MW polymer exhibits a negative enthalpy ($-\Delta H$) behavior in which the polymer-subphase interaction is favorable (lower energy) as compared to the polymer-polymer interaction.

The Chemical Structure of the Repeat Unit

Other than the polymer backbone, two types of moieties attached to the ring in the repeat unit are expected to affect the rotation of the external single bond leading to conformational changes: the ester side groups and the methylene hydrogens in the ring.

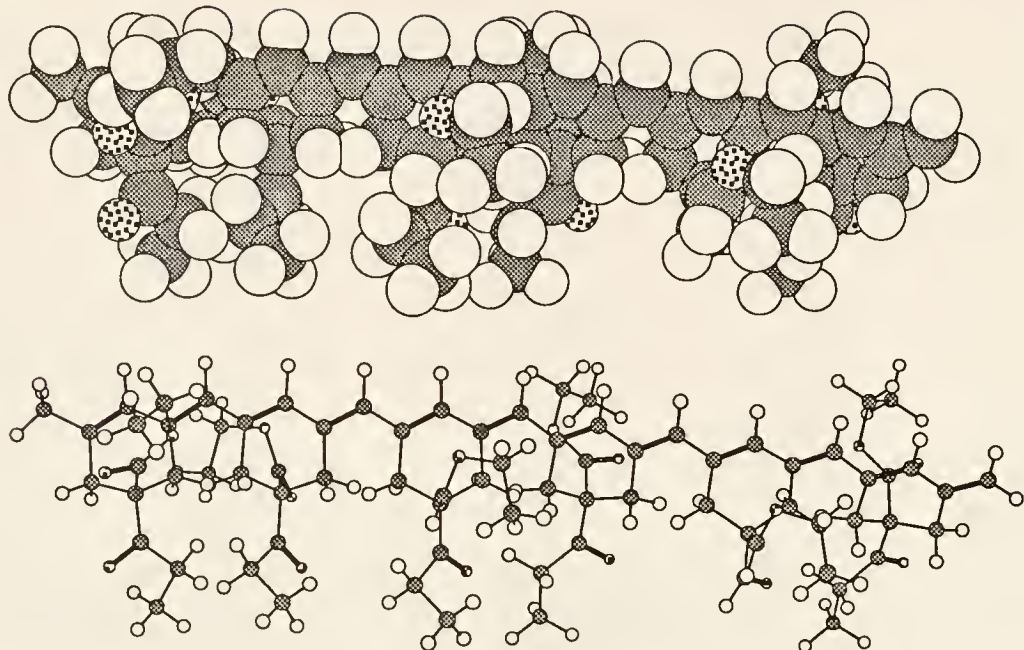
The ester side group

Figure 5-17. Corey-Pauling-Kulton (CPK) and ball and stick modeling of a polymer chain segment with 6 repeat units. A head to tail classification is possible if the methylene C adjacent to the double bond is considered the head. Ball and stick model viewed on the X-Z plane, with the backbone extending along the x-axis direction. Solid gray-C, white-H, and dotted-O.

According to a substituted polyacetylene backbone classification (Appendix B), the polymer can be classified as having a head to tail *trans-transoidal* configuration as shown in Figure 5-17. A *cis* configuration on the exo double bond as well as a *cisoidal* or *transoidal* configuration for the external single bond is possible. No pseudoassymmetric carbon is expected from the backbone other than a *cis* or *trans* configuration in the exo double bond.²²³

As mentioned above, the polymer backbone can be considered as being immersed in an ethyl ester matrix. The density of this matrix can be estimated from the % mass/volume contribution of the two ester groups over the total repeat unit density. As shown in Figure 5-17 and 5-18, the volume occupied by the ester group per repeat unit is considerably large compared to the rest of the repeat unit constitution. In general, with compression at the interface, the polymer chains are expected to "feel" the ester groups first before the backbone. This is also clearly seen in the ball and stick models of the polymer repeat unit. At high surface areas, the predominant functionalities are the ester groups, which are affected by both hydration and dipole cohesive forces. The cyclic ring in the repeat unit assumes a half-chair conformation (Figure 5-19) and therefore the two conformers of this ring will tend to place the ester groups with equal probability on either side of the polymer backbone.¹⁵⁴ In principle the disposition of these ester groups from one side to the other affects the ring conformation and indirectly, the planarity of the backbone. This results from the interconversions between two energetically equivalent half chair conformers (≈ 5 Kcal/mole for an isolated half chair cyclohexane ring).¹⁵⁴ The energy barrier to these rotations is unknown though and calculations should take into account the presence of the neighboring repeat unit. At low pressures or high areas, hydration of the ester groups is expected to be the predominant mode of interaction. However, at higher pressures (lower area), dipole interactions between esters are more predominant (along the carbonyl dipole). Therefore, the changes made on the interaction of the esters at different conditions should affect the conformation of the polymer via changes in the ester interaction.

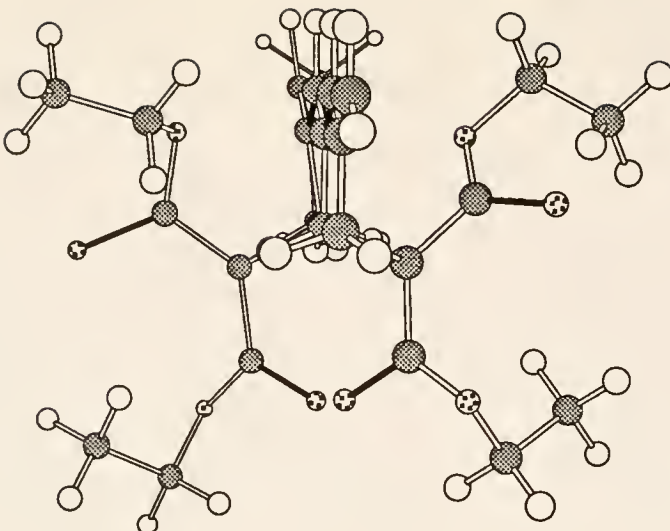


Figure 5-18. Ball and stick model of a two repeat unit segment of pDDM viewed down the X-axis (polymer backbone). The ester groups extend laterally (Y-Z plane)

Compression to high pressures should lead to stronger dipole interactions between the ester groups. Also by compressing only to pressures below the collapse, hydration and dipole interactions are sufficiently balanced, to give good hysteresis behavior. These pressure induced changes are also more clearly observed with the low MW polymers since hydration and dipole interactions are more balanced. The high MW polymers form condensed films upon spreading because the long chains increase intractability. In the longer chains, the predominant interaction is the dipole forces between the ester groups, resulting in a strong cohesive force. This results in no observable pressure effects as well as apparent absence of hydration by the subphase. Hydration should be thus limited to the domain boundaries. This is why the high MW polymer did not show much change with pressure either below or above collapse.

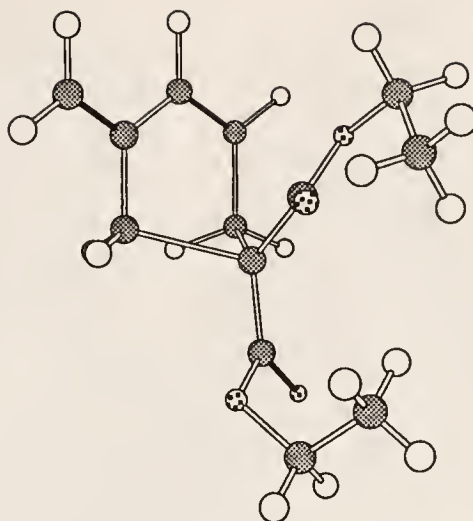


Figure 5-19. Ball and stick model of a single pDDM repeat unit in perspective view. The half chair conformation of the ring is highlighted with an equivalent conformer possible if the out of plane quaternary carbon (where the esters are attached) is oriented to the other side of the ring.

Methylene hydrogens

Alternatively, conformational changes can also be correlated to the methylene hydrogens of the ring in the repeat unit. As shown in Figure 5-17 and 5-20, the two methylene hydrogens, interact with the other methylene hydrogens of the adjacent repeat unit. These interactions can be mainly regarded as steric in origin and can have a considerable effect in maintaining the chain planarity. Recently, the effect of steric strain between the methylene carbons of an alkyl-substituted polyacetylene has been investigated by Tripathy et al using CNDO/2 calculations.¹⁶⁶ A potential energy barrier of 40 Kcal/mole has been found on going from a *transoidal* to a *cisoidal* conformation for a *trans*-polypropylene. However, the authors reasoned out that this value may be unrealistically large because the repulsive forces between nonbonded atoms were not allowed to be alleviated by changes in geometry. A value of 3.4 Kcal/mole has been calculated for a *trans*-polyacetylene.²²⁴ Similarly,

modeling studies by Le Moigne et al. showed the considerable contribution of the first two methylene carbons in reducing backbone planarity.^{62,47} This steric interaction has a direct effect on the dihedral angle, ϕ (between 0° to 180°), from rotations on the single bond along the backbone (Appendix B).^{125,223} The methylene hydrogens, if interdigitated with each other (close to ϕ between 0° to 10°), should prevent rotations about the external single bond (assumes a "locked" position). However, if the hydrogens are removed from this position, the possibility of more relaxed non-planar conformations (ϕ between 20° to 180°) is greatly increased. Since this interaction is steric in origin, thermal and pressure induced changes should affect the extent of this strain. Alternatively, the disposition of the ester groups from one side of the backbone to the other also affects the steric strain in these methylene hydrogens indirectly. This results from interconversion between the two half chair conformers, disrupting the interactions between the methylene hydrogens in between conversions.

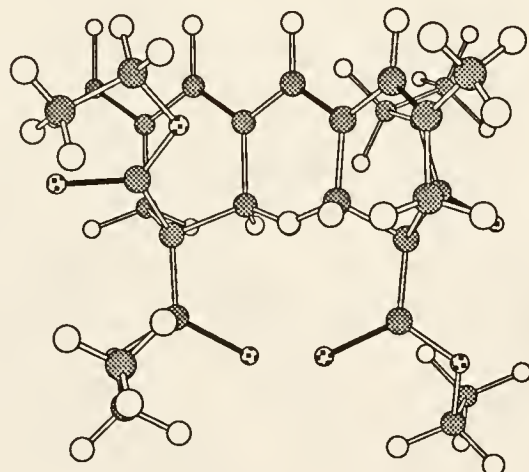


Figure 5-20. Ball and stick model of pDDM segment with two repeat units viewed along the X-Z plane (ring plane facing the viewer). The methylene hydrogen interactions between two adjacent rings are highlighted at the middle of the picture.

Thus, changes in the polymer conformation can be correlated to the ester functional group and the conformation of the ring as highlighted by the methylene hydrogens. Dipole interactions and hydration forces should have a direct effect on the disposition of the ester group, whereas pressure and temperature effects should be important on the steric interaction between the methylene hydrogens. Macroscopic changes reflect the viability of these interactions, as is consistent with the behavior of the ester group at the interface in general.

What has not been emphasized up to this point is the role of the semi-rigid polymer backbone in the monolayer film behavior. The initial polymer conformation, as a consequence of spreading or rapid evaporation of solvent can affect the compression behavior. To further probe this contribution and distinguish it from those of the ester and methylene carbon groups, hysteresis and annealing studies were made based on the compression-expansion cycle. By detailed investigation on several compression and expansion cycles, the contributions of each functional group in the polymer can be distinguished.

Hysteresis: Compression -Expansion Cycles.

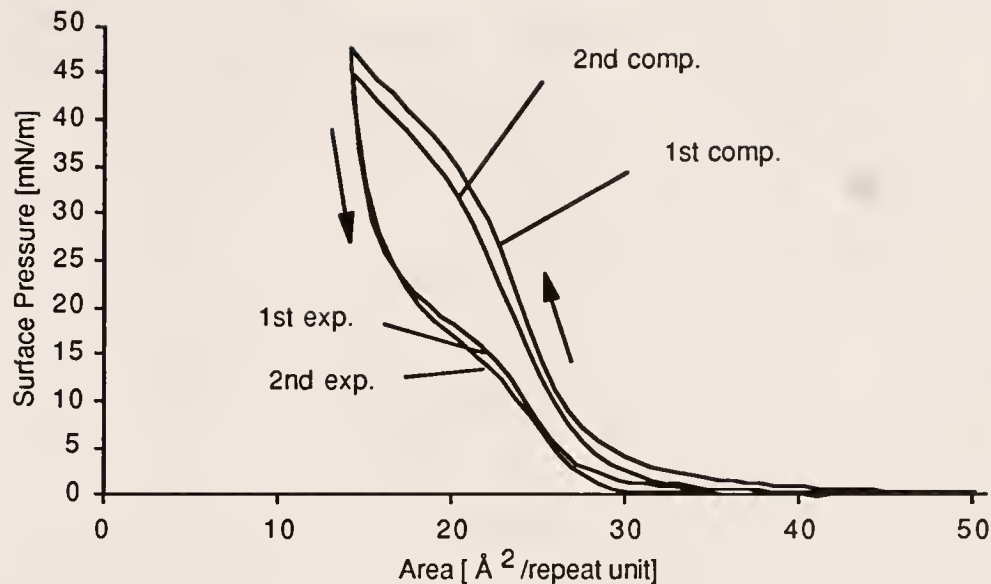
Compression-expansion cycle studies were made in order to study polymer film behavior in more depth. The compression and expansion rate used was $3\text{\AA}^2/(\text{repeat unit} \times \text{min.})$, at the median range of the speed dependence of the monolayer. Measurements were made at room temperature. Two regions were of interest: the region immediately below and above the collapse point. Differences were expected from the polymers between these two regions, especially for the low MW polymer. The effect of monolayer history on film properties was also studied. A number of analytical

techniques described previously were used. A model is proposed to account for the behavior.

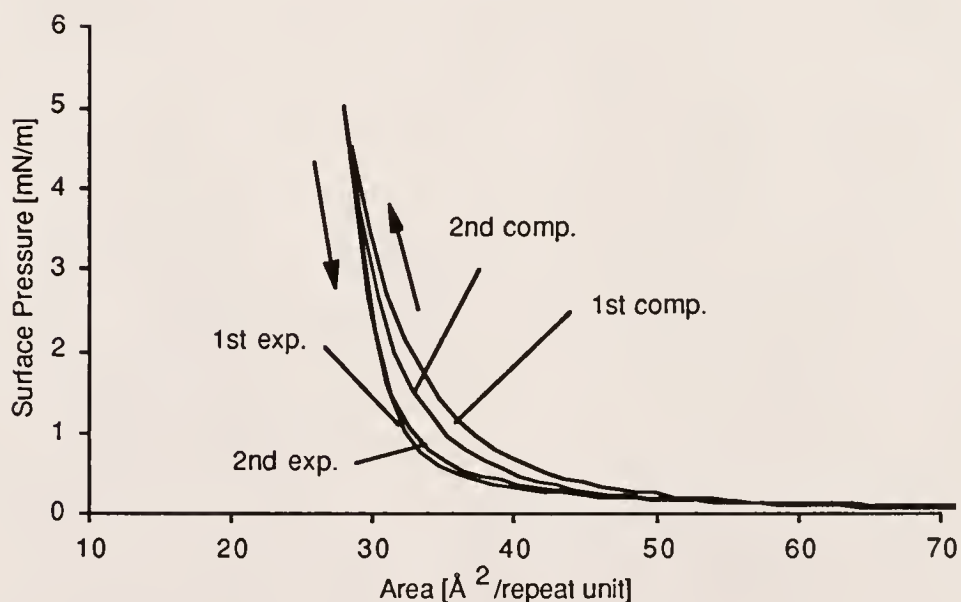
Surface pressure-area isotherm hysteresis behavior

For the low MW polymer, compression beyond collapse of the surface pressure-area isotherm showed significant hysteresis upon expansion (Figure 5-21). However, subsequent recompression and reexpansion retraced the original curves. Classically, this type of behavior would have been classified as *reversible collapse* according to Gaines.¹¹³ Since, the reversibility was evident only on the second cycle, the term *not instantaneously reversible collapse* seems to be more appropriate.¹⁹⁴ Typically, there was a minimal decrease in the extrapolated area on subsequent recompression. Since, the time scale of the compression-expansion cycle lasted less than an hour, this could not be associated with evaporation effects but possibly a morphological change (sensitive to the film balance) as a result of compression to the overfilm region. In contrast, compression and expansion cycle below the collapse region showed little hysteresis upon expansion as shown in Figure 5-21b (Note the difference in the Y-axis scale as compared to Figure 5-21a). Subsequent cycles showed the same behavior. This means that the monolayer morphology is not grossly affected with compression at regions below the collapse.

As shown in the previous sections, the overfilm region is a high pressure environment which is commonly associated with transition to a bilayer or bulk phase.⁸⁵ That a reversible collapse behavior was observed despite compression up to this region is interesting in terms of the viscoelastic properties of a polymer with a semi-rigid backbone.



(a)



(b)

Figure 5-21. Π -A hysteresis curve for the low MW polymer at (a) above and (b) below the collapse pressure. Compression and expansion rate at $3\text{\AA}^2/(\text{repeat unit} \times \text{min.})$

A reversible collapse behavior was observed on studies made with smectic liquid crystalline polymers having a flexible polydimethylsiloxane backbone.²²⁵ Generally, on other systems with a flexible backbone such as poly(n-butylmethacrylate), a reverse collapse behavior was observed as well.¹¹³ This means that despite the semi-rigidity of the polymer backbone, an elastic restoring force allows the monolayer film to reform to its pre-compressed morphology to a certain extent. A reversible collapse behavior has been observed with rigid hairy-rod polymers such as poly (γ -methyl-L-glutamate-*co*- γ -alkyl-L-glutamates)²²⁶ and on certain derivatives of poly(silanes)¹². On the other hand, *irreversible* collapse was observed with a similarly semi-rigid poly-3-BCMU upon compression to the overfilm region (blue form).²²⁷ In these systems, the importance of the side group and its interactions was emphasized in explaining the reversible collapse behavior. Similarly, for the pDDM polymer, this elastic restoring force could be attributed to the ester side group and its interactions. This means that upon expansion, a metastable state is observed in which with time and the availability of higher surface areas, the monolayer is able to relax and regain some of its initial pre-compressed properties. This means that the overfilm region is capable of inducing changes on the polymer conformation and that this observed reversibility on recompression is not necessarily reflected in the expansion curve. This could be due to a rehydration of the ester groups that have been removed from the subphase as a result of compression. That the monolayer is capable of doing this at higher areas is seen in the reversibility of the isotherms at pressures below collapse. This reversibility might be associated to insufficient distance between ester dipoles to effectively alter the film morphology.

It is interesting to note that the similarly semi-rigid poly-3-BCMU has an *irreversible* collapse behavior upon compression to the overfilm region.^{227,172}

These polymers are known to undergo reversible color changes (related to the planar conformation of the backbone) in both solution and in bulk.²²⁸ At the interface, this irreversibility has been attributed to the formation of a stabilized rigid rod conformation in which the intramolecular hydrogen bonding is favored over the subphase interactions.²¹⁸

The high MW pDDM film gave a *rearrangement* type of behavior upon compression to the overfilm region beyond the collapse.¹¹³ A similar behavior was observed even at pressures below collapse. This is understandable as the high MW polymer did not exhibit a true monolayer behavior but a heterophase film as observed by Brewster angle microscopy.

To further associate this behavior at the molecular level, complementary compression-expansion cycle studies with other surface analytical techniques are necessary.

Surface potential-area isotherm hysteresis behavior

Figure 5-22 shows the surface potential - area isotherms for the expansion-compression cycles of low MW pDDM. With compression of the film beyond the collapse point (Figure 5-22a), it is apparent that a large difference was observed between the first and second cycle. The second cycle achieved higher potential (V) values and a large hysteresis was clearly observed. The first expansion though was nearer in value to the first compression, but did not reproduce the curve. This behavior is in contrast to the surface pressure-area isotherm in which a reversible collapse behavior was observed with subsequent compression-expansion cycles. On the other hand, little hysteresis was observed with the surface potential when compressed to pressures below the collapse. This behavior is consistent with that observed in the surface pressure-area isotherm.

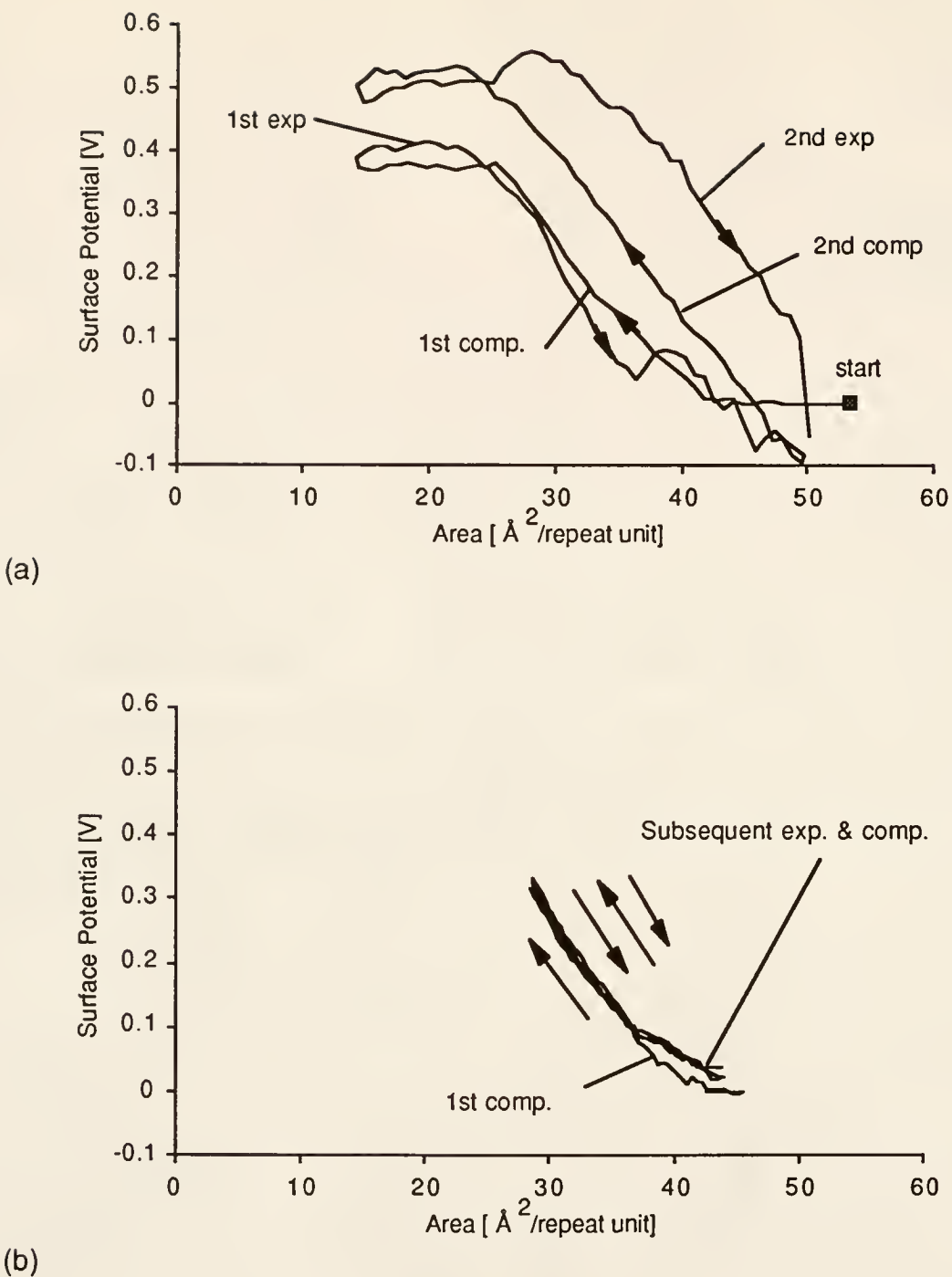


Figure 5-22. Surface potential-area isotherm, compression-expansion cycle for low MW polymer at 25 °C and 3 Å²/(repeat unit x min.) compression rate. The figures represent (a) beyond collapse and (b) below collapse.

As discussed earlier, morphological changes were expected with compression to the overfilm region. Therefore, a rearrangement of the surface dipole contributions should also be expected. This is clearly observed with the difference in behavior for the first cycle upon compressing below and above the collapse point. In Figure 5-22a, the first expansion (upon compressing beyond collapse) did not follow the first compression curve. Qualitatively, this would signify that the surface dipoles have rearranged, though as discussed previously, it was not possible to account for the exact orientation of the dipoles. This is because of the various contributions to the observed potential especially with polymers.¹⁷⁴ At the beginning, the hysteresis behavior for the second cycle (Figure 5-22a) was somewhat perplexing in that only a change in the shape of the curve was expected but not in the net potential values. However, Brewster Angle Measurements (described in the proceeding section) on the compression -expansion cycle beyond the collapse point revealed a combination of concentration effect and a net dipole rearrangement for the second cycle.

The net increase in the potential would be due to the formation of a more dense film brought about by compression up to the overfilm region. One must remember that pressure changes at the air-water interface are usually 2 orders of magnitude greater than normally observed, e.g. a 20 Å thick film with a pressure of 20 mN/m is approximately equivalent to a 100 atm across the thickness of the monolayer.¹²⁰ This film densification is reasonable, considering analogous systems on bulk polymeric materials.²²⁹ The rearrangement of the dipoles at higher pressures would tend to increase the cohesive forces between the polymer chains as a result of increased van der Waals forces and dipole doublet formation (two carbonyls oriented at opposite directions). Compression would allow the filling up of interstitial spaces in the

excluded volume of the polymer chains (limited by the bounding dimensions, e.g. radius of gyration, R, and contour length, L) as originally spread at higher areas.¹²⁵ Recent neutron reflection studies reveal that polymer films at the air-water interface have thicknesses comparable to the radius of gyration in solutions.²³⁰ This would mean that the presence of a high surface pressure environment should have a considerable effect on the surface density of polymer films.

Since, the increased potential was observed with subsequent recompression, expansion simply did not allow a considerable rehydration of these chains. However, Brewster angle microscopy and UV-vis measurements showed that a rehydration process was always in effect during expansion. As is the case with the surface-pressure area isotherms, kinetic factors should be taken into consideration, since these measurements were taken from constant speed isotherms. However examination of these measurements at lower speeds resulted in a similar irreversibility, except that the magnitude of change appeared to be lower.

Brewster angle microscopy (BAM) and reflectivity-hysteresis

Direct visualization of the morphology showed that at compression beyond collapse, the low MW polymer formed small domains upon expansion as shown in Figure 5-23. The film fluidity seemed to be lost with expansion. However, with recompression, the fluidity of the monolayer seemed to be partially restored as the film appeared to be slightly fluid but small domains remained. These differences can be clearly observed in the sequence of BAM pictures in which the compressed and expanded films are markedly different, though the 1st and 2nd compression images have some similarity. Since the low MW polymer would be more easily hydrated than the high MW polymer, the

time it takes for the film to expand at high areas allow the rehydration of some ester groups (as observed by BAM), though not necessarily altering the backbone conformation. To observe the dependence of these domains with time, the expanded film was allowed to relax for an hour before recompression. The result was the film became more fluid than the freshly expanded film though some small domains were still observable. This means that the rehydration process has a time component and was also observed with the in-situ UV-Vis measurements.

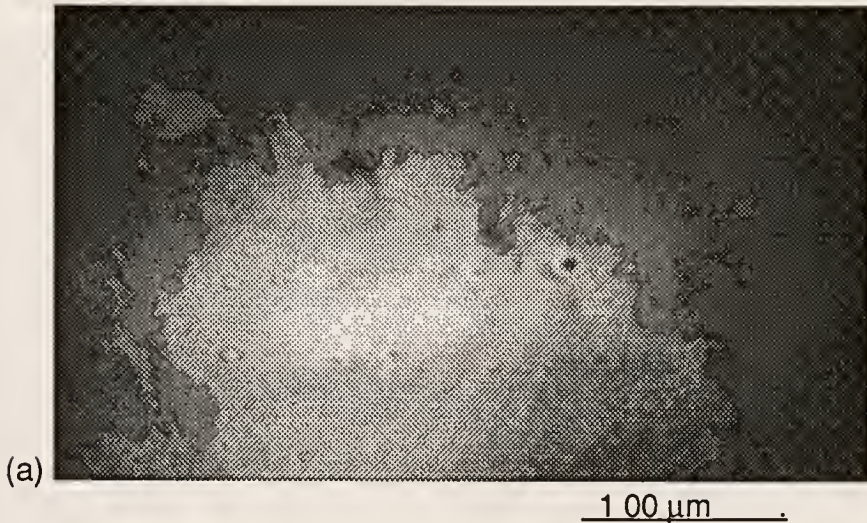


Figure 5-23. BAM images taken during the compression-expansion cycles at 25 °C. Gain kept constant and cross-polarizers were set at 90°. The notation is given as, e.g. 22;1C, meaning 22 Å²/(repeat unit), 1st compression. The images were taken from the following areas : (a) 26:1C, (b) 22;1C, (c) 24;1E, (d) 45;1E, (e) 32;2C, (f) 30;2E, (g) 35;2E. Refer to Figure 5-21 for the isotherm.

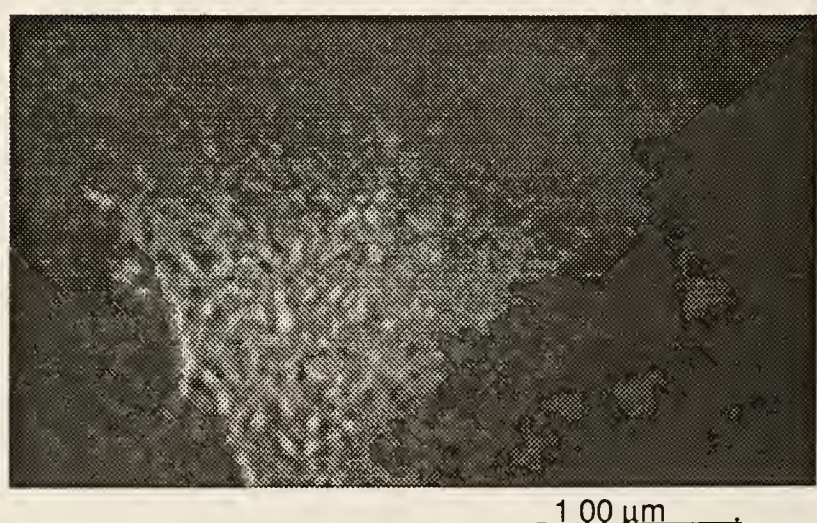


Figure 5-23 (continued)

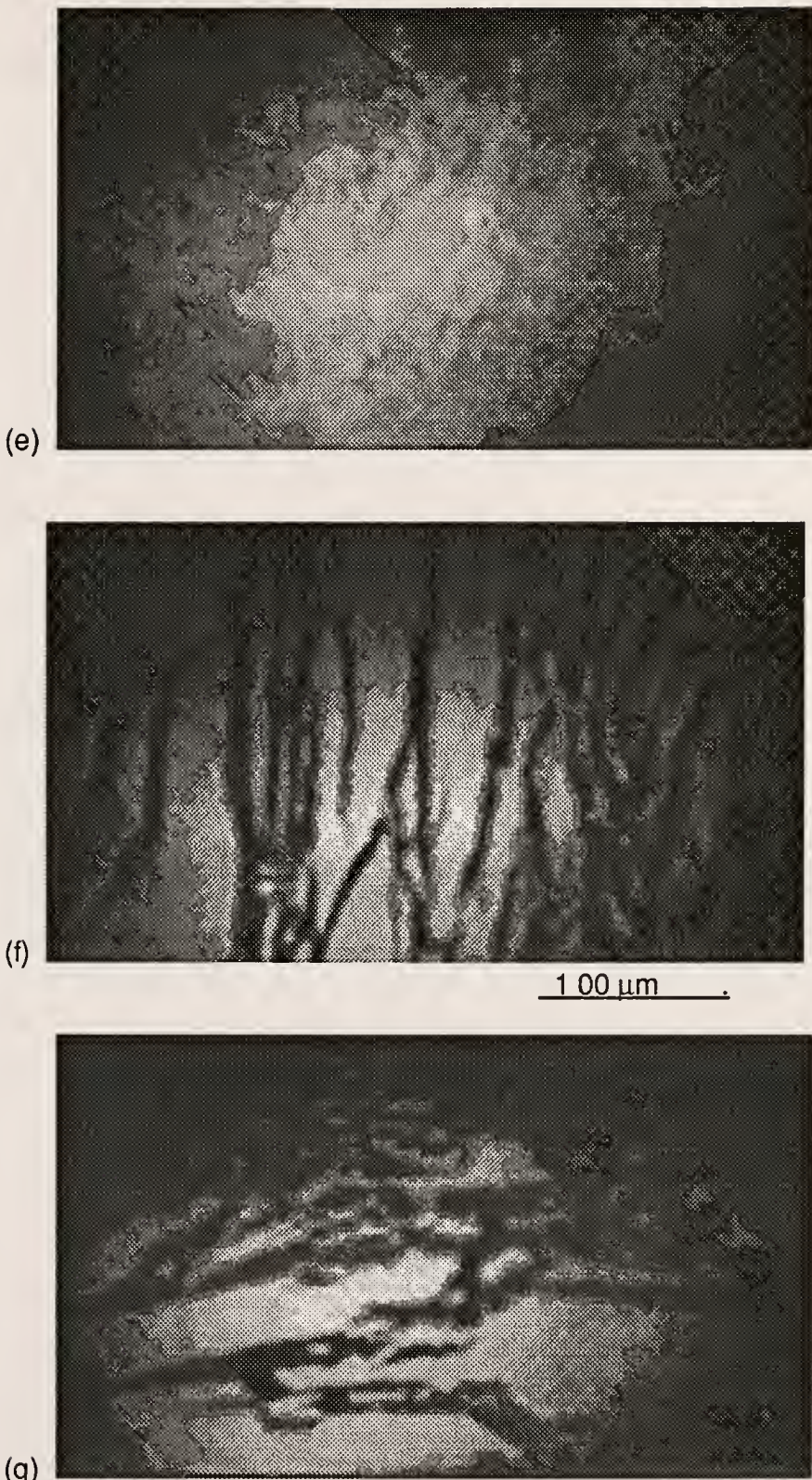


Figure 5-23 (continued)

The reversible behavior was also shown with the reflectivity measurements for the low MW polymer. Compression gave a smooth curve which increased nonlinearly up to the collapse region. Upon expansion, fluctuations were observed in contrast to the smooth curve obtained from the initial compression. These fluctuations, corresponded to the passing in and out of domains from the field of view of the microscope.²⁰¹ Recompression likewise, gave a smoother curve in the reflectivity isotherm which followed the initial compression curve closely.

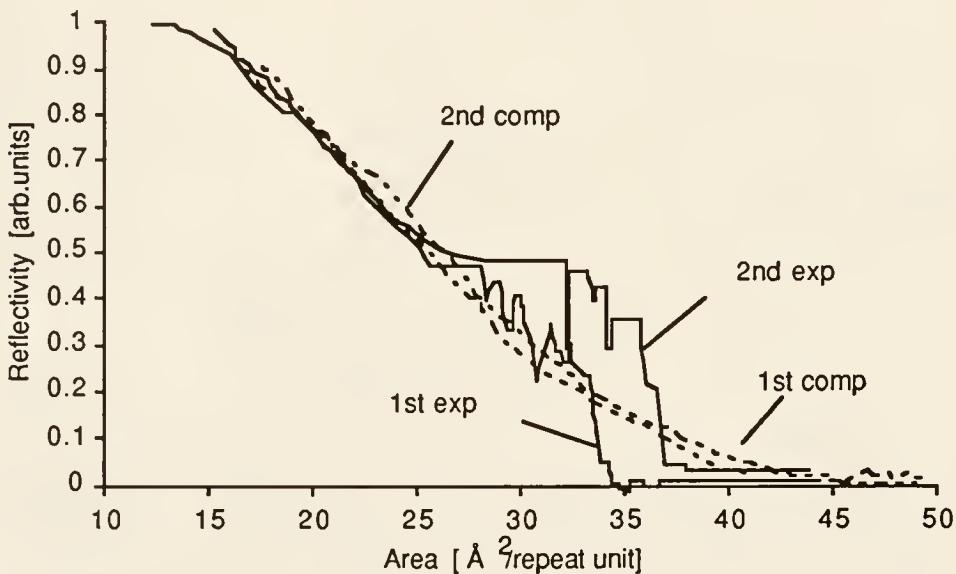


Figure 5-24. Reflectivity hysteresis for pDDM1L obtained during compression-expansion cycles at $3\text{\AA}^2/(\text{repeat unit} \times \text{min.})$

This reflectivity area isotherm hysteresis, is in contrast to the smooth curves of the surface-pressure area isotherm, which seemed to be less sensitive to such morphological changes. In relation to the surface potential - area measurements the lack of increase in relative thickness with the second

compression is consistent with a densification process for the monolayer rather than a volume expansion with compression. Likewise, compression-expansion cycles below the collapse region also gave little hysteresis with the reflectivity-area isotherms.

All of these observations point to a fluid polymer monolayer in which compression to the overfilm results in a morphological change that is partially reversible. Though the recompressed films have some similarities with the initially compressed film, the history of the film is still evident. This irreversibility can be associated with events at the molecular level, since compression brings about a high pressure environment to the chains.²³¹ It shows that the monolayer or more specifically the polymer chain has two components: one which is *inelastic*, and a majority which is *elastic*. That the monolayer is not totally elastic, means that it displays a non-Newtonian viscoelastic behavior at the interface.²³² This was observed with the kinetically and time dependent morphological changes on the film.

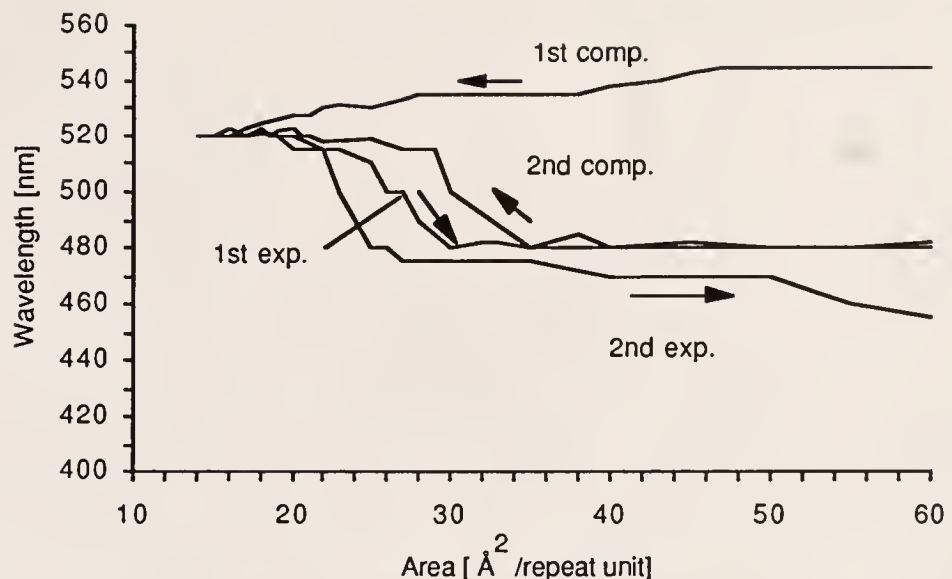
Since the most dominant structure, especially at high areas is the ester group, it is likely that the elasticity is mainly due to the interactions of this group. The polymer backbone, by virtue of its semi-rigidity and greater geometrical constraints comprises the inelastic component. This component is most dominant especially at low areas or high pressures, where gross deformations occur. To directly probe the effects of compression in this inelastic component, UV-vis spectroscopy was used.

In situ UV-vis spectroscopy

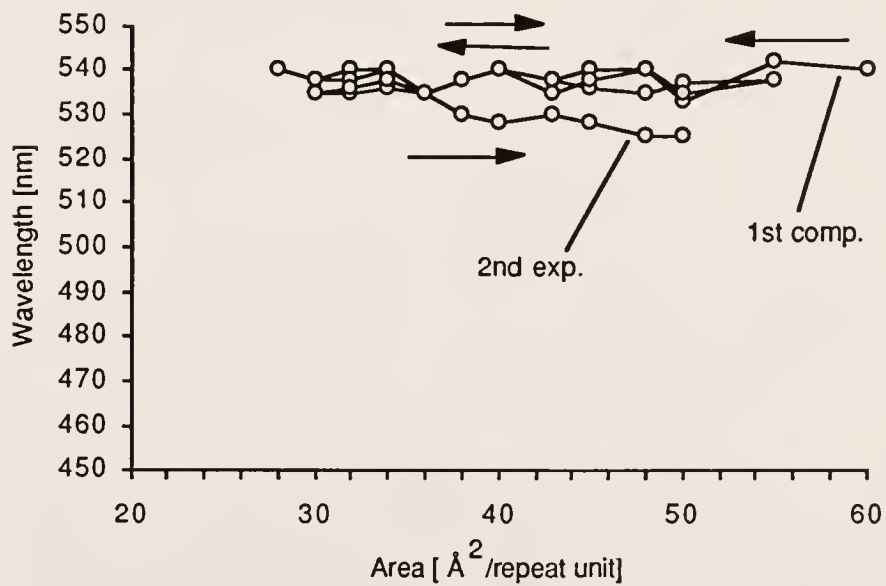
The best direct observation of conformational changes on the ribbon-like semi-rigid backbone would be with changes in the wavelength and absorption properties of the polymer at the interface.²³³ The absorption properties are a consequence of the planar conjugated segments in the polymer backbone which are affected by conformational dynamics at the air-water interface. As discussed previously, no solvatochromic effects were apparent with spreading at the water subphase although the effect on the molar extinction coefficient, ϵ , was unknown. For the low MW polymer, compression up to the overfilm region was shown to result in a slight blue shift on the absorbance wavelength-area isotherm (Figure 5-13). The difference between the low and high MW derivatives became more evident at subsequent expansion and compression cycles beyond the collapse point. Figure 5-25a and Figure 5-26 show a comparison of the absorption spectra for both polymers with 2 cycles of compression and expansion.

Compression was first made beyond the collapse pressure. The film was then expanded to higher areas. While the high MW derivative showed a blue shift up to 20 nm at the most, the low MW polymer showed magnitudes of up to 80 nm with expansion. Furthermore, greater variability was observed with the low MW polymer curves on several trials.

A red shift was observed though with the 2nd and subsequent compressions but to a maxima lower than the original. Further blue shift was observed with the second and subsequent expansions. For both polymers, expansion-compression cycle at pressures below the collapse showed reversible behavior with little or no change in the maxima (Figure 5-25b). Again the differences between the molar extinction coefficient, ϵ , of the high and low MW polymer at the interface was unknown.



(a)



(b)

Figure 5-25. UV-vis spectroscopy. Change in wavelength with area for the low MW polymer (a) above collapse (b) below collapse. Note: (b) is plotted with a different scale on the y-axis for greater resolution of the curves. Y-axis with ± 5 nm uncertainty. Scan rate of 1 spectra/40 sec. with an exposure time of 1 sec.

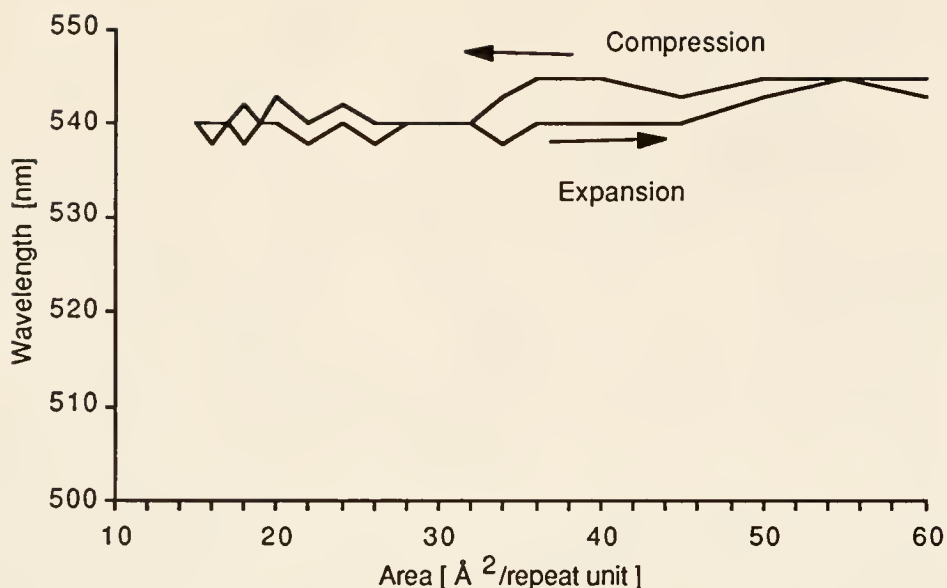


Figure 5-26. UV-vis spectroscopy. Change in wavelength with area for the high MW polymer, one cycle. Scan rate of 1 spectra/40 sec. with an exposure time of 1 sec.

Clearly, the UV-visible absorption properties of the low MW were most affected by these wavelength-area isotherm hysteresis studies. This behavior was consistent with both the surface pressure-area, reflectivity-area and more sensitively with the surface potential-area isotherms. For the high MW polymer however, the cycle did not affect much the local ordering of the monolayer. Likewise, at pressures below the collapse, not much change was observed. This confirmed the overall rigidity of the high MW polymer films in which even at the microscopic level, only minimal changes in conformation were observed despite the pressure of two-dimensional compression.

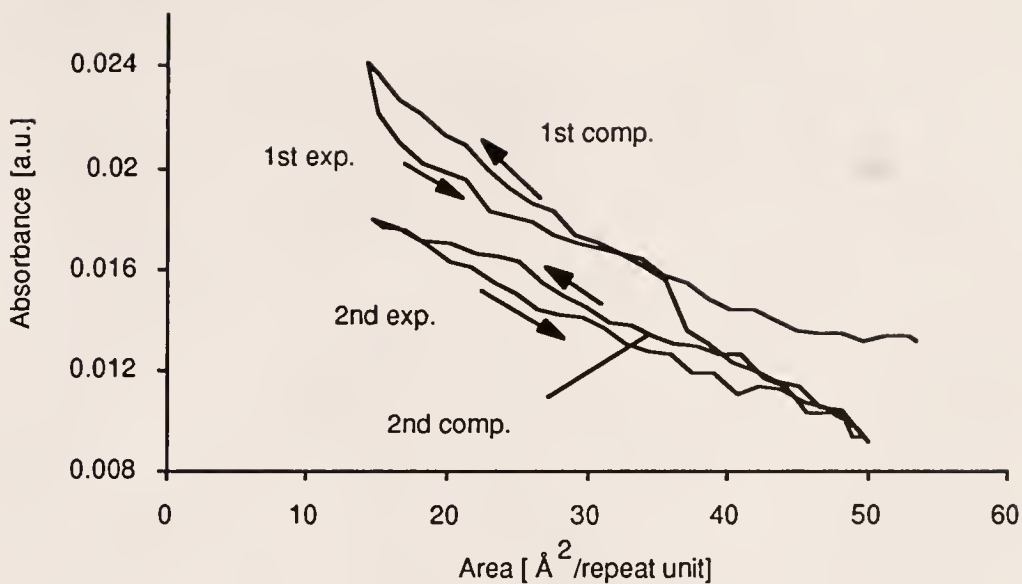


Figure 5-27. Absorbance intensity-area isotherm compression-expansion cycle at 25 °C at $3 \text{ Å}^2/(\text{repeat unit} \times \text{min.})$ speed, Intensity was taken from $\lambda_{\text{max}} = 550 \text{ nm}$. Scan rate of 1 spectra/40 sec. at an exposure time of 1 sec. Intensity values within $\pm 5 \times 10^{-4}$ uncertainty.

Figure 5-27 shows the change in absorbance of the polymer monolayer with compression-expansion cycles. Since only the conjugated polymer backbone is responsible for giving $\pi-\pi^*$ transitions near the visible region, changes in the absorption intensity could be related directly to the conjugated segments in the backbone. Upon expansion to the same area, the absorption intensity was noticeably lower than the intensity at the same area on the first compression. Likewise, with subsequent recompression and reexpansion to the same areas, the absorption intensity was also observed to be lower. Although the exact molar extinction coefficient, ϵ (ϵ_{max} if taken from λ_{max}), could not be calculated with a certain degree of accuracy (no data on film thickness), qualitatively the change in intensity with subsequent cycles is significant. This relationship is governed by Beer's Law:²¹⁶

$$A = \epsilon c l \quad (5.3)$$

With the concentration at the interface, c , and the path length, l , (assumed to be constant at a given area with monolayer compression and expansion at the interface) the decrease in absorbance, A , would indicate a decrease in the overall ratio of conjugated segments at the interface. At first, the possible increase in concentration, c , (at a given area) due to monolayer densification by compression seemed counter-intuitive with the decrease in absorbance. That is, the first compression would have resulted in a net increase in film density due to monolayer compaction. However, the fact that a decrease was observed suggests that in this case, the changes in extinction coefficient, ϵ_{\max} , have greater sensitivity than just concentration effects. Net changes in conformation would result, rather than just a filling-up of the excluded volume in the polymer chains during compression (densification). Thus, the decrease in absorbance resulted in the formation of more non-planar conformations which decreased the net amount of conjugated sequences in the chain. This would mean that although the λ_{\max} might give similar values within the same area, the amount of conjugated sequences in the backbone responsible for this absorbance decreased with subsequent cycles.

In comparison with the polydiacetylene system, poly-n-BCMU, studied by Prasad et al., no red shift was observed with compression.^{218,172} For the polydiacetylenes, the red shift signified a conformational change from a coil to a rod form, signifying an increase in conjugation length for the planar sequences. On the other hand, for the pDDM, first compression to the overfilm region resulted in a blue shift of the order of 20 nm. This would mean that compression up to this region resulted in a backbone conformation with a slight decrease in planarity.

The classical model of "loops" and "tails" formed at higher pressures would result in certain parts of the chain "buckling up" resulting in a break in the planarity.^{120,122} The majority of the segments (both plan and nonplanar) would comprise the "trains," which contribute much to the surface pressure build up. The loops that buckle up would mostly likely come from segments which are nearer to the water sub-phase or air, e.g. twists that do not allow complete hydration and dipole interactions with other polymer chains.

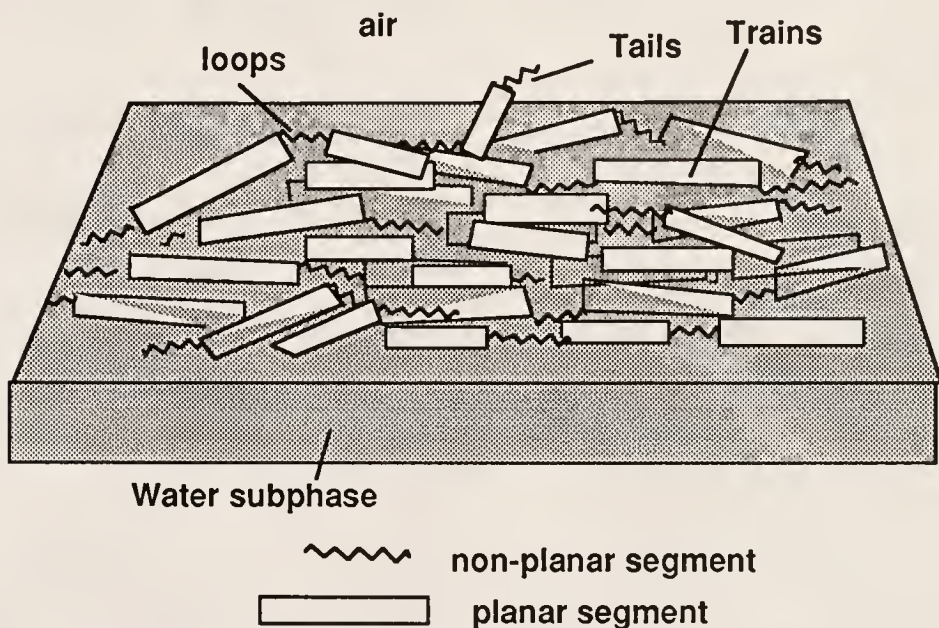


Figure 5.-28. Schematic representation of the different conformations adopted by the polymer at the interface.

Normally, for a reversible collapse in polymeric monolayers, there should be little hysteresis with expansion. Expansion should bring about a global relaxation to the monolayer film from the compressed state. In principle, the immediate availability of the free surface area upon expansion, acts as an elastic force, restoring the backbone to the original conformation. However, compression has brought about changes in the cohesive forces in the polymer

monolayer, e.g. strengthened dipole interactions or reduced hydration. Compression at the surface would bring the chains into close contact, filling up the excluded volumes of the neighboring polymer chains (as discussed earlier). Upon expansion, the chains could either separate or remain conformationally bound together. Since the expansion of the monolayer is a dynamic process, the forces acting on the chain would be an equilibrium between the hydration forces, as well as the elasticity of the dipole interactions. Both contribute to the total free energy of the chain segment. Since the tendency is to minimize this free energy, the event with greater contribution towards minimization would tend to be favored.

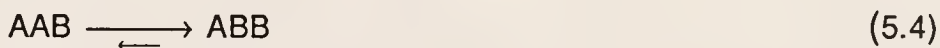
Based on the BAM images, the monolayer seemed to have formed a metastable heterogeneous domain structure upon expansion which resulted in a blue shift. However, a more fluid monolayer was observed with recompression resulting in a red shift. To test the temporal dependence of this metastable process, in one measurement, the re-expanded monolayer was allowed to relax for 30 minutes before the second compression. Upon second compression, the initial wavelength maxima was 30 nm higher than when it was last expanded. Furthermore, the monolayer seemed to be more fluid, compared to a film that was instantaneously recompressed. Although the value did not return to the original wavelength, this implied that the monolayer reformation process approaching that of the original film has a time dependent component.

Both the ester groups and the entropic behavior of the conjugated backbone could play a role in this reformation process. Since the dipole interactions between the esters are strengthened with compression, the expansion of the monolayer film could result in the polymer backbone being stretched as the dipole interaction between the ester groups are detached from each other with expansion. Rehydration by subphase water molecules would

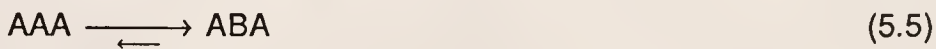
also have a tendency to spread the chains apart. In doing so, the breaking of the dipole interactions would tend to produce non-planar conformers on the originally planar sequences since an increase in entropy is favored (more disorder).

Since conformational changes in macromolecules are cooperative processes (i.e. each conformation is influenced by the conformation of neighboring bonds), the initial coils or loops formed with compression would have affected or even accelerated the formation of more non-planar conformers. It's as if the formation of loops in the initial compression, brought about a "nucleation" of further conformational twists.²³⁴

If planar conformations (dihedral angle close to 0° and 180°, e.g. transoidal or cisoidal, see Appendix B) could be denoted as A and non-planar conformations (dihedral angle in between 0° and 180° e.g. gauche) could be denoted as B, the process¹²⁵



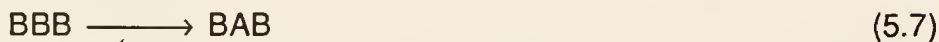
describes the *propagation* of already existing nonplanar conformations B (or reversibly, A), an equilibrium constant K_p can be assigned to this process. In the process



the nonplanar sequence, B is begun (or destroyed) and an equilibrium process K_n can likewise be assigned as a *nucleation* process. K_p is related to K_n by the following equation:

$$K_n = \sigma K_p \quad (5.6)$$

The cooperativity of conformational transitions is therefore given by the factor, σ . If $\sigma < 1$, the segments preferentially take on the conformation of the neighboring groups (for a diad, AA or BB is preferred over BA or AB). For $\sigma = 1$, $K_n = K_p$, no cooperativity exists (conformation is frozen). There are no known cases of a negative cooperativity or anti-cooperativity with $\sigma > 1$. The nucleation process in the interior of a chain should be microscopically reversible (equal probability between planar and non-planar conformations), that is, equation 5.4 could also be represented as:



with the equilibrium constant denoted as $K^{-1}\sigma$. At each end of the chain, the conformations have only one neighboring conformation. Similarly, at junctions between two segments having different conformations, only one side will have an odd conformation. The σ values for these cases should be different from those of the chain interior, depending on the type of conformation (A or B) at the chain ends. In most calculations involving conformational dynamics of the substituted polyacetylene backbone, the non-planar conformation always has the lower energy (where there is an absence of stabilizing intermolecular forces of attraction).¹⁶⁶ Equilibrium between conformational transitions tend to favor non-planar conformations (B). In this case, this model would be consistent with the observed blue shift upon expansion of the pDDM monolayer in that, the existing non-planar conformation (B) would tend to propagate the formation of more non-planar conformations as a result of relaxation due to release of the compression strain. In the case of nucleation of a non-planar (B) conformation at the interior of a planar conformation (A) with a certain persistence length, L , this would result in drastic changes in the absorption properties of the polymer.

This again is consistent with the large λ_{\max} blue shift observed upon expansion. The reversibility of this interior nucleation process (equation 5.5 and 5.7) is observed with the λ_{\max} red shift upon recompression. The opposite conformational transition (reformation of the conjugated sequence) is in equilibrium, thereby the introduction of a restoring force such as compression reforms the conjugated sequence. Since the recompression of the monolayer did not bring about complete reversibility, an irreversible component (within the thermodynamic or kinetic limitations) could be assigned. This would probably be attributed to the conformational transition at the chain end or junction point, which would have less probability to reform to a planar conformation because of the asymmetry in the energy barrier (favoring the neighboring non-planar conformer).

Incorporating the constitutional contributions as well as the conformational transition model given above, the following generalizations can be made. There are two mechanisms in operation that affect the polymer conformation transitions at the air-water interface:

(i) *polymer backbone dominated* - which is observed mostly with spreading and initial compression to high pressures. It is irreversible at least with respect to the time frame of the experiment, and

(ii) *ester group dominated* - which is observed mostly with expansion and is fairly reversible within the time frame of the experiment

These processes lead to conformational defects (non-planar conformations) which can be classified to two types according to the model above: *interior and lateral* conformational defects. The polymer, as initially synthesized, would have an average conjugated sequence (persistence length) of 30-45 carbon lengths as estimated from the absorbance maxima, the narrowness of its distribution can be inferred by the width of this peak.¹⁹⁰

Breaks in the conjugated sequence, assuming the absence of configurational and chemical defects would come as conformational twists (Appendix B). Perturbation on the system such as two-dimensional compression could lead to additional non-planar conformational "twists" in the conjugated sequences. As mentioned above, this could be in the form of extensions of the original twist leading to *lateral* defects or new breaks at the middle of the conjugated sequence leading to *interior* defects. The main difference of these induced conformational defects would be on the observed absorption properties of the conjugated segments. If a break occurs near the original twist, only a small blue shift would be observed. However, if a break occurs at the middle, this would result in a large blue shift. The differences are summarized in the following diagram:

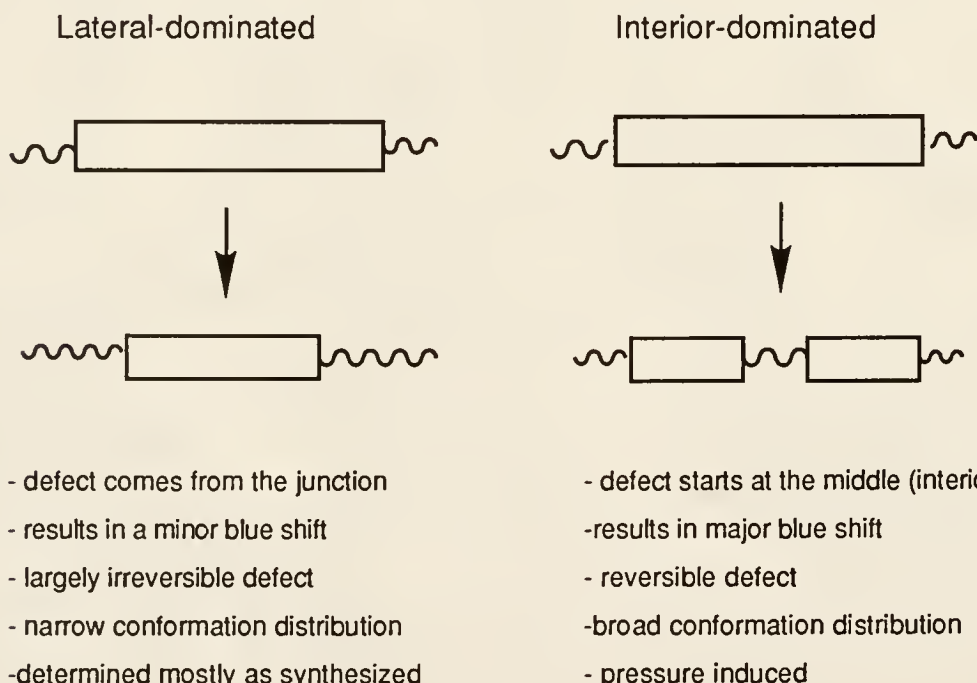


Figure 5-29. Two different conformational defect origins in the conjugated sequences. The block represent the planar conjugated segment. Coils represent the nonplanar conformers(or segments)

Using this graphic illustration to support the difference between a polymer backbone and ester dominated defects, it seemed that the defects near an existing twist should be more a property of backbone-dominated defects and that the middle defects are associated with the ester-dominated defects. Based on the observations and the initial analysis of the defects, this classification seem justifiable. The polymers, as initially spread, would have a morphology in which some pre-determined conformational order exists, e.g. spreading condition, or as-synthesized conformations will be present. The initial compression would bring about increasing interaction between the dipoles of the esters as well as filling up of the excluded volumes between the polymer chains. Hence at low surface areas, a relatively compact film is produced in which increasing conformational defects near loops and tails would come mostly from the pre-existing backbone conformation. The extension of these pre-existing conformational twists would result in a blue-shift. Upon expansion, net changes on the dipole interactions will occur as a result of pulling away of the ester groups from each other as well as increased hydration forces. Since the ester group is a property of each individual repeat unit, and not macroscopically, the disruption of this interaction would lead to a change in conformation of the ring, and indirectly, the polymer backbone. The probability of observing this change is observed for all repeat units, but more so within the conjugated sequence where the dipole interactions are strongest. Thus a conformational twist is introduced within the region of the conjugated sequence as a result of disruption of this interaction. A larger shift is expected since a defect is introduced along the middle of the conjugated sequence.

The conformational dynamics of these polymers were investigated using various surface analytical techniques. In particular, in situ UV-vis spectroscopy gave a direct observation of surface pressure induced changes on the semi-

rigid polymer backbone. Isotope labeling experiments if done (which have been very useful for studies of helical conformations of proteins at the air-water interface) could complement these studies.^{235,236} Likewise, ellipsometric measurements at the air-water interface, if done carefully, could provide data on the refractive index and thickness of the polymer film.²³⁷

Deposition to Substrates

Multilayer Deposition of Pure Polymers

With the monolayer behavior studied and the isobaric stability of the films verified, the polymer monolayers were deposited onto glass, quartz, and silicon wafer substrates. No deposition was achieved with hydrophilic glass substrates (results in nearly complete desorption of the film on downstroke cycles). However, the initial deposition of a stearic acid layer prior to deposition of polymer achieved similar results as using a hydrophobicized substrate. The high MW polymer can be deposited to produce films with good transfer ratios (y -type) despite its tendency to form domains at the interface. For the low MW polymer, good transfer was obtained using the conventional vertical dipping technique, only in the upstroke mode though. A constant applied surface pressure of 15 mN/m (minimum) and 10 mm/min dipping speed was found to be optimum for the low MW polymer. To maximize the deposition to higher order of layers on the upstroke mode, the alternate dipping technique was employed. The substrate was first passed through a clean surface, then an upstroke was made through the polymer monolayer and the cycle iterated. Transfer ratios of 1.0 ± 0.05 were obtained up to 30 layers on each side of the

substrate (total of 60 for the whole substrate). Typical transfer ratio data at room temperature is shown in Figure 5-30.

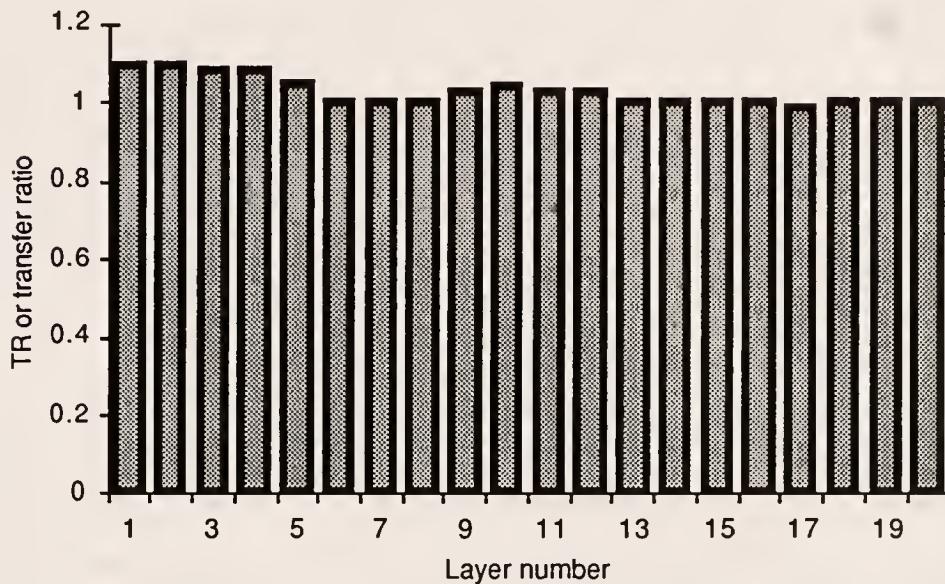


Figure 5-30. Typical Deposition ratio data for low MW Polymer LB film at 25 °C using the alternate trough. Pressure was at 15 mN/m and speed of 10 mm/min. Deposition was in the upstroke mode (z-type)

Polarized ATR-FTIR

To determine the orientation of IR active groups in the polymer such as the carbonyl stretching band of the ester group, polarized Attenuated Total Internal Reflection-Fourier Transform Infrared (ATR-FTIR) spectroscopy was made on the LB layers of the low MW polymer. Measurements were done by Mr. Houston Byrd of Prof. D. Talham's group (Department of Chemistry, University of Florida). The spectra were recorded at 1000 scans with 2.00 cm^{-1} resolution from LB films of 1 to 3 layers (further description of instrumentation is in Chapter 2). The phase of the polarized light was varied between 0° and 90°

to determine the tilt angle of the carbonyl group from the dichroic ratio. The absorbance of each additional layer was ratioed from the previous background layer and the dichroic ratio and tilt angle calculated according to the method of Ulman et al.^{238,239} The results are summarized in Table 5-3.

Table 5-3. Summary of results from ATR-FTIR measurements from 1-3 layers deposited on a Si crystal. All spectra were taken at 1000 scans with 2 cm⁻¹ resolution.

Layer Difference	Absorbance $\pm .0001$	Dichroic ratio $D = A_0/A_{90}$	Tilt Angle $\pm 5^\circ$
1-2	$A_{90} = .0031$	0.87	4°
	$A_0 = .0027$		
2-3	$A_{90} = .0057$	0.87	4°
	$A_0 = .0050$		

From the absorbance data, the dichroic ratio, D, defined as:

$$D = (A_x + A_z)/A_y \quad (5.8)$$

was calculated where $(A_x + A_z)$ is the absorbance with p-polarized light and A_y is the absorbance with s-polarized light. The small tilt angle from the normal reveals that the carbonyl groups are predominantly nearly orthogonal to the surface plane of the substrate. Assuming that the orientation at the monolayer was maintained even after film transfer, these results give support to the hypothesis that the carbonyl groups (ester) are hydrated by water as supposed from surface potential measurements.

Alternating Multilayers

To demonstrate the versatility of the multilayer film forming properties, an interesting architecture was made in which alternate layers were made with stearic acid. Various alternations were obtained using the alternate trough with the layers of the stearic acid and the low MW polymer. The alternations provide a unique superlattice structure in which an active NLO material (polymer) can be incorporated in between layers of non-active material (stearic acid) and the thickness controlled. As much as 30 alternating layers with different composition ratios were produced on silicon and quartz substrates. The data on the various alternations obtained are summarized in the following table:

Table 5-4. Summary of results for alternate deposition of polymer (P) and stearic acid (S) layers at 25 °C and 15 mN/m applied pressure using the alternate deposition apparatus. TR is for transfer ratio,

LB film	Alternation repeat unit	Average TR ± 0.05	Number of Layers
1	P	1.03	30
2	S:P	1.02	30
3	S:S:P	1.07	30
4	S:P:P	0.98	26
5	S:S:S:P	1.10	20

All the multilayers were deposited at 15 mN/m and 19 mN/m constant pressure for polymer and stearic acid respectively and 10 mm/min dipping speed. For the high MW polymer, alternate multilayer deposition was also

attempted with poor results as incomplete transfer was achieved with the transfer of stearic acid (ratio of 0.4-0.5)

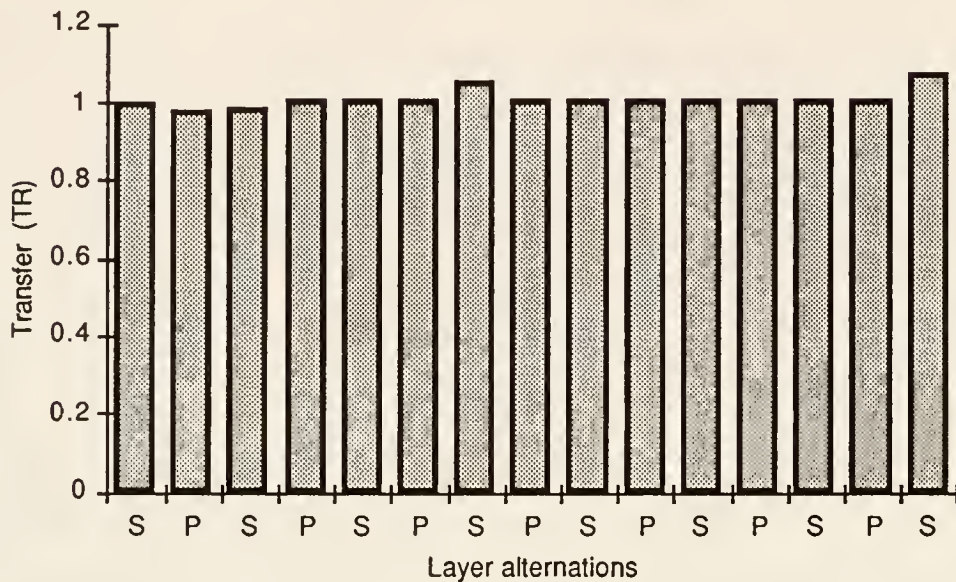


Figure 5-31. Typical Deposition data for alternating layers of pDDM and stearic acid at 25 °C on a Si substrate. The layers were deposited on the upstroke mode (z-type) at 10 mm/min. Refer to Table 5-4 LB film 2.

Small Angle X-ray Analysis

To verify the layer ordering of the multilayers, small angle X-ray diffraction of the multilayers were done on a Rigaku 18-kW rotating anode diffractometer (measurements made by Dr. Jing Fei Ma of Prof. S. Nagler's group, Physics Department, University of Florida). Diffraction data on 30 layers of the pure polymer revealed no discernible Bragg peaks (for three different films). However, for the various alternating films, well defined layer order was observed with the appearance of up to the 9th harmonic Bragg peak for Film 2 (S:P repeat unit).

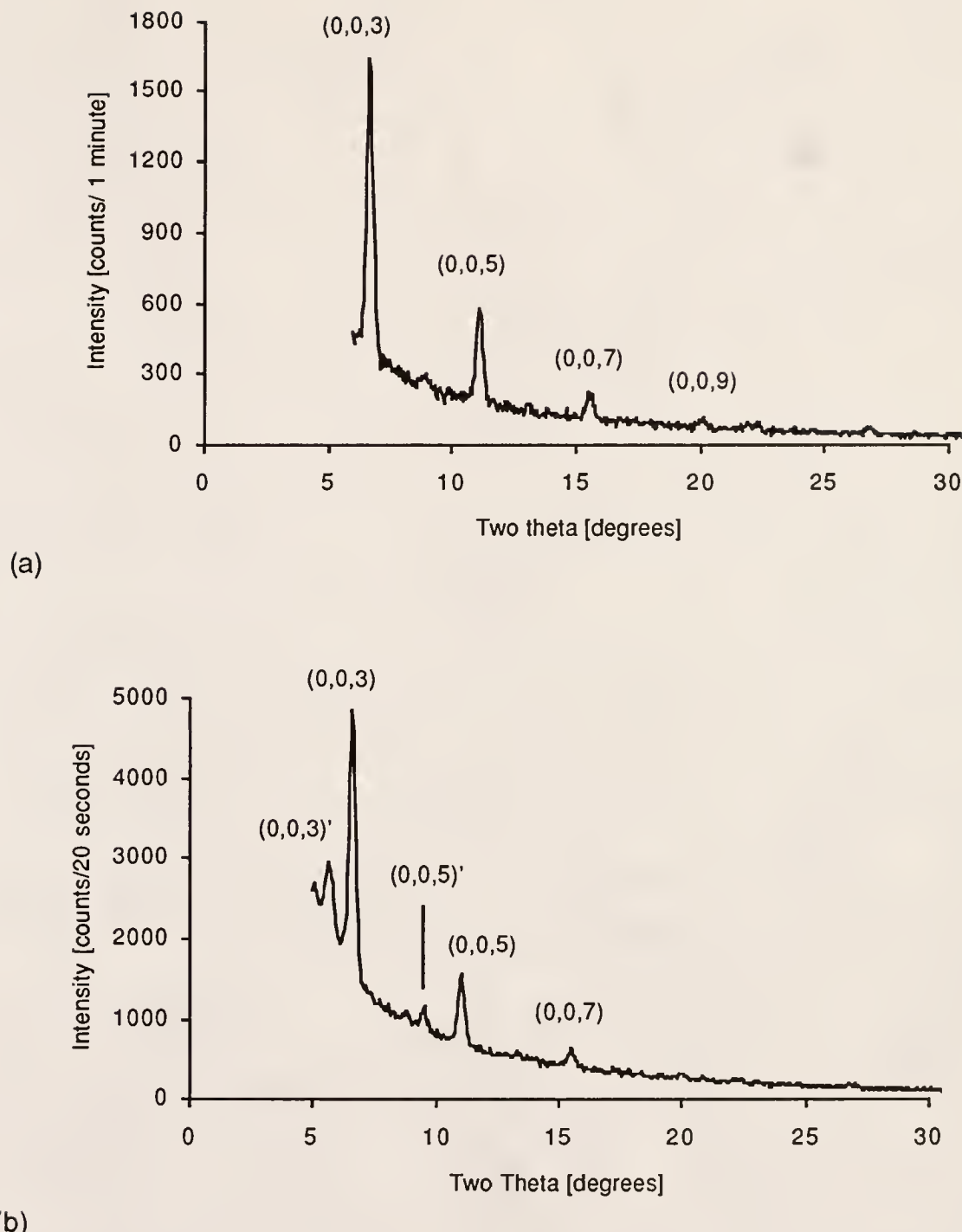


Figure 5-32. X-ray diffraction patterns for Films 2(S:P) and 3(S:S:P), showing the high degree of organization within the layers. The numbered maxima correspond to the d-spacings in Å: (a) Film 2(S:P) (3 - 13.30, 5 - 8.04, 7 - 5.71, 9 - 4.42), (b) Film 3(S:S:P) (3 - 13.20, 5 - 8.04, 7 - 5.71) ($3'$ - 15.3, $5'$ - 9.7).

The lack of Kiesig fringes (interference subsidiary maxima) in between the Bragg peaks may indicate some surface disorder either on the outermost layer or substrate surface.²⁴⁰ The appearance of two sets of Bragg peaks for Film 2 (S:S:P) implies that there are two sets of layers due to the superlattice structure. At first the absence of any Bragg peaks from the pure polymer multilayers was unexpected as good transfer ratios were observed during the dipping process. However, since the polymers have a very high aspect ratio in the direction of the chain lying parallel to the interface, the thickness of the monolayer as calculated from approximate bond lengths is only about 6 Å. It is entirely possible that the polymer chain undulations would have magnitudes of the same order as the layer periodicity. Also interlayer overlapping of the chains could occur. Either of these would effectively smear out any electron density periodicity.

For the alternating films, applying Bragg's law for the periodicity of the peak positions in the diffractogram, the most intense peak was assigned as a third order peak with a d-spacing of about 13.3 Å for Film 2. This assignment was valid on the basis of the higher order peaks of N = 5, 7, 9 obeying Bragg's law

$$N\lambda = 2d_{\text{Bragg}} \sin\theta \quad (5.9)$$

where N is the order of reflection, λ is the wavelength of the incident x-ray beam, d_{Bragg} is the periodicity distance, and θ is the diffraction angle. This means that a d-spacing of ≈ 40 Å (2.31 two theta) can probably be assigned for a first order peak which is not visible in the diffractogram since the measurement was initiated at 6 two theta (to maximize S/N ratio). If this is the case the d-spacing is almost twice in comparison to an all-*trans* conformation of stearic acid (23 Å). Since no available data is given for smaller angles (lower

than 6 two theta) no exact assignment or possible explanation can be given at this point. A theoretical value of 29 Å was expected for Film 2 if the 6Å value for the polymer was additive to an all *trans*-conformation of stearic acid layers with 23 Å d-spacing. Variations in d-spacing observed can be related to three possibilities: penetration of the carbonyl (acid) or terminal alkyl chains of stearic acid into the polymer matrix, tilting of the alkyl chains, and gauche conformations of the alkyl chain. Also, the observed peaks need to be related to the dipping behavior and possible layer overturning. Further X-ray diffraction studies will be conducted at the National Synchrotron Light Source in Brookhaven to further verify the stacking nature of these multilayers.

Summary

This study has shown the monolayer and multilayer LB film properties of poly(diethyldipropargylmalonate) or pDDM. The synthesis of the polymer was done using a MoCl₅ catalyst in dioxane under vacuum. Molecular weight control was achieved by controlling various reaction conditions such as the time of polymerization. Characterization of the polymer was done with NMR, IR, UV and polymer properties such as MW by GPC and thermal stability by TGA.

Langmuir monolayer film investigations allowed the examination of the contribution of various functional groups to the conformational dynamics of the polymer. At the same time, the technique highlighted the differences in the film forming properties of the low and high MW derivatives of the polymer. Various techniques such as surface potential, Brewster angle microscopy, and *in situ* UV-vis spectroscopy proved to be important. Compression up to the overfilm region (high pressure or collapse) always resulted in a net change for all the measurements. This kinetically unstable region would represent a high

pressure environment for the polymer chains in which the formation of more helicoidal non-planar conformations are energetically favored. This is brought about by the "squeezing" out of the chains from the polymer rich phase to both the air and water subphase. A direct consequence of this stress anisotropy at the interface is the filling up of the excluded volume in the polymer chains resulting in irreversible changes on the backbone conformation. The equilibrium between the inter- and intramolecular dipole interactions as well as the hydration dynamics at the interface were responsible for the enthalpy behavior of the polymers, i.e. spreading properties. The contribution of the semi-rigid polymer backbone to film behavior was examined in detail by a series of compression-expansion cycle studies. The two regions in the isotherm, below and above the collapse pressure, represented opposite environments for the polymer film. Compression to the overfilm region resulted in irreversible changes in the conformation of the polymer while good hysteresis behavior was observed at pressures below the collapse. This again highlighted the difference between the low and high MW derivatives in which the stress of compression is less evident for the high MW derivative. The equilibrium of conformational transitions for planar and non-planar (conformational defect) sequences was analyzed in terms of differences in propagation and nucleation behavior. A model was put forth to distinguish the contribution towards formation of conformational defects. The mechanism for this defect contribution was classified either as an *ester* or *backbone* dominated defect. The defect originating either from the *lateral* or *interior* region of the conjugated sequences. In situ-UV vis measurements proved to be invaluable in directly observing the conformational dynamics of the polymer at the interface. Other techniques for directly observing chain dynamics at the interface could complement these studies, e.g. isotope labeling, ellipsometric measurements, etc.

To demonstrate the utility of the technique in thin film fabrication, multilayer LB films of both derivatives are possible. Interesting architecture of alternating layers of stearic acid and polymer, demonstrate the versatility of these polymers and possible applications for thin film nonlinear optical materials. Further characterizations are needed though to define the film integrity and the multilayer film structures with other techniques. The scope of which is subject to further research.

CHAPTER 6

CONCLUSION: COMPARISON OF APPROACHES AND PROCESSABILITY OF SUBSTITUTED POLYACETYLENES

This work showed several routes towards two-dimensional ordering of substituted polyacetylenes for nonlinear optical film applications. The study comprised both the synthetic aspect as well as film forming properties of these polymers. It showed that thin films of substituted polyacetylenes could be obtained from two different major routes: *ordered monomer* and *preformed polymer* approach. The use of the Langmuir-Blodgett technique was critical as outlined in the introduction. It is important for device fabrication requirements and fundamental studies of such materials for nonlinear optics. The polymerization parameters for ordered monoacetylenic monomers was initially investigated. The majority of the dissertation though, addressed the Langmuir monolayer film properties of these polymers at the air-water interface. The synthetic aspect showed the importance of configuration and conformation for these polymers. The presence of a lateral alkyl chain substituent and low molecular weight were found to be important characteristics for good polymer monolayer behavior.

Polymerization of LB films: reactive functional group and initiators

For the first approach, the work showed that it was possible to polymerize ordered LB multilayers of monoacetylene monomers to form substituted polyacetylenes. The liquid crystalline monoacetylene allowed ordering of the

monolayer at lower temperatures and with the use of a stabilizing interactant. LB film deposition was possible for such monolayers with good stacking properties and sufficient lateral ordering. While polymeric products were formed as shown by UV and GPC, degradation of the side groups probably occurred because of the high energy mode of initiation. Better polymerization geometries and functional groups would therefore be needed in order to maximize the effectiveness of this technique. This could possibly be done by chemical modification of the reactive functional group and the use of initiators that could easily be activated at ordinary conditions.

Poly(ethynylbenzoate): configuration and lateral alkyl side chain length

For the polyethynylbenzoate polymers, the different substituents played an important role in determining the local conformational behavior of the polymers and their chain microstructure. The higher *trans* ratio was a consequence of substituent effect and the type of catalyst used. Modeling suggested that the *trans-transoidal*, head to head placement combination, would be the only configuration capable of giving substituted polyacetylenes free from steric interaction between the substituents. Regiospecific catalysts (as alternate mechanisms to chain addition) should play an important role in achieving this configuration. During formation, the polymers essentially retained their configuration and conformation. The substituents "locked in" the backbone conformation, the degree of which was dependent on the stiffness of the substituent and presence of flexible side chains. Thus the conformation observed as polymerized was essentially retained at the air-water interface. The stiff substituent contributed little to enhancing film forming properties but highlighted the role of the alkyl chain attached to the substituent. The effect of a longer alkyl chain pendant to the backbone enhanced the monolayer behavior

as well as deposition properties for this class of polymers. This was observed with the (Polymer 1) PPAC-16 derivative which exhibited excellent film forming properties. The consequence of the shorter chain length as well as stiff phenyl substituents resulted in stronger cohesive forces between the polymer chains, decreasing spreadability. Multilayer film deposition was possible only with the presence of a longer alkyl chain and blending with stearic acid.

Poly(diethyldipropargylmalonate): molecular weight and alternate layers

The poly(diethyldipropargylmalonate) showed an improved configuration over the poly(ethynylbenzoate) polymers. The molecular weight was controlled to produce low and high MW derivatives. It was found that the low MW polymer exhibited excellent film forming properties as compared to the high MW polymer. The measurements in the hysteresis cycle experiments showed the possibility of in-situ observations on the conformational dynamics of the polymer backbone with pressure. The UV-vis measurements gave a direct evidence on these conformational changes not possible with most polymers spread at the air-water interface. The various contributions of the functional groups to the conformational dynamics of the polymer backbone was likewise analyzed. The observed conformational transitions were proposed to be balanced between the nucleation and propagation of non-planar sequences. Two main mechanisms of defect formation were classified as either ester or backbone dominated defects. The terms *lateral* and *interior* defects were proposed to characterize the site of defect formation in conjugated sequences. Thus, long and short range forces of interaction determined the film behavior of the polymer. To demonstrate the utility of this polymer for thin film fabrication, multilayer LB films of both derivatives were made. Interesting architecture of alternating layers of stearic acid and polymer demonstrated the versatility of

these polymers and possible applications for thin film nonlinear optical materials. ATR-FTIR and small angle X-ray diffraction measurements were done to verify interlayer ordering. Further characterizations could be done to define the intralayer ordering. The scope of which would be subject for further research.

Finally, although much work has been done on polydiacetylenes as a class of polymers, to the author's knowledge, no comprehensive work has been done in literature to investigate two-dimensional ordering of substituted polyacetylenes most especially with a two-fold approach. It is now possible to design other substituted polyacetylene systems incorporating the design and approach criteria obtained from these studies. For future work, nonlinear optical measurements for $\chi^{(3)}$ will be made on these films.

APPENDIX A

NONLINEAR OPTICS: THE THEORETICAL VIEWPOINT

Maxwell's Equations

Nonlinear effects in electricity (E) and magnetism (B) are characterized by the well-known Maxwell equations relating higher order effects with linear phenomena.²⁴¹ Similarly, the same treatment can be made on the optical phenomena which normally occur with high intensity laser beams. The presence of an optical field is described by the polarization, P (dipole/unit volume or polarization density) as a complicated nonlinear function of E. This constitutive relationship is given by a Taylor power series expansion in various forms:

$$P = P_0 + P(1) + P(2) + P(3) + \dots \quad (A.1)$$

$$P = P_0 + \chi^{(1)} \cdot E + \chi^{(2)} \cdot EE + \chi^{(3)} \cdot EEE + \dots \quad (A.2)$$

$$P_i = P_i^{(0)} + \chi_{ij}^{(1)} E_j + \chi_{ijk}^{(2)} E_j E_k + \chi_{ijkl}^{(3)} E_j E_k E_l + \dots \quad (A.3)$$

where the first terms refer to the spontaneous polarization, the second term being the linear term (e.g. absorption, reflection, etc.), and the third and fourth term being the nonlinear susceptibilities. The odd orders are always present even in isotropic medium whereas the second order vanishes in a medium with centrosymmetry. Since the susceptibilities, $\chi^{(n)}$, depend on the frequencies of light present in the material, other forms of this expression therefore contain the Fourier components labeled by frequency, ω , which are used to describe the

various nonlinear optical effects observed, e.g. second harmonic generation, linear electro-optic effect (Pockel's effect), etc. Analogously, the polarization per molecule, p , can be expanded in terms of the molecular nonlinear response in powers of electric field, E . This represents the microscopic nonlinear susceptibility:

$$p = \mu + \alpha \cdot E + \beta \cdot EE + \gamma \cdot EEE + \dots \quad (A.4)$$

where α is the linear, β the second order, and γ the third microscopic nonlinear susceptibilities. At best, the relationship between microscopic nonlinear susceptibilities and macroscopic hyperpolarizabilities is an approximation due to the multiple frequencies present. Dispersion, degrees of freedom, spatial distributions, relationship of driving force frequencies to natural frequencies, variable magnetic and electric fields, affect the overall predictability of the relationship. In systems where the molecules are weakly interacting, the macroscopic susceptibility can be assumed to be additive over the microscopic susceptibilities. In this case, only the orientational order must be considered in detail since positional ordering effects can be described in an average sense by local field factors:

$$\chi_{ijk}(2n) = N \sum_{m=0} n \xi_{ijk}(2m+1) \langle P_{2m+1} \rangle \quad (A.5)$$

$$\chi_{ijk}(2n+1) = N \sum_{m=0} n+1 \xi_{ijkl}(2m) \langle P_{2m} \rangle \quad (A.6)$$

where equation A-5 and A-6 describe the even and odd order susceptibilities, $\xi_{lmn}^{(k)}$ is a function of the tensor components of the k th order susceptibility, N the number density and where the angular average $\langle P_{2m} \rangle$ depends on the orientational order.

Wavefunction Overlap

Considering a two-level model for simplicity e.g. ground state and excited state, the behavior of the nonlinear optical response can be related to the shape of the wave function. The following guidelines are useful for the analysis.⁸

Second Order Nonlinearity:

1. To promote wavefunction overlap between the ground and excited states, the oscillator strength ,f, where $f \propto \langle e/r/g \rangle^2$ needs to be increased. The coordinate operator, r, is a coordinate associated with the position of the electrons (summation over all electrons). This is related to the transition dipole moment , μ , by the electric charge $er=\mu$)
2. To promote wavefunction separation between the ground and excited states, increasing the dipole moment difference, Pe-Pg (dipole moment, $\Delta\mu$ e.g), where $Pe = \langle e/r/e \rangle$ and $Pg = \langle g/r/g \rangle$ in terms of the r operator.

Second order nonlinearity would then be proportional to the product of f and Pe-Pg, consistent with the two level model expression for molecular second order nonlinear susceptibility,

$$\beta \propto f (Pe - Pg) \quad (A.7)$$

Third Order Nonlinearity

1. To promote wavefunction overlap between the ground and excited states, the oscillator strength $f \propto \langle e/r/g \rangle^2$ needs to be increased.

2. To promote wave function differences between the ground and excited states, increasing Le-Lg, where Le and Lg are measures of wave function distribution.

Third order nonlinearity would then be proportional to the product of f and Le-Lg. Considering one excited state, $|e\rangle$, which has a major transition matrix element with the ground state $|g\rangle$ and neglecting the energy denominator, molecular third order nonlinear susceptibility can be roughly expressed as:

$$\gamma \propto S_n \langle g/r/e \rangle \langle e/r/n \rangle \langle n/r/e \rangle \langle e/r/g \rangle \quad (\text{A.8})$$

$$\approx \langle g/r/e \rangle \langle e/r^2/e \rangle \langle e/r/g \rangle$$

Then assuming $\langle e/r^2/e \rangle \propto$ Le-Lg the difference in expected values of r^2 between ground and excited states in the analogy of Pe-Pg and b, we obtain

$$\gamma \propto f(\text{Le-Lg}) \quad (\text{A.9})$$

For both second and third order nonlinearities, however, note that f and Pe-Pg , or f and Le-Lg are not independent, but are a tradeoff. Therefore a balance of the wavefunction overlap and wave function separation (or difference) must be considered simultaneously in optimizing nonlinear effects e.g. for second order organic crystal, it must be noncentrosymmetric and the conjugation length cannot be too long (oscillator strength) without equivalently raising the dipole moment of the system (wavefunction difference).

Applications:

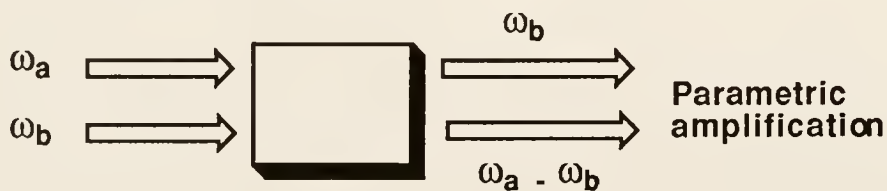
In general, all applications arising from nonlinear optical properties of materials are: modulation in the refractive index in the presence of an electric field and the generation of harmonic frequencies. The following are representative applications in a simplified description.²⁴²

Effects occurring Through $\chi^{(2)}$

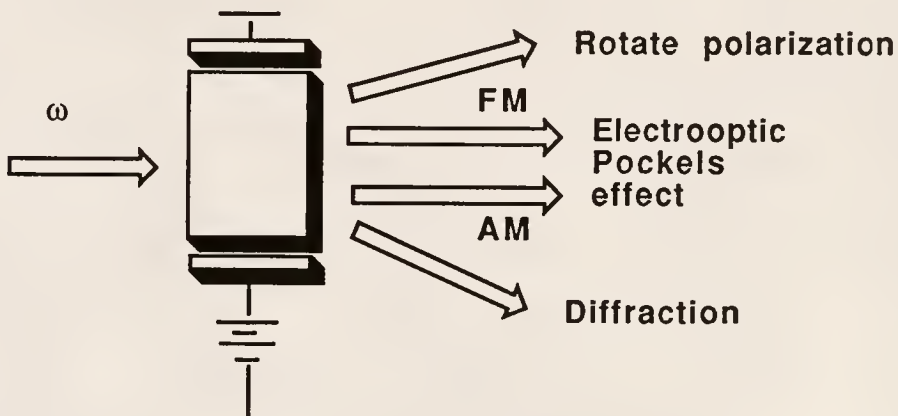
1. Second Harmonic Generation (SHG) - Nonlinear polarization is created in a medium which contains a Fourier Component at 2ω which acts as a source of electro-magnetic radiation. The outcome is phase dependent, that is, the amplitude is dependent on the phase relationship between the harmonic and fundamental frequencies. Application: For generating low wavelength lasers.



2. Frequency Mixing - Depending on the phase relationship, the output wave can show enhancement of an input frequency. Application: enhancement of weak signals for spectroscopy and optical repeaters, IR up conversion, parametric amplifiers.



3. Linear Electrooptic or Pockels Effect - Occurs from interaction of the optical and DC field in the nonlinear medium results in altering the propagation characteristics of light in the medium. Application: waveguiding, amplitude modulation, matrix effects

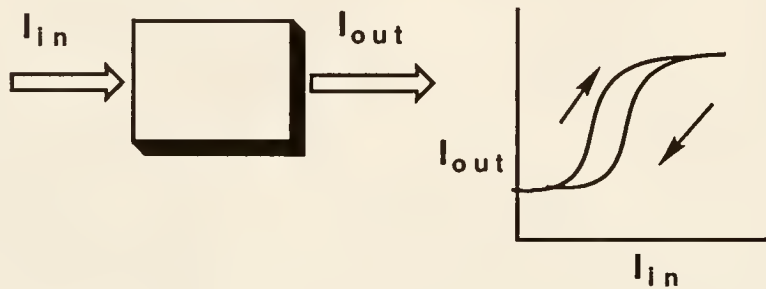


Effects Occurring Through $\chi^{(3)}$

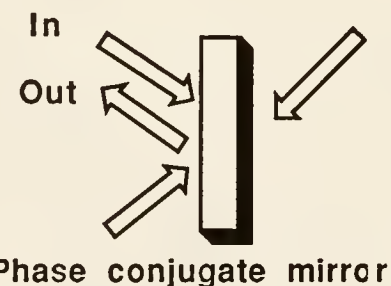
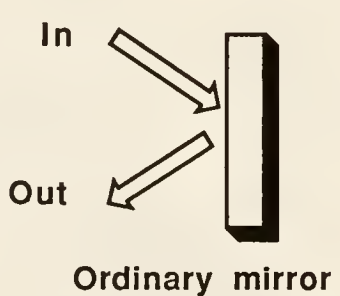
1. Third Harmonic Generation (THG). - Arises from the Fourier component of the nonlinear polarization at 3ω acting as a source of electromagnetic radiation. A major difference between even and odd order nonlinear interactions is that a response can occur at the fundamental frequency in media exhibiting odd order responses. Application: Changing laser wavelengths to the third harmonic



2. Optical Bistability. - Light intensity induced changes in the refractive index of the medium in a resonant cavity (optical Kerr Effect). This results in different beam propagation effects. Application: This is an optical analog of a transistor, optical switch for optical computers.



3. Phase Conjugate Mirrors - Results from degenerate four wave mixing process in which two beams interfere to form a phase grating and the complex conjugate of the phase front of the incoming beam is created as an outgoing beam. Application: signal enhancement, phase conjugation, powerful lasers.



APPENDIX B

THE CONJUGATED POLYMER BACKBONE

Conformation

The conformational dynamics of the semi-rigid, single-double bond polyene backbone are dependent on rotations along the single bond. The term *conformation* (or microconformation) is always used with respect to the single bond.¹⁵⁴ In some occasions, torsion stereoisomers produced by rotation about double bonds or partial double bonds are sometimes included. In which case, the concepts of conformation and configuration are partially merged by this extension. Thus, there are a large number of microconformations in the backbone and a macromolecule adopts an overall macroconformation. The macroconformation in turn determines the shape of the molecule. Of the infinitely large number of theoretically possible conformations, only some will be energetically favorable. These conformational isomers are called *conformers*, *rotational isomers*, or *rotamers*.

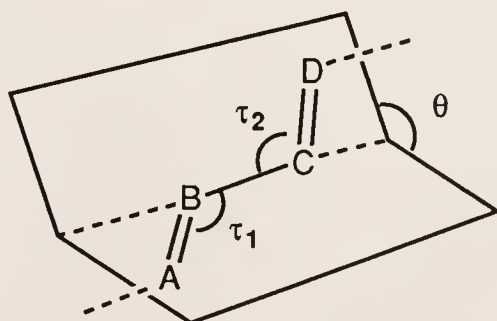


Figure B-1. A microconformation from a single-double bond sequence of the polyene backbone is defined by the dihedral angle. The dihedral angle, θ , is the angle formed between the A-B-C and B-C-D plane. τ_1 and τ_2 are the bond angles.

The dihedral angle, θ , (conformation angle, rotation angle, or torsion angle) is used to distinguish between the various conformers in a polymer backbone.¹²⁵ As shown in Figure B-1, the angle is defined as the angle between the plane A-B-C and B-C-D. The dihedral angle is measured from -180° to 180°. A positive value is obtained if the A-B bond has to be rotated less than 180° to the left (clockwise) to make it superimposable to C-D. In the illustration, the angle is negative if viewed along the B-C axis. In addition, analogous terms to various conformers of small organic molecules are used for macromolecules : *cis* (0°), *gauche* (120° or -60°), *anti* (-120°) , and *trans* (\pm 180°). For the polyene backbone, since the terms *cis* and *trans* are used to describe the configuration of double bonds, the terms *cisoidal* (0°) and *transoidal* (\pm 180°) are used instead (Figure B-4). Enantiomeric conformations are given the same name when they do not deviate from the ideal conformation by more than \pm 30 °.

The chain segment is an arbitrary term for a sequence in the polymer backbone with n number of repeating units. A classification on the polyene backbone can thus be made based on the general conformation of a segment as defined by the dihedral angles. In Figure B-2, the deviation from a theoretically all-planar conformation (could apply for both substituted polyacetylene or polydiacetylene backbone) is given by the height of the line connecting the substituent to the backbone. For simplicity, the conjugated backbone is simply represented by a straight horizontal line.²²⁸ A totally planar conformation is represented by all the main chain-substituent bonds lying in the same plane (0° angle or full vertical height). Deviations from the plane (enantiomeric conformations) are represented by variations on this height with a minimum represented by zero height (\pm 90°). In principle, the greater the dihedral angle, the lesser the probability of maintaining the segment

planarity as limited by energy barriers to rotation. Within the segment, conformational diads, triads, etc., can also be classified.

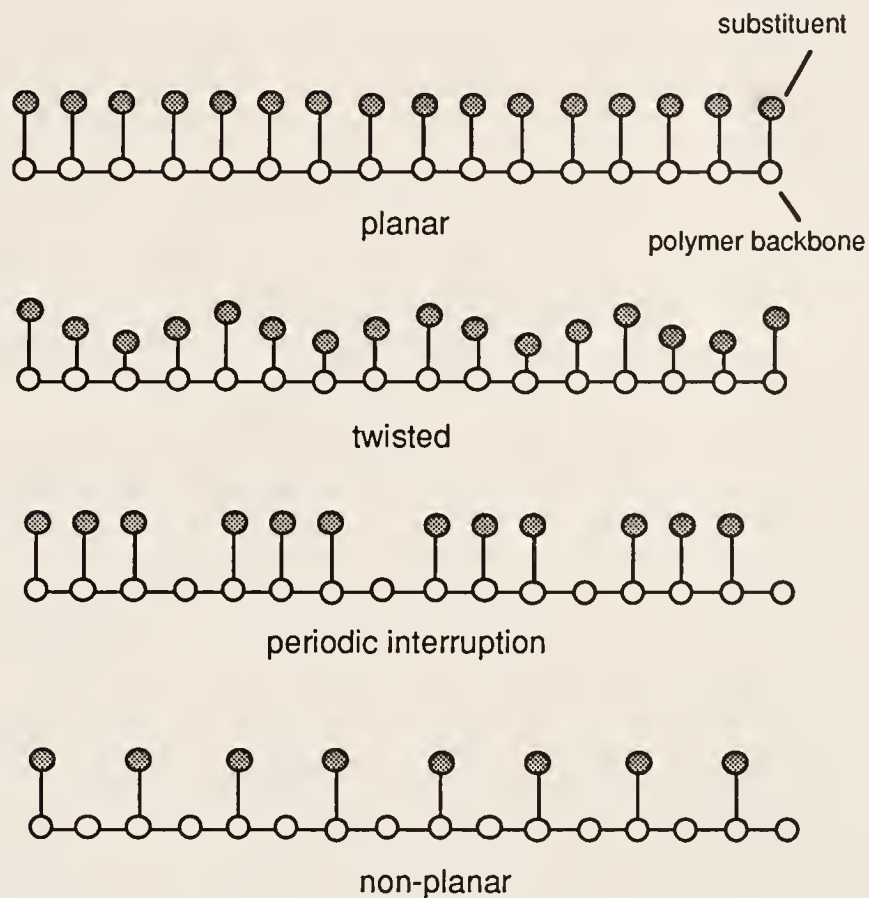


Figure B-2. Segment conformation for a conjugated polymeric backbone based on dihedral angles (planar or non planar). The degree of deviation from 0° is represented by the height of the line connecting the substituent to the polymer backbone (between 0° and $\pm 90^\circ$).

Defects on the backbone

The rigid nature of the polyacetylene backbone results in increased crystallizability. For the substituted polyacetylene, this is usually counteracted by greater geometric packing restraints, resulting in an amorphous state. On the other hand, the presence of the substituent greatly increases the

processability of these polymers. The influence of various substituents on the backbone conformation has been widely studied. However, little attention has been given to the effect of configuration in setting the initial energy barrier conditions for free rotations. The influence of the synthetic method and in particular the catalyst for coordination polymerization, also often produces irregular chemical structures on the backbone. With the planar polyenic backbone being the ideal model, all types of deviations from the planar conjugated structure could be classified as defects. In this manner, *conformational*, *configurational*, and *chemical* defects can be classified in the backbone.⁴⁷ The parameters that can determine this classification are broader in scope which could include: catalyst, preparation method, solvent, thermal effects, etc. Some specific perturbations are described as follows:

1. The presence of secondary molecular interactions in the substituents e.g. H-bonding, dipole interactions, van der Waals forces
2. The presence of molecules that can intercalate in between the polymer chains e.g. solvents, plasticizers, etc.
3. Thermal effects which increases the internal energy of the polymer resulting in less relaxed conformations such as coils for the backbone (trans-transoidal if free from steric interactions is the most relaxed conformation for polyacetylene).
4. Anisotropy of stress as in the application of pressure or release of pressure upon the chains e.g. monolayer compression, dipping.
5. The solution properties of the polymer and its hydrodynamic effects. The interaction of the polymer to a solvent and a non-solvent. The interaction at the interface of these two solvents.

6. Backbiting mechanisms during chain propagation which results in saturated chemical defects in the backbone.

7. Effect of catalyst on monomer placement during coordination of monomer to catalyst. This determines the configuration for monoacetylenes.

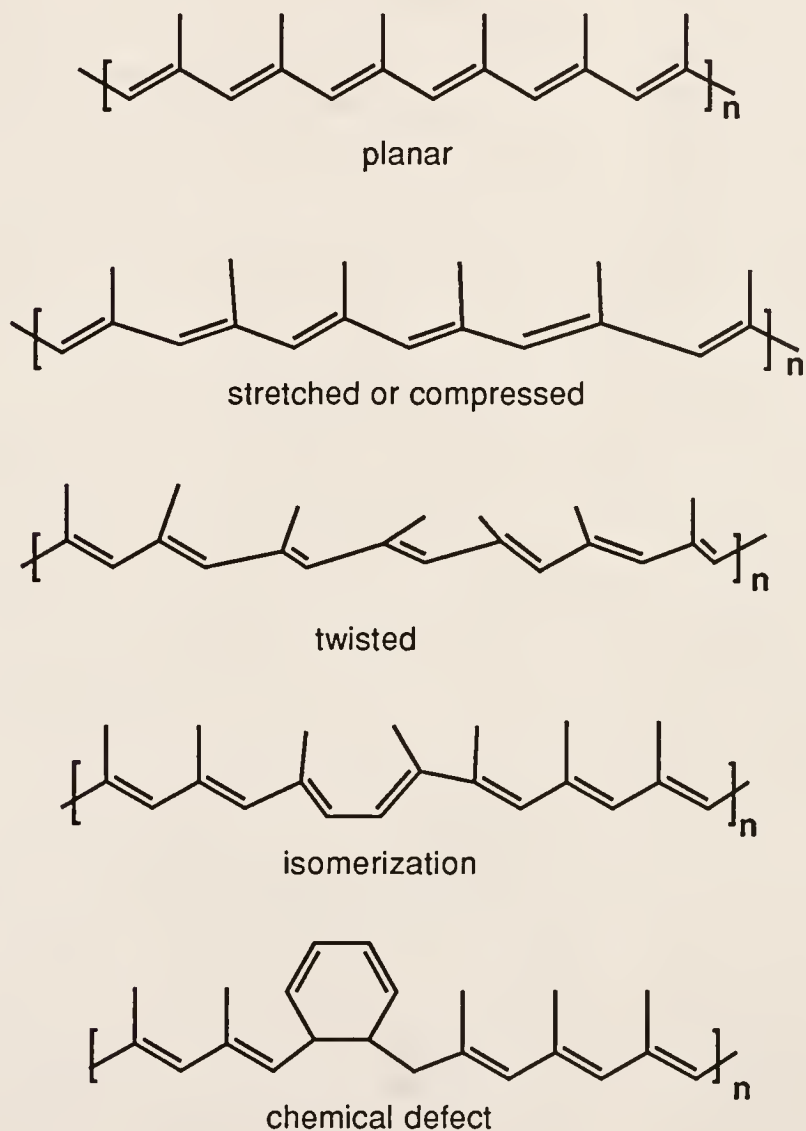


Figure B-3. The ideal backbone is shown at the topmost. All other classes result in a backbone defect. Typical substituent is a methyl group, poly(propyne).

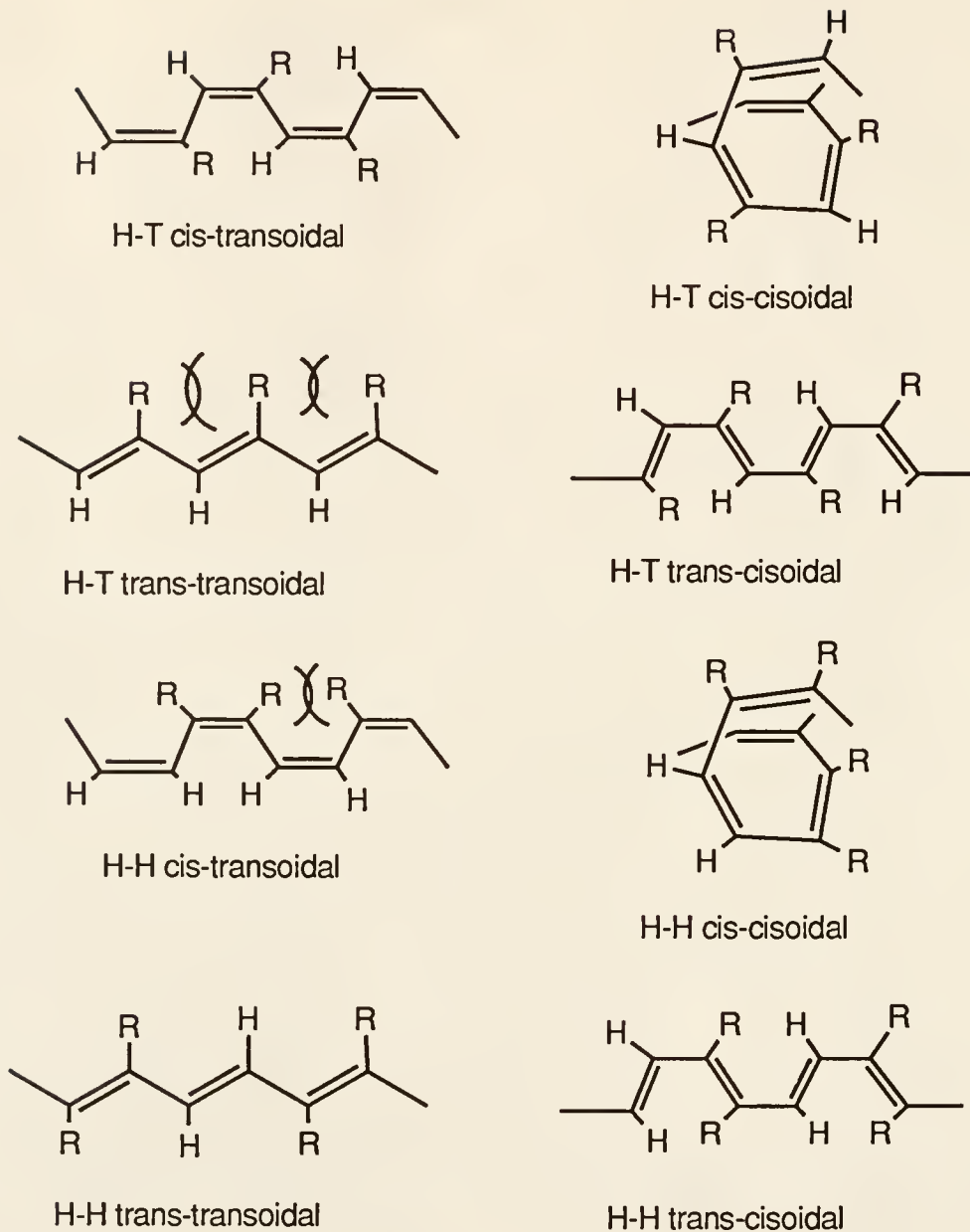
Classification by configuration

Figure B-4. Classification of the substituted polyacetylene backbone based on the configuration. Head (H) and tail (T) for placement, *cis* or *trans* for the double bond, and *cisoidal* or *transoidal* for the single bond. Notice the steric strain on each particular configuration and the eventual loss of planarity.

The substituted polyacetylene backbone can also be classified according to configuration.⁴² This is usually determined during the coordination of the monomer to the catalyst in coordination polymerizations (though classification holds true with other possible polymerization mechanisms). The placement of the monomer results in variations of head, H, (carbon with substituent) and tail, T, (carbon with hydrogen) arrangements e.g. H-H or T-T and H-T.¹⁶³ The double bond configuration can either be a *cis* or *trans*. The single bond can either be *cisoidal* or *transoidal*. These result in a combinatorial factor of three, leading to eight possible configurations ($C = 2^3 = 8$).

In principle, both regio- and stereospecific control would allow the formation of a well defined backbone configuration. Considering the various routes toward the polymerization of substituted acetylenes, one needs to control important parameters and possible limiting factors. Initiators such as Ziegler-Natta catalysts, are known to preferentially give *cis* isomers via the insertion mechanism.⁴² *Trans* isomers are obtained thermally by heating up to 150 °C (a post double bond isomerization).⁵² Group 5 and 6 metal catalysts can have either a pre- or a post-double bond isomerization, in which case, *trans* isomers are formed prior to double bond formation.^{163,165} In addition, one needs to consider conditions such as steric factors from the substituent, solvent interactions, temperature, homogeneous or heterogeneous catalysis, etc.. Any of these factors can affect the polymerization mechanism and the final configuration of the polymer backbone. Radical and photochemical polymerization afford even less geometric isomer control.⁴² Perhaps routes such as acyclic diene metathesis (ADMET) or ring opening metathesis (ROMP) could afford better control through a systematic monomer architecture and oligomerization.^{55, 56}

APPENDIX C

SURFACE POTENTIAL AND DIPOLE MOMENT

The change in phase boundary potential produced by an interfacial film is defined as the *surface potential* (interfacial potential), ΔV , measured in mV.⁸⁵ This change in potential is a reflection of changes in the electrical dipole density at the surface. In theory, it is possible to evaluate the surface potential and apparent surface dipole moments by assuming a molecular orientation and summing vectorially the known dipole moments for all groups that constitute a molecule. The surface potential depends chiefly on three factors: These are the concentration of film molecules, the contributions from the dipole in the film, and in the case of the charged monolayer, the electrical potential, ψ_0 , in the plane of the charged groups. An equation that has been used in interpreting surface potential is called the Helmholtz equation:^{134,120}

$$\Delta V = 4\pi n \Delta \mu / D + \psi_0 \quad (C.1)$$

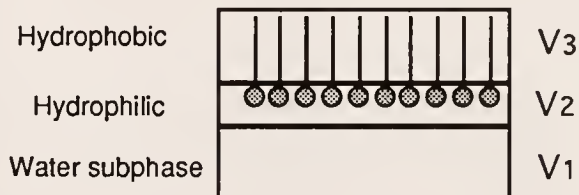
$$\Delta V = V_{\text{monolayer}} - V_{\text{air-water}} \quad (C.2)$$

where n ($1/A$) is the number of dipoles (usually molecules) per unit area, $\Delta \mu$ is the effective surface dipole moment in the perpendicular direction (measured in milli Debye), and $D(\epsilon_0)$ is the dielectric constant, which is normally assumed to be unity. Since this derivation is analogous to the potential difference between the plates of a parallel condenser, assuming an interfacial film consisting of a planar array of dipoles, a similar treatment can be made at the air-water interface. This model is based on the Demchak and Fort approach which is actually a refinement of the Helmholtz-Davies model.¹⁷⁴ It assumes that a

monolayer at the air-water interface may be divided into three layers, with each layer making a distinct and unique contribution to the surface potential, dV . Likewise as in the equation above, for ionized monolayers, the term ψ_0 , is included in the double layer potential. Thus:

$$\Delta V = V_1 + V_2 + V_3 + \psi_0 \quad (C.3)$$

where V_1 , V_2 , V_3 are contributions from (a)the reorientation of the water molecules in the subphase induced by the presence of the monolayer, (b) the group dipole moments associated with the hydrophilic headgroup region, and (c) the group dipole moments associated with the hydrophilic tail region of the monolayer.



More specifically, the equation can be written as :

$$\Delta V = (\mu_1/\epsilon_1 + \mu_2/\epsilon_2 + \mu_3/\epsilon_3) / A\epsilon_0 + \psi_0 \quad (C.4)$$

where μ_n is the average vertical component of the dipole moment per molecule (apparent) and ϵ_n , the local dielectric constant in each of the three layers and A is the average area per molecule.

REFERENCES

1. Ringsdorf, H; Schlarb, B.; and Venzmer, J. *Angew. Chem. Int. Ed. Engl.* **1988**, *27*, 113-158.
2. Franken, P.A.; Hill, A.E.; Peters, C.W.; Weinrich, G. *Phys. Rev. Lett.* **1961**, *7*, 118.
3. Groh, W.; Lupo, D.; Sixl, H. *Angew. Chem. Int. Ed. Eng. Adv. Mater.* **1989**, *18*, 1548-1559.
4. Kroschwitz, J. Ed. *Electrical and Electronic Properties of Polymers: State of the Art Compendium*, John Wiley & Sons, New York, **1988**.
5. Garito, A.F.; Singer, K.D., *Laser Focus*, **1982**, *18*, 59.
6. Williams, D.J. Ed. *Nonlinear Optical Properties of Organic and Polymeric Materials*, Plenum Press, New York, **1983**.
7. Flytzanis, Ch. in *Nonlinear Optical Effects in Organic Polymers*. Messier, Kajzar, Prasad, Ulrich Eds. Kluwer Academic Publishers, London, **1989**.
8. Yoshimura, T., *Optics Comm.* **1989**, *70*, 535-537.
9. Grossman, C.; Helfin, J.; Wong, K.; Zamani-Khamiri, O; Garito, A. in *Nonlinear Optical Effects in Organic Polymers*. Messier, Kajzar, Prasad, Ulrich Eds. Kluwer Academic Publishers, London, **1989**.
10. Delhalle, J. Dory, M.; Fripiat, J.; Andre, J. in *Nonlinear Optical Effects in Organic Polymers*. Messier, Kajzar, Prasad, Ulrich Eds. Kluwer Academic Publishers, London, **1989**.
11. Bredas,J.; Dory,M.; Bodart,V.; Delhalle,J.; Andre,J. in *Nonlinear Optical Properties of Polymers* Heeger, Orenstein, Ulrich Eds. Materials Research Society, Pittsburgh, **1988**.
12. Embs, F.W.; Wegner, G.; Neher, D.; Albuoy, P.; Miller, R.D.; Wilson, C.G.; and Schrepp, W., *Macromolecules* **1991**, *24*, 5068-5075.
13. Sinclair, M.; Moses, D.; Akagi, K.; Heeger, J. in *Nonlinear Optical Effects in Organic Polymers*. Messier, Kajzar, Prasad, Ulrich Eds. Kluwer Academic Publishers, London, **1989**.
14. Jenekhe, S.A.; Agrawal, A.; Yang, C.; Osaheni, J.; Chen, W. *Polymer Preprints* **1991**, *32*, 71-72.

15. Bubeck, C.; Neher, D.; Kalbeitzel, A.; Duda, G.; Arndt, T.; Sauer, T. and Wegner, G. *Nonlinear Optical Effects in Organic Polymers*. Messier, Kajzar, Prasad, Ulrich Eds. Kluwer Academic Publishers, London, 1989.
16. Chance, R.R. and Shand, M.L. in *Nonlinear Optical Properties of Organic and Polymeric Materials*, Williams, D.J. Ed. Plenum Press, New York, 1983.
17. Carter, G.; Chen, Y.; Tripathy, S. in *Nonlinear Optical Properties of Organic and Polymeric Materials*, Williams. Ed. Plenum Press, New York, 1983.
18. Rickert, S.; Lando, J.; and Ching, S. in *Nonlinear Optical Properties of Organic and Polymeric Materials*, Williams. Ed. Plenum Press, New York, 1983.
19. Sauteret, C.; Hermann, R.; Frey, R.; Pradere, F.; Ducuing, R.; Baughman, H.; Chance, R. *Phys. Rev. Lett.* 1976, 36, 956.
20. Garito, A.; Teng, C.; Wong, K.; Khamiri-Zamani, O. *Mol. Cryst. Liq. Cryst.* 1984, 106, 219.
21. Chollet, P.A.; Kajzar, F.; Messier, J. *Synth. Met.* 1987, 18, 459.
22. Le Moigne, J.; Thierry, A.; Chollet, P.; Kajzar, F.; Messier, J. *J. Chem. Phys.* 1988, 88, 6647.
23. Jenekhe, S.A.; Osaheni, J. *Polymer Preprints* 1991, 32, 154-155.
24. Prasad, P. in *Nonlinear Optical Properties of Polymers* Heeger, Orenstein, Ulrich Eds. Materials Research Society, Pittsburgh, 1988.
25. Bubeck, C.; Kalbeitzel, A.; Grund, A.; Leclerc, M. *Chem. Phys.* 1991, 154, 343.
26. Bubeck, C.; Kalbeitzel, A.; Lenz, R.; Neher, D. and Stenger-Smith, J.; Wegner, G. in *Nonlinear Optical Effects in Organic Polymers*. Messier, Kajzar, Prasad, Ulrich Eds. Kluwer Academic Publishers, London, 1989.
27. Wegner, G.; Bubeck, C.; Kaltbietzel, A.; Neher, D.; Stenger-Smith, J.D.; Wolf, A. in *Electronic Properties of Conjugated Polymers III*. Kuzmany, Mehring, Roth Eds. Springer-Verlag, Berlin, 1989.
28. Jenekhe, S.A.; Yang, C. *Polymer Preprints* 1991, 32, 165-166.
29. Reinhardt, B. *Trends in Polymer Science* 1993, 1, 4.
30. Jenekhe, S.A.; Agrawal, A. *Polymer Preprints* 1991, 32, 124-125

31. Dalton, L.R. in *Nonlinear Optical Effects in Organic Polymers*. Messier, Kajzar, Prasad, Ulrich Eds. Kluwer Academic Publishers, London, 1989
32. Yu, L.P.; Dalton, L.R. *Synth. Met.* 1989, 29, E463.
33. Lindle, J.R.; Bartoli, F.J.; Hoffman, C.; Kim, O.; Lee, Y.; Shirk, J.; Kafafi, Z. *Appl. Phys. Lett.* 1990, 56, 712.
34. Miller, R.; Michl, J. *Chem. Rev.* 1989, 89, 1359.
35. Kajzar, F.; Messier, J.; Rosillo, C. *J.Appl. Phys.* 1986, 60, 3040.
36. Baumert, J.; Borklund, G.; Jundt, D.; Jurich, M.; Looser, H.; Miller, R.; Rabolt, J.; Sooriyakamuran, R.; Swalen, J., Twieg, R. *Appl. Phys. Lett.* 53, 1988, 1147.
37. Hilberer, A. Ph.D. Dissertation University of Louis Pasteur, Strasbourg, France, 1993.
38. Kajzar, F.; Etemad, S.; Baker, G.; Messier, J. *Synth. Met.* 1987, 17, 563.
39. Drury, M. *Solid State Comm.* 1988, 68, 417.
40. Prasad, P.; Swiatkiewicz, J. and Pfleger, J. *Mol.Cryst. Liq.Cryst.* 1988, 160, 53.
41. Meredith, G.; Butchhalder, B.; Hanzlik, C. *J. Chem.Phys.*, 1983, 78, 1533.
42. Chien, J. *Polyacetylene*; Academic Press: Orlando, Florida, 1984.
43. Neher, D.; Kaltbeitzel, A.; Wolf, A.; Bubeck, C.; Wegner, G. *J.Phys. D: Appl. Phys.* 1991, 24 , 1193-1202.
44. Masuda, T.; Iguchi, Y.; Tang, B.Z.; Higashimura, T. *Polymer* 1988, 29, 2041.
45. Tsuchihara, K.; Masuda, T.; Higashimura, T. *J. Poly. Sci. A: Chem.* 1991, 29, 471-478.
46. Le Moigne, J.; Hilberer, A.; Strazielle, C. *Polymer Preprints* 1991, 32, 96-97.
47. Le Moigne, J.; Hilberer, A.; Strazielle, C., *Macromolecules* 1992, 25, 6705.
48. Neher, D.; Wolf, A.; Bubeck, C.; Wegner, G. *Chem. Phys. Let.* 1989, 163, 116-122.
49. Wolf, A. Ph.D. Thesis, University of Mainz, Mainz Germany 1989.

50. Simionescu, C.I., Percec, V.: *Prog. Polym. Sci.: Reviews*, 1982, 8, 133..
51. Chauser, M.; Rodionov, Y.; Misin, V.; Cherkashin, M. *Russ. Chem. Rev. (Eng. Trans.)* 1976, 45, 348.
52. Wegner, G. : *Angew. Chem. Int. Ed. Engl.* 1981, 20, 361.
53. Masuda, T.; Hasegawa, K., Higashimura, T. *Macromolecules* 1974, 7, 728.
54. Masuda, T.; Higashimura, T., *Adv. Polym. Sci.* 1987, 81, 121.
55. Tao, D. Ph.D. Dissertation, University of Florida, 1994 and unpublished results on substituted acetylene polymerization.
56. Grubbs, R.; Gilliom,L *J. Am. Chem. Soc.* 1986, 108, 73.
57. Wagener, K.B.; Boncella, J.; Nel, J.; Duttweiler, R.; Hillmyer, M. *Makromol. Chem.* 1990, 191, 365.
58. Klavetter, F.; Grubbs, R. *J.Am. Chem. Soc.* 1988, 110, 7809-7813.
59. Katz, T.; Hacker, S.; Kendrick, R.; Yannoni, C. *J. Am. Chem. Soc.* 1985, 107, 2182.
60. Okano, Y.; Masuda, T.; Higashimura, T. *Polym.J.* 1982, 14, 477.
61. Masuda, T.; Higashimura, T. *Macromolecules* 1979, 12, 9.
62. Le Moigne, J.; Hilberer, A.; Kajzar, F. *Makromol. Chem.* 1992, 192, 515.
63. Butler, G.B.; Angelo, R. *J. J. Am. Chem. Soc.* 1957, 79, 3128.
64. Butler, G. B. *Acc. Chem. Res.* 1982, 15, 370.
65. Guiata, M. in *Cyclopolymerization and Polymers with Chain-Ring Structures* Butler and Kresta Eds. American Chemical Society, Washington D.C. 1982.
66. Stille, J.K. and Frey, D. *J. Am. Chem. Soc.* 1961, 83, 1697.
67. Hubert, A.J. and J. Dale *J. Chem. Soc.* 1966, 3160.
68. Gibson, H.; Bailey, F.; Epstein, A.; Rommelmann, H.; Kaplan, S.; Harbour, J.; Yang, X.; Tanner, F. and Pochan,J . *J. Am. Chem. Soc.* 1983, 105, 4419.
69. Jin, S.; Cho, H.; Choi, S. *J. Polym. Sci. Part A. Polym. Chem.* 1993, 31, 69-74.

70. Jin, S.; Kim, S.; Cho, H.; Choi, S.K. *Macromolecules*, 1991, 24, 6050.
71. Jin, S.; Choi, S.J.; Ahn, W. Cho, H and Choi, S.K. *Macromolecules*, 1993, 26, 1487-1492.
72. Kang, K.; Kim, S.; Cho, H.; Choi, K. and Choi, S.K. *Macromolecules*, 1993, 26, 4539-4543.
73. Han, S.; Kim, U.; Kang, Y. and Choi, S. *Macromolecules*, 1991, 24, 973.
74. Ryoo, M.; Lee, W.; Choi, S.K. *Macromolecules*, 1990, 23, 3029.
75. Cho, O.; Kim, Y.; Choi, K. and Choi, S.K. *Macromolecules*, 1990, 23, 12-14.
76. Fox, H. and Schrock, R. *Organometallics* 1992, 11, 2763-2765.
77. Franklin, B. *Philos. Trans. R. Soc. London*. 1774, 64, 445.
78. Rayleigh, L. *Proc. R. Soc. London*, 1890, 47, 364.
79. Pockels, A. *Nature (London)* 1893, 48, 152.
80. Blodgett, K. *J.Am. Chem. Soc.* 1935, 57, 1007.
81. Adam, N.K., *The Physics and Chemistry of Surfaces*, 3rd. Ed. Oxford University Press, London , 1941.
82. Davies, J.T. and Rideal, E.K. *Proc. Royal Soc. (London)* 1948, A194, 417.
83. Crisp, D.J. *Surface Chemistry*, Butterworths, London, 1949.
84. Harkins, W.D. *The Physical Chemistry of Surface Films*. Rheinhold, New York, 1952.
85. Gaines, G.L. *Insoluble Monolayers at Liquid Gas Interfaces*. John Wiley & Sons , New York, 1966.
86. Biography of H.Kuhn in Proceedings and Primer, *Sixth International Conference on Organized Molecular Films (LB6)* July, 1993.
87. Roberts, G. *Langmuir Blodgett Films*. Plenum Press, New York, 1990.
88. Ulman, A. *An Introduction to UltrathinOrganic Films: From Langmuir Blodgett to Self Assembly*, Academic Press: San Diego CA, 1991.
89. Ringsdorf, H. and Schupp, H. *J. Macromol.Sci. Chem.* 1981, A15, 1015

90. Möbius, D.; Orrit, M.; Gruninger, H.; Meyer, H. *Thin Solid Films* **1985**, *132*, 41.
91. Mohwald, H. *Thin Solid Films* **1988**, *59*, 1.
92. Wegner, G.; Lieser, G.; Tieke, B. *Thin Solid Films* **1980**, *68*, 77-90.
93. Lando, J. and Day, D. *Macromolecules* **1980**, *13*, 1478-1483.
94. Adamson, A.W. *Physical Chemistry of Surfaces*, 4th Ed. John Wiley & Sons, Inc., New York , 1982.
95. Brooks, J.H. and MacRitchie, F.J. *Colloid Sci.* **1961**, *16*, 442.
96. Fromherz, P. *Rev.Sci. Instrum.* **1975**, *46*, 1380.
97. Verger, R. and de Haas, G.H. *Ann. Rev. Biophysics, Bio Eng.* **1976**, *5*, 77.
98. Langmuir, I and Schaefer, V. *J. Am. Chem.Soc.* **1938**, *60*, 1351.
99. Roberts, G.G. *Adv. Phys.* **1985**, *34*, 475.
100. Embs, F.; Funhoff, D.; Laschewsky, A.; Licht, U.; Ohst, H.; Prass, W.; Ringsdorf, H.; Wegner, G.; and Wehrmann, R. *Adv. Mater.* **1991**, *3*, 25.
101. Pockels, A. *Nature*, **1892**, *46*, 418.
102. Devaux, H.C. and Hebd, R. *Seances Acad. Sci.* **1935**, *201*, 109.
103. Katz, J.R. and Samwell, P.J.P. *Naturwissenschaften* **1928**, *16*, 592.
104. Harkins, W.D.; Carman, E.F.; Ries, H.E. *J.Chem. Phys.* **1935**,*3*, 692.
105. Crisp, D.J. *J. Colloid Sci.* **1946**, *1*, 49, 161.
106. Takahashi, A.; Yoshida, A.; Kawaguchi, M. *Macromolecules* **1983**, *16*, 956.
107. Gabrielli, G.; Pugelli, M. and Baglioni, P. *J.Colloid Interface. Sci.* **1982**, *86*, 485.
108. Gabrielli, G. ; Baglioni, P.; Feroni, E. *Colloid Polym. Sci.* **1979**, *257*, 121.
109. Ferroni, E.; Gabrielli, G.; and Pugeli, M. *Chim.Ind. (Milan)* **1967**,*42*, 147.
110. Gaines, G.L. ,Jr. *Adv. Chem.Ser.* **1975**,*144*, 338.

111. Noll, W.; Steinbach, H.; and Sucker, C. *J.Poly. Sci.; Part C.* **1971**, *34*, 123-139.
112. Fowkes, F. *J.Phys. Chem.* **1964**, *68*, 3515.
113. Gaines, G.L.Jr., *Langmuir* **1991**, *7*, 834.
114. MacRitchie, F. *J. Colloid Sci.* **1963**, *18*, 555.
115. Danielli, J.; Rosenberg, M.; Cadenhead, D., *Progress in Membrane and Surface Science*, Academic Press;New York, 1973.
116. Zhou,H.; Stern,R.; Batich,C.; and Duran, R.S. *Makromol. Chem. Rapid Comm.* **1990**, *11*, 409.
117. Fukuda, K.; Kato, T.; Machida, S.;Shimizu, Y. *J. Colloid Int. Sci.* **1979**, *68*, 82.
118. Sanchez, I. *J. Macrom. Sci. Rev. Chem.* **1974**, *c-10* , 113.
119. Lavielle, L; Schultz, J. *J.Colloid Int.. Sci.* **1985**, *106*, 446.
120. MacRitchie, F. *Chemistry at Interfaces*. Academic Press, San Diego, **1990**.
121. Malcolm, B. *J. Colloid. Int. Sci.* **1985**, *104*, 520-529.
122. Singer, S. J. *J.Chem.Phys.* **1948**, *16*, 872.
123. Rondelez, F. and Villanove, R. *Phys.Rev.Lett.* **1977**, *39*, 95.
124. Andrade, J.D., *Polymer Surface Dynamics* Plenum Press, NewYork, **1988**.
125. Elais, H.G. *Macromolecules.1 Structure and Properties* Plenum Press, New York, **1984**.
126. Wu, S. *Polymer Interface and Adhesion*, Marcel Dekker, New York, **1982**.
127. Lee, H., *Adhesion and Adsorption of Polymers* Plenum: New York, **1980**.
128. Seymour, R.; Stahl, G., *Macromolecular Solutions* Pergamon Press, New York, **1982**
129. Ozcayir, Y.and Blumstein, A. *Mol.Cryst.Liq. Cryst.* **1996**, *135*, 237.
130. Vogel, A. *Textbook of Practical Organic Chemistry* 4th edition Longmans, New York **1986**.

131. Neises, B.; Steiglich, W. *Angew. Chem. Int. Ed.*, 1978, 17, 522.
132. Austin, W.; Bilow, N.; Kelleghan, W.; Lau, K. *J. Org. Chem.* 1981, 46, 2280-2286. '
133. Schrock, R.R.; Crowe, W.E.; Bazan, G.C.; DiMare, M.; O'Regan, M.B.; Schofield, M.H. *Organometallics* 1991, 10, 1832.
134. Davies, J. and Rideal, E. *Can.J. Phys.* 1955, 33, 947.
135. Priestley, E.B. *Introduction to Liquid Crystals* Priestley, Wojtowicz, Sheng. eds. Plenum Press, New York, 1974, 903.
136. Gray, W.G.; Goodby, J.W. *Smectic Liquid Crystals, Textures and Structures*, Hill: London, 1984.
137. references cited in Ringsdorf, H.; Schlarb, B.; Venzmer, J. *Angew. Chem. Int. Ed. Eng.* 1988, 27, 113-158.
138. Heesemann, J. *J.Am. Chem.Soc.* 1980, 7, 102, 2167- 2176.
139. Blumstein, A. in *Advances in Macromolecular Chemistry* Pasika ed., Vol. 2, Academic Press, New York, 1970
140. Cohen, M.D.; Schmidt, G.M.J. *J.Chem.Soc.* 1964, 1996.
141. Wegner, G. *J.Pure & Appl. Chem.* 1977, 49, 443-454.
142. LeMoigne, J.; Soldera, A.; Guillon, D.; Skoulios, A. *Liquid Crystals* 1989, 6, 627-639.
143. Zhang, X.; Ozcayir, Y.; Feng, C.; Blumstein, A. *Polymer Preprints* 1990, 31, 597-598.
144. Ogawa, K., *J. Phys.Chem.* 1989, 93, 5305-5310.
145. Oh, S.Y.; Ezaki, R.; Kazuo, A.; Shirakawa, H. *J. Poly. Sci. Part A: Chem.* 1993, 31, 2977-2985.
146. Xiu, X.; Era, M.; Tsutsui, T.; Saito, S. *Thin Solid Films* 1989, 179, 65.
147. Heesemann, J. *J.Am. Chem.Soc.* 1980, 102, 2176-2181.
148. Tieke, B. *Adv.Polym.Sci.* 1985, 71, 79
149. O'Brien, K.; Long, J.; Lando, J.B. *Langmuir* 1985, 1, 514-518.
150. Tieke, B.; Lieser, G.; Wegner, G. *J.Polym.Sci.Polym.Chem.Edu.* 1979, 17, 1631.

151. Tieke, B.; Wegner, G. ; Graf, J.; Naegele, B.; Ringsdorf, H.; Banerjie, A.; Day, D. and Lando, J. *Colloid and Poly. Sci.* **1977**, *255*, 521-531.
152. Labana, S. J. *Macro. Sci.:Rev. in Macro. Chem.* **1974**, *C11*, *2*, 299-318.
153. Ogawa, K.; Tamura, M.; Hatada, M. and Ishihara, T. *Langmuir* **1987**, *4*, 195-200.
154. Lowry, T. and Richardson, K. *Mechanism and Theory in Organic Chemistry*, Harper and Row Publishers, New York, 1987.
155. Malatesta, V. and Sciano, J. *J. Org. Chem.* **1982**, *47*, 1455.
156. Tsuchihara, K.; Masuda, T.; Higashimura, T. *J. Poly.Sci. Part A: Poly.Chem.* **1991**, *29*, 471-478.
157. Schnabel, W. *Polymer Degradation Principle and Practical Application* Hanser International, 1981.
158. Fouassier, J.; Tieke, B.; and Wegner,G. *Isr. J. Chem.* **1979**, *18*, 227.
159. Winter, S.; Tredgold, R.; Vickers, A.; Khoshdel, L and Hodge, P. *Thin Solid Films* **1985**, *134*, 49-55.
160. Nishikata, Y.; Komatsu, K.; Masa-aki, K. and Imai, Y. *Thin Solid Films*, **1992**, *210/211*, 29-31.
161. Simionescu, C.; Percec, V.; Dumitrescu, S. *J. Polym. Sci.. A: Chem. Ed.* **1977**, *15*, 2497.
162. Sanford, T.; Allendorf, R.; Kang, E.; Ehrlich, P. *J. Polym. Sci. Phys. Ed.* **1980**, *18*, 2277.
163. Percec, V; Rinaldi, P. *Polym. Bull.* **1983**, *9*, 548.
164. Furlani, A.; Napoletano, C.; Russo, M.; Feast, W. *Polym. Bull.* **1986**, *16*, 311.
165. Percec, V. *Polym.Bull.* **1983**, *10*, 1.
166. Clough, S.; Sun, X.; Tripathy, S.; Baker, G. *Macromolecules* **1991**, *24*, 4264-4269.
167. Kawaguchi, M.; Sano, M.; Chen, Y.; Zografi, G.; Yu, H. *Macromolecules* **1986**, *19*, 2606.
168. Rennie, A.; Crawford, R.J. ; Lee, E.M.; Thomas, R.K.; Crowley, T.L.; Roberts, S. Qureshi, M. Richards, R. *Macromolecules* **1989**, *22*, 3466.

169. Sansone, M.; Rondelez, F.; Peiffer, D.; Pincus, P.; Kim, M.; Eisenberger, P. *Phys. Rev. Lett.* **1985**, *54*, 1039.
170. Kawaguchi, M.; Nagata, K. *Langmuir* **1991**, *7*, 1478-1482.
171. Matuo, H.; Rice, D.; Balthasar, D.; Cadenhead, D. *Chem. Phys. Lipids* **1982**, *30*, 367.
172. Biegajski, J.; Cadenhead, D.; Prasad, P. *Langmuir* **1988**, *4*, 689-693.
173. Schulman, J.; Hughes, A. *Proc.R.Soc. London Ser.A* **1932**, *138*, 430.
174. Oliviera, O.N.; Taylor, D.M.; Morgan, H. *Thin Solid Films* **1992**, *210/211*, 76-78.
175. Henon, S. and Meunier, J., *Thin Solid Films* **1992**, *210*, 121.
176. Vogel, V and Mobius, D. *Thin Solid Films* **1988**, *159*, 73-81.
177. Alexander, A. and Schulman, J. *Proc. Roy.Soc. London* **1937**, *A161*, 122.
178. Honig, D. Mobius, D. *Thin Solid Films* **1992**, *210/211*, 64-68
179. Ballauf, M. *Angew.Chem.* **1989**, *28*, 253.
180. Watanabe, I; Hong, K.; Rubner, M. *Langmuir* **1990**, *6*, 1164-1172.
181. Brinkhaus, R. and Schouten, A.J. *Macromolecules* **1992**, *25*, 6173-6178.
182. Odian, G. *Principles of Polymerization* 2nd. ed. Wiley Interscience, New York, 1970.
183. Advincula, R.C.; Duran, R.S.; Le Moigne, J.; Hilberer, A. *Macromolecules* **1993**, *26*, 3895-3903.
184. Eglinton, G.; Galbraith, A.R. *J. Chem. Soc.* **1959**, 889.
185. Masuda, T. ; Matsumoto, T.; Yoshimura, T.; Higashimura, T. *Macromolecules* **1990**, *23*, 4902-4907.
186. Masuda, T. ; Hamano, T.; Tsuchihara, K.; Higashimura, T. *Macromolecules* **1990**, *23*, 1374-1380.
187. Masuda, T. ; Okuhara, K.; Ueda, T.; Yoshimura, T.; Higashimura, T. *Macromolecules* **1991**, *24*, 6054-6058.
188. Kuhn, H. *Fortschr. Chem. Org. Naturst.*, **1959**, *7*, 404.

189. Baughman, R.H.; Chance , R.R. *J.Polym. Sci. Polym Phys.* **1976**, *14*, 2037.
190. Craig, G.; Cohen, R.; Schrock, R.; Silbey, R.; Pucetti, G.; Ledoux, I; Zyss, J. *J. Am. Chem. Soc.* **1993**, *115*, 860-867.
191. Reich, L.; Shindler, A. *Polymerization by Organometallic Compounds* , Wiley Interscience, New York, 1966.
192. Tait, P. in *Coordination Polymerization* Chien ed., Academic Press Inc., New York, 1975.
193. Sawada, H. *Rev. Macro. Chem.* **1970**, *4*, 313-395.
194. Brinkhaus, R.H.G.; Schouten, J. *Macromolecules* **1991**, *24*, 1487-1495.
195. Kato, T. *Langmuir*, **1990**, *6*, 870-872.
196. MacRitchie, F.; Alexander, A. *J. Colloid Sci.* **1963**, *18*, 458.
197. Macritchie, F. *J. Colloid. Interface Sci.* **1985**, *105*, 119.
198. Yoo, K-H.; Yu, H. *Macromolecules* **1989**, *22*, 4019-4026
199. Motomura, K. *Adv. Colloid Interface Sci.* **1980**, *12*, 1.
200. Duran, R.; Adams, A.; Buske, A. *Macromolecules* **1993**, *26*, 2871-2877.
201. Henon, S. and Meunier, J., *Thin Soild Films* **1992**, *210*, 121.
202. Davies, J. T. ; Rideal, E.K. *Interfacial Phenomena*, Academic Press, New York, 2nd ed. **1963**.
203. Ajuha, R.; Caruso, P.; Mobius, D.; Wildburg, G.; Ringsdorf, H.; Philip, D.; Preece, J.; Stoddart, F. *Langmuir* **1993**, *9*, 1534-1544.
204. Schulman, J.H. and Hughes, A.H. *Proc. R. Soc. London. Ser. A* **1932**, *138*, 430.
205. Oliviera, O.; Taylor, D.M. ; Morgan, H. *Chem. Phys. Lett.* **1989**, *161*, 147.
206. Seelig, J.; McDonald, P.; Scherer, P.G. *Biochemistry* **1987**, *26*, 7535.
207. Wilson, M.; Pohorille, A.; Pratt, L. , *J. Chem. Phys.* **1988**, *88*, 3281.
208. Vogel, V. ; Mobius, D. *J. Colloid Interface Sci.* **1988**, *26*, 408-420.
209. Oliviera, J. O.; Taylor, D.M., Lewis, T.J., Salvagno, S.; Stirling, J.M. *J. Chem. Soc. Faraday. Trans.* **1989**, *85*, 1009.

210. Takahashi, A.; Yoshida, A.; Kawaguchi, M. *Macromolecules* **1982**, *16*, 1196.
211. Hildebrand, J. *An Introduction to Molecular Kinetic Theory* Reinhold Publishing Corporation, New York, **1963**.
212. Tredgold, R.; Vickers, J.; Winter, S.; Khoshdel, C ;Hodge,P. *Thin Solid Films* **1985**, *134*, 49-55.
213. Lavielle, L.; Schultz, J. *J. Colloid, Int. Sci.* **1985**, *106*, 446.
214. Clementi, E. *Determination of Liquid Water Structure* Springer Verlag: New York, **1976**.
215. Hatefi, Y.; Hanstein, G. *Biochemistry* **1969**, *62*, 1129.
216. Williams, D.; Fleming, I. *Spectroscopic Methods in Organic Chemistry*, Third. ed. McGraw-Hill, Great Britain.**1980**.
217. Fadel, H.; Percec, V.; Zheng, Q.; Advincula, R.; Duran, S. *Macromolecules* **1993**, *26*, 1650-1655.
218. Cadenhead, D.; Biegajski, J.; Burzynski, R.; Prasad, P *Macromolecules* **1986**, *19*, 2459-2461.
219. Carpenter, M.; Paras, P.; Griffin, A. *Thin Solid Films* **1988**, *161*, 315-324.
220. Kawaguchi, M.; Tohyama, M.; Mutoh, Y.; Takahashi, A. *Langmuir* **1988**, *4*, 407.
221. Hoenig, D.; Moebius, D.; Overbeck, G. *Adv. Mater.* **1992**, *4*, 419.
222. Frank, H. and Evans, M. *J. Chem. Phys.* **1945**, *13*, 507.
223. Bovey, F. *Polymer Conformation and Configuration* Academic Press, New York, **1969**.
224. Bredas, J.; Heeger, A. *Macromolecules* **1990**, *23*, 1150.
225. Thibodeaux,A. Ph.D. Dissertation, University of Florida, **1993**.
226. Motschmann, H.; Reiter, R.; Lawall, R.; Duda, G., Stamm, M.; Wegner, G.; Knoll, W. *Langmuir* **1991**, *7*, 2743-2747.
227. Gabrielli, G.; Nocentini, M.; Sbrana, G.; Grando, D.; Sottini, S.; and Ventura, G. *Thin Soid Films* **1992**, *210/211*, 551-554.
228. Patel, G. ; Miller, G. *J. Macrom. Sci. Phys.* **1981**, *B20(1)*, 113-131.

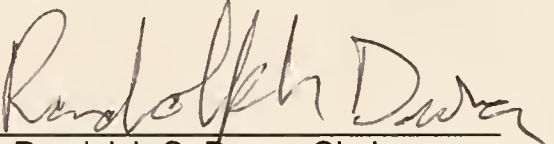
229. Ward, I. *Mechanical Properties of Solid Polymers* Wiley-Interscience, London, 1971.
230. Rennie, A.; Crawford, R.; Lee, E.; Thomas, R.; Crowley, T.; Roberts, S.; Quereshi, M.; Richards, R. *Macromolecules* 1989, 22, 3466.
231. Shaw, D. *Introduction to Colloid and Surface Chemistry*, Butterworths:, London. 1970.
232. Fourt, L.; Harkins, W. *J. Phys. Chem.* 1938, 42, 897.
233. Kawai, T.; Umemura, J.; Takenaka, T. *Langmuir* 1989, 5, 1378-1383.
234. Gabrielli, G.; Guarini, G.; *J. Colloid Sci.* 1978, 64, 185.
235. MacRitchie, F.; Ter-Minassian-Saraga, L. *Colloids Surf.* 1984, 10, 53.
236. Malcolm, B. *Proc.R.Soc. London* 1968, A305, 363.
237. Kawaguchi, M.; Tohyama, M.; Mutoh, Y.; Takahashi, A. *Langmuir* 1988, 4, 407.
238. Tillman, N.; Ulman, A.; Schildkraut, J.; Penner, T. *J. Am. Chem. Soc.* 1988, 110, 6136-6144.
239. Haller, G.; Rice, R. *J. Phys. Chem.* 1970, 74, 4386-4393
240. Kiessig, H. *Ann. Phys.(Leipzig)*, 1931, 10, 769.
241. Shen, Y.R. *The Principles of Nonlinear Optics* John Wiley & Sons, New York, 1984.
242. Williams, D.J., *Electronic and Photonic Application of Polymers, Adv. Chem. Series*, 1988, 218, 297-330.

BIOGRAPHICAL SKETCH

The author was born on the 31st day of October 1967, in Manila, Philippines. The eldest son of a lawyer-businessman, he was one of six children. Having obtained his high school education from a special science curriculum, he set out to become a medical doctor after accepting a scholarship in chemistry at the University of the Philippines. Later in his "pre-med" endeavors, he discovered the challenge of doing research as a chemist and henceforth decided to pursue chemistry as a career. After graduating with a B.S. degree in chemistry, he decided to become an instructor at the University and at the same time start on a master's degree program. Hoping to fulfill a desire to do research in the U.S., the author decided to apply for graduate school in the U.S. During the months leading to his preparation, the author became engaged to Carolyn whom he met at the Christian church where he belonged. They married right before departing for the U.S.

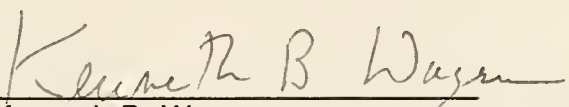
The author entered graduate school in chemistry at the University of Florida in the fall of 1989. After five years of studying and research under the direction of Dr. Randy S. Duran, he finally defended his dissertation research and graduated April 1994. After graduation, the author accepted a position to do postdoctoral work at the Max Planck Institute in Mainz, Germany, with the group of Dr. Wolfgang Knoll.

I certify that I have read this study and that in my opinion it conforms to acceptable standards of scholarly presentation and is fully adequate, in scope and quality, as a dissertation for the degree of Doctor of Philosophy.



Randolph S. Duran, Chairman
Assistant Professor of Chemistry

I certify that I have read this study and that in my opinion it conforms to acceptable standards of scholarly presentation and is fully adequate, in scope and quality, as a dissertation for the degree of Doctor of Philosophy.



Kenneth B. Wagener
Professor of Chemistry

I certify that I have read this study and that in my opinion it conforms to acceptable standards of scholarly presentation and is fully adequate, in scope and quality, as a dissertation for the degree of Doctor of Philosophy.



John Zoltewicz
Professor of Chemistry

I certify that I have read this study and that in my opinion it conforms to acceptable standards of scholarly presentation and is fully adequate, in scope and quality, as a dissertation for the degree of Doctor of Philosophy.



Martin T. Vala
Professor of Chemistry

I certify that I have read this study and that in my opinion it conforms to acceptable standards of scholarly presentation and is fully adequate, in scope and quality, as a dissertation for the degree of Doctor of Philosophy.



Christopher D. Batich
Professor of Materials Science and
Engineering

I certify that I have read this study and that in my opinion it conforms to acceptable standards of scholarly presentation and is fully adequate, in scope and quality, as a dissertation for the degree of Doctor of Philosophy.



Jacques Le Moigne
Director of Research
Institute of Physics and Chemistry of
Materials, Strasbourg, France

This dissertation was submitted to the Graduate Faculty of the Department of Chemistry in the College of Liberal Arts and Sciences and to the Graduate School and was accepted as partial fulfillment of the requirements for the degree of Doctor of Philosophy.

April 1994

Dean, Graduate School

LD
1780
1994
. A244

UNIVERSITY OF FLORIDA



3 1262 08557 0868